



**HAL**  
open science

# Grafting of organic thin films to act as dry boundary lubricants for the protection of electrical contacts

Alessandro Benedetto

► **To cite this version:**

Alessandro Benedetto. Grafting of organic thin films to act as dry boundary lubricants for the protection of electrical contacts. *Polymers*. Université Paris XI, 2008. English. NNT: . tel-03745002

**HAL Id: tel-03745002**

**<https://theses.hal.science/tel-03745002>**

Submitted on 3 Aug 2022

**HAL** is a multi-disciplinary open access archive for the deposit and dissemination of scientific research documents, whether they are published or not. The documents may come from teaching and research institutions in France or abroad, or from public or private research centers.

L'archive ouverte pluridisciplinaire **HAL**, est destinée au dépôt et à la diffusion de documents scientifiques de niveau recherche, publiés ou non, émanant des établissements d'enseignement et de recherche français ou étrangers, des laboratoires publics ou privés.

Thèse de doctorat de l'Université Paris XI

Spécialité : Chimie Physique

Présentée par

Alessandro BENEDETTO

Pour obtenir le grade de Docteur de l'Université de Paris XI

Sujet de la thèse :

Films minces organiques greffés pour une  
lubrification limite appliquée à la protection  
des contacts électriques

Soutenue le 6 octobre 2008

devant la commission d'examen :

Président : Mme Liliane LEGER

Rapporteurs :

M. Philippe KAPSA

M. Eric LEVILLAIN

Examineurs :

M. Bharat BHUSHAN

Mme Catherine COMBELLAS

Mme Sophie NOEL

M. Pascal VIEL



*Altissimu, onnipotente bon Signore,  
Tue so' le laude, la gloria e l'honore et onne benedictione.*

*Ad Te solo, Altissimo, se konfano,  
et nullu homo ène dignu te mentovare.*

*Laudato sie, mi' Signore cum tucte le Tue creature,  
spetialmente messor lo frate Sole,  
lo qual è iorno, et allumeni noi per lui.  
Et ellu è bellu e radiante cum grande splendore:  
de Te, Altissimo, porta significatione.*

*Laudato si', mi Signore, per sora Luna e le stelle:  
in celu l'ài formate clarite et pretiose et belle.*

*Laudato si', mi' Signore, per frate Vento  
et per aere et nubilo et sereno et onne tempo,  
per lo quale, a le Tue creature dàì sustentamento.*

*Laudato si', mi' Signore, per sor Aqua,  
la quale è multo utile et humile et pretiosa et casta.*

*Laudato si', mi Signore, per frate Focu,  
per lo quale ennallumini la nocte:  
ed ello è bello et iocundo et robustoso et forte.*

*Laudato si', mi' Signore, per sora nostra matre Terra,  
la quale ne sustenta et governa,  
et produce diversi fructi con coloriti flori et herba.*

*Laudato si', mi Signore, per quelli che perdonano per lo Tuo amore  
et sostengono infirmitate et tribulatione.*

*Francesco d'Assisi, 1226*



## Ringraziamenti



- **Pascal Viel** qui a été le directeur de thèse idéal que chaque doctorant voudrait avoir. Merci pour m'avoir accompagné dans ces trois ans, m'avoir initié aux mystères de l'électrochimie et m'avoir passionné à cette discipline. Merci pour tout ce qui m'a appris sur la chimie des surfaces, la physico-chimie, le fonctionnement du laboratoire. Merci pour le support scientifique et morale. Il est et il restera toujours la personne la plus importante pour moi dans ces trois ans de doctorat vécus à Paris et sur le plateau de Moulon.
- **David Alamarguy** pour le partage de ce travail coude à coude sur le projet nanoconnect et pour être une des personnes plus généreuses que je connaisse.
- **Mirela Balog** pentru o foarte frumoasă moleculă. Avem avut puțin din ocazia sa lucra împreună dar au fost foarte fericite.
- **Sophie Noël** pour m'avoir suivi dans le travail au LGEP et pour sa grande disponibilité.
- **Serge Palacin** pour avoir été un excellent chef de laboratoire toujours (ou presque) de bonne humeur et d'une compétence énorme. Je le remercie pour avoir corrigé tous mes articles et rapports avec une disponibilité et une vitesse extraordinaires.
- **Bruno Jusselme** pour m'avoir laissé jouer avec son sel de diazonium avec le complexe de ruthénium et le benzenediazonium qui c'est en suite révélé fondamentale pour cette thèse.
- Tout le laboratoire LCSi et les personnes qui le forment. Ça été un lieu de travail très agréable et gai.
- Merci au maître ingénieur (et bien tôt docteur) **Pierre-Jean Alet** pour avoir été un bon compagnon de thèse.
- Les amis angevin **Franck Le Derf** et **Marc Sallé** qui ont fait partie du projet nanoconnect et avec lesquels a été très agréable de travailler et correspondre.
- Je remercie aussi **Philippe Kapsa** et **Eric Levillain** d'avoir accepté d'être rapporteur de cette thèse.
- As **Bharat Bhushan**, **Catherine Combellas**, and **Liliane Léger** to be in the examining committee.
- Ringrazio i miei genitori **Maria** e **Gianni** per avermi sostenuto e permesso di arrivare fino a qui. Così come mia sorella **Enrica** alla quale per di più ho subappaltato il "pot de thèse".
- Ringrazio anche tutti i miei amici **Angelica**, **Anton**, **Claudio**, **Dorota**, **Elisa**, **Enrico**, i **Franceschi**, **Laurent**, **Marie-Hermine**, **Matteo**, **Sylwia**, **Xavier** (e tutti quelli che sicuramente ho dimenticato) per avermi aiutato a portare a termine questo dottorato risolvendomi l'umore e regalandomi tanti momenti allegri. Ringrazio specialmente quelli che da vicino o da lontano sono venuti il 6 ottobre ad ascoltare la passionante storia sulle superfici lubrificate dai polimeri.
- La signa **Monteforte** per essere arrivata nella mia vita come il vento di primavera ed avermi strappato dal mio zittellaggio scientifico. Nonché per aver attivamente contribuito a rallentare la stesura di questa tesi di dottorato per altro con mio grande piacere.

- Le **Grand Céleste** et tous les **célestins** pour m'avoir donné des moments de souffle, d'amusement, d'amitié, de création et de distraction au cours des ces ans de doctorat à Paris. Je n'oublierai jamais cet endroit magique qui comme dans un rêve a disparu avec la fin de mon temps doctorale et surtout je n'oublierai jamais les personnes que j'y ai connues.
- A **Océane Boyer** pour avoir été un soutien dans les jours les plus durs de la rédaction du mémoire de thèse et car sans être d'abord passé par la méthodologie russe du trapèze ballant jamais j'aurais eu assez de discipline et de courage pour arriver à la fin de ce manuscrit. A **Léa Pessard** pour m'avoir initié à l'art du trapèze fixe et avoir été à la fois une amie et une enseignante.

## Summary

Ringraziamenti.....	5
Summary.....	7
1 Introduction.....	8
2 Methodologies .....	18
3 Grafting of aromatic diazonium salts.....	28
4 Grafted poly(methacrylate)s.....	63
5 Composites of grafted poly(methacrylate)s and conductive charges .....	83
6 Discussion and comparison of tribological behaviors .....	148
7 General conclusion and outlook.....	159
Appendix A - List of acronyms and abbreviations.....	163
Appendix B - Introduction to electrical contacts.....	165
Appendix C - Introduction to EIS.....	170
8 Index.....	178
9 Bibliography.....	182

# 1 Introduction

## 1.1 Objective of the work

“God made solids, but surfaces were the work of the devil”. This citation belongs to the great physicist Wolfgang Ernst Pauli. Although surfaces can upset theoretician physicists and be a hard work for experimentalist researchers life is based on surfaces.



*Figure 1. Gecko, mussel and water strider: animals that have developed stunning “intelligent” surfaces to live in their natural environment [1].*

Animals represented in Figure 1 know that very well. Nature has developed stunning strategies to modify the surface of the legs of water strider and gecko to allow them to better survive in their natural environment [2-4] and an excellent chemistry for the glue that allow mussels to solidly hold on sea rocks [1] beaten by the waves.

But controlling the surface properties is also extremely important for the mankind [5] because they play a fundamental role in our life of every days and in many technological applications. The durability of our computer hard disk, the soft sound of a violin, the way in which rain roll off our car windows, the texture of food, the good working of surgery tools, and the opening of a car airbag in case of accident: these are few examples in which surface science and surface modification play a fundamental role.

Moreover with the increasing miniaturization of device components and high-performance materials, the surface-to-volume ration increases, and the properties of the surfaces become increasingly more important [6].

In between all the vast panorama of cases where surface science plays a fundamental role we are concerned by the lubrication of electrical contacts in electronic devices.

Every kind of electrical contact for electronic (low dc currents) needs to be protected. The two principal reasons reside in lubrication for the reduction of wear and the protection from environmental corrosion.

Electrical contacts, such as in connectors, are subjected to wear either because of insertion/removal or simply because of the vibrations to which a device is inevitably submitted during its life. In a pure metal/metal contact configuration the strong adhesion can quickly lead to a severe wear, the formation of a poorly conductive oxidized layer and finally to the contact failure (that means a large increase of the electrical contact resistance).

For that reason the substrate material of the electrical component (usually copper based) is coated by another more appropriate to electrical contacting such as e.g. tin, silver and gold. This latter layer can finally be coated by a protective film constituted of an adsorbed liquid lubricant. For gold one of the most used family of lubricants is that of Fomblin® by Solvay Solexis that is constituted of perfluoropolyethers (PFPE) of high molecular weight (in the order of 1000 u). Another technological solution resides in poly(phenylethers) (PPE). The choice of their molecular structure is a compromise in between many needs such as low surface energy (which leads to often fluorinated solutions) to reduce adhesion in between the two components of the contact, good adherence to the substrate (which is often controversial with the former one), low evaporation and migration, resistance to the temperature...

A second reason to coat electrical contact with an organic film is to reduce environmental corrosion which also leads to oxides formation and eventually contact failure. This is particularly present in the case of gold coated contacts where the presence of the noble metal enhances the corrosion of the copper substrate. For that reason a nickel inter-layer is usually present to separate gold from copper and reduce the corrosion rate.

If the protection of liquid lubricants is almost the only solution that is applied today it presents many limitations. The reader should have experimented at least once in

his/her everyday life the break down of a device because of the failure of an electrical contact.

Moreover liquid lubricant can not be applied in many applications in extreme conditions such as in aerospace (because they are subject to migrations and evaporation), ultra high vacuum machines and in extremely miniaturized machines (MEMS and NEMS) [7]. In those cases one has to rely entirely on the tribological properties of dry surfaces [5].

Therefore the functionalization of metallic surfaces with organic molecules to impart “lubricating” properties without degrading electrical conduction becomes a subject of major interest both from fundamental and technological point of view.

The objective of this thesis is to study the covalent grafting of thin lubricant films on metals surface to act as boundary lubricants for the protection of electrical contacts.

## **1.2 Previous works on the tribology of grafted organic films**

Boundary lubrication is a regime where the tribological properties (such as friction and wear) are determined by the solid surface properties and lubricant properties other than its viscosity [8].

This situation is obtained when the lubricant is constituted of a thin film (a monolayer or a few monolayers thick) adsorbed on the contacting surfaces. In the years 1900-1920 Langmuir experimentally showed that a monolayer of organic molecules is sufficient to produce a lubricant effect.

Although the phenomenon of boundary lubrication is known since a long time insight on the microscopic mechanism were obtained much later with the development of the appropriated experimental techniques [9] such as the surface-force apparatus (SFA), the atomic-force and friction force microscopes (AFM and FFM) and the quartz microbalance.

SFA was developed in the late 1960s and is commonly employed to study both static and dynamic properties of molecularly thin films sandwiched between two molecularly smooth surfaces.

The introduction of the atomic force microscope in 1985 provided a method for measuring ultra-small forces between a probe tip and a surface, and has been used

for topographical measurements of surfaces on the nanoscale, as well as for adhesion and electrostatic force measurements. Subsequent modification of the AFM led to the development of the friction-force microscopy (FFM) designed for atomic-scale and microscale studies of friction.

The early and more widely studied families of films studied by these techniques are that of fatty acids. In that case it was shown that the interesting tribological properties results from the molecules being adsorbed on the surface by the polar extremity while the rest of the chains forms a compact brush-like carpet whose terminal surface is constituted of  $-CH_3$  groups with a very low surface energy [10]. Successive studies conducted [6, 11-13] in Jacob Israelachvili research group allowed to clarify fundamental aspects of tribology such as the relations between the friction and adhesion on such film family. They have shown that for a fat acid monolayer adsorbed on a mica surface the friction coefficient increases with the hysteresis measure on adhesion as measured from approach-redraw curves [13].

Another family of widely studied molecular films as boundary lubricant is that of silanes. Their interest resides in the fact that they can be easily bonded to the oxide present on silicon surface. Therefore they can be applied to the lubrication of devices based on silicon technology such as MEMS [7, 14].

MEMS are one of the most interesting examples to show the importance of controlling the surface energy of the device by chemical bonding of a molecular film. Unless adhesion is strongly suppressed, micro- and nanomachines do not work because stiction phenomenon: their “moving” parts spontaneously collapse together and remain adherent [15].

Because MEMS may have surfaces in normal or sliding contact, friction and wear are also important issues [16]. Because at that length scale surface-to-volume ratio increases and surface and capillary forces become predominant on other forces behaviors different from the macroscopic world can be found.

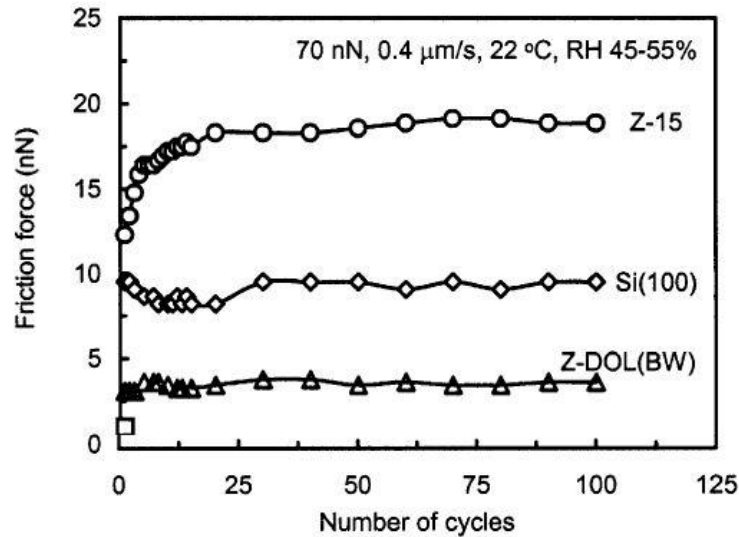


Figure 2. Friction force and coefficient of friction versus the number of sliding cycles for unlubricated Si(100), lubricated with Z-15 (liquid lubricant) and Z-DOL(BW) (same lubricant but silane grafted) [14].

Figure 2 is extracted from an article of Liu et Bhushan [14] which show the importance of a grafting lubricant in MEMS lubrication. It reports the evolution of the coefficient of friction during a micro-tribological test for an unprotected Si(100) surface, for the surface lubricated by a perfluoro poly ether lubricant (Z-15) and for a surface lubricated by grafting a monolayer of a silane having the same molecular structure (Z-DOL(BW)). In that case it can be seen that while the grafted monolayer ameliorates the tribological properties by reducing the coefficient of friction the ungrafted lubricant degrades them with respect to the native surface.

A great number of works exists on other families of thin graded molecular films acting as boundary lubricants: thiols [17, 18] have been studied for the lubrication of gold, phosphanates [19] and silanes [20] for the lubrication of aluminium.

Of course this paragraph can not be exhaustive but it simply attempts to show the great interest that resides in the study of grafted boundary lubricants both from theoretical and applicative aspects.

### 1.3 Specific studies on the lubrication on electrical contacts

If many works have been conducted on grafted molecules and a great number of publications exists on the subject fewer studies have been conducted on the specific application to the lubrication of electrical contacts where both tribological and electrical properties have to be considered.

Electrical connectors are normally constituted of copper-based materials. They need therefore to be protected against the different degradation mechanism and especially against oxidation. Copper is therefore coated by other metallic layers:

- Tin: for low cost connectors. In that case friction is high and connector performances are low.
- Gold: for higher performances connectors.

In the latter case, to reduce fabrication costs, the gold layer is thin and not anymore covering. The presence of a not covering noble metal on copper quickly enhances connector corrosion. For that reason a nickel infra-layer is interposed between copper and gold to reduce corrosion rate.

Therefore, because of friction (in the case of tin coated connectors) or corrosion (in the case of gold coated connectors) a further protective layer is necessary.

An existing solution is that of liquid lubricants. But they present many problems as polymerization, migration, evaporation, etc.

For that reason it is of interest to look for immobilized lubricants that will be stable, inert, reducing friction and oxidation without increasing electrical resistance.

In the past in the LGEP the lubrication of electrical contacts by grafting of thiols on polycrystalline nickel was studied [21-23]. It was shown that it was possible to graft SAM on nickel covering and with a good organization. But the reoxidation of nickel substrates make not possible a direct application to industrial electrical contacts.

Then a do-deposition process of thiols and perfluoropolyether was developed [24]. Excellent results were found in terms of protection against wear and corrosion and a patent was deposited [25].

Anyway the grafting kinetics are slow and need a fine tuning of the formulation depending on the specific application.

Another solution studied for the boundary lubrication of electrical contacts was the use of a partially pyrolyzed poly(acrylonitrile). Thin polyacrylonitrile films were electrografted on nickel [26-30] in order to obtain a covalently grafted film on the metal.

Then a rapid thermal treatment was executed at different temperatures between 350 °C and 700 °C in order to induce bonds between adjacent polymer chains with the

formation of a graphite like structure (see Figure 3). The thermal treatment was effectuated in order to reduce the electrical resistance and ameliorate the tribological behavior (by increasing the hardness). The best results from both electrical conductivity and tribological and wear properties were obtained for the highest treatment temperature. This severely limits the transfer of the proceeding to an industrial application [31].

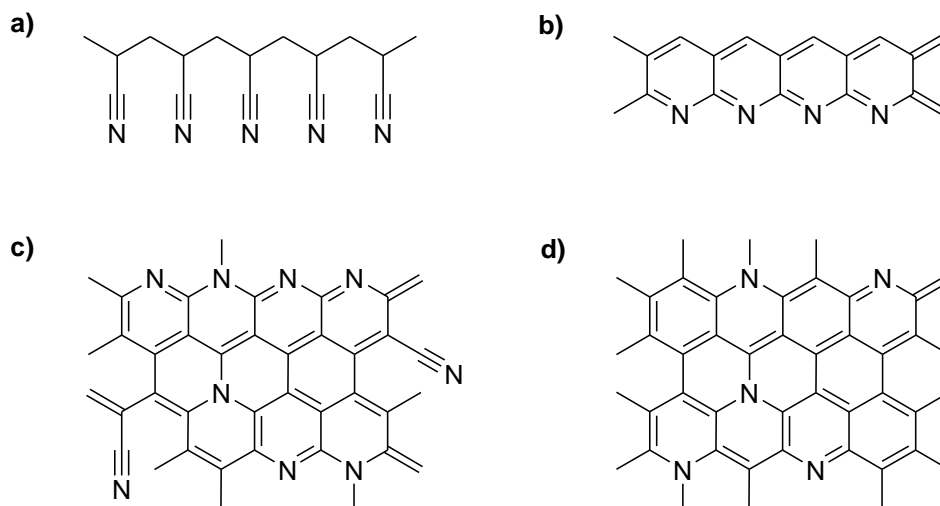


Figure 3. Schematical illustration of the thermally-induced evolution of the polymer structure [29].

Moreover even at the highest treatment temperatures the lubricating effect of the pyrolyzed polymer remains low [29] and a liquid lubricant had to be added to obtain satisfying behavior.

#### 1.4 Electrografting. A versatile method for covalent surface functionalization

In the former sections we have shown some molecule families used to functionalize surfaces in order to boundary lubricate them.

Principally they are self-assembled monolayer (SAM), it means that the lubricant molecules react spontaneously in liquid or vapour phase with the surface to give a monolayer with a certain degree of organization.

Many of them are restricted to pairs functional group/specific surface. It means that a specific functional group allows for bonding on a specific surface, i.e. phosphanates for aluminium, silanes for silicon, thiols for gold. Although this is quite schematic, because we have shown that for example thiols can functionalize different kinds of

metal surfaces, it is true that specificity exists in between the functional group and a small family of substrates.

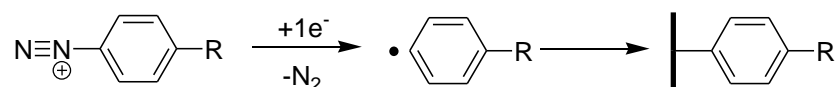
We present below two different ways to functionalize substrates by using electrochemistry. One of their great advantages resides in the capability to functionalize almost any kind of conducting or semiconducting surface.

The other great advantage resides in the nature of the bond that is created with the surface. Both of them bring to the formation of a strong covalent bond with the surface. This is of great interest for an application as boundary lubricant because it has been shown that resistance of the film strongly depend from the strength of the bond with the surface [9].

### Grafting of aromatic diazonium salts

Grafting of aromatic diazonium salts upon electrochemical reduction was first described by Pinson et al. [32] as a method for modifying the surface of carbon fibers.

The grafting mechanism is reported in Scheme 1.



*Scheme 1. Diazonium salts grafting mechanism.*

Electrochemical reduction of the aromatic diazonium salt leads to the formation of a substituted benzyl radical. The loss of the nitrogen molecule has been proved to be concerted with the electron transfer [33]. Then the reactive radical, generated in the proximity of the surface, grafts.

If electrochemical reduction is continued multi-layer can grow by a mechanism of substitution on the already grafted aromatic rings.

Since the first publication the electrochemical grafting of diazonium salts was reported a great number of articles were published on the subject. Electrochemical grafting of diazonium salts has proven to be a simple and efficient way to functionalize a wide number of conductive and semi conductive surfaces [34] as metals (gold [35], iron [36], copper [37], zinc [37], ...), silicon [38] and diamond [39, 40].

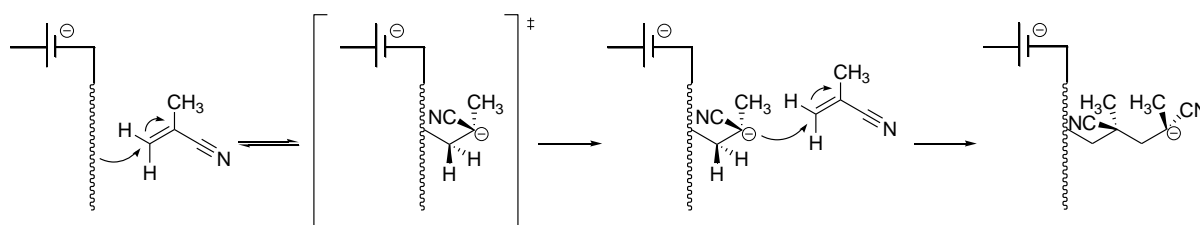
Surface covalent grafting is widely accepted by scientific community [34] and DFT calculations have shown the covalent bond to be energetically favorable [41]. Direct spectroscopic demonstration was obtained on iron [42, 43] by XPS and on carbon [44-47] by Raman spectroscopy and SIMS.

The advantages in surface functionalization by diazonium salts reside in the possibility of bonding different functional groups by changing the substituent on the aromatic ring and the possibility of easily functionalize a wide spectrum of surfaces.

### Electrografting of poly(methacrylate)s

Cathodic electrografting of polyacrylonitrile on metals has been published earlier [48] with respect to aromatic diazonium salts grafting. Application of a negative potential in anhydrous acetonitrile to a surface in an acrylonitrile solution was reported to bring to the formation of a highly adherent polyacrylonitrile film.

The mechanism (Scheme 2) involves the formation of a radical anion that grafts on the surface. Then the chemisorbed anion initiates an anionic polymerization at electrode surface [49]. Polymerization is terminated by the anion reacting with a proton in the solution or by taking a hydrogen atom to the solvent.



*Scheme 2. Polyacrylonitrile grafting mechanism*

A competitive mechanism with respect to surface polymerization involves in step number 2 the radical desorption followed by polymerization in the solution.

The same mechanism has been proven to be effective to graft vinyl monomers bringing an electron withdrawing group as poly(acrylate)s and poly(methacrylate)s which allows for a great choice in functional groups [50, 51]. Cathodic electrografting has proven to be an efficient way to functionalize many different conductive (nickel, copper [52], gold [53], platinum [54], carbon [55], ...) and semi conductive surfaces as doped silicon [53].

The degree of polymerization of the chains attached to the surface is much smaller than what expected from traditional polymerization in solution and is in the order of about 1000 monomer unities [56] which correspond to a film thickness that typically is below 20 nm [49].

Although studied since a long time spectroscopic evidence of covalent polymer grafting on metal surface as been reported more recently [57].

For some aspects cathodic electrografting of vinyl monomers is comparable with aromatic diazonium salts grafting. One of the common aspects is the use of negative potentials that make possible the grafting on oxidable metals allowing for almost any kind of conductive and semi conductive surface functionalization.

On the other hand the reduction of diazonium salts needs low negative potentials while vinyl monomer electrografting has to be conducted at highly negative potentials. Therefore while diazonium salts can be grafted from aqueous acid solutions [58] vinyl monomer electrografting has to be performed in organic solvents. Moreover the occurring of an anionic polarization requires the use of anhydrous solvents and a highly purified atmosphere (dry box) [59].

More recently processes have been published allowing for the surface grafting of vinyl polymers from aqueous solution by a diazonium salts reduction initiated polymerization [60, 61].

## 2 Methodologies

### 2.1 ANR Project NANOCONNECT

Studying the lubrication of electrical contact requires studying phenomena spreading from many different disciplines and it is situated at a true knowledge crossroad. The synthesis of lubricants requires knowledge in organic chemistry, and often in organic fluorinated chemistry, that presents differences from traditional organic chemistry. Moreover surface science knowledge is needed to functionalize the substrate, to characterize it, to study how it evolves. Tribology and electrical engineering proves also to be necessary in order to simulate the contact working in real environment and to determine if its performance is acceptable for its application.

All these expertises are hardly found in a single laboratory. This is probably one of the main reasons because the development of boundary lubricant is still limited until today although solutions in the field could be very interesting from a technological and economical point of view.

Because of all those reasons stated above, this thesis was a brick in a bigger project concerned with the development of innovating solutions for the dry lubrication of electrical contacts. The project whose acronym is NANOCONNECT was principally financed by the French governmental agency “Agence Nationale de la Recherche”.

The following laboratories were involved in the project:

- ✓ CIMA (Laboratory of Chemistry and Molecular Engineering) at Angers university that has a wide expertise in organic synthesis ;
- ✓ CSI (Chemistry of Surfaces and Interfaces Laboratory), which is a Surface Chemistry laboratory at Commissariat à l’Energie Atomique in Saclay specialized in surface functionalization;
- ✓ LGEP (Laboratory of Electrical Engineering of Paris) which has a longtime expertise in electrical contact behavior and lubrication;

in order to put together all the knowledge that was needed to study a such vast question.

The work of this thesis was mainly effectuated at CSI and partly at LGEP and is a part of the NANOCONNECT project. Of course it will not be possible to be accomplished without the contribution of all the others part of the project.

## 2.2 Molecules choice and design

As presented in the previous chapter it is known [9] that the solidity of a boundary lubricant film depends on the strength of the bond with the surface and the stability and durability of the films decreases in the following order: chemical reaction films, chemisorbed films, and physisorbed films.

Therefore the choice of the lubricant films was oriented toward the electrografted films, present in the former chapter, bonded to the surface by a covalent bond [34, 49].

Moreover electrografting is possible on a vast choice of conducting substrates that means almost any kind of metals possible to be used for building an electrical contact. This is a great advantage with respect to boundary lubricants families widely presented in the literature such as phosphanates and silanes that are used to functionalize a small set of specific metal surfaces.

We studied both the family of organic films obtained from the grafting of diazonium salts and from the reduction of vinyl monomer because they lead to the formation of different macromolecular structures (see Figure 4).

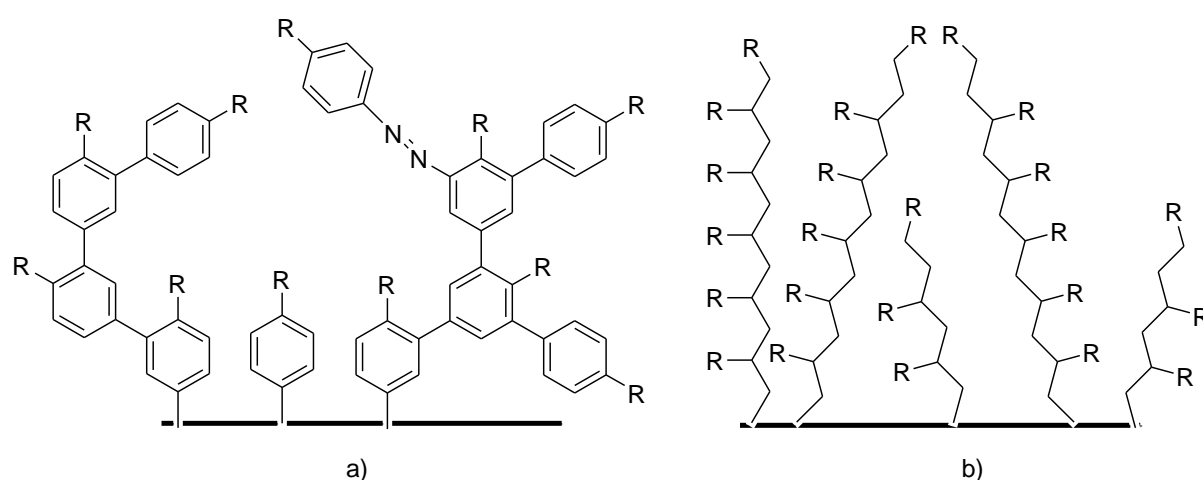


Figure 4. Structures of grafted films obtained from the reduction of a) aromatic diazonium salts, b) vinyl monomer.

The grafting of aromatic diazonium salts leads to the formation of a poly(phenylene) like structure where the main chain is formed by carbons having a  $sp^2$  hybridisation. On the contrary the electrografting of vinyl monomers leads to the formation of carbons chain having a  $sp^3$  hybridisation.

A macromolecule with a  $sp^2$  skeleton is expected to be more rigid with respect to the ones  $sp^3$  constituted. Therefore we expect the films from diazonium salts to be more rigid and hard with respect to the vinyl electrografted films in the same way that for bulk polymers a Bakelite is harder than a poly(ethylene). Harder materials are expected to behave have better tribological and wear resistance with respect to soft ones.

But at the same time a  $sp^2$  rigid material results often to have a brittle behaviour, that is of course not a good propertied to withstand wear. This is also one of the reasons that make Bakelite a material for museum objects while poly(ethylene) has become the largest commodity polymer used in the world.

It is therefore of interest for this thesis to inquire whether for dry lubrication it is better to have the rigid behaviour of poly(phenylene) like films or the plasticity of vinyl monomer electrografted films.

One of the best families of liquid lubricants used for electrical connector is that of perfluoropolyethers of high molecular weight (e. g. the commercial lubricants family Fomblin®)

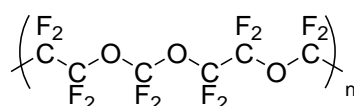


Figure 5. Structure of Fomblin®, a family of perfluoropolyethers used as lubricant.

The molecular weight and the terminal group of the macromolecular chain vary and different kinds of lubricant are sold depending on the application.

To better understand why highly fluorinated lubricants are used, let consider the definition of friction coefficient.

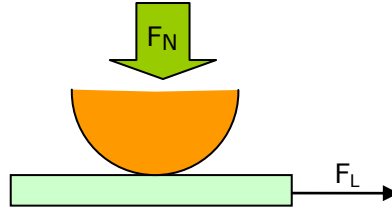


Figure 6. Ball plane contact.

When a normal force  $F_N$  is applied between a sphere and a plane, because of friction, it will be necessary to apply a lateral force  $F_L$  to keep the two in relative motion. The friction coefficient is defined as:

$$\mu = \frac{F_L}{F_N}$$

That expresses the idea that some of the energy of the system is dissipated by friction. This coefficient can be separated in two terms:

$$\mu = \mu_{def} + \mu_{ad}$$

The first one  $\mu_{def}$  expresses the loss of energy due to the deformation of materials during motion and it depends on the mechanical properties of the material such as hardness and geometrical characteristics such as surface roughness distribution.

The second one  $\mu_{ad}$  is due to adhesive forces in between the two components of the interface. Therefore reducing the surface energy of the two materials is expected to reduce this term of the friction coefficient.

Clean metals surface energies are in the order of  $10^3$  mJ m<sup>-2</sup>. Organic matter surface energies range typically from 5 to 50 mJ m<sup>-2</sup>. Therefore introducing an organic layer at the interface between two metals drastically reduces the adhesion between them and lowers the friction coefficient resulting in a lubricant effect.

Surfaces presenting fluorine atoms are the one presenting the lowest energy [8]. That is the reason because usually fluorinated lubricants bring to low friction coefficients.

Other interests in fluorinated lubricants reside in high thermal and chemical stabilities of fluorinated compounds.

For all those reasons we decided to use fluorinated monomers for the construction of electrografted films in the idea of being able to transpose the benefits of fluorinated liquid lubricant to the grafted films.

During this work the properties of fluorinated compounds was compared to that of analogue aliphatic ones to see whether the presence of fluorine produced the expected effects.

The diazonium salts reported in Figure 7 were synthesised at CIMA laboratory of Angers University. Their structures were designed as such for the reasons stated above.

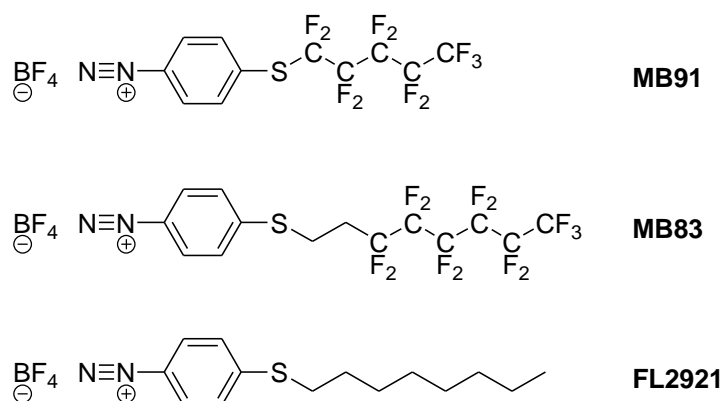


Figure 7. Structures of the molecules synthesized as building blocks for electrografting poly(phenylene) like lubricant films with the abbreviations used to designate them.

The vinyl monomers used for electrografting of poly(methacrylate)s are commercial, were purchased from Sigma Aldrich. Their structures are reported in with the abbreviation used to designate them.

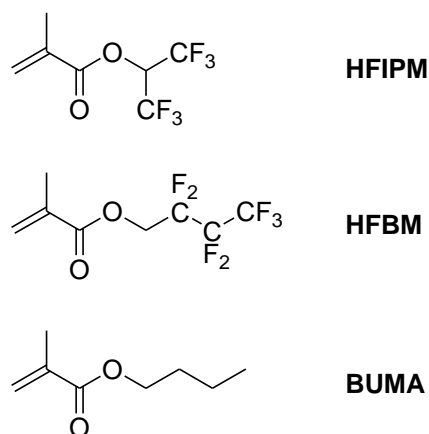


Figure 8. Structure of vinyl monomer used for electrografting with the abbreviations used to designate them.

### 2.3 The role of this thesis in the NANOCONNECT project

The work of this thesis has been conducted mainly at the Chemistry of Surfaces and Interfaces laboratory and partly at the Laboratory of Electrical Engineering of Paris.

One of the first points of the work, conducted at the Chemistry of Surfaces and Interfaces laboratory, was to study the electrochemical activity of the molecules synthesised in Angers and of the fluorinated vinyl monomers (to our knowledge no publication existed prior to this work on the subject).

Then their ability to be grafted on electrode to form homogenous and adhesive thin film has been inquired. Traditional surface science characterization techniques (XPS, ATR-IR and AFM) have been used to get insights of the structure of the films and to check whether the obtained films corresponded to what expected.

Successively the macroscopic tribological and electrical properties of the films have been studied at the Laboratory of Electrical Engineering of Paris with the aim to determine whether the films were good materials for the protection of the electrical contacts and what was the effect of the molecular structure of the film on contact electrical resistance, friction and wear.

Further studies are in progress at the Laboratory of Electrical Engineering of Paris on the film considered most interesting for potential applications. This kind of studies concerns the relationships in between macro- and micro-tribology properties, nano-mechanical properties (such as nanofretting) and conduction modes across the film.

### **2.4 Substrates**

Different kinds of substrates were used:

- ✓ “Evaporated gold” - Obtained in the laboratory by vacuum evaporation of 7 nm of chromium and then 200 nm of gold (purity 99,99%) on glass at room temperature, evaporation speed 5 nm min<sup>-1</sup>, in a Balzers BAK600 evaporator. The chamber residual pressure was 2E-7 bar. This kind of substrates have a polycrystalline surface and has a roughness  $R_a = 2,4$  nm. They were mainly used for physical-chemistry characterizations.

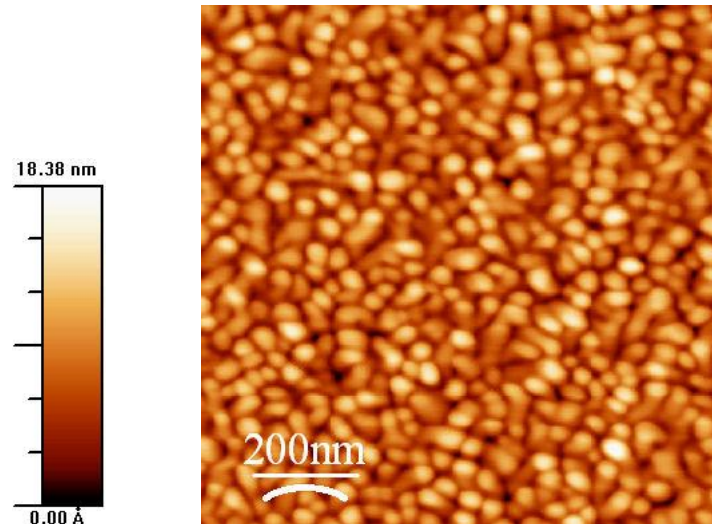


Figure 9. Tapping AFM image of “evaporated gold”.

- ✓ “epitaxied gold” – Constituted of epitaxial gold Au(111) on mica. They were used for studying the influence of crystallographic orientation on diazonium salts grafting. They are near to an “ideal” surface, they have a roughness of 0,08 nm and are constituted of pillars presenting the Au(111) face on the surface. The topography of such gold is visible on Figure 10.

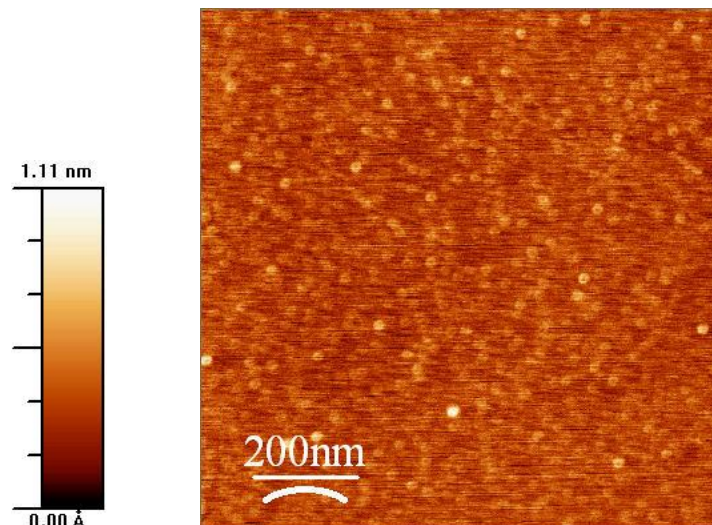


Figure 10. Tapping AFM image of epitaxial Au(111) on mica.

- ✓ “Gold coupons” – Obtained by deposition of 2 μm of nickel and then 2 μm of gold by galvanoplasty on bronze coupons. These substrates were realized by MicronOr company (Paris). They are technological substrates composed of the same material that is currently used in electrical connectors fabrication. The surface “quality” is poor, presenting a roughness  $R_a = 0,25 \mu\text{m}$ .

Because of the roughness of “gold coupons” the characterization of the thin grafted films is difficult on such substrates. This is the reason why the grafting process was studied before on the “evaporated gold” substrates, in order to follow the process by common surface techniques. At the end it was transferred on the “gold coupons” to perform the tribological test in conditions nearer to the real conditions of an electrical connector.

Optical profilometry images reported in Figure 11 report the topography of these substrates. In the top view vertical stripes can be seen, corresponding to lamination features introduced by fabrication of bronze strips which are reproduced when nickel and gold are deposited by galvanoplasty (which follow the original substrate profile. The 3D view of the “bronze coupon” illustrates substrates roughness.

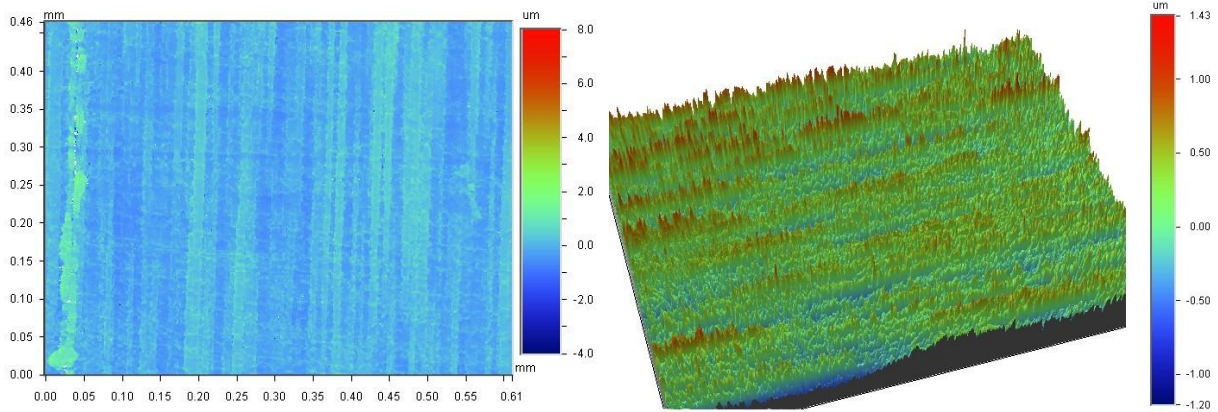


Figure 11. Optical profilometry images of “gold coupons” substrates. Left: top view, Right: 3D view.

- ✓ “Platinum electrodes” - Obtained by sputtering 1  $\mu\text{m}$  of platinum on glass. As for “evaporated gold” a thin layer of chrome (5 nm) was deposited on glass prior to platinum sputtering to enhance the adhesion and the stability of the platinum. These substrates were used for preliminary studies on the electropolymerization of PEDOT and fluorinate PEDOTs as these experiments need the application of electrical potential more positives that gold redox potential (as discussed in chapter 5).

## 2.5 General experimental details

### Electrochemical equipment

All the electrochemical experiments conducted during the work of thesis have been performed under an argon dry box (unless differently stated). The amount of residual water vapor and oxygen are kept at level of 1 ppm and 5 ppm respectively, by continuously recirculation of the dry box atmosphere through various purifiers (zeolites, active carbon and BTS).

Traditional three-electrode electrochemical cells have been used and potentials are expressed with respect to the reference electrode (Ag|AgClO<sub>4</sub> 10<sup>-2</sup> M), which potential is 0,3 V with respect to (Ag|AgCl<sub>sat</sub>).

A graphite plate, having a surface with an area much bigger than the working electrode, was used as auxiliary electrode. Unless differently stated TEAP 0,05 M was used as supporting salt.

Cyclic voltammetry was performed using an EG&G potentiostat, model 273A.

Electrochemical Impedance Spectroscopy (EIS) experiments were conducted on a Solartron 1286 potentiostat equipped with a Solartron SI 1255 HF frequency response analyzer. Measurements were made in the frequency range from 1 MHz to 0,01 Hz, with ac voltage of 10 mV amplitude superimposed on different dc potentials.

Electrochemical Quartz Crystal Microbalance experiments were carried on a SEIKO EG&G Quartz Crystal Analyzer QCA917. The electrochemical was a standard three-electrode cell, composed by a platinum counter electrode foil, a reference electrode (Ag/AgClO<sub>4</sub> 0,01 M) and the working electrode constituted by an AT 9 MHz cut crystal quartz platinum or gold coated (area 0,2 cm<sup>2</sup>). The quartz microbalance was calibrated by Cu electrolytic deposition.

### Surface spectroscopies

Infrared spectra were obtained with a Bruker Vertex 70 spectrometer (resolution 2cm<sup>-1</sup>, spectra were collected with 256 scans, MCT detector), equipped with a Pike Miracle plate for ATR or with an Hyperion Microscope and a reflection-absorption spectroscopy (IRRAS) GIR x15 objective, grazing angle 80°.

XPS spectra were recorded on a first time on Vacuum Generator ESCALAB 210, using an Al K $\alpha$  source monochromatized at 1486,6 eV. We used a hemispheric analyzer working at pass energy of 50 eV for the survey spectrum, and 20 eV when focusing on the sole core levels.

In a second time XPS experiments were conducted on KRATOS AXIS ULTRA spectrometer. A Al K $\alpha$  source monochromatized at 1486,6 eV. In this latter case the sample were mounted by interposing an insulating material in between the sample and the sample-holder. Charge was neutralized by an electron gun. Just after taking sample spectra the Au 4f<sub>7/2</sub> peak was measured on a pure gold sample determining the binding energy shift and allowing recalibration of energies.

### Contact angle measurements

Contact angle measurements were performed with water (Millipore), diiodomethane (Sigma Aldrich) and hexadecane (Sigma Aldrich). Liquid surface energy was tested before measurements by pending drop shape analysis.

The measurements were performed on a Krüss DSA 10 contact angle measuring system, equipped with Krüss drop shape analysis software.

### Tribology experiments

A configuration ball/plane was used for tribological tests. We used bronze balls, covered by galvanoplasty with a 2  $\mu$ m nickel and 2  $\mu$ m gold layers, with diameter 2,40mm. The contact with the plane, where the film was deposited, was submitted to reciprocating wear cycles of 2 mm long at a constant speed of 0,5 mm/s with a constant normal load of 1 N or 2,5 N. A well-suited tribometer

allows recording the values of the tangential force  $F_t$  during sliding, 600 values are measured during a cycle. From these values a mean value of the friction coefficient is calculated as

$$\bar{\mu} = \frac{\sum_{i=1}^{600} F_t}{F_N}$$

At the end of each traverse the contact resistance  $R_c$  is measured with a four point device while the tangential force is maintained at zero value. This ensures that the contact resistance is measured in a macroscopically no-slip condition. Plots of the friction coefficient in the rest of the thesis reports the value of the average friction coefficient  $\bar{\mu}$ . Local friction coefficient "cartographies" have also been

constructed by plotting the values  $\mu_i(N)$  where  $\mu_i = \frac{F_t}{F_N}$ ,  $x$  the position in the wear track and  $N$  the cycle number. In that case just a half cycle has been represented corresponding to the "forward" displacement (in reciprocating wear each cycle is composed of a "forward" and a "backward" displacement).

The planes were constituted of bronze coupons that were alloy CuSn4 constituted (that is currently used for the fabrication of electrical connectors) and coated by galvanoplasty by the society MicronOr - Paris.

### Atomic force microscopy

Atomic force microscopy measurements have been conducted on a Veeco Nanoscope IIIa under ambient conditions.

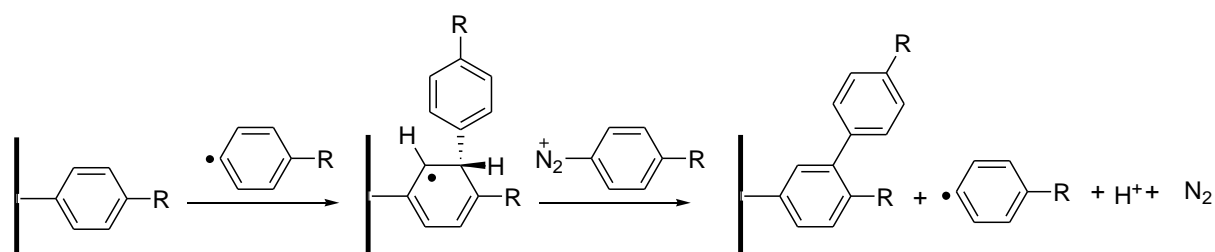
Conducting AFM measurements were effectuated with a special amplification and conversion device, called "Resiscope". A constant bias voltage (1 V) was applied between the sample and the conducting cantilever tip. The conducting (tip-lever) system was made out of n-doped monocrystalline silicon. A thin layer of conductive (p-doped) diamond is deposited on the tip.

### 3 Grafting of aromatic diazonium salts

#### 3.1 Introduction

As described in section 1.4 the electroreduction of diazonium salts is a facile method to functionalize surfaces with a covalently bonded organic thin film.

Although in specific experimental conditions a monolayer of substituted benzene attached to the surface can be obtained [38, 62] usually multilayers are grown more easily. The growth of multilayers proceeds by Aromatic Homolytic Substitution: radicals formed by the electrochemical reaction attack the phenyl rings already attached to the surface as shown in Scheme 3 [47].



*Scheme 3. Mechanism of growth of multilayers from diazonium salt reduction.*

A film with a substituted polyphenylene-like structure is obtained. Because such films are compact and insulating the electrode surface is passivated. This prevents electron transfer to other active molecule and the film growth is somewhat “self-limiting”. The maximum thickness of the film depends on the substituent group on the benzene and on the surface but typically, if no other mechanism takes part in the growth, it remains below 50 nm.

Adenier et al. [63] reported the formation of micrometric thick film in the case of the electro reduction of benzenediazonium tetrafluoroborate on iron electrodes. The authors claim that a conductive polyphenylene film is formed. The film not being current blocking does not preclude electron transfer, radicals can continue to be formed and thick films are grown.

Grafting of diazonium through electrochemistry has been first conducted in organic solutions [64, 65]. It was later shown [58] that film grafting was also possible in acidic solutions, which is of great interest from the point of view of “green” chemistry and costs reason for an industrial process application.

In this chapter we will present the works conducted on studying the grafting process of diazonium salts on gold substrates and the results of tribology experiments. All the electrochemical studies were effectuated in organic solution because fluorinated diazonium salts proved to be insoluble in acidic solutions.

## 3.2 Experimental section

### Reagents and electrochemistry

Molecules **BD**, **MB91**, **MB83**, **FL2921** were synthesized, purified and characterized at CIMA at Angers' University. Please refer to the work of M. Balog for further details.

4-nitrobenzenediazonium tetrafluoroborate (**NBD**) (purity  $\geq 97\%$ ) and acetonitrile (anhydrous grade) were purchased from Sigma-Aldrich.

TEAP (purity 95%) was purchased from Acros Organics. Prior to use it was dried under vacuum by heating at 80 °C for at least 24 h. It was used as supporting salt.

For electrochemistry experiments, unless differently stated diazonium salts were dissolved in anhydrous acetonitrile at a concentration of 5 mM and TEAP (0,05 M) was used as supporting electrolyte.

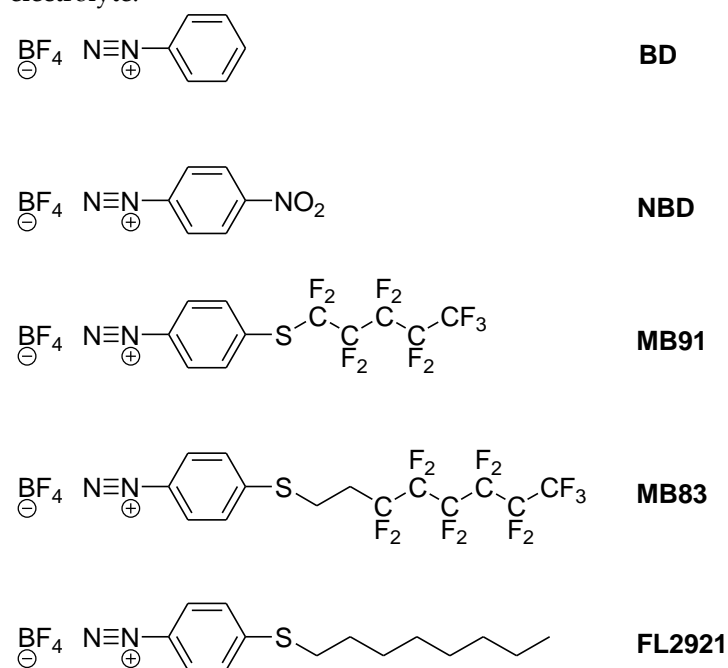


Figure 12. Diazonium salts that were grafted with the abbreviations used to designate them throughout the text.

### 3.3 Electrochemical grafting of diazonium salts on polycrystalline gold substrates

The electrochemical grafting of diazonium salts on conducting substrates [34] (such as metals [35, 42, 66] or carbon [67]) is associated with the observation of a cyclic voltammetry peak at “low” negative potential as reported by many authors.

The peak observed corresponding to the reduction of the diazonium salts on “evaporated gold” exhibits a multiple peaks shape as reported in Figure 13.

The phenomenon is especially evident for **MB91** with two narrow peaks at 0,14 V and 0,03V and a broader peak at -0,45 V. The presence of three distinct peaks on “evaporated gold” is reproducible on clean freshly evaporated substrates, although the two peaks at 0,14 V and 0,03 V are sometimes convoluted in a single one with visible shoulders at the given potentials.

For **MB83** just two broad peaks are visible at -0,24 V and -0,64 V. Peaks are broader for **FL2921** and around -0,2 V and -0,85 V. The presence of just two peaks for these molecules and the fact that they are broader let us suppose that the first peak can be the convolution of two.

The position of the peaks shows the electronegative effect of the perfluorinated chain on the reduction potential of the diazonium salts. Because the perfluorinated chain is directly bonded to sulphur atom in **MB91** this molecule starts to reduce much earlier.

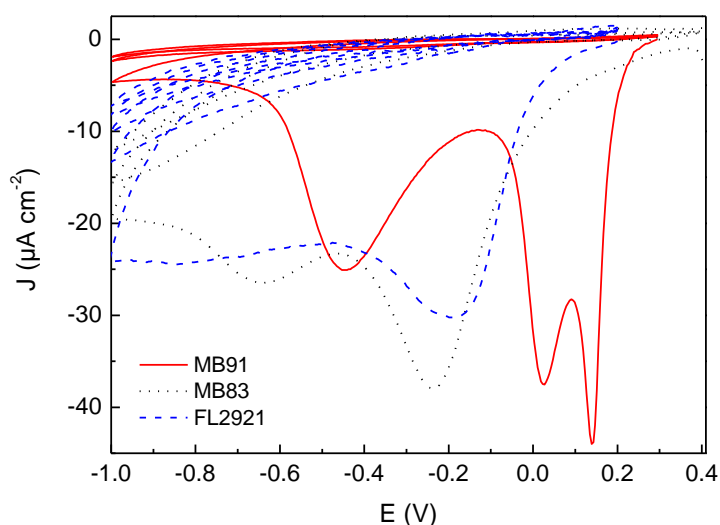


Figure 13. Cyclic voltammetry of **MB91** (solid line —), **MB83** (dashed line - - -) and **FL2921** (dotted line .....), scan rate 20 mV/s.

Although the big number of article in the literature this phenomenon of peak splitting was scarcely reported. Cyclic voltammetry showing multiple peaks were reported in a few articles by Bélanger [68] and Downard [69] groups working on carbon electrodes and others authors published diazonium cyclic voltammetry peaks

exhibiting shoulders [66] on gold. Anyway the peak splitting did not reach such intensity.

We observed that the cleanness of substrates is fundamental to observe multiple peaks. When working on contaminated surfaces, as “old” surfaces that were stocked long time in air, we observe only one broad peak corresponding to the reduction of **MB91**.

We also studied the reduction of 4-nitrobenzenediazonium tetrafluoroborate (**NBD**) a “textbook” diazonium salt frequently used in literature [34, 62, 69]). The comparison between the cyclic voltammetry of **NBD** and **MB91** is reported in Figure 14.

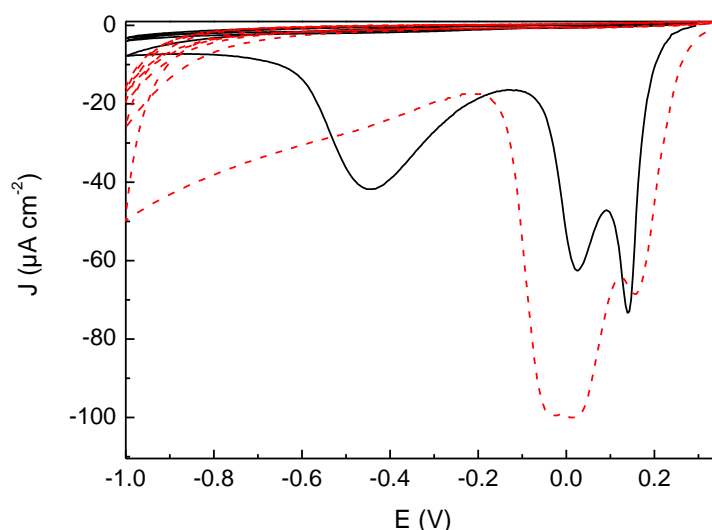


Figure 14. Comparison of the cyclic voltammetry of **NBD** and **MB91**, scan rate 20 mV/s.

For **NBD** only two peaks at 0,15 V and 0,00 V are observed, with a less pronounced splitting than for **MB91**. The third peak at lower potential is not observed in the same condition used for the other molecules.

We explain the observation of different peaks as the reduction of the diazonium salts on different crystallographic sites and the differences in the intensity of peak splitting as a different degree of passivating character for the molecules.

The vacuum-evaporation process used to prepare the substrates leads to the formation of a polycrystalline substrate presenting microcrystals with an average

size of 20 nm, as measured by AFM and SEM (see page 23). Hence, different crystallographic orientations of gold are present on the electrode surface.

The influence of crystallographic orientation on electrochemical behaviour has already been widely discussed, particularly for hydrogen adsorption as shown by Clavilier group [70-72] and other authors working on single crystal surfaces. They have shown that the positions of the peaks corresponding to hydrogen and oxygen adsorption shift depending on the crystallographic orientation of the crystal. These shifts are due to the differences in surface electron work function that are dependent on the crystallographic structure. Lipkowski et al. [73] have also shown that the molecular adsorption of pyridine is dependent on the electronic structure of the working electrode and evidenced differences in the potential dependence on Au(111), Au(100) and Au(311). Lang et al. also showed that the electropolymerization of 3-methylthiophene is influenced by the crystallographic orientation of platinum substrates. By successively increasing the applied potential films were grown in a first time just on Pt(111) then on Pt(111) and Pt(100) and finally on the whole surface [74].

The concept of work function of a surface with a particular (*hkl*) orientation, as can be measured by UHV techniques, is translated in electrochemistry by the concept of potential of zero charge. The two are correlated by the relation [75]:

$$PZC(hkl) = \Phi_{hkl} + \delta\chi^M - g^S \psi_{hkl} + \text{const}$$

where  $\delta\chi^M$  is the modification of the electron distribution at the metal surface upon contact with the solution, and  $g^S \psi_{hkl}$  is the contribution to the interfacial potential drop brought by any preferentially oriented molecules of the solvent. The constant term depends only on the properties of the reference electrode. At potential more negative than PZC the surface has a negative charge excess and at more positive potential there is a positive surface charge.

When the potential is swept from equilibrium potential to more negative ones, the molecule starts to be reduced on the crystallographic facets that exhibit the highest PZC and where electrons with the highest energy can be transferred on the LUMO level of the molecule, while no reduction occurs on the other facets. As reduction leads to a covalent grafting on the working electrode, the former facets will likely be

passivated by electrografting before the latter ones for proximity reasons. The surface passivation of the facets is responsible for the decrease in the current that leads to the formation of the first sub-peak.

When the electrode potential reaches the PZC of the second facets (with respect to the work function scale) the current increases again as electrons are again transferred to the molecule, and then decreases because of the passivation leading to the formation of the second sub-peak and so on.

According to references [75, 76] the decreasing order of the work function for gold crystal facets is  $\Phi_{(111)} > \Phi_{(100)} > \Phi_{(110)} > \Phi_{(10\bar{1}0)} > \Phi_{(10\bar{1}1)} \dots$

Therefore we tentatively associate the first peak observed upon the reduction of **MB91** with the reduction on Au(111) facets and the second one with the reduction on Au(100). The third and broader peak can be attributed to the convolution of the reduction on Au(110), Au(311), other crystal facets with high Miller indexes and faults such as grain boundaries.

To observe the effect of the different work functions present on the surface it is necessary to work on carefully clean surfaces [77]. Therefore the experiments were conducted under a purified atmosphere in an argon dry box on freshly evaporated gold.

The need to work on clean surfaces is probably a critical point explaining the lack of results of diazonium multiple peaks in literature.

The peak splitting is significantly stronger with **MB91** rather than with **NBD** or other diazonium salts already described in literature. Indeed, the presence of the “bulky” sulphur atom and the long fluorinated chain on the grafted film are expected to better prevent the electronic transfer from the electrode to the molecules in the solution. That steric hindrance and the fluorinated moiety increases the current blocking behaviour of the **MB91**-grafted film with respect to other salts reported in literature such as **NBD**, resulting in sharper voltammetric peaks.

Moreover while for **MB91** the current intensity drops to zero at the half of the first cycle, some current is still flowing for **NBD** for the cycles following the first one. The diffusion length of the corresponding radical species generated by the electroreduction should also play a role in the different behavior observed for **MB91**

and **NBD**. Indeed, the smaller nitrophenyl radical should diffuse more easily than the bulky fluorinated radical issued from **MB91**.

It is noteworthy that **MB91** and **NBD** are reduced within the same potential range, although **MB91** bears a thioether and **NBD** a nitro group directly linked to the benzene ring. However the presence of the perfluoro chain linked to sulphur strongly modifies its character from electron-donating to electron-withdrawing, which brings the reduction of salts **MB91** and **NBD** in the same potential range.

The peak splitting of the CV peak is observed with less intensity for **MB83** and **FL2921**. This shows that the passivation character is stronger for a purely perfluorinated chain. The addition of a spacer in the chain or the use of an aliphatic chain reduces the current blocking character of the film grafted on the electrode. This can also be seen by observing the current reduction after the first voltammetry cycle and the followings. While for **MB91** almost no current is observed for cycles following the first for **MB83** and **FL2921** some current is still observed at the second cycle and for the following.

The highly passivating properties of the **MB91**-grafted films were evidenced by Electrochemical Quartz Micro Balance (EQCM). Figure 15a shows the mass variation on the working electrode with respect to the potential sweeping during **MB91** electrografting. The figure clearly evidences that almost all the mass variation occurs during the first potential scan, which is consistent with a very high passivation by **MB91** grafting.

Voltammograms recorded during EQCM experiments exhibit almost no peak splitting; the commercial substrates used indeed behave similarly to “gold coupons” substrates, with only one broad peak corresponding to the reduction. That is the reason why no variation of the slope during the first scan was observed as should be expected for a voltammogram presenting multiples peaks. This observation confirms the need to work on very clean surfaces to observe the splitting of the Cyclic Voltammetry peak.

As a comparison Figure 15b gives the same mass variation during the grafting of **NBD** in the same conditions. Although a large mass variation could be observed during the first scan, the film growth clearly goes on during the following scans

which is therefore justified by a less efficient passivation with diazonium salt **NBD**, devoid of long fluorinated chains.

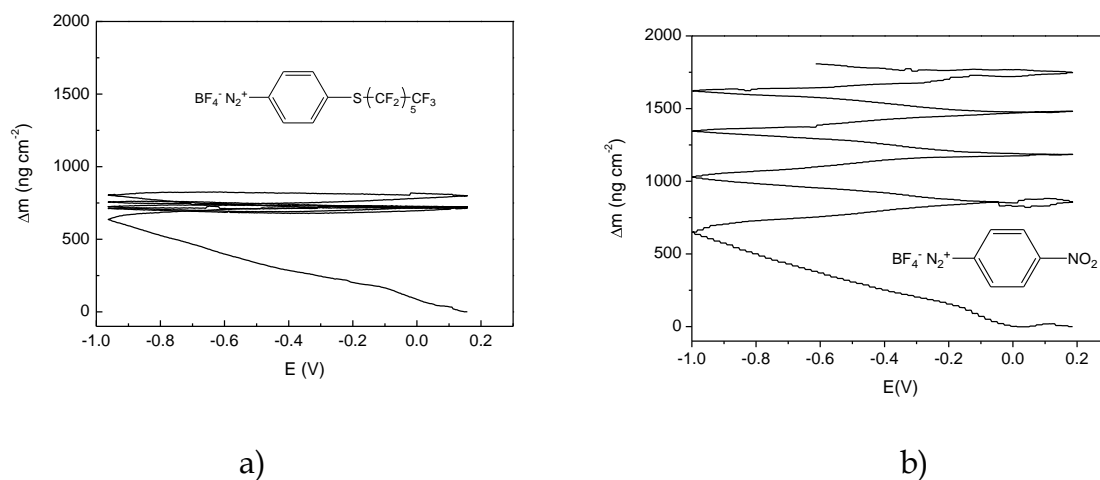


Figure 15. a) Electrografting of **MB91** followed by Electrochemical Quartz Crystal Microbalance. b) Comparison with **NBD** film grafting.

In order to corroborate our hypothesis we studied the electroreduction of **MB91** on the two other substrates with distinct crystallographic distributions: gold epitaxied on mica “epitaxied gold”, which gives a pure Au(111) surface, and “gold coupons” poorly crystallized gold deposited by galvanoplasty on bronze coupons. Results are reported in Figure 16. Au(111) substrates epitaxied on mica exhibit almost only one very narrow peak at  $0,13\text{V}$ . This result confirms the assignment of the first peak observed on “evaporated gold” to the reduction of **MB91** on Au(111) facets. Other very small peaks are also present on the recorded voltammogram on “epitaxied gold”, which may arise from electroreduction on crystallographic defects, grain boundaries and crystallographic steps which are inevitably present on a centimetre-scale gold-on-mica surface.

On the other hand, the reduction of **MB91** on “gold coupons”, substrates based on electrochemically-deposited gold on bronze coupons, exhibits only a broad peak spanning over the whole range of reduction potential of the diazonium salt. This result is a direct consequence of the crystallographic disorder exhibited by such rough surfaces.

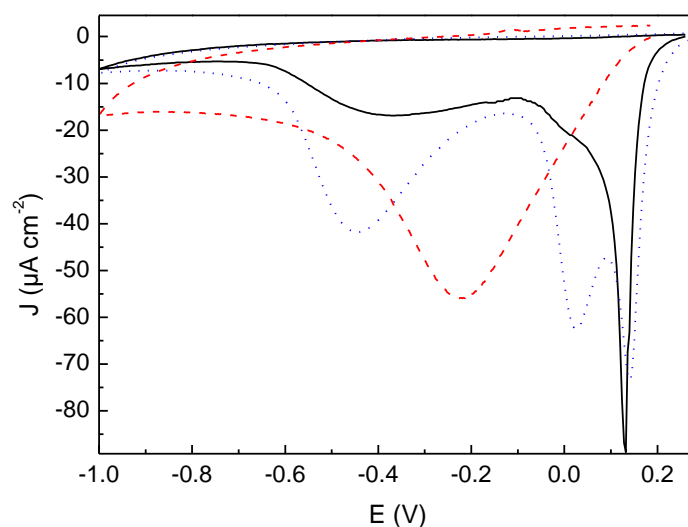


Figure 16. Cyclic voltammetry upon the reduction of **MB91** on “evaporate gold” substrates (dotted line .....), on “epitaxied gold” on mica (solid line —) and on “gold coupons” (dashed line - - -).

Results reported in Figure 17 further confirm the assignment given above. A gold working electrode prepared by vacuum-evaporation on glass (“evaporated gold”) was swept from the equilibrium potential until -0,13 V in the presence of **MB91**. As shown by the solid black line on Figure 17, two peaks at 0,13 V and 0,03 V are observed on the first sweep, which almost vanished upon the next potential sweeps. The corresponding surface is thus passivated by electrografting of **MB91** on the crystallographic facets concerned by the potential range of that first experiment. Then the same sample was cycled from the equilibrium potential to -1V. As shown by the dashed red line Figure 17, the peaks at 0,13 and 0,03 V are not visible anymore, but the broad peak at -0,45 V is now showing up, indicating that the gold facets that were not concerned by the former potential sweeps (between the equilibrium potential and -0,13 V) are still electrochemically active for the electroreduction of **MB91**.

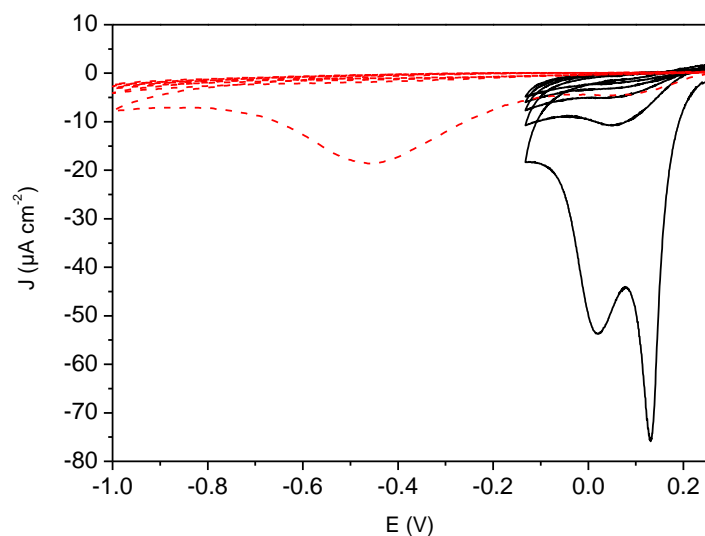


Figure 17. **MB91** cyclic voltammetry on “evaporated gold”. Solid line — and dashed line - - - represent experiments that were conducted successively on the same substrate, scan rate 20 mV/s.

It is noteworthy that the height of the peak at -0,45 V in Figure 17 is reduced with respect to what is measured when cycling directly to -1V (Figure 13), and the peak current intensity decreases from  $-42 \mu\text{A cm}^{-2}$  to  $-19 \mu\text{A cm}^{-2}$ . Hence the "electroactivity" of the corresponding facets is higher on "fresh surfaces" (i.e. surfaces that never experienced any cathodic potential) than on surfaces that were already cycled from the equilibrium potential to -0,13 V. This could be explained by a "long-distance grafting", i.e. part of the phenyl radicals electrogenerated during the first two peaks in the proximity of Au(111) and Au(100) facets diffuse and graft at other electrode regions. It was already shown [34, 38, 39] that the actual efficiency of electrografting of diazonium salts is below unity and part of the generated radicals eventually react in solution. Hence, gold facets unconcerned by the first potential sweeps in Figure 17 could be partially grafted by radicals issued from Au(111) and Au(100) facets. We can however expect the grafting to be more efficient on the Au(111) and Au(100) facets for obvious statistical reasons. This assumption is confirmed by the second scan in Figure 17 (dashed line) which shows almost no current corresponding to the peaks at 0,13 and 0,03 V.

The effective grafting of the organic film for each peak present in the voltammogram was measured by Electrochemical Impedance Spectroscopy (EIS). First, **MB91** was

electrografted on “evaporated gold” by cycling the potential from the equilibrium potential to 0,13 V, 0,03 V and finally to -1 V. Then we measured the EIS response of the corresponding grafted films in a aqueous solution of  $\text{Fe}(\text{CN})_6^{3-/4-}$  5 mM as electrochemical probe.

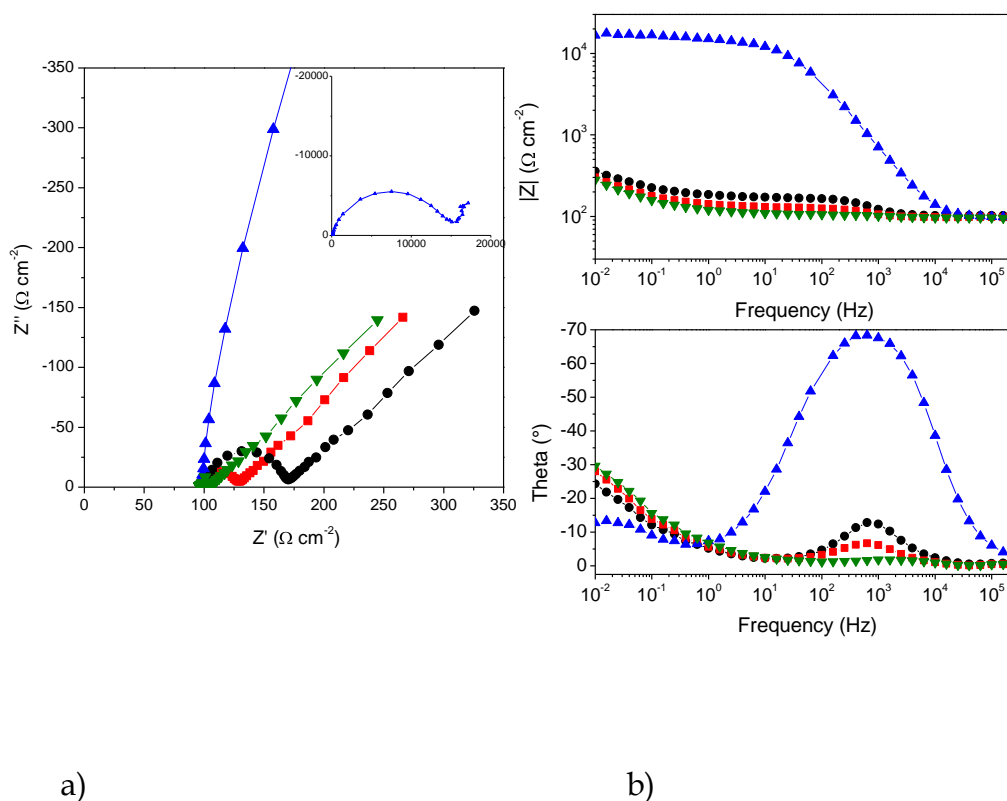


Figure 18. a) Nyquist and b) Bode Electrochemical Impedance Spectroscopy diagrams on films obtained from compound **MB91** at different vertex potentials in water with  $\text{KCl}$  0.1 M and  $\text{Fe}(\text{CN})_6^{3-/4-}$  0.005 M.  $\blacktriangledown$  uncoated substrate,  $\blacksquare$  vertex potential at 130 mV,  $\bullet$  30 mV,  $\blacktriangle$  -1V. The experiments were performed on “evaporated gold” substrates.

Results are reported in Figure 18, subsequently to the electrochemical scans that were stopped at 0,13 V and 0,03 V, the charge transfer resistance (estimated from the width of the semicircle in the Nyquist plot) increased from  $9 \Omega \text{ cm}^{-2}$  for uncoated gold to  $32 \Omega \text{ cm}^{-2}$  and  $74 \Omega \text{ cm}^{-2}$  respectively. The increase in the charge transfer resistance is the direct consequence of the partial passivation of gold electrode that reduces the ability of the redox probe to access the surface of the working electrode. The charge transfer resistance remains however very low because the iron complexes can still freely access to the ungrafted part of the electrode. At this stage, the electrode behaves as a partially covered gold surface which total impedance is dominated by the uncoated gold areas. When the potential is swept to -1 V the whole surface is passivated and

the charge transfer resistance increases to  $15\,500\ \Omega\ \text{cm}^{-2}$  (inset in Figure 18a), as expected for a totally passivated gold electrode.

The explanation of our experimental results given above indeed applies to the peak splitting observed on gold substrates, but also on any polycrystalline metal surface showing strong anisotropy in work functions values with crystallographic orientation. We effectively observed voltammetry peak splitting with compound **MB91** on polycrystalline sputtered platinum electrodes. Similar results could be expected on clean polycrystalline silver surfaces [78].

Except for HOPG, carbonaceous surfaces used as electrodes in electrochemistry are normally constituted of a mosaic of hexagonal and trigonal graphitic crystallites, amorphous matrix, diamond-like domains interconnected by different kind of carbons hybridizations. The state of the surface is strongly dependent on the process used to produce it and may be poorly reproducible [79].

The patchy structure of carbonaceous surface, with the presence of domains having different crystallization degrees and structure causes a spatial inhomogeneity in work function distribution. Kelvin probe force microscopy (an atomic force microscopy technique sensitive to local work function) was performed on carbonaceous materials [80] and actually showed a patchy structure in work function values.

Therefore we suggest that also on carbonaceous materials the peak splitting is caused by successive reduction on sites having a different crystalline surface structure. The complicated topography of carbon surfaces makes it not possible to establish a direct correspondence between work function values and crystallographic sites as for well defined gold surfaces. The lack in carbon surfaces reproducibility might be responsible for the lack of reproducibility reported on peak splitting on glassy carbon [68].

### **Electrochemical grafting of benzenediazonium tetrafluoroborate (BD)**

The grafting of benzene diazonium tetrafluoroborate has already been reported by Adenier and al. [63]. They claimed a different behaviour for this kind of molecule with respect to other “classical” diazonium salts such as **NBD**.

They reported the film obtained on iron electrodes being much less passivating than **NBD**. Current continued flowing in the circuit after the first cycle and the peak corresponding to the reduction of the diazonium salt was observed until the 12<sup>th</sup> cycle with intensity comparable with the peak recorded at the first cycle.

This phenomenon was explained by the semi conductive character of the films that was assumed to allow electron to be transferred from the metal/film interface to the film/interface solution and therefore allowing the reduction of the diazonium molecules in the solution.

They reported the formation of more than 2  $\mu\text{m}$  thick films on iron, copper and zinc electrodes.

We studied the reduction of **BD** on “evaporated gold” electrodes. A cyclic voltammetry is reported in Figure 19. On gold electrodes we found that the molecule behaves as “classic” diazonium salt.

A peak it is observed in correspondence of the reduction of **BD** at -0,35 V during the first cycle. A shoulder is visible at -0,05 V that we assume having the same origin of the sub peaks discussed above.

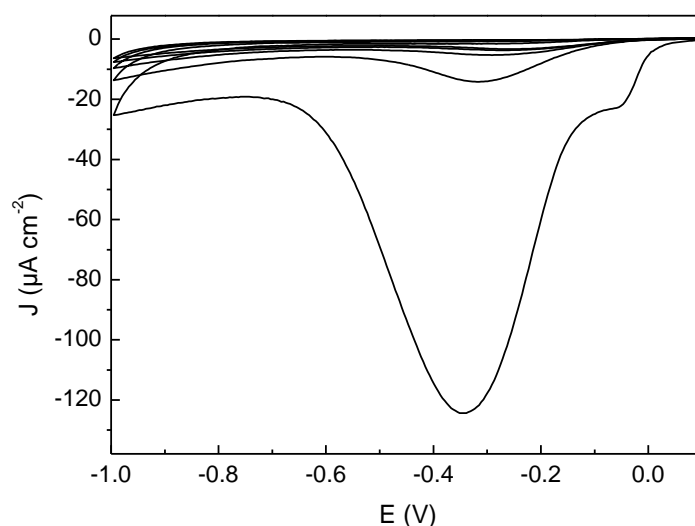


*Figure 19. Cyclic voltammetry of **BD** reduction on “evaporated gold” electrodes. Scan rate 20 mV/s*

During the second cycle the intensity of the peak is greatly reduced and almost no current is observed to flow in the cell after the third cycle. Therefore in our

conditions **BD**-grafted films behave as insulating films that prevent further electron transfer from the metal electrode to the solution.

The modified electrodes were rinsed and dried. The film is not visible to naked eye but characteristic bands were observed by ATR-IR. Therefore thickness has to be less than 10 nm.

Other experimental parameters for electrochemistry were used, as changing sweeping speed, vertex potential, performed chronoamperometry but it was impossible to grow thicker films. The same behaviour was observed on ITO and platinum electrodes.

### 3.4 Physical chemistry characterization of the films

#### Infrared spectroscopy

The aromatic diazonium salt present a characteristic peak at about  $2250\text{ cm}^{-1}$  corresponding to the  $\text{N}\equiv\text{N}^+$  stretching. This can be easily observed on Figure 20 (dashed line) for **FL2921**.

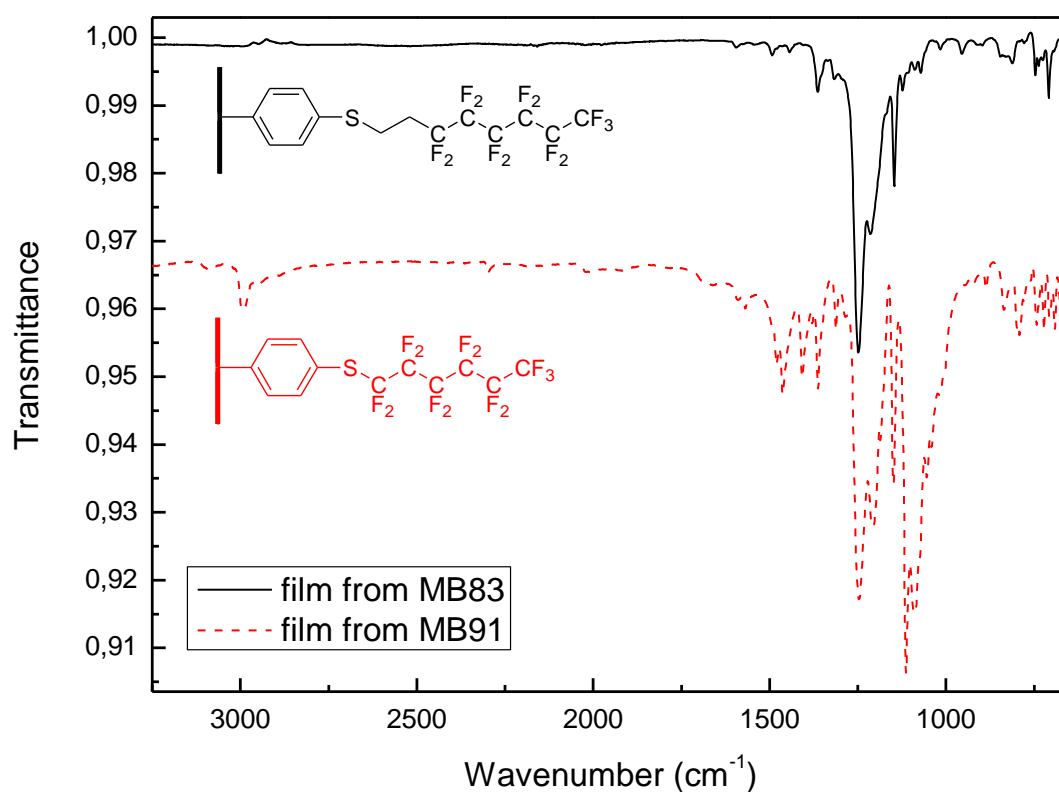


Figure 20. ATR-IR spectra of **FL2921** molecule (dashed line) and the film deposited on gold after electrochemical reduction (solid line)

This peak is not present anymore in the film spectrum because  $-N\equiv N^+$  is electrochemically reduced to a substituted aryl radical concerted with the loss a nitrogen molecule [33]. Then the phenyl radical bond on the metal surface or to another phenyl ring already present on the surface (by substitution of a hydrogen atom on the ring). Bands between 3100 and 2800  $\text{cm}^{-1}$  correspond to the stretching of aliphatic and aromatic  $-C-H$ . In the film spectrum, the intensity of the aromatic  $-C-H$  peak stretching at 3100  $\text{cm}^{-1}$  is greatly reduced with the formation of weak and broad peaks at lower wavenumbers. This is probably due to the substitutions on the aromatic ring (growth of multilayers).

The bands between 1610 and 1420  $\text{cm}^{-1}$ , corresponding to the deformation of benzene rings, are also modified by the bonding on the surface and the substitutions.

The out-of-plane  $-C-H$  aromatic deformations between 900 and 675  $\text{cm}^{-1}$  are useful to determine the type of aromatic substitution. The film spectrum shows a peak between 860 and 800  $\text{cm}^{-1}$  that can correspond to a para-disubstituted benzene (i.e. the formation of a monolayer grafted on the surface) or to a 1,2,3,4-tetrasubstituted benzene [81] (corresponding to a multi-layer). Both probably coexist on the surface. However the films are too thin to get the signal of the bands due to the combinations and overtones of  $C-H$  out-of-plane deformation vibrations in the 2000-1660  $\text{cm}^{-1}$  region. So we can not confirm definitively the substitutions on phenyl ring.

Comparable results are found for **MB91** and **MB83** (see Figure 21). For polyfluorinated compounds very strong bands are expected between 1360 and 1090  $\text{cm}^{-1}$  due to coupling of  $C-F$  and  $C-C$  vibrations. This is effectively found for the film grafted from the two molecules. In this case it is even more difficult to assess for the way in which the benzene ring is substituted during the growth of multilayer because  $C-F$  vibrations also give bands in the region 830-520  $\text{cm}^{-1}$  which therefore superpose with the out-of plane  $-C-H$  aromatic deformations.

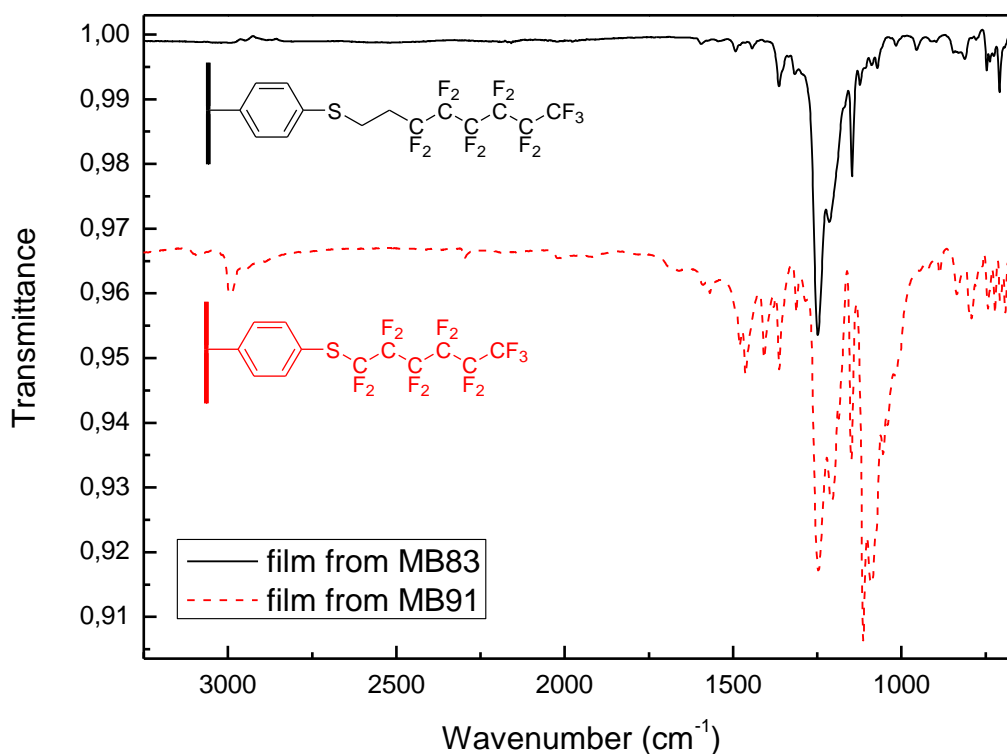


Figure 21. Infrared spectra of film grafted upon reduction of **MB91** (red dashed line) and **MB83** (solid black line)

The ATR-IR spectrum of the gold surface modified by the electrochemical reduction of **BD** is reported in Figure 22. It reports the same absorption of the spectrum that was published by Adenier et al. [63]. The greatest difference consists in the intensity of the absorptions. While they could obtain bands with an intensity of more than 20% in our case the most intense band is below 1%. This is of course due to the difference in the thickness obtained. While the reduction of the molecule on iron, copper and zinc lead to micrometric thick films, on gold we obtain films that are certainly below 10 nm (films are not visible at naked eye).

Anyway the spectrum presents all the characteristics of a disordered phenylene-like film. Band in between 3150-3020 cm<sup>-1</sup> corresponds to the symmetric and asymmetric stretching of aromatic -C-H bond.

Aromatic -C=C- vibrations are visible at 1600, 1500 and 1450 cm<sup>-1</sup>. In the region of the aromatic out-of-plane -C-H vibrations and ring out-of-plane vibrations can be seen four peaks: two of weak intensity at 915 and 845 cm and two strong at 762 and 703 cm<sup>-1</sup>. In the case of pure 1-4 disubstitution just one peak in between 860-800 cm<sup>-1</sup> should be expected. This confirms that the reduction of **BD** leads to a polyphenylene-

like structure but disordered and not linear as for a good semiconductive poly(phenylene).

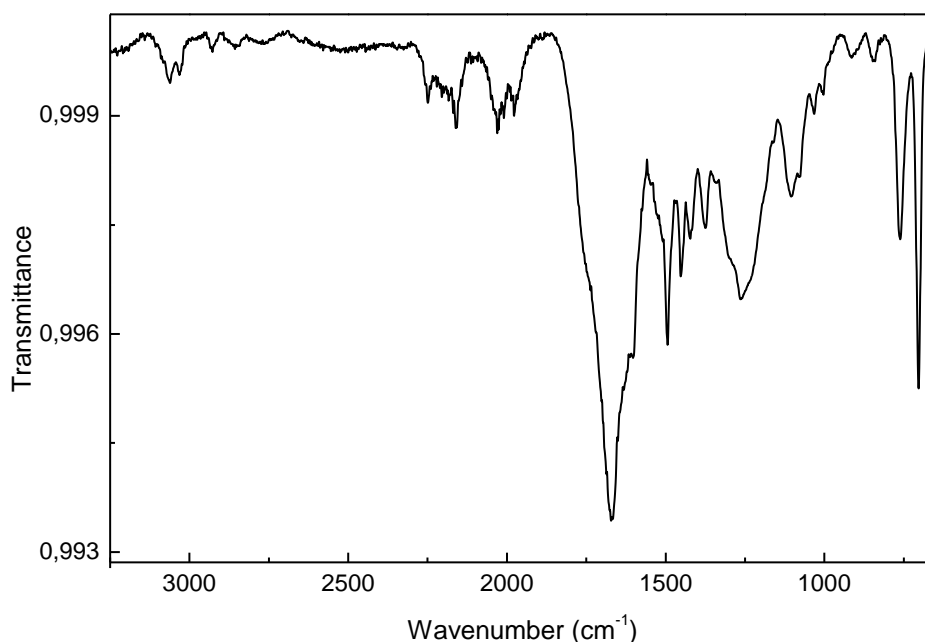


Figure 22. Infrared spectrum of film grafted upon reduction of **BD**.

The absorptions in the region  $900\text{-}675\text{ cm}^{-1}$  indicate the presence of different types of aromatic substitutions such as monosubstitution, 1-3, 1-4-disubstitution, and trisubstitutions. On the basis of IR absorption 1,2,3,4-tetrasubstitution could be possible but seems likely to be excluded on a steric basis.

The absence of a linear order in the case of conjugated polymers greatly reduces the conjugation length of the polymer and the delocalization of the charges. Therefore it seems unlikely that the only reason that allowed Adenier et al. [63] to obtain thick film on iron, zinc and copper was the increased conductivity due to the non substitution of the phenylene-like structure that seems to be disordered as in all other films obtained by diazonium salts reduction.

The nature of substrates seems to play an important role. They reported that film obtained on other substrates such as TiN or TiN/Ta were much thinner.

Moreover on copper, zinc and iron grafting of diazonium salts was reported to be spontaneous [82-84] because the reduction potential of these metals is sufficiently low to oxidize spontaneously diazonium salts in solution.

The interface of the metal with the solution must be not perfectly stable; the diazonium salts are oxidizing and can attack the surface when the electrical potential is bring to the most positive values. Therefore a great number of aryl radical is generated not only by the electrical reduction but also by the spontaneous reduction due to the substrate metal. The film builds up on a surface that is being destroyed.

Probably the small benzenediazonium cation, that is smaller than other "classical" diazonium cations, can more easily diffuse until the metal surface. Moreover the absence of lateral group probably reduces the passivating nature of the films also because of steric reasons. All this considerations, together with the increased conductivity because of the absence of electron attractive substituent group on the polyphenylene-like structure, made possible to grow micrometric thick films on metals as iron, copper and zinc.

The substrates that we used (mainly gold, but also platinum and ITO) are much more inert. In that case no spontaneous reduction of diazonium salts can be obtained due to the substrate metal oxidation and the conductivity of the films is not yet sufficient to allow for efficient electron transfer to the film/solution interface. Therefore on such inert substrates we obtain much thinner films.

### **X-ray photoelectron spectroscopy**

Films deposited were further characterized by XPS to confirm the IR bands and to check that no other reactions occur to the radical obtained by electrochemical reduction (such as cleaving).

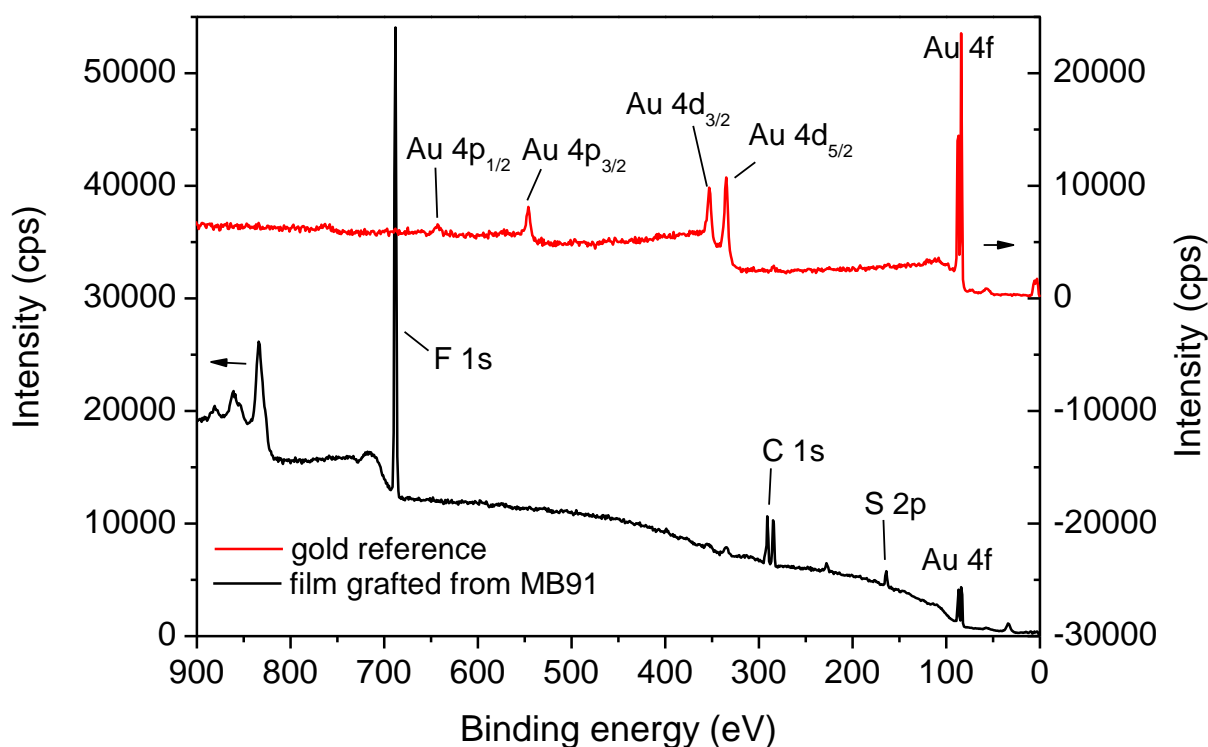


Figure 23. Survey XPS spectrum (lower, black line) of a film grafted from **MB91** and the reference spectrum of gold substrate (upper, red line).

The survey spectrum of a film grafted from **MB91** is reported in Figure 23. Film thickness is expected below 20 nm because Au 4f peaks are still visible. Fluorine 1s, Carbon 1s and Sulphur 2p peaks are visible at about 686, 285 and 164 eV.

More information about the diazonium salt grafting is obtained from core spectra reported in Figure 24.

C 1s peak shows clearly at least three different components. The one at highest energy 293,3 eV is assigned to the carbon  $-\text{CF}_3$ . A second component is visible at 291,0 eV and was assigned to  $-\text{CF}_2-$ . At lower energy there is a wider peak at 284,7 eV. Because of its width we tentatively decomposed it into two components at 285,6 and 284,6 eV, the one at the highest energy being assigned to the carbon directly bonded to sulfur atom and the other to the others aromatic carbon atoms.

F 1s shows just a large peak at 688 eV which probably is the sum of more different components. S 2p was decomposed to account for S 2p<sub>1/2</sub> and S 2p<sub>3/2</sub> components.

More interestingly an asymmetric peak at 399,1 can be observed in correspondence to N 1s level.

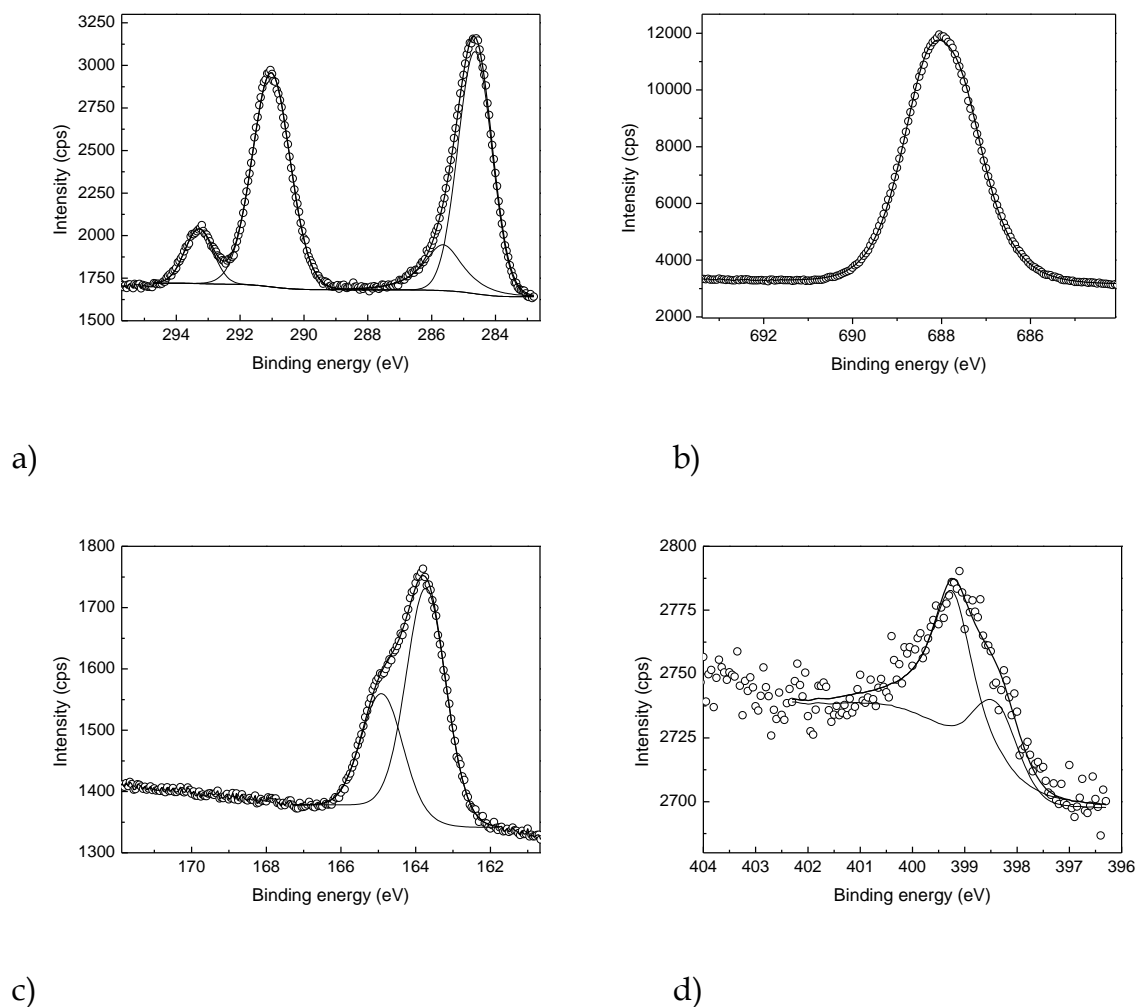


Figure 24. XPS core spectra of film grafted from **MB91** a) C 1s, b) F 1s, c) S 2p, d) N 1s

The presence of a peak at that energy indicate the presence of azo  $-N=N-$  bonds within the film.

The reason of the presence of diazo bonds has been widely studied by Pinson [33, 85]. The diazenyl radical has been shown to be highly instable, and the loss of the nitrogen molecule concerted with the reduction of the diazonium salt [33]. Therefore no diazo  $-N=N-$  bond should be expected in the film.

The presence of diazo group (observed experimentally) was explained by Pinson by the growth of multiple layers, by a mechanism were a radical present on the already grafted film attack a diazonium molecule in the solution [85]. The question is still controversial and in Belanger group experimental data have been advanced showing the presence of the diazo bond between the surface and the phenyl ring [86].

Integration of core peaks area and normalization by Scofield factor allows determining the stoichiometry of the deposited film. Deviation in atomic ratio between the stoichiometry determined from the formula and measured by XPS are less than 5%, which prove that diazonium salts graft as previewed and that no modification to the lateral chain occurs during the electrochemical reduction. These results are reported in Table 1.

	C <sub>calc</sub>	C <sub>exp</sub>	N <sub>calc</sub>	N <sub>exp</sub>	S <sub>calc</sub>	S <sub>exp</sub>	O <sub>calc</sub>	O <sub>exp</sub>	F <sub>calc</sub>	F <sub>exp</sub>
<b>FL2921</b>	93%	90%	0%	1%	7%	7%	0%	2%		
<b>MB83</b>	46%	52%	0%	1%	4%	4%	0%	2%	46%	41%
<b>MB91</b>	46%	50%	0%	1%	4%	5%	0%	1%	50%	44%

*Table 1. Atomic percent expected from molecular formula (calc subscript) compared with ratios measured by XPS (exp subscript).*

Because of environmental pollution an excess in oxygen atoms content is found. Correspondingly the amount of carbon is higher than what will be expected simply from the molecular structure of the films.

Some nitrogen is always found in the films around 1%. This corresponds to about 1 phenyl which grafts with a “azo bridge” for 10 molecules grafted.

### 3.5 Surface energy measurements

Surface energies were calculated from angles measurements by using the Owens-Wendt equation[87]:

$$\frac{\gamma_L}{\sqrt{\gamma_L^D}} (1 + \cos \theta) = 2\sqrt{\gamma_S^D} + 2\sqrt{\gamma_S^P} \sqrt{\frac{\gamma_L^P}{\gamma_L^D}}$$

$\gamma_L$ ,  $\gamma_L^D$ ,  $\gamma_L^P$  refer to liquid tension and its dispersive and polar components,  $\gamma_S$ ,  $\gamma_S^D$ ,  $\gamma_S^P$  refer to solid surface energy and its dispersive and polar components and  $\theta$  is the contact angle between the liquid sessile drop and the solid surface. Therefore measuring the contact angle with different liquids which parameters are known allows for determining the solid surface energy components by a linear fitting procedure. As liquid we used water ( $\gamma_L^D = 21.8 \text{ mN m}^{-1}$ ,  $\gamma_L^P = 51 \text{ mN m}^{-1}$ )[88]; diiodomethane( $\gamma_L^D = 50.8 \text{ mN m}^{-1}$ ,  $\gamma_L^P = 0 \text{ mN m}^{-1}$ )[88] and n-hexadecane( $\gamma_L^D = 27.47$

$\text{mN m}^{-1}$ ,  $\gamma_L^P = 0 \text{ mN m}^{-1}$ )[89]. Table 2 reports the weighed average of the contact angle and the surface energies calculated from different samples.

	$\theta_{\text{H}_2\text{O}}$ (°)	$\theta_{\text{CH}_2\text{I}_2}$ (°)	$\theta_{\text{C}_{16}\text{H}_{36}}$ (°)	$\gamma_S^P$ (mN/m)	$\gamma_S^D$ (mN/m)	$\gamma_S$ (mN/m)
<b>MB91</b>	$114.7 \pm 0.8$	$90.0 \pm 0.5$	$59.6 \pm 0.7$	$0.5 \pm 0.1$	$12.7 \pm 0.2$	$13.2 \pm 0.2$
<b>MB83</b>	$105.3 \pm 0.6$	$89.8 \pm 0.6$	$59.4 \pm 0.4$	$2.4 \pm 0.1$	$14.5 \pm 0.2$	$15.7 \pm 0.2$
<b>FL2921</b>	$86.14 \pm 1$	$34.7 \pm 0.4$		$1.4 \pm 0.2$	$42.2 \pm 0.2$	$43.6 \pm 0.3$

Table 2. Contact angles on films grafted on gold from **MB91**, **MB83** and **FL2921**. Surface energies were calculated by fitting experimental data with Owens-Wendt model. Films were electrografted on “evaporated gold” substrates.

On unmodified film the effect of terminal fluorinated perfluoro chain with respect to aliphatic chain is evident. Films from **MB91** and **MB83** present a surface energy that is much lower than films from compound **FL2921**. A solid presenting  $-\text{CF}_2-$  groups on the surface (as for Teflon) is expected to have energy of about  $18 \text{ mN m}^{-1}$  (that is what is effectively found for Teflon) [8]. The fact that the energy found is lower suggests that the perfluoro chains are oriented vertically and that  $-\text{CF}_3$  are exposed on the surface.

Vertical alignment of perfluoro chain was already claimed for others films obtained from the reduction of fluorinated diazonium salts [42]. But in the case of a surface presenting just  $-\text{CF}_3$  group a surface energy of about  $6 \text{ mN m}^{-1}$  is expected [8]. The surface energy calculated for our samples remains significantly higher than such a value. This suggests that the vertical orientation is just partially obtained. Moreover it can be seen that values measured for films from compound **MB83** have higher values than the ones from **MB91** and this could not be explained if the chains were completely vertically aligned. This hints for some remaining disorder and the surface energy on the whole chain is determined not just from the final groups but also from the whole chain.

### 3.6 AMF approach/withdraw curves

AFM approach/withdraw curves (D-R curves) were done to probe the microscopic mechanical properties of the films [90]. Films were electrografted on evaporated gold substrates to reduce the effect of the roughness. In such curves the tip of the

microscope is pressed against the sample to penetrate in the film. The deflection of the tip ( $D$ , which is proportional to the normal force in between the tip and the sample) is measured as a function of the excursion on the z-axis ( $R$ ). Values measured during the approach are plotted in grey and values measured during the withdrawal in black.

### FL2921 diazonium salt modified gold sample

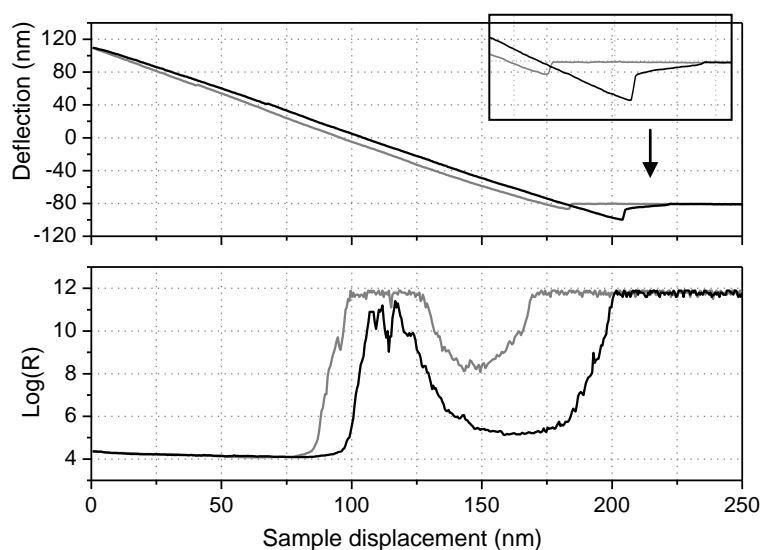


Figure 25.  $D$ - $R$  curves acquired with a conducting tip on **FL2921** diazonium salt modified gold electrode (inset : deflection around the jump-to-contact).

Figure 25 refers to an experiment performed on **FL2921** diazonium salt modified gold electrode. For the first cycle, during the approach phase, after the mechanical contact between the tip and the film surface called jump-to-contact, the sample must be displaced further (about 12 nm in the figure) to measure an electrical current (the detection threshold is  $10^{-12}$  A). After the jump-to-contact, the repulsive forces immediately dominate as for a hard wall contact whereas the tip is not yet in contact with the gold surface. While the sample displacement continues, the resistance value goes through a minimum ( $R = 10^8 \Omega$ ) before it increases again, reaches the saturation level ( $R > 10^{12} \Omega$ ) for 25 nm and finally rapidly drops down to a low and stable level ( $R \sim 10^4 \Omega$ ) corresponding to the true tip/gold surface electrical contact. The resistance minimum at  $10^8 \Omega$  indicates that the tip did not penetrate completely through the film, but was close enough to the gold surface to allow a tunnelling

current. The sudden increase of  $R$  can be explained by a very high value of the film compactness and the granular morphology of the gold substrate as explained by Guo et al [91]. At a given penetration depth, the tip/surface contact equilibrium is unstable and to compensate further displacement the tip slides to a more stable contact spot where the coating is thicker. In Figure 25, the value of displacement necessary to go from the mechanical contact of the tip with the top of the diazonium film to the mechanical contact with the gold coating is referred to as the mechanical/electrical shift ( $\Delta_{m/e}$ ). For this diazonium film,  $\Delta_{m/e} \sim 100$  nm, this corresponds to  $\sim 200$  nN. This value is large bearing in mind that for bare gold the current is detected at the jump to contact (thus  $\Delta_{m/e} = 0$  nm); it shows that the film is very compact. It is also shown to be compact by the observation that the repulsive forces dominate just after the jump-to-contact. After the maximum applied load ( $\sim 380$  nN), the sample displacement is reversed. During the withdrawal phase, the electrical measurements show similar trend to the one observed during the approach phase, with lower resistance values during the unstable phase. The current is below the detection threshold a few nanometers before the jump off contact, while the tip and the surface are still in mechanical contact. This leads us to think that some grafted molecules in the tip/sample interface are compressed. This shows that the film is not damaged by the indentation and recovers its initial shape.

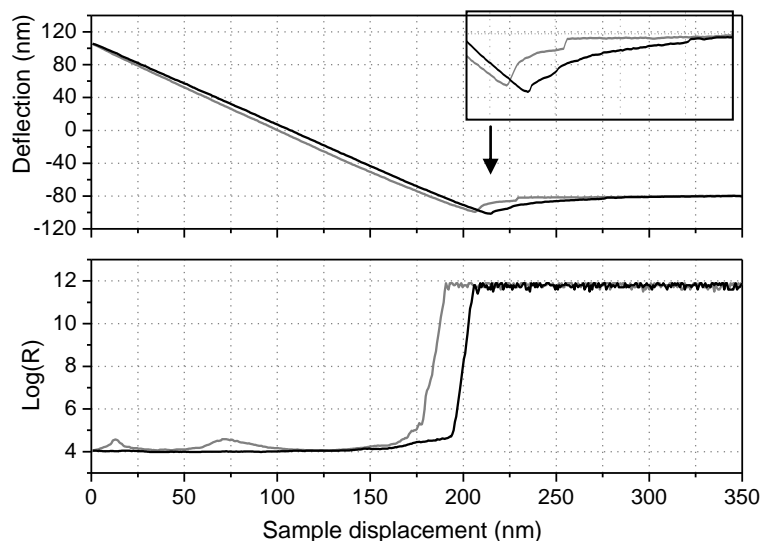
**MB83 diazonium salt modified gold sample**

Figure 26. D-R curves acquired with a conducting tip on **MB83** fluorinated diazonium salt modified gold electrode (inset : deflection around the jump-to-contact).

The **MB83** fluorinated diazonium salt modified gold electrode presented a very different behaviour during the D-R curve acquisition. For the approach phase, just after the jump-to contact, a phase of slow increase of the attractive force takes place and lasts while the sample is displaced for about 23 nm. After this phase the repulsive forces dominate and the electrical current is detected after a further displacement (about 15 nm in the figure), showing that the cohesive energy of the molecules at this depth is difficult to overcome. Then the resistance value drops down quickly and steadily to the value corresponding to the tip/gold electrical contact ( $\sim 10^4 \Omega$ ) indicating that the tip has gone through the diazonium film. The mechanical/electrical shift  $\Delta_{m/e}$  is about 70 nm. During the withdrawal phase, the current stops being detected 8 nm before the jump-off contact. This shows that the deep part of the film can recover back to its initial conformation; a very small jump off contact is observed followed by a huge slide off contact ( $\sim 80$  nm). This phase corresponds to the stretch and breaking of the adhesion meniscus. This behaviour is drastically different compared to that of the first sample displaying a significant jump off contact and a much smaller slide off contact phase ( $\sim 15$  nm). To sum up, the slow increase of the attractive force shows that the top of the film is not very compact

(and not very well organised). The mechanical/electrical shift shows that the deeper part of the film is more compact.

Summing up the results on approach/withdraw curves it is found that while the films obtained from **FL2921** are compact the ones obtained from **MB83** present an external part that is soft (easily penetrated by AFM tip) and an inner part that is compact.

We can tentatively interpret the results by the different organization of fluorinated and hydrogenated substituent chains. It was reported [92] that hydrogenated thiols SAM are more compact than their fluorinated counterparts. A similar behavior could be expected for the substituent chains of the poly(phenylene)-like film if a nearly monolayer is grafted.

The outer part of the film will be mainly composed by the fluorinated or aliphatic chains and the inner part by the phenyl rings. Fluorinated chains being less compact are more easily penetrated by AFM tip than the hydrogenated ones. When the tip reaches the inner part of the film, mainly composed of the phenyl rings, a hard film is found in the two cases.

### **3.7 Tribological tests**

#### **Effect of the fluorination**

The effect of using as substituent on the phenyl ring an aliphatic chain or a fluorinated/perfluorinated chain on the tribological properties was tested by comparing the tribology results between **FL2921** grafted films and **MB83/MB91** grafted films. A normal force of 1 N was applied, which is the force currently used in designing industrial gold coated low-level connector.

Differences between the molecules are small although significant.

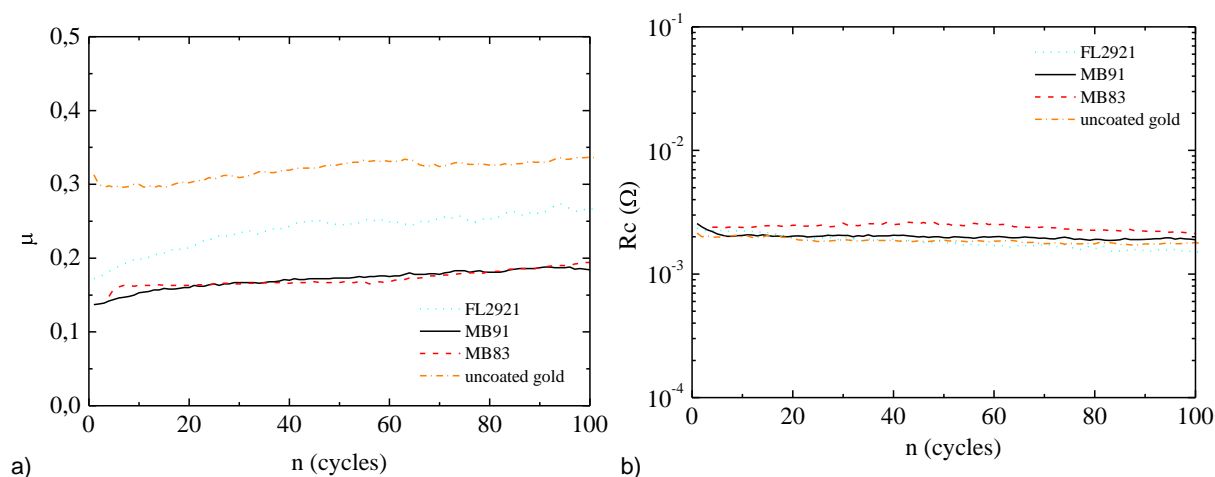


Figure 27. a) Evolution of the average friction coefficient with the number of wear cycle for films grafted from **FL2921**, **MB91** et **MB83**. b) Electrical contact resistances measured at one track end at the end of each wear cycle. Applied normal force 1 N.

Figure 27a reports the evolution of the average friction coefficient on 100 cycles at an applied normal force of 1 N for films grafted from the three molecules.

Films from **MB91** and **MB83** show almost the same behaviour. This shows that the effect of the aliphatic spacer is not noticeable from the tribological point of view. The surface energy of the two films were calculated to be  $13,2 \text{ mN m}^{-1}$  for **MB91**-grafted films and  $15,7 \text{ mN m}^{-1}$  for **MB83**-grafted films. The difference in between surface energies ( $2,5 \text{ mN m}^{-1}$ ) is therefore too low for inducing effects on the adhesion term of the friction.

The difference is sensible in between the aliphatic films **FL2921**-grafted films and the fluorinated films. On 100 cycles at 1 N the friction coefficient is around 0,15-0,175 for fluorinated films but starts from 0,175 for the hydrogenated film but increases rapidly until 0,25.

From the point of view of the electrical contact resistance all the films behave very well. Industrial specifications for gold coated low level connectors fix as limits 10 m $\Omega$  to contact resistance.

During the experiments the contact resistance is around 2-3 m $\Omega$  (Figure 27b) and remains constant. This means that the films are thin enough for allowing the electrical current to flow trough the interface (probably in places were the film is pinned in between the asperities) and that no external insulating particles are generated in the wear track. This, together with the fact that the friction coefficient remains low and constants, for all the length time of the experiments presented in

Figure 27, tell us that the films are not worn (or very little) during this kind of test. This is confirmed by the difficulty to observe at the microscope the wear track produced by experiments at 1 N for 100 wear cycles. In many cases the only phenomenon that was observable was the flattening of coupons lamination stripes. Therefore, during this kind of tests, the diazonium grafted organic films acted as an excellent protective film for electrical contacts.

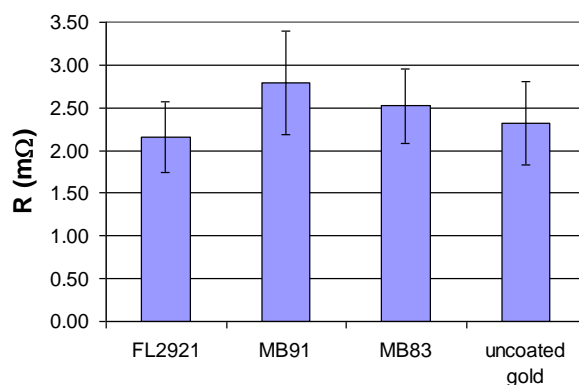


Figure 28. Static contact electrical resistances before starting friction experiment. Statistics are on 5 measures for **FL2921**, on 8 measures for **MB91**, on 5 for **MB83** and on 15 for gold. Applied normal force 1 N.

Figure 28 reports the static electrical contact resistance that was measured before starting the experiment for each kind of diazonium grafted thin film and for the uncoated gold.

The difference in electrical contact resistance in between the coated samples and the bare gold is very small and is not significant.

The electrical resistance being that low could mean that the film is thin enough to allow direct metal/metal contacts or tunnel contacts in between the asperities to be established.

It is anyway surprising that no significant difference is found with the uncoated substrate. This will mean that the same amount of direct contacts is established when the gold is coated and when it is not. But this is somewhat controversial with the low friction coefficient measured during friction and the fact that no adhesion plates are observed in the wear track of the coated substrate after an experiment as in Figure 27. Another possibility that could explain such low contact resistance is that the electrical conduction is effectuated through the organic film. Actually the grafting of the diazonium salts leads to the formation of a structure that is poly(phenylene)-like. The

presence of the substituent group prevent the coupling of the phenyl rings to be done on 1-4 positions as it will be necessary to have the formation of a semiconductive organised linear polyphenylene. The structure of the films was discussed in section 3.4. Although it is not linear it is constituted of coupled phenyl rings that are bonded to form a polyconjugated skeleton. To our knowledge no data exists on the electronic structure of such films to know whether they can be electronic conductor when extremely thin as in our case. Some data about the electronic structure of the films will be presented in the chapter 6.

For the moment it is not possible from our experimental data to clearly state if the conduction is limited to direct metal to metal contacts or there is a contribution of the film. Studying the variation of the electrical resistance with the temperature could be a good way for obtaining meaningful data. This kind of experiment will allow observing whether the interface behaves as completely metallic, in that case pure asperities conduction can be assumed, or whether there is a semiconducting contribution to conduction, and in that case a contribution from the film can be expected.

Although the results obtained at 1 N applied normal force are already satisfying for an industrial application we effectuated same tests at 2,5 N of applied normal force in order to see whether it was possible to delineate greater differences in between the different diazonium salts grafted films.

The evolution of the friction coefficient is reported in Figure 29 for a test at 2,5 N for 800 cycles on **FL2921** and **MB91**-grafted films. The results on unprotected gold are reported for compaireson.

The friction coefficient for the uncoated gold at 2,5 N is characterised by a rapid increases from about 0,25 to 0,6 (but this latter values could vary with the different experiments form 0,4 to 0,6). Then the ball and the surface flatten out, the friction coefficient decreases and reaches a plateau around 0,4. This behaviour was reproduced for the different experiments.

At 2,5 N of applied normal force the behaviour is more different in between hydrogenated and fluorinated films.

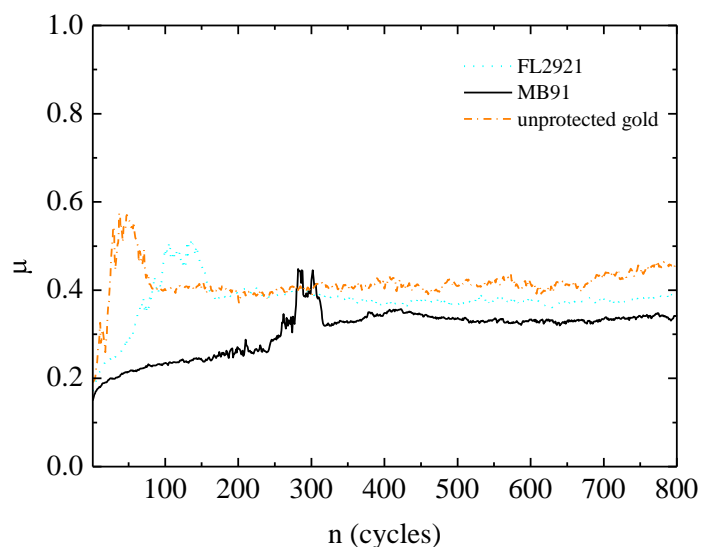


Figure 29. Evolution of the average friction coefficient with the number of wear cycle for **FL2921**, **MB91** and unprotected gold. Applied normal force 2,5 N.

The **MB91** grafted film starts from low friction coefficient (0,15) which increases but remain around 0,2 for at least 200 cycles. Then the a “rupture” of the film is observed. The friction coefficient increases showing oscillation and reaches a plateau which value is comparable to that of uncoated gold.

In the case of the hydrogenated film, grafted from **FL2921**, “rupture” happens much sooner and around 50 cycles the film shows “breaking down”.

The breaking down of the films is more easily seen by plotting a “cartography” of the friction coefficient as done in Figure 30. The friction coefficient is calculated (by measuring the instantaneous lateral force on the ball) for 600 positions in the wear track. The intensity of the friction coefficient is represented by a colour scale. Each line along the x-axis represents the friction coefficient for a cycle. Cycles are then stacked along the y-axis. That means that the friction coefficient measured for the first cycle is represented on the bottom of the figure and that the friction coefficient measured for the last cycle is represented on the top.

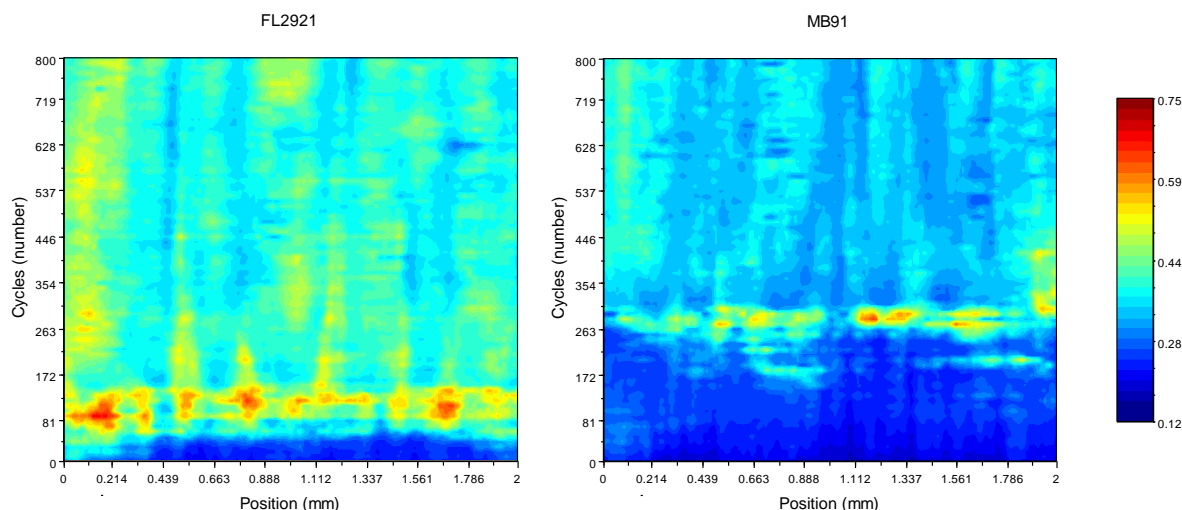


Figure 30. “Cartography” of the evolution of the friction coefficient in the wear track corresponding to curves reported in Figure 29.

Both cartographies showed in Figure 30 presents “vertical stripes”. These stripes correspond to oscillation in the friction coefficient values because of the lamination stripes in the substrate that are orientated perpendicular to ball motion direction. As a consequence stripes showing higher friction values and stripes showing lower friction values can be observed.

The “rupture” is clearly visible on those maps. It shows up as a “catastrophic” event. By this we mean that the film damage (that we can suppose from higher friction coefficients) is not localized in a specific point in the wear track but it is homogenous in the entire track. When the rupture happens is characterized by a rapid increase in the values of the friction coefficient (that corresponds to the peak visible in the curve of the average friction coefficient evolution, Figure 30). Then the friction coefficient decreases somewhat, but remains anyways to values much higher that the beginning of the experiments.

In the case of **FL2921** films the rupture happens for values of wear cycles number much lower than for **MB91**.

This seems likely to be due to adhesion properties rather than to film mechanical properties. Recorded D-R curves (see section 3.6) tell us that hydrogenated films show better supramolecular organization, are more compacts and more difficult to be penetrated by a tip that their equivalent fluorinated films.

The weakest resistance to wear and the higher friction measured by tribology test for hydrogenated films with respect to fluorinated ones has therefore to come from adhesion regulated aspects. For severe test with high load (2,5 N) the difference in surface energy between hydrogenated and fluorinated films (about 30 mN m<sup>-1</sup>) plays an important role. For low loads (1 N) it resulted just in a recorded slight difference in friction coefficient for the two kinds of films. For high loads it becomes fundamental for resistance to wear and can change greatly the point at which the rupture of the films is reported.

### Effect of the lateral group

D-R approach/withdraw AFM curves have shown (section 3.6) that the inner part of the diazonium film, that means the part that is constituted of the aromatic rings, is the most solid part and is the most difficult to be penetrated by the AFM tip.

We therefore studied the tribological behavior of substrates functionalized by the electrografting of benzene tetrafluoroborate (**BD**) which is the simplest aromatic diazonium salt and brings no lateral group (structure in Figure 12).

For this kind of films the values of surface energies can not be as low as for the fluorinated salts but the effect of having a mechanically tough polymers could results in interesting tribological properties.

Results for severe wear test (applied load 2,5 N) for a surface functionalized with this molecule are reported in Figure 31 and compared to the results obtained for **MB91**. The tribological behavior of the **BD** grafted surface is stunning. The friction coefficient remains low for all the length of the experiment and its shape is extremely smooth. Values are around 0,15.

The same smooth shape is found for the values of electrical contact resistance. It is interesting to compare the behavior of the electrical contact resistance for the two films. Two curves are plotted for each film which represents the values that are measured at each one of the ends of the wear track.

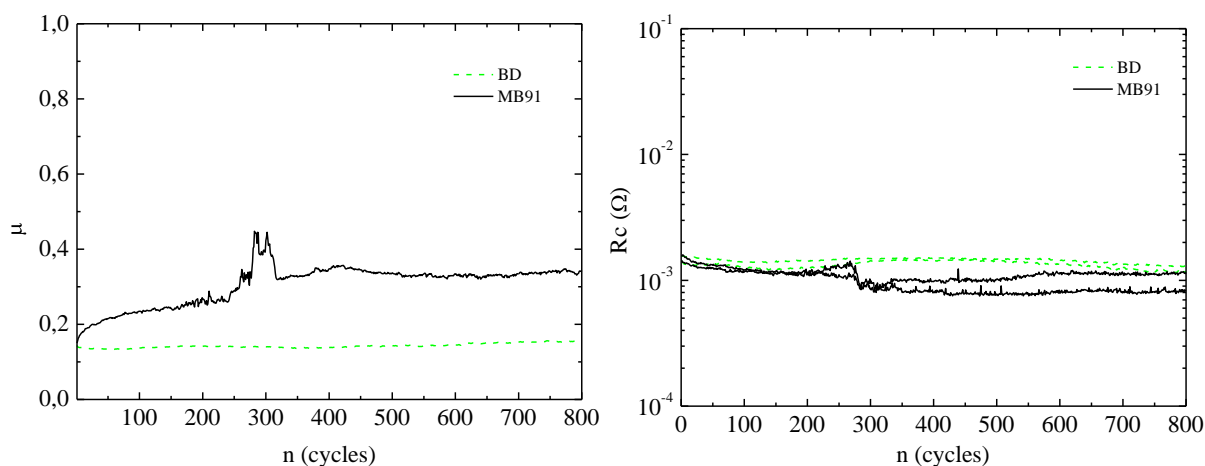


Figure 31. Evolution of the average friction coefficient with the number of wear cycle for film grafted from **MB91** and **BD**. Applied normal force 2,5 N.

The two values are almost equal for the **MB91**-grafted sample until about cycle number 200. Then the film breaks down and this can be seen because of course on the values of the friction coefficient increases as discussed above. The rupture of the film is anyway also visible from the electrical resistances records. In the moment of the rupture the contact electrical resistance decreases, probably because a contact of greatest area is generated. From that point the values of the resistance at the two end of the track start to be different that means that some matter is accumulated preferentially at one end. That means that the organic film is pushed at one of the wear track when it breaks down.

On the contrary for the **BD**-grafted surface the values of the contact electrical resistance remain smooth and the resistances measured at the two different ends remain equals. This shows no degradation of the film and that no “catastrophic” event happens inducing a preferential accumulation of matter to one of the two track ends.

Although no degradation can be observed from the evolution of the average friction coefficient or the contact electrical resistance because they remain constant some more information can be obtained by friction coefficient “cartography”. The “cartography” correspondent to the experiment of Figure 31 is reported in Figure 32. The behaviour is radically different with respect to what reported for the films grafted from **FL2921** or **MB91** (see above).

Some degradation is visible in friction coefficient “map”. It is not observable as a sudden increase of the friction coefficient at a specific cycle but looks like more

gradual. Actually it can be seen that the friction coefficient starts increasing at the track ends.

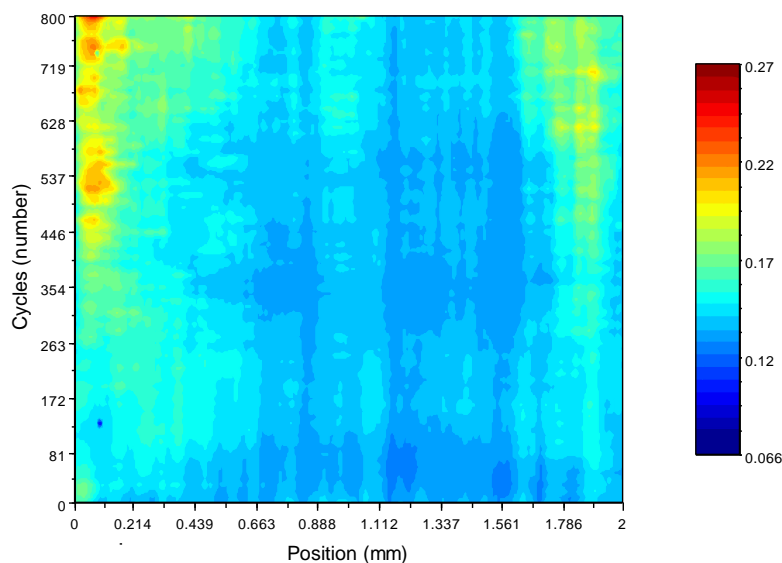


Figure 32. “Cartography” of the evolution of the friction coefficient in the wear track for and **BD**-grafted film. The friction coefficient “map” corresponds to the curve reported in Figure 31.

In a reciprocating tribological test, as the one we applied, the wear is more severe at the ends of the track.

As a consequence the film start to be worn at the track ends and the friction coefficients values increases from about cycle number 300. The augmentation of the friction coefficient being localised just in these specific points is almost not visible on the mean friction coefficient reported in Figure 31 that averages all the values recorded in the track. Also this “cartography” shows anyway that films obtained upon the reduction of **BD** withstands wear in an exceptional good way.

The behaviour presented by such films seems even more surprising when compared to the film obtained by the electro reduction of **FL2921**, **MB91** or **MB83**.

The presence or the absence of the lateral chain radically changes the wear modes in the film. In the case of the films with the aliphatic or fluorinated substituent chain one measures a “catastrophic” rupture. In the case of the non substituted film the wear process precedes gently probably with a slow and constant erosion of the organic matter.

### 3.8 Chapter conclusions

In this chapter we have shown that the electroreduction of fluorinated and hydrogenated diazonium salts leads to the formation of thin poly(phenylene)-like films grafted on gold surfaces.

We have shown that the voltammetric peak of diazonium salts can be split into sub-peaks. The phenomenon was explained by the presence of different reduction sites corresponding to different crystallographic orientations. The observation of peak splitting requires working on clean polycrystalline substrates and the grafted film needs to have passivating properties.

AFM approach/withdraw curves have shown that hydrogenated films have a better supramolecular compactness with respect to fluorinated ones.

At low loads the tribological behaviour of hydrogenated and fluorinated films is similar. For more severe tests, fluorinated films withstand better wear with respect to hydrogenated ones. This is probably dictated by adhesion contribution to friction and wear.

Finally, films grafted from benzene diazonium tetrafluoroborate (**BD**), which bring no lateral substituent chain, have shown excellent properties as solid lubricant for electrical contacts. They present a persistent low friction together with low contact electrical resistances.

## 4 Grafted poly(methacrylate)s

### 4.1 Introduction

As presented in section 1.4 applying a negative potential in appropriate conditions to some vinyl monomer solutions in organic anhydrous solvents leads to the formation of a thin covalently bonded polymer film on electrode surface.

The grafting mechanism (presented in Scheme 2) involves the chemisorptions of a radical anion on electrode surface followed by an anionic polymerization. Thus the mechanism requires vinyl monomers with an electro attractive substituent group. Strictly anhydrous conditions and aprotic solvents are needed because of the anionic polymerization.

The most studied monomers that can form electrografted films belong to two big families: acrylonitrile and derivatives [50-52], acrylates and methacrylates [93, 94]. Other monomers that have been electrografted are vinylpyridine [55], 4-chlorostyrene [95] and 1-vinyl-2-pyrrolidone [96].

Film grafting has been effectuated by chronoamperometry at a given potential [97], chronoamperometry pulses [29, 98] and cyclic voltammetry [49, 50, 94].

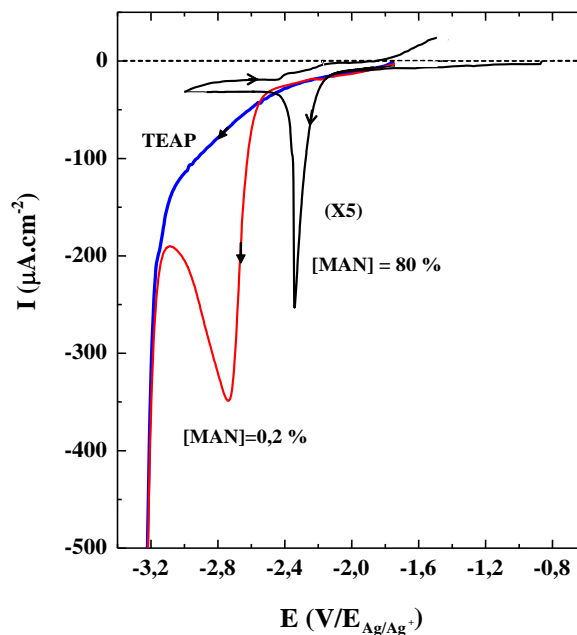


*Figure 33. Plot of the reduction current versus potential during linear sweep voltammetry ( $200 \text{ mV s}^{-1}$ ) of a solution containing the supporting electrolyte alone (TEAP  $5 \times 10^{-2} \text{ M}$  in acetonitrile), a 0.2% MAN solution in acetonitrile and an 80% MAN solution in acetonitrile including the reverse scan [99].*

When film grafting is conducted by cyclic voltammetry a narrow peak is sometimes observed (depending on the system monomer/solvent) before the monomer diffusion peak. The thickness and the structure of the film have been found to be independent from the shape of this first peak [99]. This peak, whose origin was discussed for some time [100, 101], is now named “polymerization peak”. It is attributed to a rapid depletion of monomer in the electrode region because of the rapid consumption due to the rapid anionic polymerization [102, 103]. This causes a quick current decrease resulting in the cutting off of the diffusion peak and the appearance of the “polymerization peak”.

The grafting ratio of the surface was studied by EIS in organic solvents [104] for poly(acrylonitrile) and poly(methacrylonitrile). By using a simple model it is found that the grafted macromolecular chains occupy at maximum 40% of the surface while the remaining it is still accessible to solvent molecules.

The electrografting of fluorinated monomer was never reported before. In this chapter we will present the results on the electrografting of methacrylates bringing a fluorinated lateral chain (see Figure 8). The tribological properties of the films will be also presented and compared to non fluorinated molecules.

## 4.2 Experimental section

### Reagents

Fluorinated monomers 2,2,3,3,4,4,4-Heptafluorobutyl methacrylate (purity 97%), 1,1,1,3,3,3-Hexafluoroisopropyl methacrylate, Zonyl® TM were purchased from Sigma-Aldrich and used without further purification.

Butyl methacrylate (purity  $\geq 99\%$ ) was purchased from Fluka and distilled under reduced pressure to remove polymerization inhibitors.

Acetonitrile, DMF and THF were bought at anhydrous grade from Sigma-Aldrich and normally used without further purification. Propylene carbonate (GC grade) was also purchased from Sigma-Aldrich.

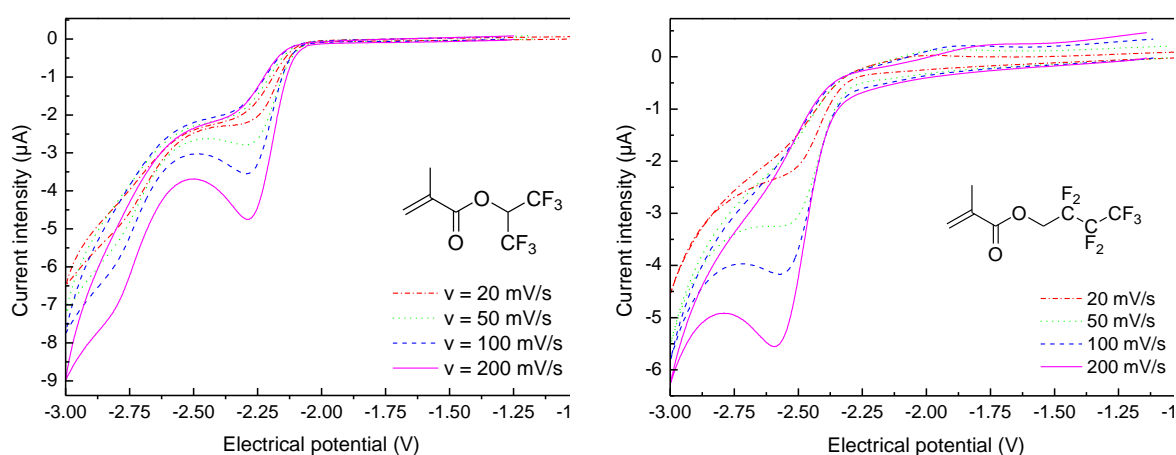
Propylene carbonate and the acetonitrile used for monomer characterizations were dried over molecular sieves and distilled in argon dry box under an argon reduced pressure.

TEAP (purity 95%) was purchased from Acros Organics. Prior to use it was dried under vacuum by heating at  $80 \text{ }^\circ\text{C}$  for at least 24 h. It was used as electrolyte (solutions concentration 0,05 M).

### 4.3 Electrochemical grafting

#### Monomers electrochemical behavior

To study the electrochemical reduction without being affected by polymerization, low concentrations are needed (and in that case the diffusion peak is not perturbed by the presence of polymerization peak). Therefore monomers solutions in acetonitrile at a concentration of 0,01 M were used.



a)

b)

Figure 34. Cyclic voltammetry of HFIPM (a) and HFBM (b) in acetonitrile at 0,01 M for different sweep rates.

Figure 2 reports the results obtained. Both molecules exhibit a reduction peak in the electrochemical domain of the system. That means that the radical anion can be formed in the solution and that film grafting can be expected.

It is interesting to observe that a small variation in the structure of the substituent group corresponds to a shift in reduction potential of the molecule. While HFIPM exhibits a peak at -2,3 V at a speed of 200 mV s<sup>-1</sup>, the potential is shifted at -2,6 V for HFBM. This observation confirms the peculiarity of fluorinated compounds chemistry. Although the structures of the two molecules are similar, and a similar electroactive character of the lateral chain is expected, a big shift in electrochemistry reduction potentials is found that could be hardly previewed before the experiment.

Methacrylates with longer fluorinated chains are more difficult to study. The commercial technical product Zonyl TM® is a mixture of 2-(perfluoroalkyl)ethyl methacrylate. The structure is reported in Figure 35.

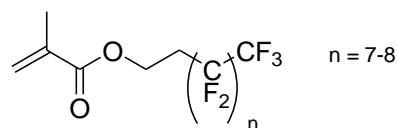


Figure 35. Chemical structure of Zonyl TM®.

The first difficulty that was encountered is that the monomer is insoluble in acetonitrile. Therefore experiments were conducted in solutions in DMF. Results are reported in Figure 36.

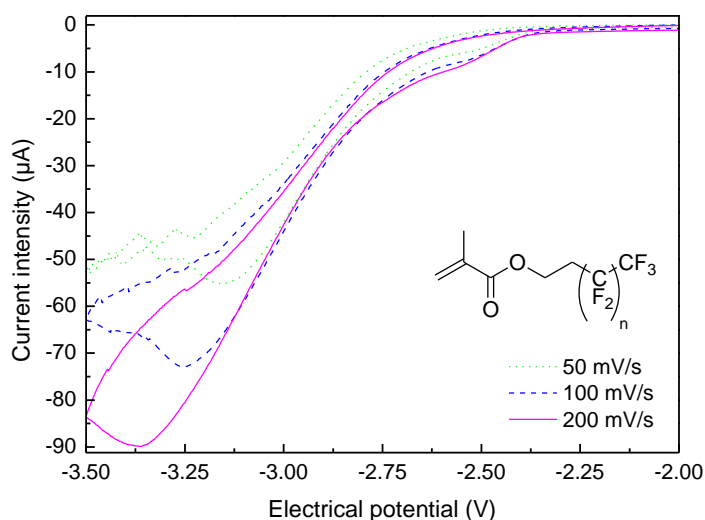
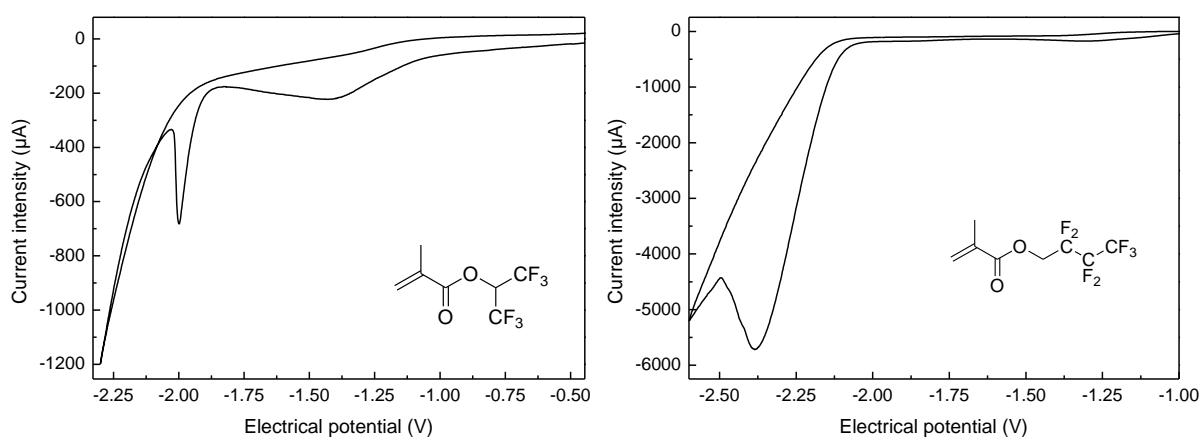


Figure 36. Cyclic voltammetry of Zonyl TM® in DMF at 0,01 M for different potential sweeping speeds.

In this case the reduction potential is even more shifted toward negative values. The peak observed at 200 mV s<sup>-1</sup> is found at -3,4 V. Such low values, at which the reduction of tetraethyl ammonium is already started, make difficult the utilisation of the monomer for film electrografting.

### Electrografting in different solvents

In a first time, films of PHFBM and PHFIPM were electrografted from the corresponding monomers in acetonitrile which is a common solvent for electrografting. The corresponding voltammograms are reported in Figure 37



a)

b)

Figure 37. Voltammograms recorded during electrografting of PHFIPM (a) and PHFBM (b) films in acetonitrile, sweep rate  $20 \text{ mV s}^{-1}$ .

HFIPM exhibits a very narrow polymerization peak which probably means that the polymerization is very efficient. For HFBBPM the peak is much wider and at lower potential but it is anyway sensibly different from the diffusion peak that was measured at lower monomer concentrations.

The films thickness was measured ex situ by mechanical profilometry. Films obtained by cycling the potential just once (such as presented in Figure 37) have thicknesses of about  $5 \mu\text{m}$ .

Such high thicknesses are due to fluorinated polymer insolubility in acetonitrile. In fact the polymerization in the solution leads to the formation of insoluble macromolecules that precipitate on the electrode surface leading to thick films.

It has been shown [104] that the grafting ratio of electrografted polymers increases by increasing the number of potential cycles.

In our case the precipitation of ungrafted macromolecular chains on the surface hindered further growth of electrografted polymers during the following potential cycles. Therefore the grafting ratio for PHFIPM and PHFBM in acetonitrile is expected to be quite low.

For that reason electrografting was tried in better solvents for the polymers. Propylene carbonate was used. Electrografting voltammograms are reported in Figure 38.

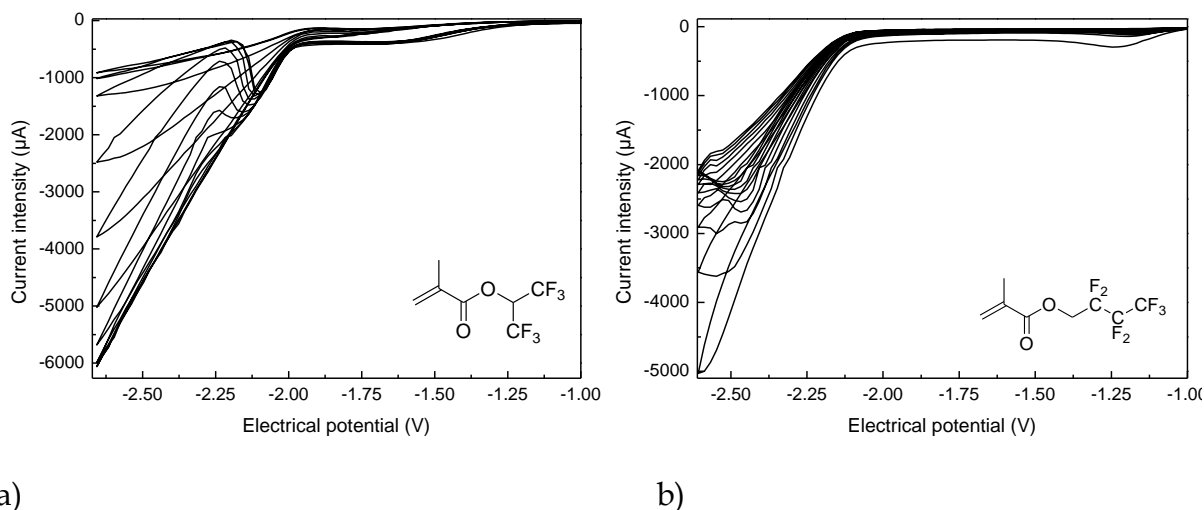


Figure 38. Voltammograms recorded during electrografting of PHFIPM (a) and PHFBM (b) films in propylene carbonate, sweep rate  $20 \text{ mV s}^{-1}$ .

While for film grafting in acetonitrile the surface passivation was almost total after the first cycle and almost no current was recorded during the next scans, in this case one can see that the surface passivation is gradual and current decreases at each cycle.

Films obtained are still very thick, in the order of  $1 \mu\text{m}$ , which means they are mainly composed of ungrafted precipitated chains although they are swelled by the solvent during the electrochemical experiment that allows for gradual passivation.

Bulk polymers solubility was tested in different solvents and the time needed for complete polymer dissolution was estimated. Acetone and THF were found to be the best polymers solvents. THF is a solvent that can be used for electrochemistry but the choice of suitable supporting salts is quite limited. Because electrografting needs the use of quaternary ammonium supporting salts, which act locally as “water molecules traps” [105] a mix of THF and DMF at 50%/50% vol./vol. was used. DMF was also found to be a solvent for the bulk polymers but polymer dissolution in this solvent needed stirring overnight while in THF it was almost immediate (solutions at about  $1 \text{ g cm}^{-3}$ ).

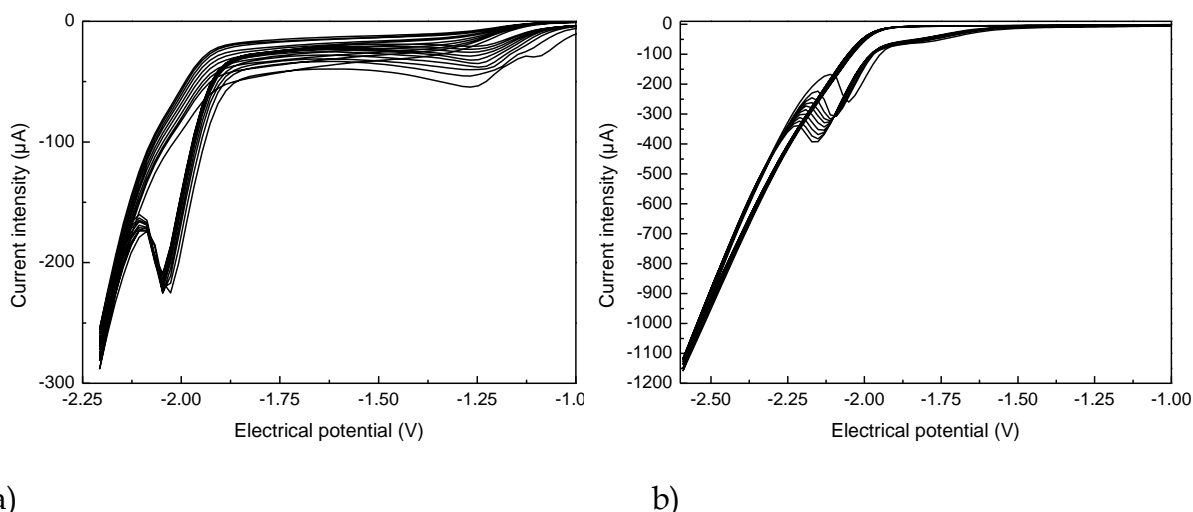


Figure 39. Voltammograms recorded during electrografting of PHFIPM films in DMF/THF for different vertex potentials, sweep rate  $20 \text{ mV s}^{-1}$ .

In that case (Figure 39) the reduction of current after each cycle is smaller than in the other solvents which indicates that almost no ungrafted polymer precipitates on the electrode. In Figure 39a were the potential is swept until  $-2,2 \text{ V}$ , the reduction of the current is almost negligible. Anyway a reduction of the current corresponding to electrode passivation is visible in Figure 39b, where the potential is swept until more negative values ( $-2,6 \text{ V}$ ). This is due to the growth of thicker films when more negative potentials are applied.

Even if electrode passivation is not observed in the case presented in Figure 39a the film is expected to grow anyway. In the case of electrografted poly(methacrylonitrile) it has been shown that the grafting starts at the beginning of the polymerization peak [96]. For PHFIPM the effective films grafting for potential below  $2,0 \text{ V}$  was verified by EQCM and by ATR-IR spectroscopy of electrode surfaces ex situ.

As already expected from monomer electrochemical characterisations the electrografting of films from Zonyl TM proved more difficult. Although in some experimental conditions a deposit could be observed it rarely was homogenous and mechanically resistant. For those reasons work has not been conducted further on that compound.

#### 4.4 Physical chemistry characterization of the films

##### IR characterization

The ATR-IR spectra of the film and of the monomers are shown in Figure 40. One can see the characteristic peak of the methacrylate  $\text{-C=O}$  stretching at  $1750\text{ cm}^{-1}$ , and for the monomer the  $\text{-C=C-}$  stretching at  $1640\text{ cm}^{-1}$ . As expected the polymerisation causes the bleaching of this peak in the film spectrum.

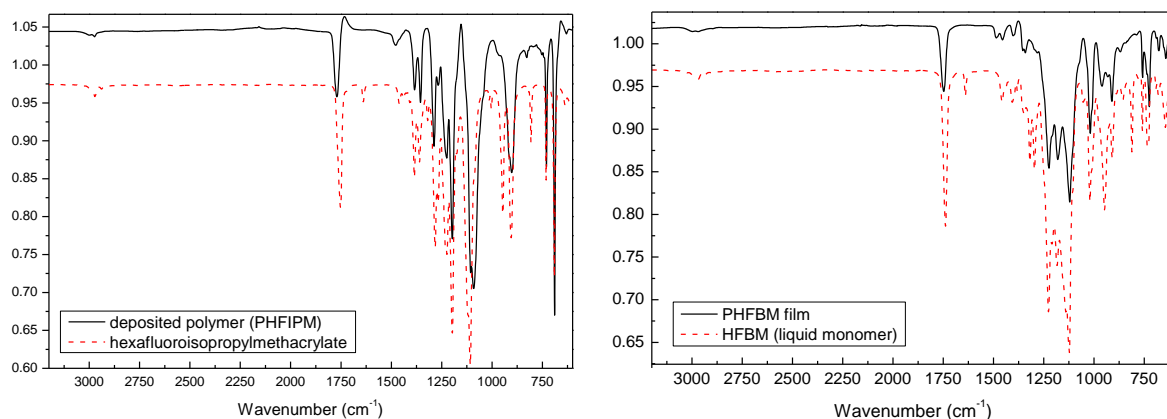


Figure 40. ATR-IR spectra of poly(methacrylate) films (solid line) compared with respective monomers (dashed line); a) PHFIPM, b) PHFBM.

$\text{-C=O}$  stretching vibration is found at values higher (in between  $1780\text{-}1760\text{ cm}^{-1}$ ) than what is expected for aliphatic methacrylates ( $1750\text{-}1725\text{ cm}^{-1}$ ) [81]. This is an effect due to the electron attractive character of the fluorinated lateral group. Electronegative group directly bonded to the alcoholic oxygen atom of the ester group tend to increase the frequency of the  $\text{-C=O}$  stretching vibration [81].

Frequencies at lower wave numbers are difficult to identify, but strong bands are expected in that region because of the  $\text{-C-F}$  stretching modes that are superposed with polymer chain collective modes. Anyway the film spectrum, except for the peak due to the  $\text{-C=C-}$  vibration, is similar to monomer that insures that the film is effectively formed of the expected polymer.

The effect of the solvent used for electrochemical grafting on the ratio between grafted/ungrafted polymer chains has been studied by sonicating the films in THF and recording the IR spectra before and after sonication.

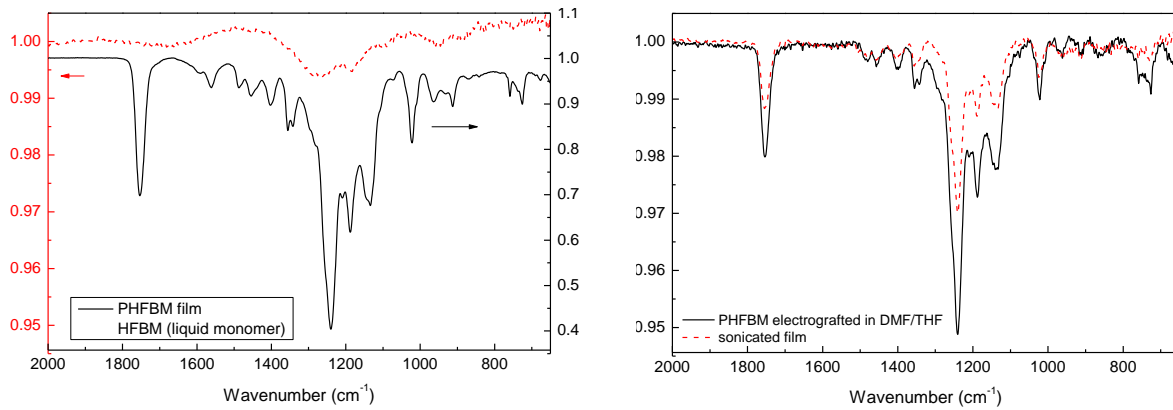


Figure 41. IRRAS-IR spectra of PHFBM film electrografted in a) acetonitrile b) DMF/THF before (solid line) and after (dashed line) 10 min sonication in THF.

As can be seen from Figure 41a electrografting of films from acetonitrile leads to the formation of thick films (the transmittance is lower than for films electrografted in DMF/THF) but they are essentially composed of ungrafted macromolecular chains because after sonication in a good solvent almost nothing is left on the surface. On the contrary electrografting performed in DMF/THF solvent mixture leads to thinner film with respect to the ones obtained in acetonitrile but they resist much better to sonication. Therefore a better ratio between grafted and ungrafted macromolecular chain is expected.

Films electrografted in propylene carbonate, which is capable to some amount to swell and solubilize polymer films, have an intermediate behavior in between films obtained in acetonitrile and in DMF/THF. Although a great quantity of films is removed by sonication, there is anyway a certain amount of grafted chains that remains after the sonication in a good solvent as measured by IR spectroscopy.

These observations remain qualitative because of the not-quantitative character of ATR-IR transmittance.

### XPS characterization

Further characterization of the films was obtained by XPS spectroscopy. Results on PHFBM films grafted on gold are reported in Figure 42.

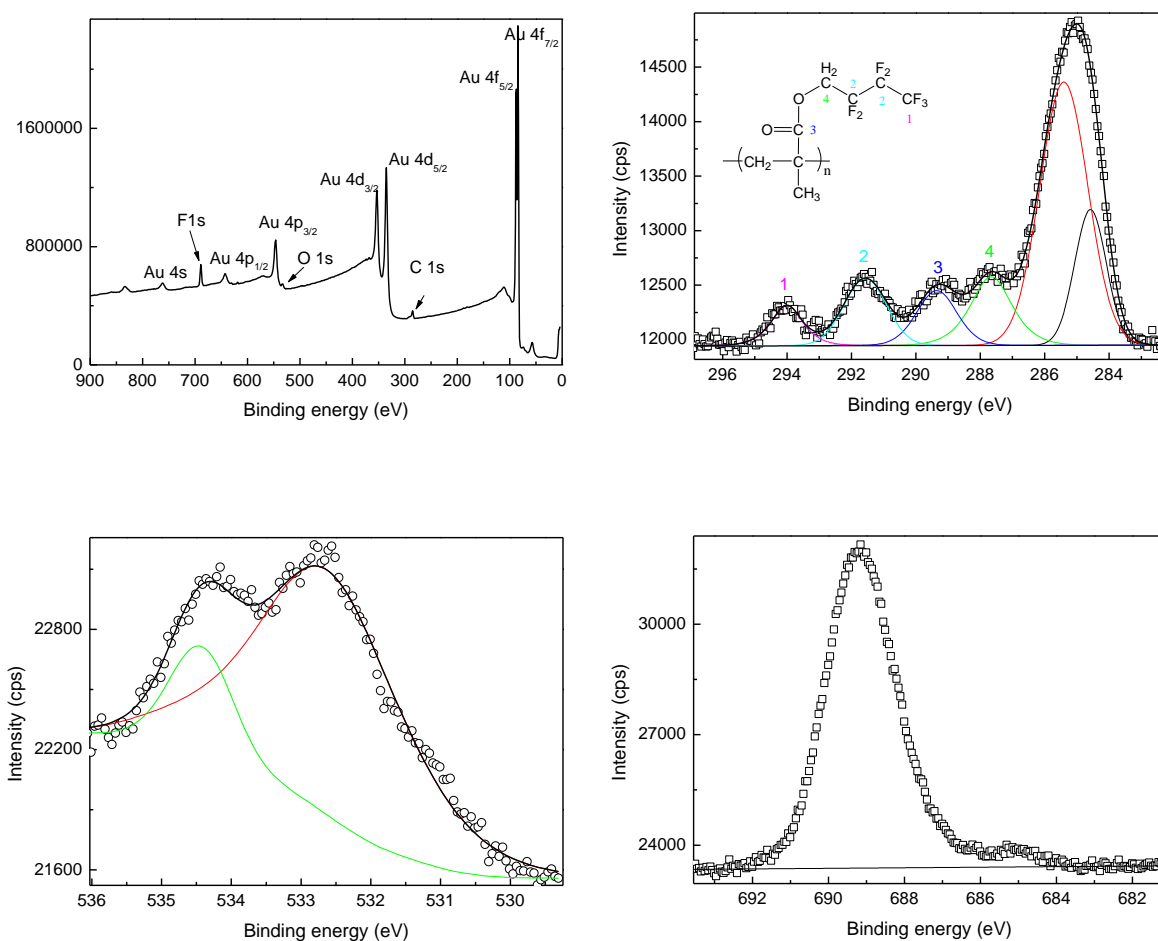


Figure 42. XPS spectra of PHFBM grafted on gold. a) Survey, b) C1s, c) O1s, d) F1s. Film grafted in DMF/THF.

Because films grafted from the DMF/THF solvent mixture are thin (thickness of the film estimated by ellipsometry was 10 nm) all the gold peaks are present in the XPS survey spectrum. The other visible peaks are C1s, O1s and F1s. C1s peaks is very characteristic and presents multiples components due to the electroactive character of adjacent fluorine and oxygen atoms. The components at the highest energy 294,0 eV is assigned to  $-\text{CF}_3$  carbons.  $-\text{CF}_2-$  carbons are found at 291,5 eV. Then the third peak at 289,3 eV has to be assigned to the carbon of the carbonyl group. The an other component is found at 287,6 eV, this is tentatively assigned to first  $\alpha$  carbon of the ester substituent that is subjected to the electroactive effect of the  $-\text{CF}_2-$  and the ester group. The big peak at 285,0 eV is found at a binding energy typical for aliphatic carbon. It is too wide to represent just a component and it was tentatively deconvoluted into two components.

O1s core peak present two components, one at 534,4 eV and one at 532,8 eV due to the presence of the two oxygen of the ester group. Deconvoluted components area ratio is not unity as it should be expected. The peak is anyway convoluted with the Au 4p<sub>3/2</sub> peak. Differences in area of the two components are also probably due to the environmental contamination.

Analogous results are found for PHFIPM electrografted films.

### Contact angle measurements

As expected the electrografted PHFIPM and PHFBM have hydrophobic surfaces. The surface energy was calculated by measuring the contact angle with diiodomethane, hexadecane and water and by fitting the data with Owens-Wendt model as in section 3.4.

	$\theta_{H_2O}$ (°)	$\theta_{CH_2I_2}$ (°)	$\theta_{C_{16}H_{36}}$ (°)	$\gamma_s^p$ (mN / m)	$\gamma_s^D$ (mN / m)	$\gamma_s$ (mN / m)
PHFBM	109,6 ± 0,4	89,9 ± 0,4	65,3 ± 0,6	0,48 ± 0,01	12,7 ± 0,2	13,1 ± 0,2
PHFIPM	103 ± 2	87 ± 5	59 ± 2	0,25 ± 0,01	13 ± 2	13 ± 2

Table 3. Contact angles with water, diiodomethane and hexadecane for the poly(methacrylate) films and the corresponding surface energies calculated by fitting with Owens-Wendt model. Films grafted on “evaporated gold” substrates.

Also in this case a value even lower than that of poly(tetrafluoroethylene) is found. This will suggest again an orientation of polymers lateral chains in order to have -CF<sub>3</sub> preferentially orientated toward the external surface.

Self organization and dewetting of fluorinated lubricant, dictated by thermodynamic surface energy causes, is a known phenomenon [106, 107]. In the case of grafted fluorinated poly(methacrylates) the lateral chain could keep a certain amount of mobility allowing it to behave as a “liquid lubricant” and to self-organize in order to minimize surface energy.

### 4.5 Tribological tests

### Effect of the solvent used for electrografting

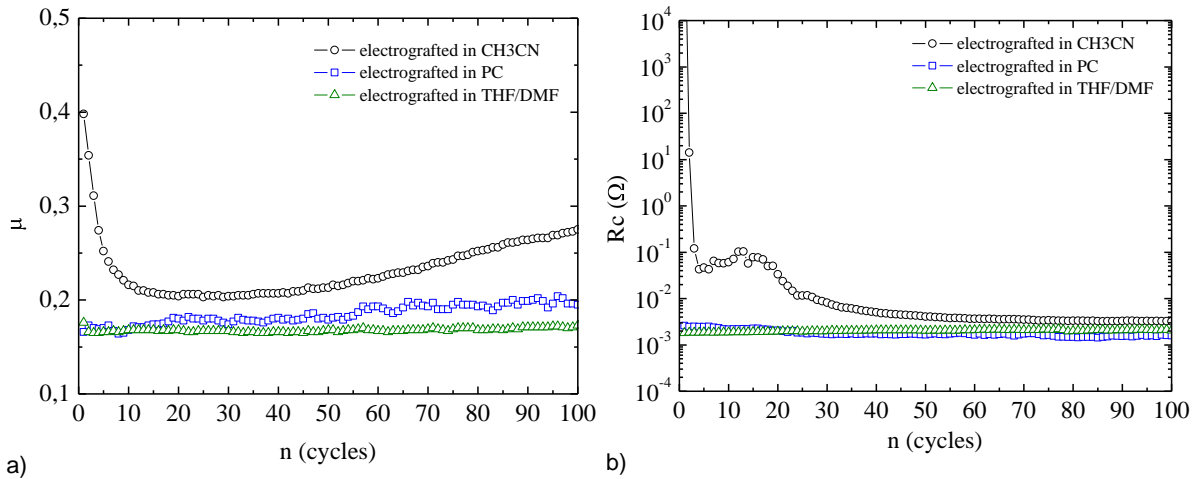


Figure 43. a) Evolution of friction coefficient with friction cycles for PHFBM films electrografted in different solvents. b) Corresponding contact resistances measured at track end. Applied normal force 1 N.

Figure 43a reports the evolution of friction coefficient for PHFBM films grafted in acetonitrile, propylene carbonate and THF/DMF. Films deposited from propylene carbonate were rinsed by acetone in order to remove ungrafted polymer chains entangled with grafted ones.

The black curve with empty circles symbols show a peculiar shape with a mean friction coefficient that start from about 0,4 and decreases to a lower values of about 0,2 that is comparable with the films obtained in PC and THF/DMF. We interpret this phenomenon as the plastic deformation of the thick ungrafted film. The polymer is pushed out of the wear track and the friction coefficient is high corresponding to the energy dissipation required by the plastic deformation. When the thickest part with the worse mechanical properties is removed from the wear track the friction coefficient stabilizes to a low value.

This assumption is also confirmed by contact resistance values measurements (Figure 43b). The contact resistance measured before starting the experiment was beyond the limit of the instrument. Then the curve of the contact resistance also shows a decreasing shape comparable to that of the friction coefficient. This confirms that the insulating matter is pushed off of the wear track and that locally direct metal to metal contacts can be established.

The shapes of the curves of the films grafted in PC and DMF/THF are quite similar. The friction coefficient is low from the beginning of the experiment and remains

stable. The contact resistance graph also shows that the films are thin enough to allow for electronic transport through the interface in between the ball and the plane.

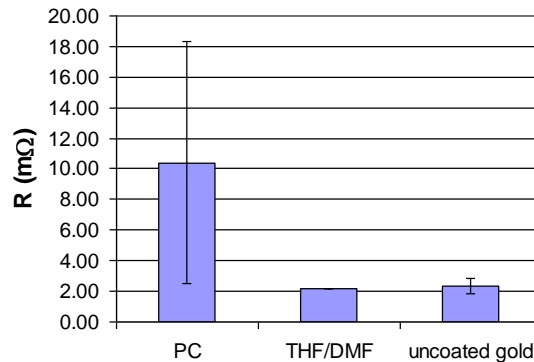


*Figure 44. Average static contact resistance measured before starting friction test for PHFBM films electrografted in PC and THF/DMF compared with uncoated gold. Applied normal force 1N. Statistics effectuated on 6 measures for PC, 3 for DMF/THF and 15 for uncoated gold.*

Anyway the removal of the entangled ungrafted polymer chains by extensive acetone rinsing for the films electrografted from PC is not total and the static contact resistance is somewhat higher than what is measured for the films electrografted in THF/DMF. Figure 44 shows that while the value of the contact resistance obtained for the films grafted from DMF/THF is not sensibly different to that of uncoated gold (about 2 mΩ) in the case of the films obtained from PC and rinsed with acetone the contact resistance is around 10 mΩ and moreover it presents a wide scattering in contact resistance values. This is probably due to a not well reproducible removal of the ungrafted polymer chains.

The effectiveness of the thin DMF/THF electrografted film in reducing wear is clearly visible by comparing the friction tracks on the planes and the wear of the balls after a tribology test for the uncoated and coated substrate.

The wear track of unprotected gold, reported in Figure 45b, shows a classical behaviour for the wear of a ball/plane contact. Adhesion plates are visible in the track and on the corresponding ball. These plates are generated by the formation of micro-soldering in between direct metal/metal contacts that are successively broken by the motion.

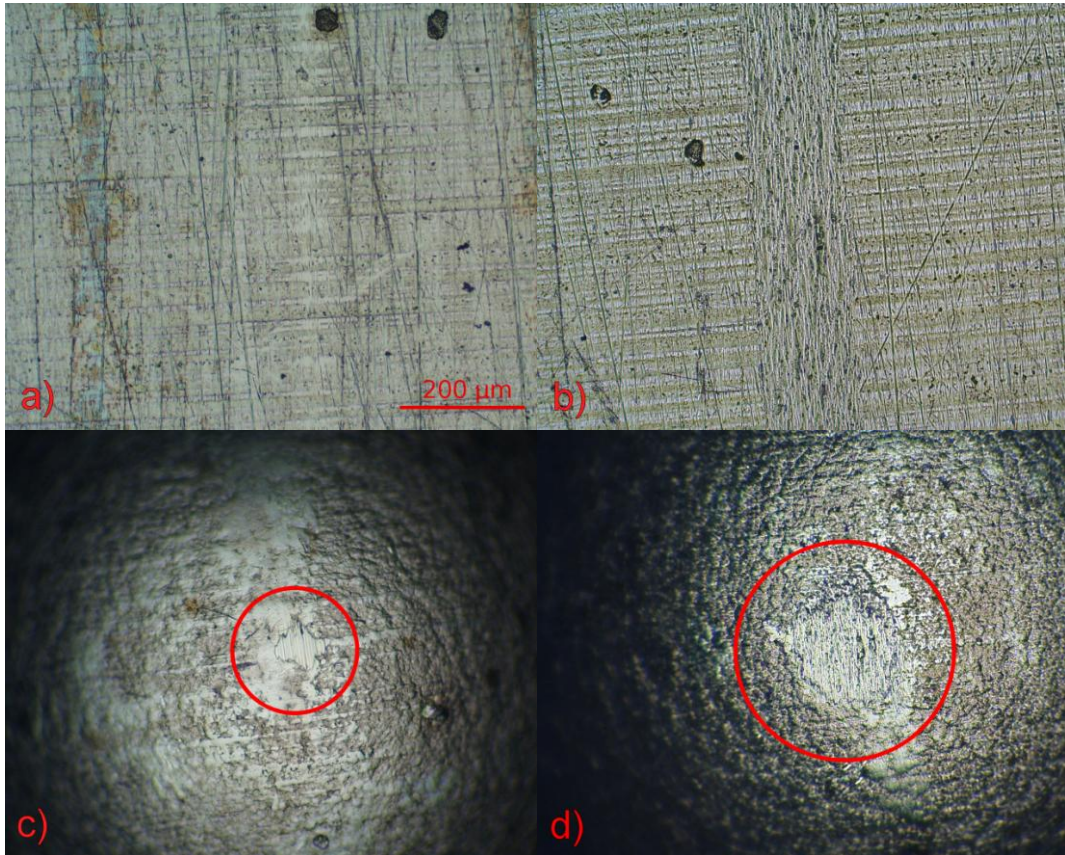


Figure 45. Wear optical microscopy pictures of balls and planes after tribological test (100 cycles at 1 N). a) wear track of a plane functionalized by PHFBM electrografted from DMF/THF; b) wear track of an uncoated plane; c) and d) corresponding balls.

This kind of feature is not visible in the track of Figure 45a which proves that the fluorinated polymer is effective in reducing the adhesion. In this case the wear track is mainly due to the plastic deformation and substrate flattening. The substrates were fabricated by lamination; therefore lamination features are visible on the sample as horizontal stripes perpendicular to the wear track. In Figure 45 the flattening of lamination features in the wear track is clearly visible while in the case of unprotected gold (Figure 44b) these features are wiped out by adhesion plates.

Wear rates can be estimated from the area of the wear region of the worn ball. This area is much smaller in the case of Figure 44c, the plane functionalized by the polymer, than in Figure 44d, the unprotected gold, which shows the beneficial effect of the organic layer in wear reduction.

### Effect of fluorination

The effect of fluorination was studied by comparing the tribological properties of thin grafted PHFBM films with PBUMA films. The latter one has the same molecular structure of PHFBM but is a completely hydrogenated polymer (see Figure 8).

The evolution of the friction coefficient is reported in Figure 46. PBUMA films were grafted in DMF which is a good solvent for the polymer in order to just have the grafted chains and obtain a film with a structure comparable to that of PHFBM.

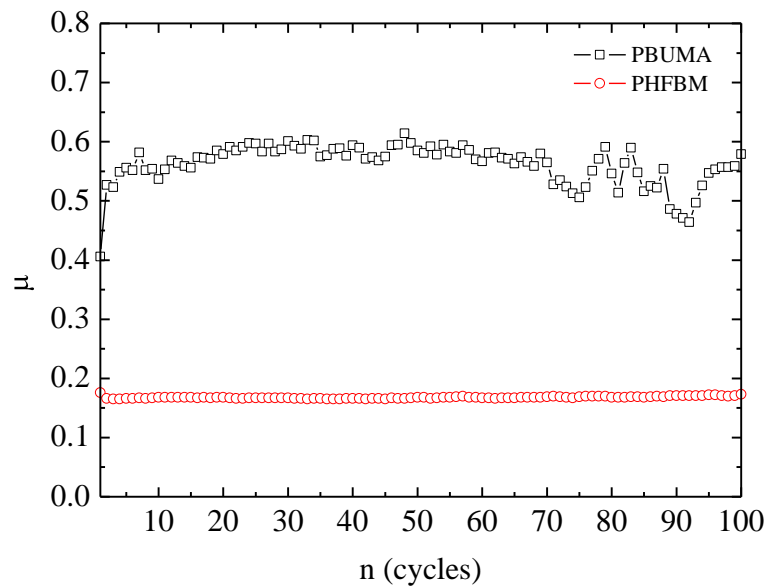


Figure 46. Evolution of friction coefficient for PBUMA and PHFBM with friction cycles. Normal force applied 1 N.

Friction coefficient measured for PBUMA is much higher than the analogous fluorinated polymer and in between 0,4 and 0,6.

Such high values are somewhat surprising for a organic coated polymer and even higher than that of the uncoated gold/gold interface (which typically presents friction coefficients in between 0,3 and 0,5).

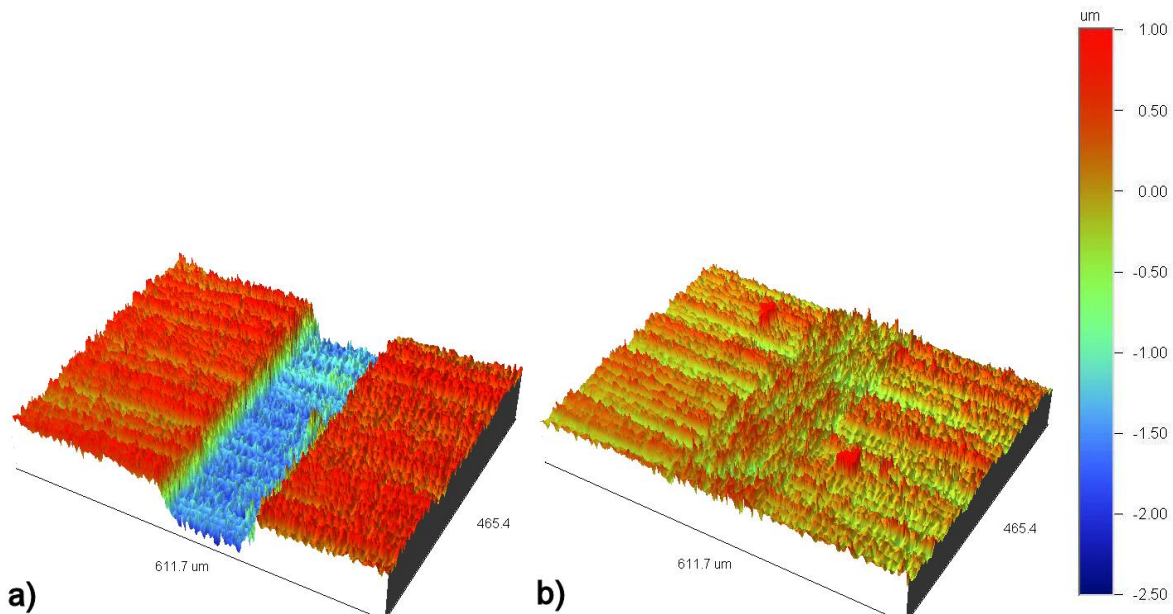


Figure 47. Optical profilometry of wear tracks: a) plane coated with PBUMA, b) uncoated plane. Tests were conducted applying a normal force of 1 N and performing 100 cycles.

The wear track of the PBUMA coated sample was imaged by optical profilometry (Figure 47). The wear of the coated sample is much higher than that of the uncoated sample and presents a surprising shape.

The borders of the wear track are sharp and on the bottom of the track the lamination feature are visible. The depth of the track is about 2  $\mu\text{m}$ .

We interpret it as a complete removal of the polymer layer together with the gold layer. The substrates were fabricated by deposition of 2  $\mu\text{m}$  nickel and 2  $\mu\text{m}$  gold on bronze coupons. Therefore the depth of the wear track is consistent with the removal of the gold until the nickel/gold interface.

This is probably due to a greater adhesion in between the PBUMA functionalized plane and the ball. This results in a greater mechanical sollicitation of the interfaces present in the plane. The interface polymer/gold is more solid that the interface nickel/gold because of the covalent bonding of the polymer and the latter one failed first.

When the gold layer is removed the friction is characterized by nickel friction that is characterised by higher friction coefficients [108-110].

### Effect of the lateral chain on tribological properties

Figure 48 reports the evolution of the friction coefficient for PHFBM and PHFIPM film electrodeposited from acetonitrile compared with the unprotected substrate. The beginning of the curve of both polymers is characterized by a decreasing of the friction coefficient as it was already discussed above.

What is more interesting to observe is the shape of the curves at high around 100 wear cycles. At that point of the experiment the friction coefficient remains below the values of the gold for PHFBM and continue to remain below it for all the experiment long (200 cycles). On the contrary for the PHFIPM (that brings a fluorinated lateral group) the friction coefficient increases all the experiment long and finally the friction coefficient of the substrate with the polymer reaches the values of the unprotected substrate.

This shows that while the lubrication effect of the PHFBM lasts at least for 200 cycles when a 1 N normal force is applied the PHFIPM starts degrading quickly and at around 100 cycles its lubricating effect is completely lost.

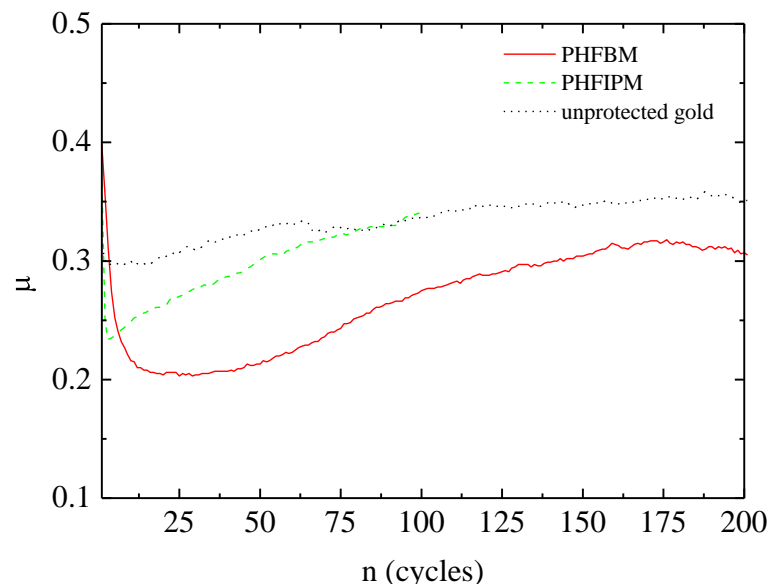


Figure 48. Evolution of friction coefficient for PHFBM and PHFIPM with friction cycles. Films deposited in acetonitrile (PHFIPM one potential cycle until -2,1 V, PHFBM one potential cycle 2,8 V). Normal force applied 1 N.

If we compare the surface energy measurements (Table 3) we can see that the surface energy of the two polymers is low and almost the same (13 mN/m). Therefore this exclude that the effect can come from adhesion phenomena and the different

tribological behaviour has to be imputed to a different mechanical behaviour of the films.

In the case of liquid lubricants it is generally believed that branched lubricants have lower friction coefficients and better performance than the analogous linear lubricants [111]. However some authors reported just minor differences in friction response of branched compound and their linear counterparts [112] and other claims better results for linear lubricants [113].

The better properties of branched lubricants are usually explained as an effect of lateral group in reducing the viscosity. When the thickness of the film is squeezed to a few monomolecular thick layer to the regime of "boundary lubrication" linear lubricants more easily organize to a "solid-like" film while the branched lubricant remain longer liquids [114].

It is however difficult to sum up bibliographic report to a general trend because of the different experimental set up and lubricants studied. The greatest part of the studies is concentrated on liquid lubricant capable of forming a bonded layer acting as a boundary lubricant when the thickness on the liquid is squeezed to a few monolayers thick (acids and esters). Anyway the bonding energy of such layers is much lower of electrografted films and their results are hardly comparable with our work.

Of greater interest for our work is the article of Pooley and Tabor [115] who studied and compared the friction behaviour of linear and ramified polymers. They compared the behaviour of PTFE with TFE-HFP copolymer. The structure of the former is constituted of a  $-CF_2-$  helix that leads to a very rigid rod-like molecule with a very smooth profile. The second is a copolymer of fluoroethylene with hexafluoropropylene. In this copolymer a bulky perfluoroalkyl ( $-CF_3$ ) group replaces a fluorine atom at intervals along the carbon chain. The molecules still have a helical structure but the bulky  $-CF_3$  group spoils the smooth profile of the molecule.

Another couple they studied was constituted of high density poly(ethylene), which is linear, and low density poly(ethylene) which is ramified.

In both case they found that the linear polymers had a lower kinetic friction coefficient than the branched analogous.

Their experimental data support the assumption that during friction a preferential orientation is induced for linear polymers (that they claim having a molecular smooth profile), with the chains laying in the direction of sliding, causing lower values in friction coefficient. When the molecular structure is modified to destroy the smooth profile of the molecule, slip between the chains, was reported to be always accompanied by more severe plunking and transfer.

In our case both polymers bring a lateral group and cannot be assumed to have a smooth molecular profile. Anyway linear substituent groups of PHFBM are more likely to align in the sliding direction rather than the bulky lateral groups of PHFIPM. Moreover polymers bringing a linear lateral group are expected to have better mechanical properties (such as hardness and tenacity) with respect to polymers with a branched lateral group.

We make the hypothesis that the better tribological properties of PHFBM with respect to PHFIPM are due to a combination of better mechanical properties and better orientation of linear lateral group. To fully confirm this hypothesis further experiments are needed.

#### **4.6 Chapter conclusions**

Electrografted poly(methacrylates) with fluorinated lateral groups used as lubricants reduces the friction and the wear of gold coated electrical contacts.

The use of fluorinated lateral chains is essential in order to have good mechanical properties. The use of a poly(methacrylate) with an aliphatic lateral chain is deleterious on contact wear.

The best results are found for thin, completely grafted films, electrografted in good polymer solvent capable of solubilizing and removing the ungrafted chains. The necessity of using thin films is very important for reducing electrical contact resistance to values acceptable for an industrial application. Lower friction coefficients were found for thin grafted films with respect to thicker films during the first wear cycles because some energy is dissipated in plastic deformation of the mechanically weaker part of thick films.

Poly(methacrylate)s with fluorinated linear lateral chain show lower friction coefficients and better resistance to wear than the analogous polymer with ramified lateral chain.

## 5 Composites of grafted poly(methacrylate)s and conductive charges

### 5.1 Chapter introduction

#### Composites with PEDOT and fluorinated PEDOT

We have already reported in section 4.1 that the electropolymerization of vinyl monomers leads to the formation of grafted macromolecular chain with a grafting ratio of at maximum 40% [104]. This means that in electrolytic organic solutions the polymer is swelled and that just 40% of the surface is inaccessible to electrolyte molecules.

As a result it is found that when electrografted vinyl polymers are put in an electrolytic cell with a good solvent capable of swelling the film the electrode surface remains still electroactive. This allows for further electrochemical modification of electrode metallic surface.

The persistence of electrode electroactivity and the low compactness of the poly(methacrylate)s film was used to build binary films of electrografted insulating films and semiconducting polymer [116]. First the insulating polymer (polyacrylonitrile or polyethylacrylate) was formed under cathodic polarization. Then the semiconducting polymer (polybithiophene or polypyrrole) was formed by electrooxidation of the parent monomer.

In more recent papers [117, 118] binary films were elaborated by using dual macromonomers containing a carbon to carbon double bond and thiophene or pyrrole ring. In a first step a polymer film was electrografted by cathodic polymerization. In a second step the semiconducting polymer was obtained by anodic polymerization with or without the presence of additional unsubstituted monomer (thiophene or pyrrole) in the electrochemical bath.

Our idea was to elaborate a composite polymer film constituted of a mechanically solid insulating fluorinated matrix and of a semiconducting polymer in order to conjugate good tribological properties with electrical conduction. The fluorinated

insulating matrix is composed of the fluorinated poly(methacrylate)s which showed good tribological properties (as reported in chapter 4).

For the semiconducting charge we thought of PEDOT. In fact this kind of polyconjugated polymer is the one which shows the best electrical conduction properties together with good chemical stability. Films will be elaborated in two steps. The first one will involve the electrografting of the fluorinated poly(methacrylate). Then the films will be put in a electrochemical bath in the presence of an EDOT monomer that will be polymerized under anodic polarization.

In order to increase the fluorination degree of the film fluorinated EDOTs derivatives were synthesized at Angers University. Their structures are reported in Figure 49.

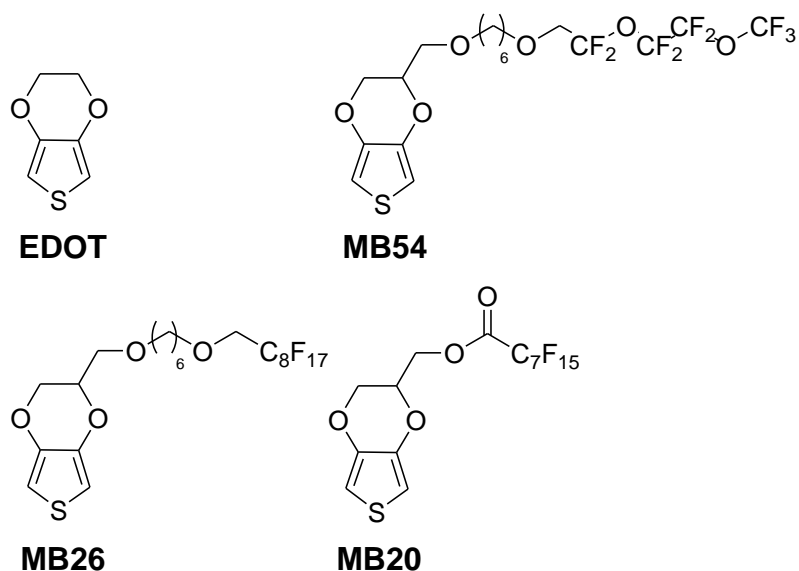


Figure 49. Molecular structure of EDOT and EDOTs derivatives used as monomers for building the semiconducting polymers intended to play the role of “conductive charge” in fluorinated poly(methacrylate)s films.

The molecules were designed in order to have lateral chains that imitate the structure of liquid lubricants currently used. In particular the structure of the lateral chain of **MB54** is similar to the structure of PFPE that is one of the best liquid lubricants for the electrical connectors.

### Composites with carbon nanotubes

Another strategy tested for improving the electrical properties of fluorinated poly(methacrylates) was to use as a nanometric conductive charge 2D-networks of carbon nanotubes.

The formation of carbon nanotubes 2D-networks on amine functionalized glass has been reported recently [119] and exploits the affinity of carbon nanotubes toward amines [120].

In [119] a flat glass plate was modified by 3-(aminopropyl)triethoxysilane, which leads to the functionalization of the surface with primary aliphatic amines. Then the plate was immersed in a single walled carbon nanotubes suspension. The plate was removed and rinsed. Successive immersions in the suspensions allowed for a progressive construction a 2D-network of carbon nanotubes laying on the surface. Electric percolation was measured across the plane.

The functionalization of the surface by primary amine allows “immobilizing” the carbon nanotubes on the substrate. The interaction energy between amine and single walled carbon nanotubes is reported to be 23 kcal/mol [121] (hydrogen bonds have energies in the order of 5 kcal/mol, covalent bonds are in the order of 100 kcal/mol).

Our idea is to build poly(methacrylate)s film charged by carbon nanotubes networks by functionalizing the gold substrate with amine functions, adsorb carbon nanotubes and then graft the polymer. Steps are schematized in Figure 50.

In the last step shown in Figure 50 two strategies have been used to graft the organic film: one way was the electrochemical cathodic grafting of poly(methacrylate)s and the second way was using the amine functions present on the surface to chemically graft an organic molecule.

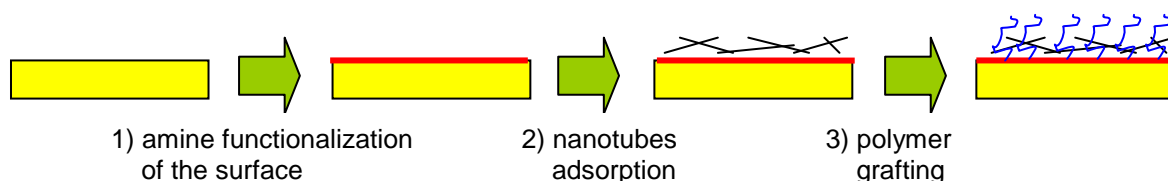


Figure 50. Steps for carbon nanotubes 2D-networks adsorption and polymer grafting.

During experiments it became evident that the immobilization of carbon nanotubes is essential for having good tribological properties and that the strength of the bond play an important role.

While the adsorption of carbon nanotubes on amine functionalized surfaces is a well known technique fewer articles exist on the covalent bonding of carbon nanotubes on

surfaces [122-126]. The published works were not adaptable to our needs and a way to covalently bond nanotubes on the surface had to be developed.

### **Present chapter structure**

The present chapter presents the results about the fabrication and characterisation of composites of fluorinated poly(methacrylate)s and conductive charges. It is composed of three parts depending on what kind of materials is studied as conductive charge in the poly(methacrylate) matrix.

The first one, from section 5.3 to section 5.5, is concerned about PEDOTs and its derivatives as conductive charge. The second one, from section 5.6 to 5.7, is about composites with adsorbed single walled carbon nanotubes networks on primary amines. The third one, from section 5.8 to 5.9, is about composites with covalently grafted multi walled carbon nanotubes.

## **5.2 Experimental details**

### **Electrochemistry and electrochemistry reagents**

Molecules **MB54**, **MB20**, **MB26**, were synthesized, purified and characterized at CIMA at Angers' University. Please refer to the work of M. Balog for further details. 2,3-Dihydrothieno[3,4-b]-1,4-dioxin (**EDOT**) was purchased from Sigma-Aldrich.

Fluorinated monomers 2,2,3,3,4,4,4-Heptafluorobutyl methacrylate (purity 97%), 1,1,1,3,3,3-Hexafluoroisopropyl methacrylate, were purchased from Sigma-Aldrich and used without further purification.

TEAP (purity 95%) was purchased from Acros Organics. Prior to use it was dried under vacuum by heating at 80 °C for at least 24 h. It was used as supporting salt.

For electrochemistry experiments, unless differently stated monomers were dissolved in anhydrous acetonitrile at a concentration of 5 mM and TEAP (0,05 M) was used as supporting electrolyte.

### **Carbon nanotubes 2D-networks adsorption and characterization**

The carbon nanotubes (NT) were purchased by Nanoleedge Brute and produced by arc discharge graphite pyrolysis. They were purified by nitric acid treatment. They are purely single-wall nanotubes and have a diameter of about 1-2 nm and a length of about 1 µm. A stable suspension of SWNTs 4.1 mg/ml in NMP was realised by sonication for 10 h.

The amine-rich substrates were covered by NT suspension for 10 min. They were then rinsed with acetone and the operation was repeated twice.

Raman spectra were collected with a dispersive T6400 spectrometer, with exciting source at 514.5 nm. Power intensity was kept below 1 mW to prevent sample heating.

### **Carbon nanofibers functionalization and grafting**

Carbon nanofibers were purchased by Sigma Aldrich. They were extensively sonicated in water for 30 min obtaining a partially stable suspension (3,35 mg/mL). Acrylic acid was added (concentration 0,1% v/v) to the suspension and kept under stirring.

1,4-phenylenediamine (10 mg/mL) in chloridric acid (0,5 M) was added to an equivalent of  $\text{NaNO}_2$  (6,9 mg/mL) to generate diazonium salt. The salt was activated by addition of metallic iron powder. The activated diazonium salt solution was added (5,13 mg/mL) to nanotubes dispersion under stirring for 10 min. After the reaction time when stirring was stopped the suspension was stable. Functionalized nanotubes were filtered on Teflon 0,22 $\mu\text{m}$  filter and rinsed with water and then dried. Functionalized nanofibers resulted easily dispersible in water without sonication.

### Carbon nanotubes 2D-networks grafting

The carbon nanotubes were purchased by Nanocyl. They are multi walled carbon nanotubes (MWCNT) with an external diameter of 4-10 nm. They were synthesized by chemical vapor deposition. A stable suspension of MWCNT 0,3 mg/mL in NMP was realized by sonication for 12h. Nanotubes bundles were removed by precipitation by centrifugation for 15 minutes at 7000 rpm.

Gold surfaces allowing for nanotubes grafting were obtained as follow. In a first time a aqueous solution of 0,1 M of 1,4-phenylenediamine (Sigma Aldrich) was realized in 0,5 M hydrochloric acid. The same volume of 0,1 M  $\text{NaNO}_2$  (Sigma Aldrich) aqueous solution was added to the same recipient. The mixture was activated by adding metallic iron powder.

Then the substrate was immersed in the reaction bath for 1 h. It was then removed, rinsed with water, ethanol and acetone. It was then sonicated for 10 min in water to remove the ungrafted part of the film. The functionalized substrate was then immersed in a 0,01 M solution of  $\text{NOBF}_4$  for 3 minutes. It was removed, rinsed with acetone and dried.

The substrate was then immersed in the MWCNT suspension in NMP and gradually heated from room temperature to 373 K. It was left at 373 K in the suspension of carbon nanotubes overnight under stirring. It was then removed, rinsed with ethanol and acetone and dried.

### Zonyl BA-L® grafting

The reactions were conducted on amine-rich surfaces prepared as described above, with or without nanotubes. The grafted polyamine samples were left under stirring in a solution of 1,6-Diisocyanato-hexane (Aldrich, 52 mg/ml in anhydrous toluene) at room temperature, for 24 h.

The samples were then left in reaction in Zonyl BA-L (Aldrich), a commercial product containing fluorinated alcohols composed of 9-11 carbon atoms chain, activated with a 1,8-diazobicyclo[5,4,0]-undec-7-ene for 48 h, under stirring at room temperature. These reactions were conducted in argon atmosphere in a dry box.

## 5.3 Electrochemical study and characterization of fluorinated PEDOTs

### Films deposition

First the electrochemical behavior of the fluorinated EDOT derivatives (**MB54**, **MB26** and **MB20**, see Figure 49) was studied to be sure that their electrochemical behavior is the same of the parent molecule. Platinum electrodes were used to avoid gold substrates oxidation question as presented further in the text (in section 5.4).

The irreversible oxidation of monomers **MB54**, **MB26** and **MB20** appears at a usual value for EDOT derivatives (ca  $E_{pa} = 1,3$  V). Electropolymerization of all monomers was carried out under similar concentration conditions. Formation of the polymer films was realized either under potentiostatic ( $E_{appl} = 1.40$  V) or potentiodynamic

conditions (-0,3 to 1,10 V) giving rise to stable films. An illustrative example is given in Figure 51, showing the film growing through potentiodynamic conditions in the representative case of monomer **MB54** (Figure 51a), as well as the corresponding electrochemical response of the modified surface (poly(**MB54**)) in a monomer-free electrolytic medium (Figure 51b). The polymerization could be carried out in acetonitrile ( $10^{-2}$  mol/L), pointing out the efficiency of the process. The CV response (Figure 51b) exhibits a very broad redox system characteristic of the poly(EDOT) doping/dedoping process in the - 0,2 V to + 0,8 V region. Finally, it has to be pointed out that all of these electrodes exhibit a remarkable stability, since no loss of the electrochemical signature has been observed upon repeated cycling, or after standing for days in solution.

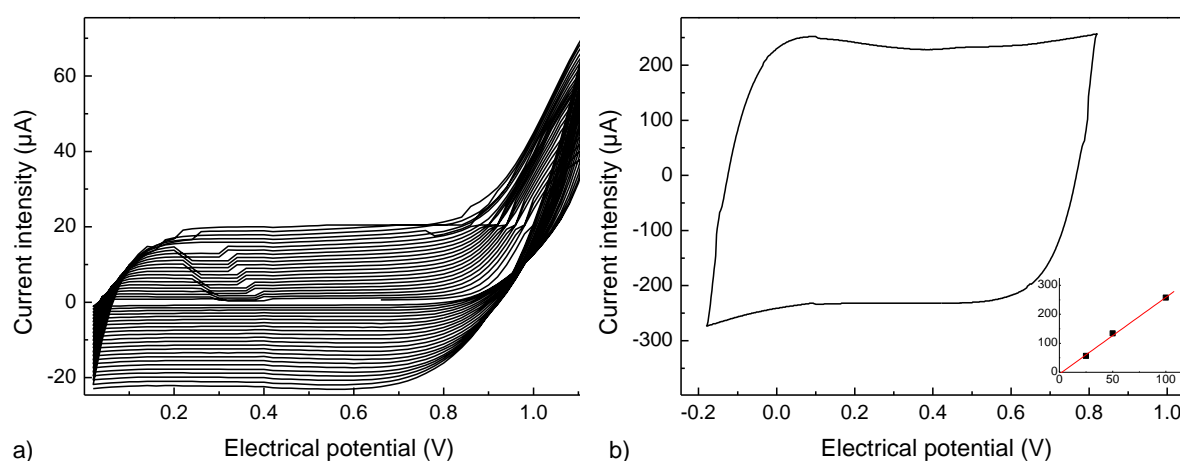
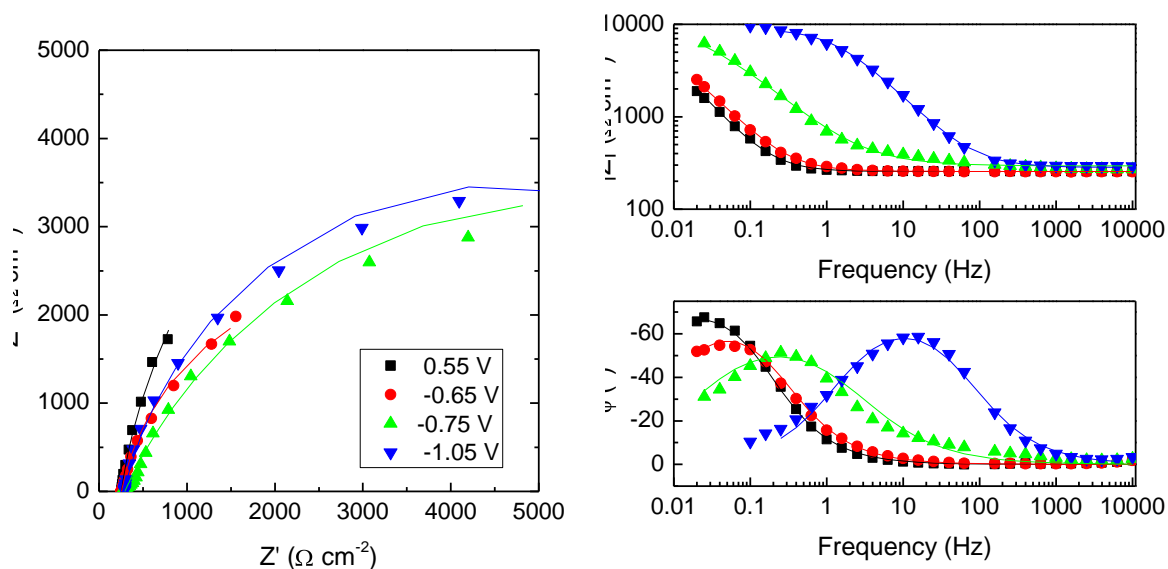


Figure 51. a) Electropolymerization of MB54 (10 mM), in 0,10 M  $Bu_4NPF_6$ ,  $CH_3CN$ , 25 cycles at  $50\text{ mV s}^{-1}$ , Pt  $\Phi = 2\text{ mm}$  (left); b) CV response of poly(MB54),  $CH_3CN$ ,  $Bu_4NPF_6$  (0,1 M),  $100\text{ mV s}^{-1}$  Pt  $\Phi = 2\text{ mm}$ ; (right) Insert : plot of the peak intensity as a function of the scan rate.

### Electrochemical impedance spectroscopy characterization

EIS spectroscopy was performed on the films obtained by electropolymerization to study the differences in the doping process and in the conduction properties of the fluorinated films with respect to parent PEDOT.

For poly(**MB54**) film, taken as an illustrative example, the dc potential was swept from 0,55 V down to -1,5 V (forward scan) and then backward to 0,55 V. Polarization for 1 min at the dc potential to reach a steady-state was performed before starting the measurement. Figure 52 reports the complex plane results during forward scan.



a)

b)

Figure 52. Nyquist (a) and Bode (b) EIS plot on poly(MB54) film taken for different dc polarization potentials. Symbols report experimental points while lines report fits results.

In the frequency window that has been considered, and for the most positive polarization (0,55 V), the film behave almost as a pure capacitor. A wide circle in the Nyquist plot starts to develop when sweeping toward more negative dc potentials. This evolution can be interpreted as a modification of electroactive film by the expulsion of perchlorate counterions. The transition from a doped “conducting state” to an undoped “insulating state” can be easily observed on the Bode diagram (Figure 52b) in the low frequencies  $|Z|$  values.

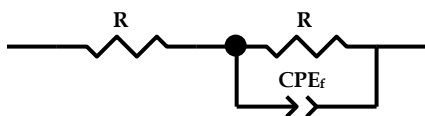


Figure 53. Equivalent circuit used for fitting EIS experimental data.

The modification of film properties with dc potential variation is expected from the theory of electroactive polymer films EIS behavior as formalized by Vorotyntsev et al [127]. This theory is based on a homogenous film model within an irreversible thermodynamic framework. The ion transport is described by a diffusional process since a supporting electrolyte large excess is used that allows the migration contribution to flux to be neglected. It considers that two mobile charge carriers

participate in the process, and due to bulk electroneutrality of the film, the coupled chemical diffusion appears in the form of a binary diffusion coefficient. In our case the charges correspond to holes (positive charges delocalized on the polymer film) that are injected at the metal/polymer interface, leading to the formation of, and to the diffusion of charge compensating perchlorate ions through the polymer/solution interface. Therefore, the concentration of the charge-compensating counterions in the films depends on the oxidation level of the polymer film.

In the case that we considered, at least for the frequency windows used for carrying on the experiments, ion diffusion is fast enough for impedance to be dominated by the capacitive behavior.

With the aim of summing up polymer films behavior more than a deep EIS analysis, we tried to fit the experimental data by the simple homogeneous film equivalent circuits presented in Figure 53. The considered parameters are sufficient for fitting our experimental data and there is good agreement between the model and the experimental points as shown in Figure 52. Symbols represent experimental data while the fit results are represented by lines. The capacitor  $CPE_f$  is modeled with a constant phase element. The impedance of this element is expressed as:

$$Z = \frac{1}{C_f (\omega)^\gamma}$$

where  $\gamma$  is a factor (between 0 and 1) to account for the non ideality of the capacitance  $C_f$ . This non ideality is often ascribed to surface roughness [128]. In our experiments  $\gamma$  was found in the range 0,6 - 0,95. Adding circuit elements such as Warburg impedance did not improve our fits.

$R_s$  accounts for solution resistance. It is found to be constant in our experimental conditions at any dc potential and equal to 261  $\Omega$ .  $C_f$  and  $R_f$  describe film capacity and resistance. Fit statistical errors are in the order of 0,5 % for  $C_f$  and 4 % for  $R_f$  for our experiments.

Fit results at the different dc potentials during forward and backward scan are summed up in Figure 54. Error bars report the fitting statistical errors. The bars in the case of  $C_f$  can not be seen because they are smaller than the symbols. One can see that the poly(**MB54**) film shows very high capacity response at oxidized potentials in the

order of 30 mF/cm<sup>2</sup>. When the potential is decreased below -0,8 V the capacitance starts to decrease and reaches a plateau with values in the order of 20 μF cm<sup>-2</sup>. A symmetrical behavior is found for R<sub>f</sub>. We interpret this as the transition from a conducting doped state down to an intrinsically semiconductor state. In the doped state the polymer shows a high capacitance corresponding to a state where positive charges carried by polymer main chain are compensated by negative counterions. In the intrinsic undoped state the capacity decreases to the normal electrochemical double-layer capacity (as found for a bare platinum surface in the same electrolyte). The resistance is presumably dominated by the ionic carrier more than the electronic component. However within the framework of the applied simple model, it is not possible to discriminate electronic and ionic charge transfer resistance components, or to know which one is dominant; but both increase when passing from a conducting state to a more resistive one corresponding to intrinsic poly(MB54), resulting in R<sub>f</sub> increase. Varying films thicknesses changed the absolute value of the impedance response but did not change the general trend that seems to be thickness independent for the studied films (from 100 to 400 nm, as measured by mechanical profilometry).

We observe a hysteresis in the value of C<sub>f</sub> and R<sub>f</sub> in between the forward and the backward scan.

The hysteresis of redox peaks on **PEDOT** CV response is a well known phenomenon, and a potential shift (0,3 V- 0,1 V) is observed between the oxidation and reduction peaks. Hass et al. [129] have also observed a hysteresis for **PEDOT** in EIS and shown that it is correlated to CV hysteresis. The EIS response they have reported for **PEDOT** films (obtained on ITO substrates for a different electrolytic medium) partially differ from what we report here, and the model used for fitting experimental data had to include a further capacitance to account for low-frequency diffusion behavior observed.

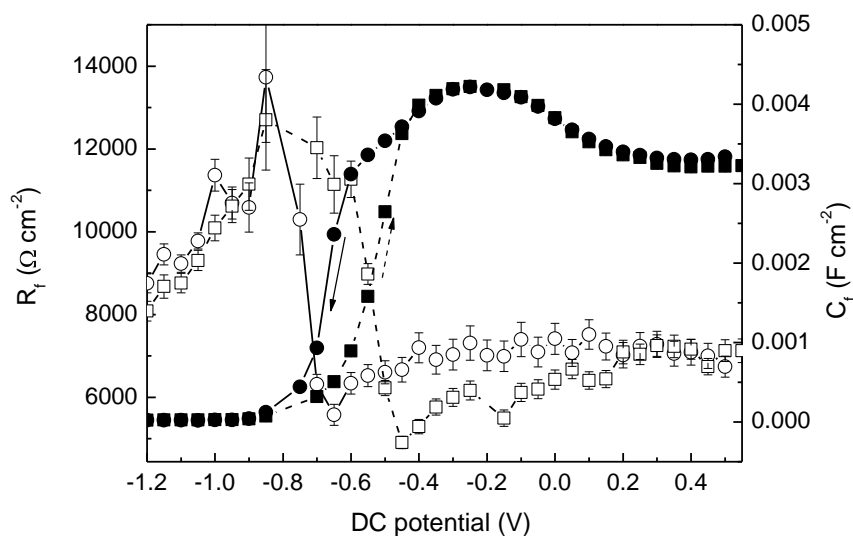


Figure 54. Parameters values obtained by fitting EIS results poly(MB54) film at different dc potentials.  $C_f$  is represented by filled symbols and  $R_f$  by empty symbols. Forward scan (from positive to negative potentials) is represented by circles and backward scan (from negative to positive potentials) by squares.

Therefore we carried out EIS on parent **PEDOT** films using the same conditions as for poly(MB54), to check whether there is an effect caused by the chemical **PEDOT** modification with the fluorinated lateral chain.

Figure 55 reports some of the EIS Nyquist and Bode diagrams taken during the forward scan. The results with the parent **PEDOT** system appear similar to that presented above for poly(MB54), showing a transition from “conducting states” in the oxidized highly capacitive form to the “insulating states” in the intrinsic form. The inset in Figure 55 reports a zoom at the highest frequencies. No particular features are observed for the frequency range used here. Effectively a semicircle at the high frequencies could be expected. Hass et al. [129] correlate this behavior at high frequencies to the interfacial properties while the medium and low frequencies behavior is correlated to the charging properties. However a complete study of the interfaces is out of the scope of our work and phenomena at high frequencies were not further studied.

Again a hysteresis between the forward and the backward scan is present (see Figure 56). In the **PEDOT** case the transition is broader, spanning from -0,1 V down to -0,5 V, while for poly(MB54), the transition is located between -0,4 V and -0,3 V. We

suggest that hysteresis phenomenon is correlated to the energy level difference between the lowest unoccupied level of the doped state when electronic injection is performed from metal to polymer under the forward scan and the highest occupied level state of the undoped state when injection from polymer to metal under backward scan occurs.

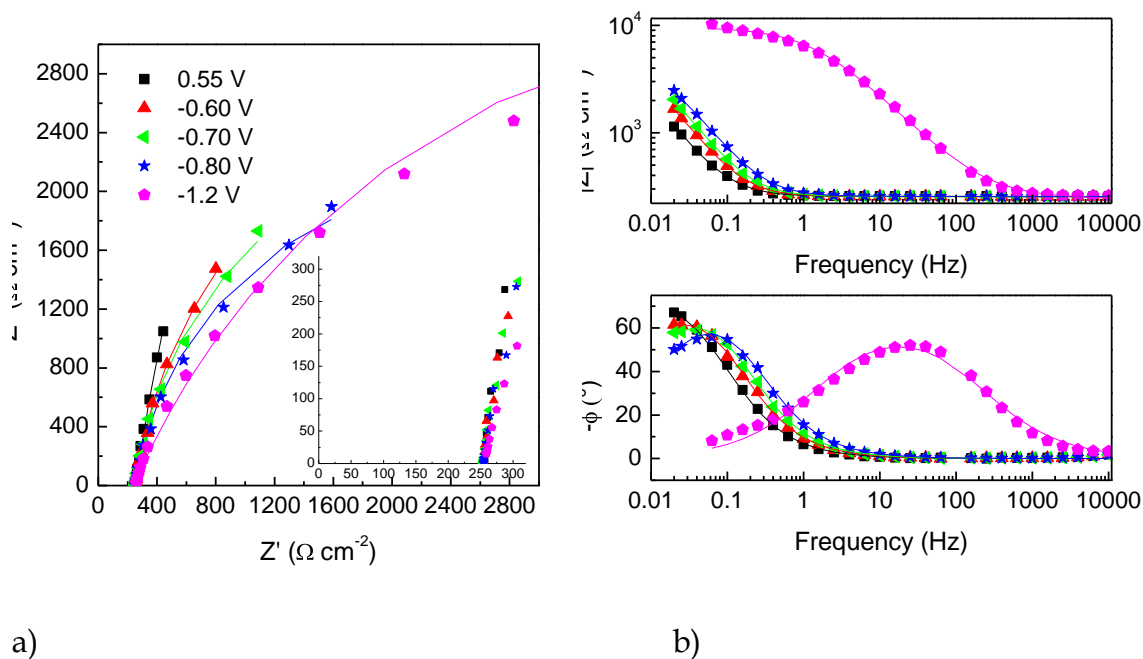


Figure 55. Nyquist (a) and Bode (b) EIS plots for PEDOT at different dc potentials. Symbols represents experimental points, lines represents fits results.

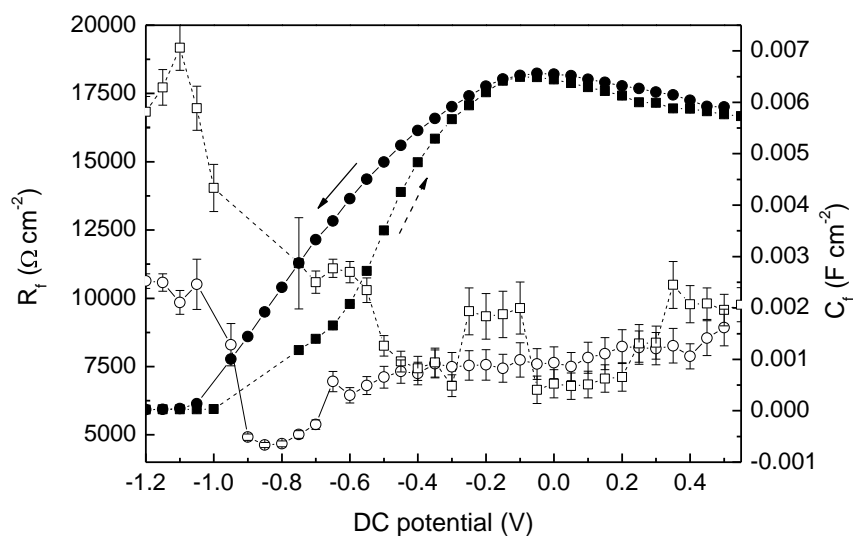
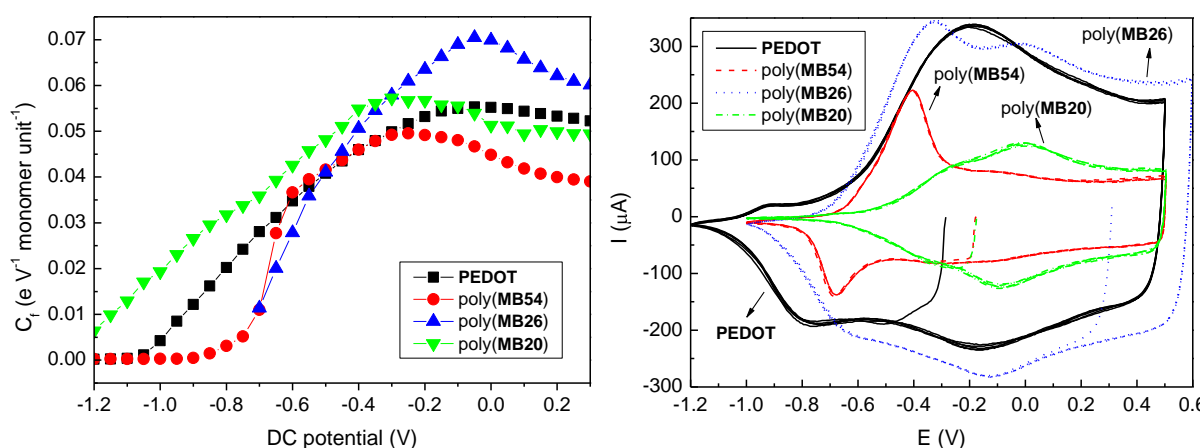


Figure 56.  $C_f$  (filled symbols) and  $R_f$  (empty symbols) values resulting from fit procedure at different applied dc potentials, during forward scan (from positive to negative potentials, circles) and backward scan (from negative to positive potentials, squares) for PEDOT.

Figure 57a reports a comparison of  $C_f$  parameter at different dc potentials for PEDOT and polymer electrodeposited from monomers MB54, MB26 and MB20. The capacitance was normalized on the number of repetitive units for each film (obtained from the charge necessary to deposit the polymer film in the approximation that the faradic yield is unitary) and expressed in elementary charge ( $1 \text{ F} = 1 \text{ C} / 1 \text{ V} \cong (1.602\text{E-}19)^{-1} \cdot 1 \text{ e} / 1 \text{ V}$ ). It can be seen that in the oxidized states the values of the capacitance for repetitive unit is similar for the different polymers, which indicates that the nature of the fluorinated side chain has not dramatic effects on the film doping.



a)

b)

Figure 57. a)  $C_f$  comparison of different polymer films (forward scan). b) Comparison of CV response for poly(1), poly(2), poly(3), and PEDOT.  $v = 20 \text{ mV/s}$ , 5 cycles, TEAP 0,05 M in acetonitrile.

One can see that all  $C_f$  curves present a maximum. For PEDOT and poly(MB26), the maximum is situated at about -0.05 V while for poly(MB54) and poly(MB20) it is shifted at about -0,025 V.

CV responses for the same potential zone are reported in Figure 57b. One can see that the films showing a broad transition from “conducting states” and “insulating states” in EIS experiments show a CV response that is also broader and characterized by ill-defined redox peaks. On the other hand poly(MB54) and poly(MB26) which show

characteristic and well defined redox peaks tend to have narrower transition in EIS experiments.

We suggest here that this difference possibly come from a different degree in polymers chains organization. It is known [130] that the presence of side chains on polyconjugated polymers, thanks to their interdigitation, leads to a better organization resulting in an increased conjugation length. Moreover the presence of fluorinated extremities is favorable to chains self-organizing [131].

Therefore the presence in poly(**MB54**) and poly(**MB26**) of a fluorinated terminal fragment in the lateral chain, separated from the conjugated polyheterocyclic backbone by a flexible aliphatic chain acting as spacer, could allow for a higher degree of organization, resulting in a narrower DOS for the energetic levels in the band gap created by the doping process with respect to parent PEDOT.

In poly(**MB20**), the CV response shows broader features which resemble those of the PEDOT again. The shorter side chain and the absence of an aliphatic spacer should be responsible for a lower organization degree.

The capacitance measured by EIS can be compared to the one measured from CV by the slope of the I (scan rate) curve (e.g. the slope in Figure 51b, insert). For poly(**MB54**) a capacitance of  $0,083 \text{ e V}^{-1} (\text{monomer unit})^{-1}$  is found at 0,0 V. From the graph in Figure 57a, we find a capacitance value, measured at the same potential by EIS, of about  $0,045 \text{ e V}^{-1} (\text{monomer unit})^{-1}$ . As expected measurements obtained by EIS give lower values of the capacitance than the ones obtained by CV. Indeed, CV correspond to a system that is not in a steady-state, and for which the current measured results from two contributions: the faradic one due to the redox processes on the polymer and the capacitive one due to the charging/discharging currents. Therefore the value of the capacitance obtained by the slope of the curve I (scan rate) overestimates the intrinsic capacitance of the electroactive film because of the contribution of the redox processes.

### **Electrochemical Quartz Crystal Microbalance analysis**

The doping process by perchlorate ions was further investigated by EQCM experiments. Figure 58 reports the EQCM signal corresponding to the deposition

process of poly(**MB54**). Figure 58b shows a peculiar stair profile for both resonant frequency variation and resonant admittance. Each step corresponds to the potential being swept at the beginning of the oxidation peak of compound **MB54**.

In the case of a thin rigid film the resonant frequency variation is directly proportional to the variation of mass as described by Sauerbrey equation [132]. Resonant admittance is related to resonance peak width. Moving from a rigid environment to more viscous one causes the widening of resonance peak and a diminution of the admittance. Such variation in energy dissipation mechanism is associated also to a resonant frequency variation as shown by Kanazawa and Gordon [133].

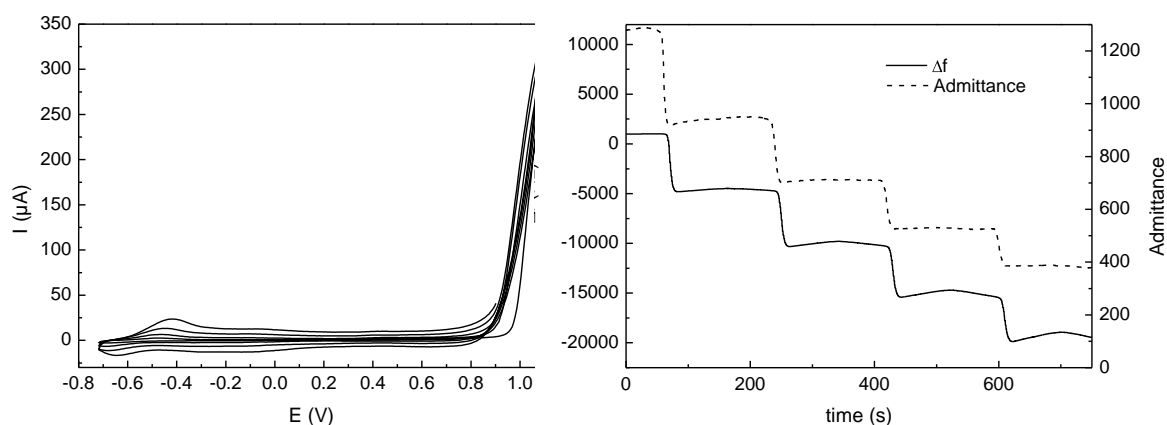


Figure 58. a) EQCM cyclic voltammogram corresponding to the electrodeposition of poly(**MB54**).  $v = 20 \text{ mV/s}$ ; b) corresponding quartz resonant frequency and resonant admittance.

In the case presented in Figure 58, the frequency steps always correspond to steps in the admittance. In such case we cannot apply the Sauerbrey approximation and the frequency variation is not directly correlated to mass increase because the deposition of the “thick” energy-dissipating polymer film causes the variation of quartz viscoelastic properties. It anyway demonstrates that for each cycle corresponding to oxidation potential of monomer **MB54**, a new polymer layer is deposited. The electrochemical doping by perchlorate ion was then studied following by EQCM the polymer response in TEAP 0,05 M in acetonitrile. CV (Figure 59a) shows a very particular redox response with two very strong peaks at ca -0,45 V (oxidation) and -0,7 V (reduction), followed by two redox processes at about -0,1 V (oxidation) and -0,25 V (reduction), The presence of such intense and narrow peaks that usually are

less visible in parent PEDOT (see Figure 57b), can be probably correlated to the transition observed in EIS response, much broader in the case of parent PEDOT.

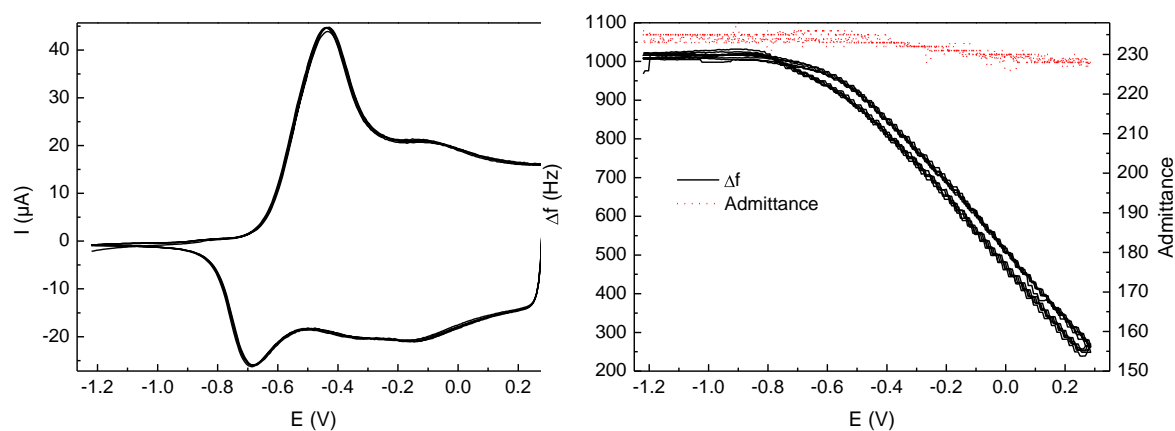


Figure 59. a) EQCM experiment, poly(MB54) CV response in TEAP 0,05 M in acetonitrile, b) frequency and admittance variation corresponding. 5 cycles,  $v = 20$  mV/s.

Figure 59b reports the corresponding variation in resonant frequency. One can see that over 5 cycles there is almost no variation in the resonant admittance and therefore we can apply Sauerbrey approximation, and consider the frequency variation directly proportional to mass variation. A diminution in frequency corresponds to an increase of resonating crystal mass. For potential lower than -0,8 V  $\Delta f$  presents a plateau, while over this potential the decrease is almost linear. We can assign this mass increase to the insertion of perchlorate ions into the electroactive films, to compensate the charge generated on the polymer chain. More interestingly we can see that the beginning of the mass increase potential, around -0,8 V, corresponds to the lowest limit of the transition observed in the EIS transition. Therefore EQCM measurements show that the “insulating states” observed in EIS correspond to the polymer that is counterions free, which means undoped.

In the case of the applicability of Sauerbray equation, our system was previously calibrated in order to associate frequency variation to mass variation [134]. It is found that a decreasing in frequency of 1 Hz corresponds to an increasing in mass of 5 ng  $\text{cm}^{-2}$ . Therefore the variation in frequency presented in Figure 59b of about -760 Hz (between -0.9 V and 0.6 V on the second scan) corresponds to a variation of ca 3.8  $\mu\text{g cm}^{-2}$ . We can express the mass increase for each repetitive unit (obtained from the charge necessary to deposit the polymer film in the approximation that the faradic

yield is unitary) that is  $1.13 \times 10^{-26}$  kg (monomer unit)<sup>-1</sup> which corresponds to 6,8 u (monomer unit)<sup>-1</sup>. If we assume that no perchlorate ion is present in the film at the lowest potential, this is equivalent to a mass gain of 0,068 perchlorate ion per monomer unit. We cannot exclude that some of the mass gain is also due to the incorporation of solvent molecules solvating the perchlorate in the film and therefore the value given is an overestimation of the doping rate of the film.

The value is comparable with what we also find by measuring the response of poly(**MB54**) by cyclic voltammetry. Integration of the current with respect to the time while cycling the polymer in the solvent in presence of the electrolyte gives the charge that is stocked in the polymer during the cycle. The ratio of the charge measured during response and the charge used for depositing the film gives an approximation of the doping level. For poly(**MB54**) on different films values of about 6 % are found. As discussed above this is also an overestimation of the doping level. In this case just the faradic component of the current should be considered to measure the quantity of perchlorate introduced to compensate the positives charges on the polymer, but it is hardly possible to separate this component from the capacitive one.

The measurements taken by EIS are made in steady-state and the fitting procedure allowed separating capacitive component from the resistive ones. Integration of the values of  $C_f$  (expressed in the measure units used in figure 7a) with respect to the potential allows for the calculation of the charge that is stocked in the polymer for each repetitive unit at a given potential.

The result of integration of  $C_f$  is reported in Figure 60. The charge is compared to the variation in mass measured by EQCM. Mass variation has been expressed in perchlorate ion mass units per monomer unit to make it comparable with the charge curve. The similarity in between the curves is striking which confirms the validity of our model. Anyway it can be seen that a multiplicative factor as to be introduced to have the curve superimposing.

That can be explained by a neutral molecule accompanying perchlorate ions entering in the film. This can be clearly the solvent molecules solvating perchlorate ions and enough strongly bounded together to induce crystal frequency shift.

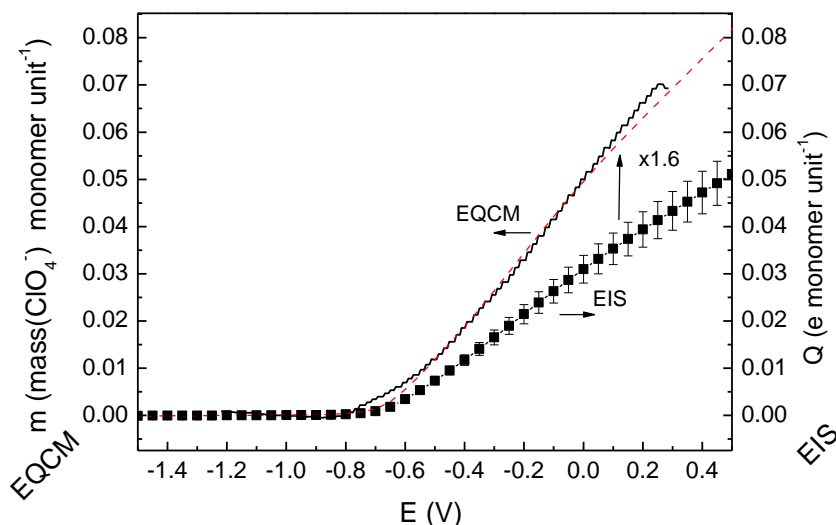


Figure 60. Comparison of data obtained from EQCM and EIS on poly(MB54) doping by perchlorate ions. The solid black curve reports EQCM mass variation expressed in perchlorate ion mass units normalized to the number of EDOT units present in the film. Squares reports the charge presents in the film obtained by integration of  $C_f$  parameter obtained by fitting of EIS data. Charge is expressed in proton charge units and normalized to the number of EDOT units present in the film. The red dashed curve was obtained by multiplying by 1,6 data represented by squares (EIS obtained).

For poly(MB54) integration of Figure 57a gives doping level of 0,043 for each monomer unit at 0,3 V. This value is lower than what estimated by CV response and EQCM, but is more likely to correspond to the true value of the doping level because the other two techniques overestimate the doping level as discussed above.

The ratio in between the doping level as measured by EQCM and the one measured from EIS is about 1,6, this can be explained by assuming that each perchlorate inserted in the film upon oxidation is accompanied in average by 1,4 solvent molecules.

At 0,5 V (that is the maximum potential we used in EIS) the doping level for repetitive unit is found at 0,053. The doping levels reported here are lower than the maximum electrochemical doping levels reported in literature for PEDOT and PEDOT derivatives [135] but the conditions used for the experiments above were not optimized in order to obtain best doping levels.

Looking more closely to Figure 58b, it is possible to observe that input/output of perchlorate ions within the films was already shown during the film growth. Actually the plateau steps shown in Figure 59b change during the growth of the film. After the first step, the  $\Delta f$  signal corresponding to the area where no oxidation of the monomer occurs is completely flat, while in the following steps it becomes more and more “roof-shaped” corresponding to the leaving of perchlorate during film reduction, followed by re-entering of ions when the film is oxidized.

As one can observe from Figure 59b the hysteresis observed in EIS measurements corresponds also to a small mass variation hysteresis due to the perchlorate ions film filling.

### XPS analysis

Polymers deposition and electrochemical doping of monomers was confirmed by XPS measurements. By integrating all elements having most intense core peaks, and normalizing areas by Scofield factor, we could estimate the chemical composition of the electrodeposited films. Ratio between the normalized areas and the chemical formulas are consistent, with average differences close to the percent (the maximum difference found was at 4%) showing that electropolymerization does not induce lateral chain degradation. The results are summed up in Table 4.

	C <sub>th</sub>	C <sub>exp</sub>	F <sub>th</sub>	F <sub>exp</sub>	O <sub>th</sub>	O <sub>exp</sub>	S <sub>th</sub>	S <sub>exp</sub>
poly(MB54)	0.53	0.50	0.27	0.31	0.18	0.16	0.03	0.03
poly(MB26)	0.50	0.52	0.39	0.38	0.09	0.08	0.02	0.02
poly(MB20)	0.43	0.45	0.43	0.42	0.11	0.11	0.03	0.03

Table 4. Atomic ratio calculated from XPS peaks area (Scofield factor normalized, exp) compared with values expected from chemical formulas (th).

The survey spectrum of a reduced-state polymer is reported in Figure 61. No platinum peak can be seen, which insures the film is thick in respect to the XPS mean free path, homogeneous and covering. The absence of chlorine peaks is also indicative of the absence of perchlorate ions in the films in intrinsic state.

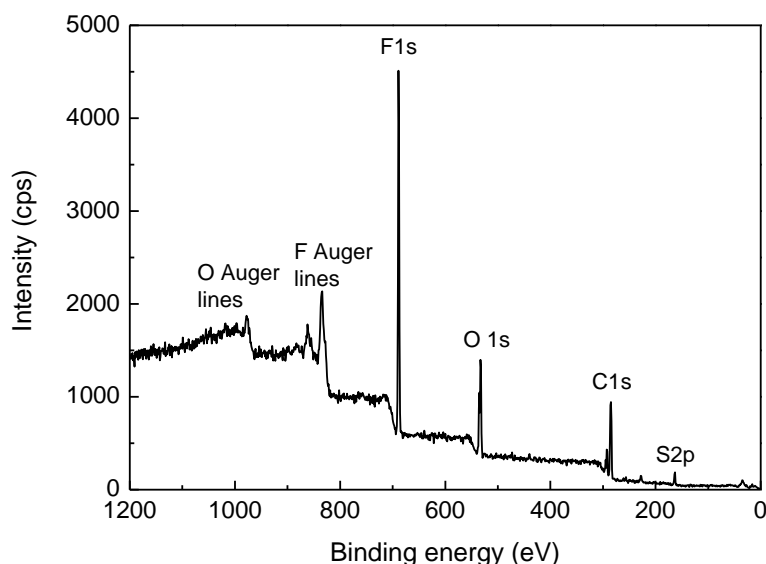
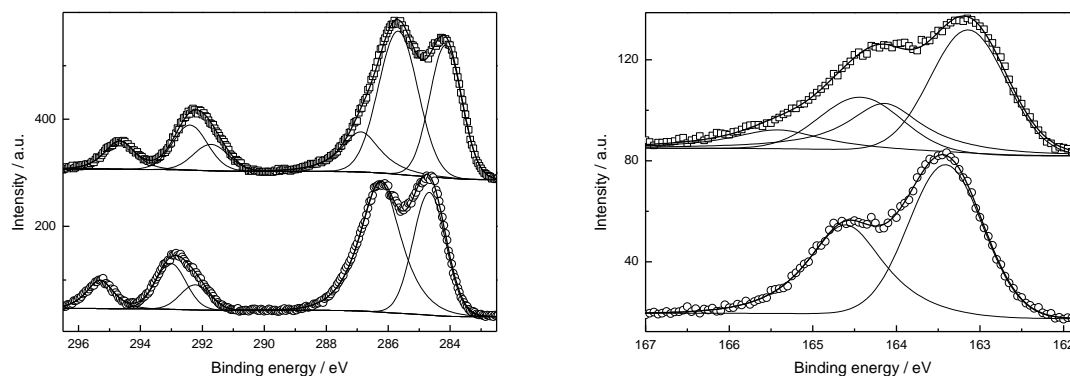


Figure 61. XPS survey spectrum of films of poly(MB54) in the reduced state.

Figure 62a (circles) reports the  $C_{1s}$  core level spectrum. One can distinguish clearly at least four peaks, the peak at 295,3 eV is assigned to the  $-CF_3$  components, the broad and asymmetric peak at 292,8 eV is assigned to a  $-CF_2-$  component, with higher energy component at 293,0 eV assigned to the carbon bonded to oxygen and another  $CF_2$  and the lower energy component at 292,2 eV assigned to carbon bonded with an oxygen atom and a  $CH_2$ . The area ratio is consistent with the hypothesis.

The component at 286,2 eV is assigned to aromatic carbons (subjected to S effect), and the component at 284,6 to aliphatic carbons.

Figure 62a (squares) reports the  $C_{1s}$  XPS core level spectrum for the same film but now electrochemically doped by applying a linear sweep at 5 mV/s in TEAP 0,05 M in acetonitrile from the equilibrium potential (-0,7 V) to 0,55 V. We observe the same peaks as above, but the broad peak between 282 eV and 289 eV shows a widening on high energy side, which needs for fitting an additional component centered around 286,7 eV. This component corresponds to the formation of delocalized positive charges on the polyconjugated chain. The presence of a positively charged carbon component for the oxidized state is also evident from peaks intensities modification, since for the unoxidized film the peak around 286 eV is more intense than the peak around 285 whereas for the oxidized film the trend is inversed.



a)

b)

Figure 62. a)  $C_{1s}$  core level spectrum of films of poly(MB54) in the reduced state (circles) and in the oxidized state (squares); b)  $S_{2p}$  core level spectrum of films of poly(MB54) in the reduced state (circles) and in the oxidized state (squares).

This presence of charge on the main chain is also shown by the  $S_{2p}$  core level spectra. For the undoped form, the  $S_{2p}$  core spectrum (shown in Figure 62b) can be decomposed in two components at 163,4 eV and 164,6 eV, accounting for the  $S_{2p_{3/2}}$  and  $S_{2p_{1/2}}$  levels. The same spectrum for the oxidized form is reported in Fig. 12b, which shows a component at higher energy accounting for positive charge presence on the polythiophenic chain [136]. It was also possible to follow the presence on perchlorate counterions by the  $Cl_{2p}$  core level peaks appearing in the oxidized form spectrum (not shown here).

#### 5.4 Grafting of poly(methacrylate)s/PEDOTs composites and physical chemistry characterizations

##### Electropolymerization of EDOT and derivatives on gold electrodes

The preliminary studies on fluorinated PEDOTs presented in the section above were conducted on platinum electrodes.

The first matter we had to consider when passing on gold substrates was the electrochemical behavior of that metal in the conditions used for the electrosynthesis on PEDOT.

A linear sweep of the gold electrode in acetonitrile and TEAP 0,05 M is reported in Figure 63. As one can see there is an anodic current starting from about 0,8 V and

constantly increasing. At 1,1 V the current reaches quite high densities (above 130 mA cm<sup>-2</sup>).

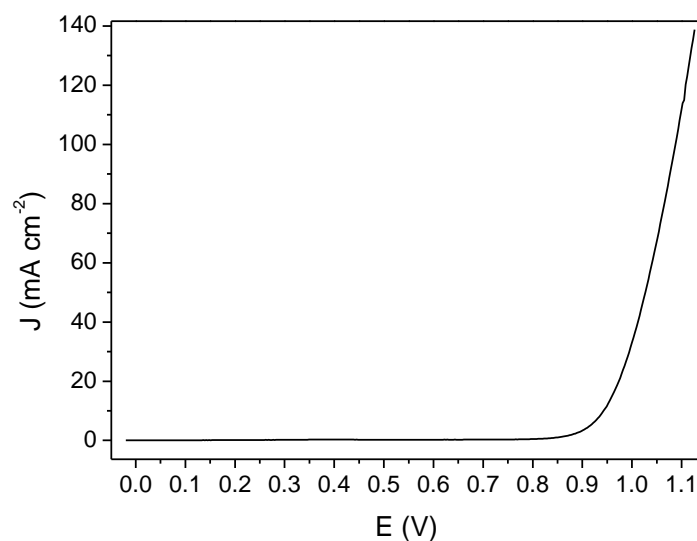


Figure 63. Potential sweep on a gold electrode (bulk gold wire) in acetonitrile TEAP 0,05M, scan rate 20 mV/s.

The measured current is due to the oxidation of gold with the corresponding dissolution of the metal in the electrolytic solution [137].

Dissolution of the electrode during the electropolymerization of PEDOT could be an issue for obtaining homogenous polymer films of the surface.

The electrosynthesis of PEDOT and other conducting polymers on platinum has been extensively studied. This metal presents the advantage of being stable in the electrochemical conditions used for the electropolymerization and therefore it is adapted for studies on the fundamental mechanisms.

Articles have also been published about the anodic electropolymerization on oxidable metals (nickel, steel, etc.). In those case strategies based on applying peculiar potential signals (trapezoidal waves) [138] or electrode surface modification by adsorbed molecules [139-141] are necessary in order to obtain adhering and homogenous films.

Fewer works have been published on the anodic electropolymerization on gold of PEDOT or other polyconjugated polymers. In those cases, to our knowledge, the matter of electrode corrosion was not treated [142].

We tried anyway to perform electropolymerization of EDOT on gold electrodes either by cyclic voltammetry or chronoamperometry. Typical cyclic voltammograms recorded during the electropolymerization of EDOT on platinum and gold electrodes are reported in Figure 64.

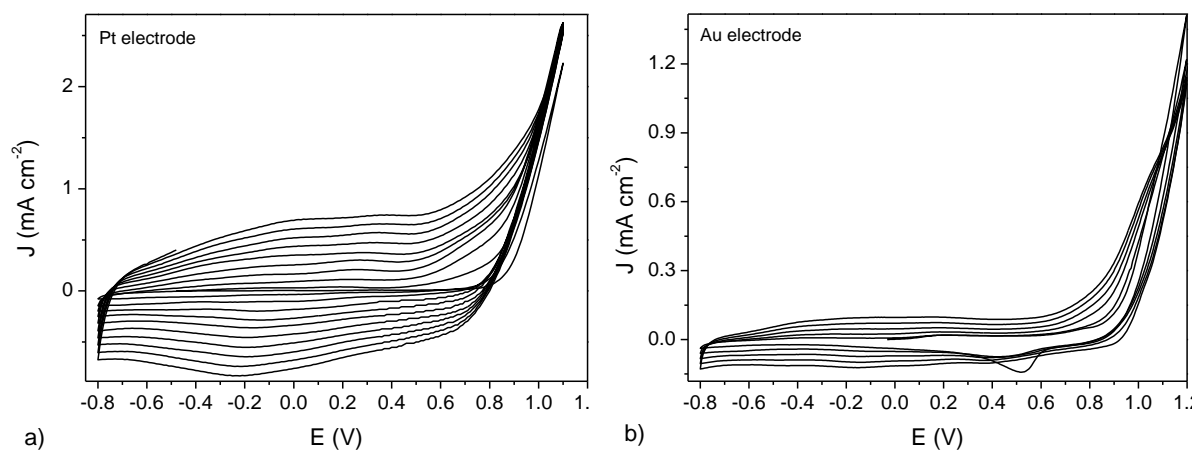


Figure 64. Cyclic voltammograms recorded during the electropolymerization of EDOT in acetonitrile TEAP 0,05 M on: a) platinum electrodes, b) gold electrodes. Scan rate 20 mV/s, monomer concentration 0,005 M.

On both metals a colored film was observed on electrode surface after the experiments. Films obtained on gold electrodes were generally more easily scratched than the ones on platinum.

In fact the oxidation potential of the monomer is in the same range of gold one. The formation of the polymer film protects the surface from dissolution. This can be seen by comparing the values of current density obtained for positive potential (e. g. 1,1 V) in the absence (Figure 63) or in presence of the monomer (Figure 64b). In the former case very high currents were measured, while the presence of the monomer, which causes the formation of a polymer film when the positive potential is applied, leads to a diminution of the current density of a factor 100.

The shape of the voltammograms recorded on platinum and gold exhibit the characteristic onion-like shape of PEDOT growth by cyclic voltammetry. For each cycle, when the potential is swept to enough positives values, more polymer is deposited on the electrode surface. Because electrochemical response of PEDOT modified electrodes is characterized by high capacity (as discussed in section 5.3) a

bigger capacitive currents is measured at each cycle resulting in the onion shaped voltammogram.

In the case of the voltammograms recorded on the platinum electrode (Figure 64a) the increase of capacitive current from one cycle to the following is bigger than that for the gold electrode (Figure 64b) (onion layers are thicker). This indicates that the film growth is more efficient on platinum rather than on gold. Two interpretation of the phenomenon are possible: the first one is that the gold oxidation is a competitive process to polymer growth; the second is that the loss of gold atoms from the surface also induces a loss of the polymer that was already present on the surface.

A feature that is present on the voltammograms recorded on gold but not in the one recorded on platinum is the presence of a reduction peak at about 0,53 V. The intensity of this peak was not well reproducible on different experiments. The peak is recorded just in correspondence of the first cycle when scanning the potential from positive to negative values. The peak is likely due to the reduction of the gold present in the electrolytic solution after the anodic dissolution.

It was reported [137] that traces of water can inhibit gold electrodes dissolution. In normal environmental conditions the gold surface is recovered by a thin film of "gold oxide". This ephemeral oxide is destroyed by immersing the surface in anhydrous organic solvents. Adsorption of water molecules on the surface results in increasing the stability of this layer [143].

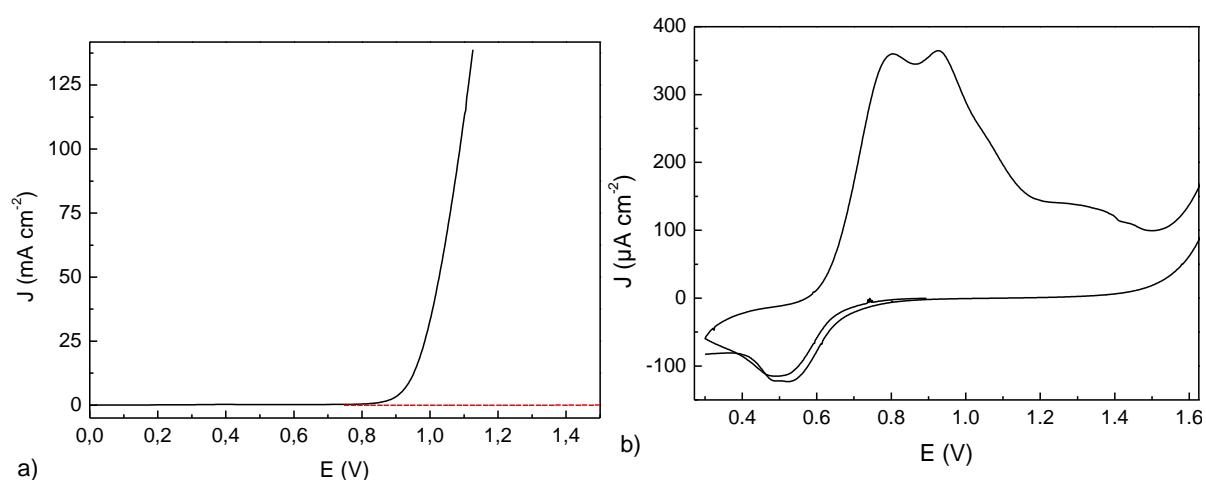


Figure 65. a) Linear sweep voltammetry of gold electrode in anhydrous acetonitrile (solid black line) and after addition of water (0,1 mM, red dashed line) b) Cyclic voltammetry of "gold oxide" layer in acetonitrile added with 0,1 mM of water. TEAP 0,05 M as supporting electrolyte, scan rate 20 mV/s.

Figure 65a reports the linear sweep of the gold electrode in acetonitrile anhydrous (solid line) and after the addition of water (dashed line). In the case of anhydrous acetonitrile, as we already reported above, the current increases continuously with the applied potential. The oxidation of gold in anhydrous acetonitrile leads to the dissolution of gold and the formation of Au<sup>+</sup> ions in the solution [137].

When the water is added the anodic current is strongly reduced.

Figure 65b reports a cyclic voltammetry recorded for the gold electrode in the acetonitrile added with water. Different features are visible. Two oxidation peaks are clearly delineated at 0,8 V and 0,92 V. A reduction peak is found at about 0,5 V.

Electrochemical oxidation of gold in aqueous solution containing perchlorate ions has been extensively studied by Antoinette Hamelin [143-147].

The proposed mechanism is the following. At potentials somewhat positives to the PZC a reversible electrostatic adsorption of water and perchlorate anions is observed. Then by increasing the potential the perchlorate anions are desorbed. The two peaks observed correspond to the two electron transfers:



where AuOH and AuO represents a chemisorbed state of OH and O on Au surface. The two peaks observe in Figure 65b) corresponds to the two electron transfer. The cathodic peak observed is due to the reduction of AuO layer. The values found are in agreement with the data reported in the literature for the oxidation of gold in neutral and acid solutions.

These findings, showing that gold oxidation is enhanced in strictly anhydrous conditions, are somewhat surprising because they demonstrate that films obtained in careful and clean electrochemical conditions will have worse properties than film obtained in less controlled conditions. Thus the electropolymerization of PEDOTs for fabricating films used in the tribology tests on “bronze coupons” substrates has been conducted outside the dry box and using technical grade acetonitrile.

The strategy used for building the dual film of fluorinated poly(methacrylate)s and PEDOTs was as follow. First poly(methacrylate) was electrografted by cathodic polymerization in DMF/THF (in a dry box and strictly anhydrous conditions). Then

the films were put in a new electrochemical bath (outside the dry box) containing the EDOT derivative monomer where we conducted anodic electropolymerization. Because the poly(methacrylate) films are insulating but swollen by the electrolytic solution the fluorinated PEDOT has to grow through them (Figure 66).

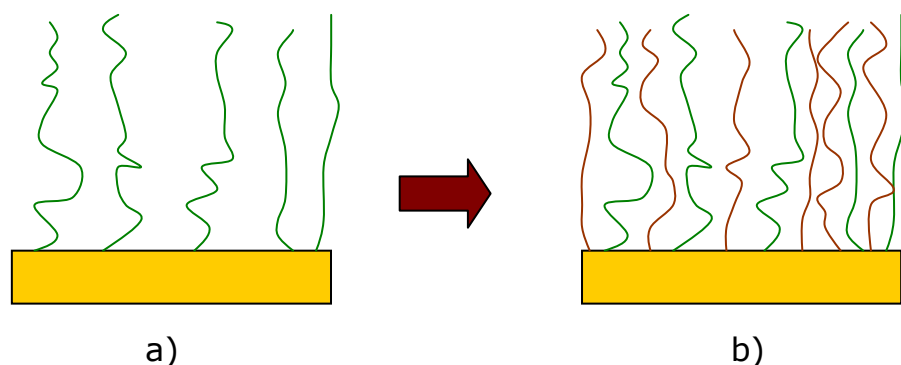


*Figure 66. Steps for the growth of composite films of fluorinated poly(methacrylate) and fluorinated PEDOT derivative. a) cathodic electrografting of the poly(methacrylate) followed by b) anodic electropolymerization of the EDOT derivative monomer.*

At this stage fluorinated PEDOT were deposited by chronoamperometry by imposing a potential of 1,1 V. The duration of the pulse was chosen by first fabricating a series of films on uncoated gold and measuring their thickness by mechanical profilometry. This allowed determining by extrapolation for what potential step duration a film between 10 and 20 nm thick on uncoated gold was obtained (about 5 s). The same time was used for the potential step applied when growing the fluorinated PEDOTs derivatives through a pre-grafted fluorinate poly(methacrylate).

### **XPS characterization**

Characterization of the dual films is necessary to insure that the deposition of fluorinated PEDOT is effective and that the anodic polarization does not cause the degrafting of the fluorinate poly(methacrylate).

Anyway characterization of a film containing both fluorinated poly(methacrylate) and fluorinated PEDOT is not straightforward with classical surface science techniques.

For that reason first composites made of parent PEDOT and PHFBM were fabricated for XPS characterization. The survey spectrum of the film is reported in Figure 67.

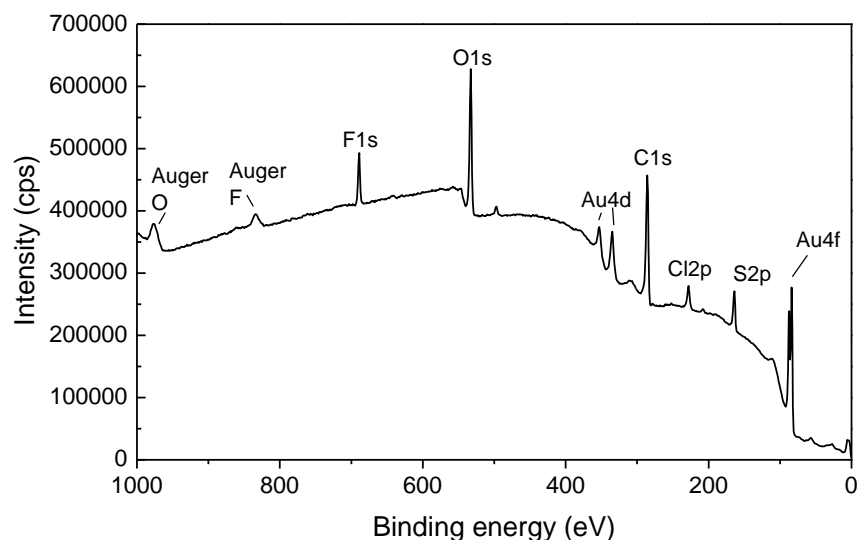
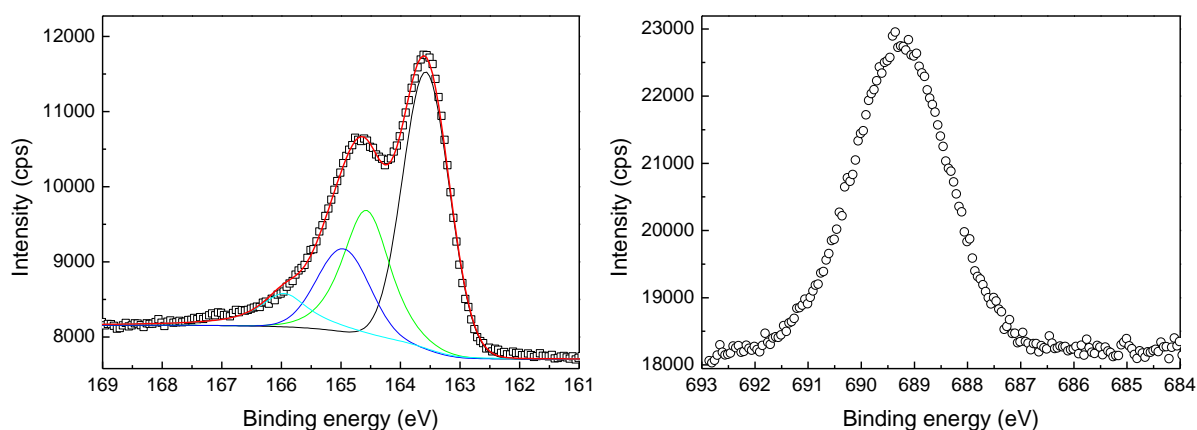


Figure 67. XPS survey spectrum of a film obtained by cathodic grafting of PHFBM followed by anodic electropolymerization of EDOT.

The presence of the sulfur atom S2p characteristic peak insures that the PEDOT is effectively present in the film. At the same time the observation of the F1s peak correspond to the presence of the grafted PHFBM. The simultaneous observation of the signatures of fluorine and sulfur also testify that the amount of the two deposited polymers is comparable. The presence of Cl2p peak is due to doping of PEDOT by perchlorate anions.

Figure 68 reports the spectrum of the Sp2 peak and F1s peak. Sp2, which has to be decomposed taking in account the Sp1/2 and S2p3/2 levels. The decomposition has to consider sulfur at higher energy because of the doping by perchlorate ions as discussed in section 5.3.



a)

b)

Figure 68. XPS core spectra of a film obtained by cathodic grafting of PHFBM followed by anodic electropolymerization of EDOT. a) S2p b) F1s.

### Infra Red characterization

Good infra red characterization was possible for composites of PHFBM and poly(**MB20**). An ATR-IR spectrum of such film is reported in Figure 69.

Parent **PEDOT** films have IR absorption bands in the region  $1500 - 800 \text{ cm}^{-1}$ . It is therefore difficult to use them to univocally identify the polymer because it is a region where IR absorptions of organic matter concentrate. Moreover it is possible to record a spectrum of the polymer showing definite peaks just for film in the undoped state. When films are in the doped state they present a broad absorption in the IR (due to the formation of polaronic and bipolaronic levels) and this masks the absorptions coming from molecular vibrations.

Spectra of poly(**MB26**) and poly(**MB54**) also do not have a characteristic signature that allows to easily identify them.

On the contrary poly(**MB20**) films IR spectra presents a characteristic peak due to the stretching of the carbonyl  $\text{-C=O}$  bond in the ester group. Moreover due to the direct bonding of the perfluorinated chain to the alcoholic atom of the ester group the stretching vibration is found at  $1790 \text{ cm}^{-1}$ . In PHFBM the electroactive effect of the fluorinated chain on the carbonyl is reduced because of the presence of the  $\text{-CH}_2\text{-}$  spacer between the alcoholic oxygen and the perfluorinated segment of the chain. Thus the stretching frequency is at lower energies, i. e.  $1755 \text{ cm}^{-1}$ . As can be see in

Figure 69 this is sufficient for separating the vibration frequencies of the carbonyl group in the two polymers.

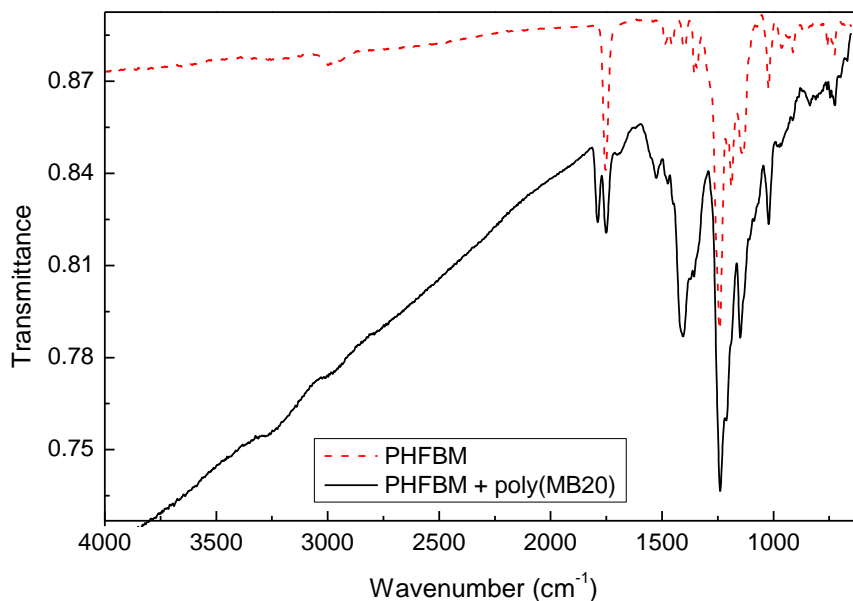


Figure 69. ATR-IR spectra taken during the fabrication step of a PHFBM/poly(MB20) composite film. Red dashed line is the spectrum recorded after the grafting of PHFBM (step 1). Solid black line is the spectrum recorded after the electropolymerization of MB20 (step 2).

The dashed red line is the spectrum that is recorded after the cathodic electrografting of PHFBM. Black solid line reports the spectrum recorded after growing poly(MB20) through the pre-grafted PHFBM matrix.

The derive of the spectrum baseline is observed after growing the poly(MB20). We always observed derive of the spectrum baseline for PEDOT and its fluorinated derivatives especially when in the doped state. The peak at 1790  $\text{cm}^{-1}$  appears which attests the presence of poly(MB20) on the surface.

For composites with PEDOT, poly(MB54) and poly(MB26) the IR spectra are less explicit and the deposition of the polyconjugated polymer resulted just in a broader absorption in the whole spectral range and in the spectrum baseline deriving.

### 5.5 Study of the tribological properties of the poly(methacrylates)s/PEDOTs composites

We already reported in section 4.5 the tribological behavior at 1 N of applied normal force for PHFBM films grafted on gold from THF/DMF electrolytic solutions.

At 1 N the behavior of the composites of PHFBM with fluorinated derivatives of PEDOT is similar to that of pure PHFBM. Results for a tribo-electrical test obtained on PHFBM and PHFBM + poly(MB20) and poly(MB54) are reported in Figure 70. The friction coefficient values are in between 0,1 and 0,2 during all the experiment which indicates a good lubrication and wear resistance of the films.

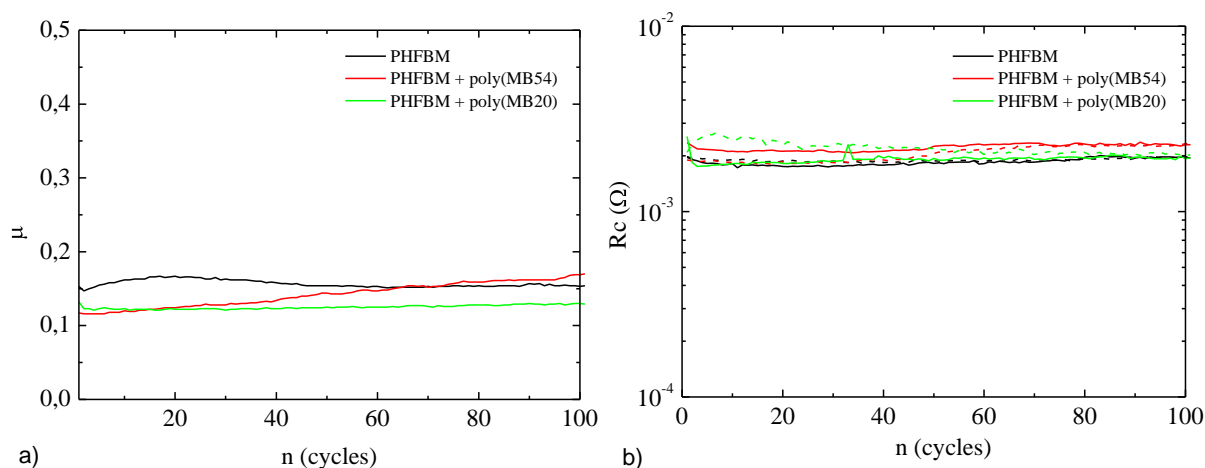


Figure 70. Tribo-electrical test on grafted PHFBM films (black lines), PHFBM/poly(MB54) (green line) and PHFBM/poly(MB20) (red line) composites. a) evolution of the average friction coefficient b) measures of the electrical contact resistances for each cycle recorded at the track ends. Applied normal force 1 N.

The results on the electrical contact resistance are reported in Figure 70b. As mentioned before two lines are present (solid and dashed) for each experiment and correspond to measurements made at the two ends of the wear track. We already discussed in section 4.5 the electrical contact resistance values for PHFBM films electrochemically grafted in DMF/THF solutions and compared them to the uncoated gold. The difference in contact resistance between the uncoated gold and the PHFBM grafted substrates is small because of the thinness of the films. The film is pinned in between the asperities allowing the current to flow disregarding the insulating materials added in the interface.

The addition of the semiconducting polymer is not reducing further the electrical contact resistance and a similar evolution is found in between the three different samples.

PEDOT has one of the best conductivity among the family of polyconjugated polymers. In the doped state the conductivity reaches values of  $650 \text{ S cm}^{-1}$ , while in the undoped state conductivities are around  $10 \text{ S cm}^{-1}$  [135, 148]. We have therefore

chosen PEDOT derivatives as best candidates for improving the electrical conduction properties of PHFBM films among all the possibility of organic semiconductors.

Anyway, if compared to metals, PEDOT conductivity remains very low. The best conductive metals as silver, copper and gold have respectively conductivities of 630 kS cm<sup>-1</sup>, 596 kS cm<sup>-1</sup> and 452 kS cm<sup>-1</sup> [149].

If no significant contribution to the electrical contact resistance comes from the insulating polymer film present at the interface and the same value of resistance is found for an unprotected direct gold/gold metal contact and for the contact with the film in the interface, it is therefore logical that the addition of a conducting film with lower conductivity with respect to gold is not able to further enhance conduction.

Although in our experimental setup it was not possible to measure a beneficial effect of the addition of conductive polymer in the PHFBM matrix this does not mean that the approach is uninteresting. In our setup the contact electrical resistances were measured in a macroscopic setup and using rough ball and plane. The roughness of the substrates  $R_a$  is about 0,25  $\mu\text{m}$ , with maximum asperities of about 20  $\mu\text{m}$  when the grafted film has a nanometric thickness. In this setup, which simulates the life of industrial wide-spread low-level electrical connectors, the contact resistance is quickly dominated by the asperities.

In some other possible application of grafted thin films as dry lubricants the different conditions could change the role of the added conductive polymer. E. g. in an application to MEMS, the area of the contact surface is going to be the same of just one of the many asperity to asperity contacts that compose a macroscopic contact. Moreover in more technological applications, like in aerospace industry, it is likely that mechanical surface finishing is going to be better and that the surfaces will be smoother than the ones we studied. In those cases the role played by the asperity contacts is going to be smaller.

Because almost no differences were observed at 1N in between the PHFBM and the PHFBM composite with PEDOTs and all the films stand the test showing much almost no wear more severe tests were effectuated at 2,5 N.

Figure 71 reports the evolution of the friction coefficient and of the contact resistance for films of PHFBM alone and for PHFBM/poly(**MB54**) and PHFBM/poly(**MB20**) composites with a 2,5 N applied normal force for 800 cycles.

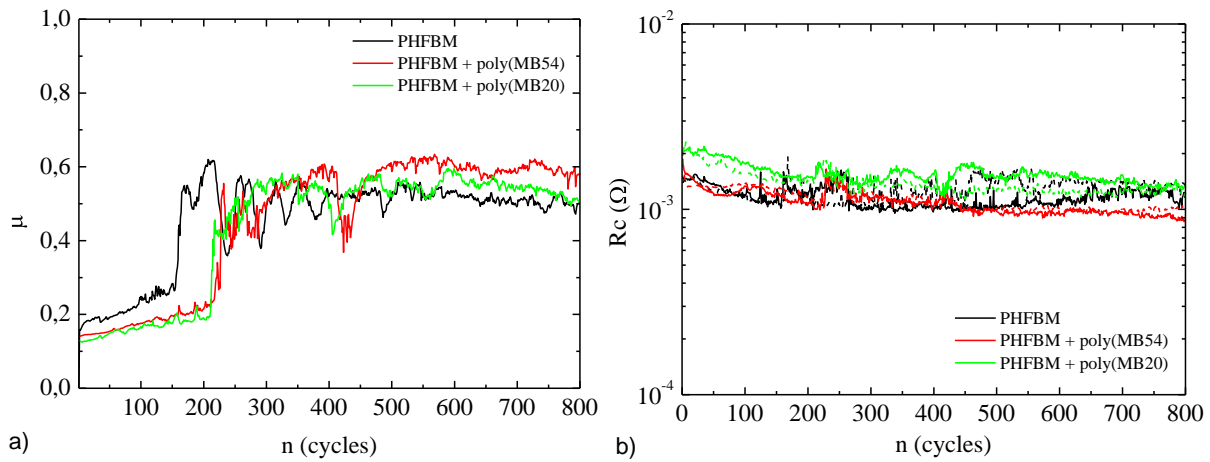


Figure 71. Tribo-electrical test on grafted PHFBM films (black lines), PHFBM/poly(**MB54**) (green line) and PHFBM/poly(**MB20**) (red line) composites. a) evolution of the average friction coefficient b) measures of the electrical contact resistances for each cycle recorded at the track ends. Applied normal force 2,5 N.

Application of that high load causes a different behavior for the evolution of the average friction coefficient. While the friction coefficient starts again from low values in between 0,1 and 0,2 for all the different kinds of sample, it does not remain constant for all the experiment as was recorded at 1 N. For PHFBM a steep variation in friction is observe at about the 150<sup>th</sup> cycle: the average friction coefficient increases to values of almost 0,6 and remain that high (with some oscillation) for all the rest of the experiment. For the composites films with poly(**MB54**) and poly(**MB20**) the steep variation is observes at about the 220<sup>th</sup> cycle.

The steep friction coefficient is even more easily seen by plotting the friction coefficient maps. Figure 72 reports the values of the instantaneous friction coefficient for the PHFBM + poly(**MB20**) which corresponds to the data presented in Figure 71. Before the cycle number 210 the friction coefficient is on low values between 0,1 and 0,2 in all the positions in the wear track. Then again a critical event happens and the friction coefficient immediately increases to high values in between 0,6 and 0,8.

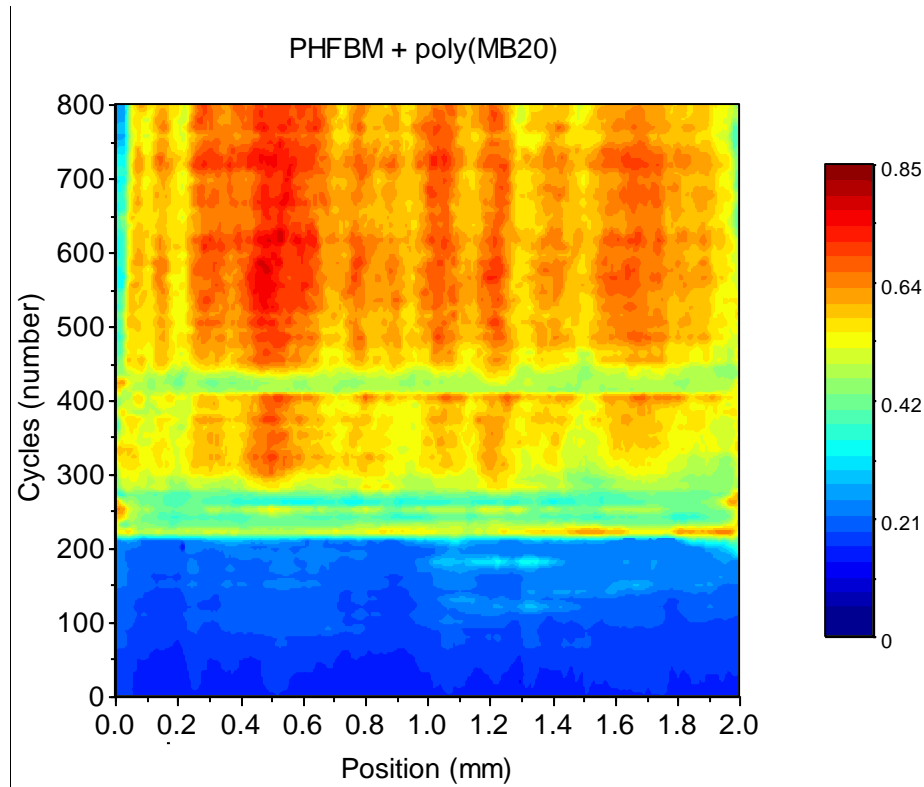
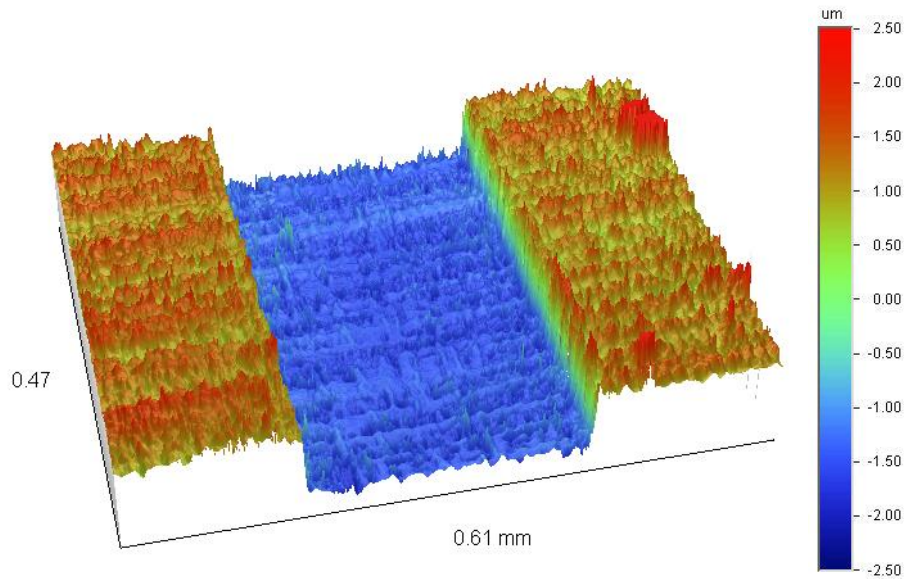


Figure 72. Color representation of the friction coefficient values at the different spatial position in the wear track ( $x$ -axis) for different cycles number ( $y$ -axis). Data presented correspond to the one in Figure 71. The applied normal force is 2,5 N.

As we already discussed in section 4.5 for the tribological properties of PBUMA films, friction coefficients greater than 0,6 are even too big to correspond to the gold on gold friction. For the uncoated gold at 2,5 N see for example Figure 29, in that case friction coefficient is in between about 0,4 and 0,6.

We hypotize that the step transition observed in the evolution of friction coefficient corresponds correspond to the failing of the gold/nickel interface in the substrate or in the ball. This is confirmed by observing the optical profilometry results obtained on the wear track (Figure 73).



*Figure 73. Optical profilometry of part of the wear track of a coupon coated with PHFBM + poly(MB20) after a tribology test of 800 cycles with 2,5 N normal force applied. The wear track corresponds to the experiment reported in Figure 71.*

A deep track of about  $2\mu\text{m}$  is observed. Because coupons were fabricated by galvanoplasty by depositing  $2\mu\text{m}$  of nickel followed by  $2\mu\text{m}$  of gold on massive bronze, the depth of the wear track corresponds to the thickness of the gold layer present on the coupons. In the bottom of the wear track the original lamination stripes of the substrate are still visible. This hints for an abrupt fail of the interface in between the gold and the nickel which will justify the abrupt transition observed in the friction coefficient.

This assumption that gold is removed and that nickel it is exposed was confirmed by taking XPS spectra in the wear track. Spectra will be reported in chapter 6 and discussed in more detail.

The PHFBM film is grafted on the gold surface by a covalent bond. This results in a mechanically stronger polymer/gold interface with respect to the gold/nickel interface. Thus the weakest part in the system is the gold/nickel interface and it is the part that fails first during the test.

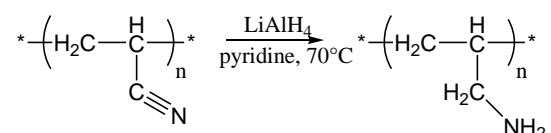
## 5.6 Elaboration of composites of poly(methacrylate)s and adsorbed nanotubes

### Grafting of PAN and chemical reduction to PAA

The first matter that had to be solved for using the technique of carbon nanotubes 2D-networks adsorption on amines as in [119, 120] was the functionalization of gold substrates by this function. In the cited works the functionalization was made by using APTS (3-(aminopropyl)triethoxysilane). This procedure works well on silicon oxide surfaces, as e. g. glass or silicon. On inert metals, as gold, this functionalization is not possible.

In our work the ideal functionalization is constituted of a covalently bonded and extremely thin organic film presenting amine functions.

The solution we implemented for grafting such a film was a two steps procedure: in the first step we grafted an ultra thin film of PAN, in the second step we chemically reduced the film by using the classical reducing agent  $\text{LiAlH}_4$ . The reaction was conducted by immersing the substrate with the grafted film in a solution of  $\text{LiAlH}_4$ . The occurring reaction is reported in the scheme below.



*Scheme 4. Chemical reduction of PAN to PAA by lithium aluminum hydride ( $\text{LiAlH}_4$ ).*

The chemical reduction of PAN by  $\text{LiAlH}_4$  leads to the transformation of nitrile groups into radical terminating with a primary amine. Therefore, if the reaction is complete, PAN is transformed into PAA (poly(allylamine)).

The reaction was followed by ATR-IR spectroscopy. Results before and after the reduction are reported in Figure 74.

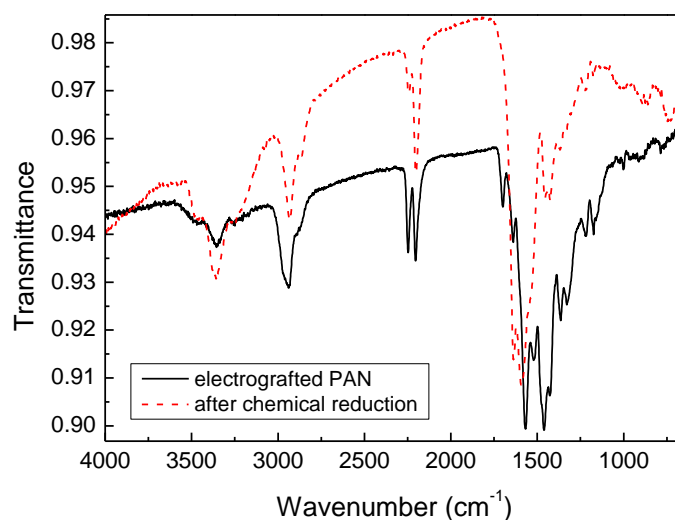
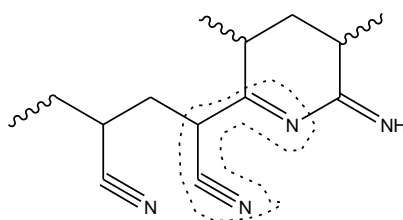


Figure 74. ATR-IR spectrum recorded for a PAN electrografted film (solid black line) and the spectrum recorded after chemical reduction to PAA (dashed red line) by  $\text{LiAlH}_4$ .

The PAN spectrum is characterized by the peak  $2247\text{ cm}^{-1}$  corresponding to the nitrile group (stretching frequency) [81]. The peak at  $2200\text{ cm}^{-1}$ , which normally is not observed for “classical” acrylonitrile solution polymerized is typically observed for PAN electrografted at “low” monomer concentration (typically  $0,5\text{ M}$ ) [150]. It is associated with the inter-reticulation during polymer chains growth with formation of the following group (outlined by the dashed line in Scheme 5):



Scheme 5. Inter-chains reticulation in electrografted PAN films, the outlined group is responsible of the IR absorption at  $2200\text{ cm}^{-1}$ .

The spectrum of the film after chemical reduction is characterized by the bleaching of the nitrile stretching peak and the formation of a massive in between  $3500$  and  $3200\text{ cm}^{-1}$  that is characteristic of primary amine stretching vibrations.

The peak at  $2200\text{ cm}^{-1}$  is not bleached that means that the inter chains reticulation is stable with regard to chemical reduction.

With the aim of obtaining ultra-thin films we fabricated the PAN films by short chronoamperometry pulses at potentials of  $-2,8$  and  $-2,5\text{ V}$ . Films were fabricated on

“evaporated gold” substrates to have a small roughness and their thickness was measured by ellipsometry (to extract thicknesses data were fitted with the simple model and the optical parameters as in [151],  $n = 1,35$  and  $k = 0$ ). Applied pulses varied from 0,02 s to 0,5 s. The electrical charge flown in the circuit was calculated by integrating the electrical current with respect to the time. An almost linear relationship is found between the thickness of the film and the charge flown in the circuit. Data are reported in Figure 75.

Data are quite scattered, this is probably due to the lack in reproducibility in the polymerization degree of the anionic polymerization. The polymerization degree is dependent on the residual water present in the electrolytic cell when the experiments are conducted ( $H^+$  terminates the polymerization).

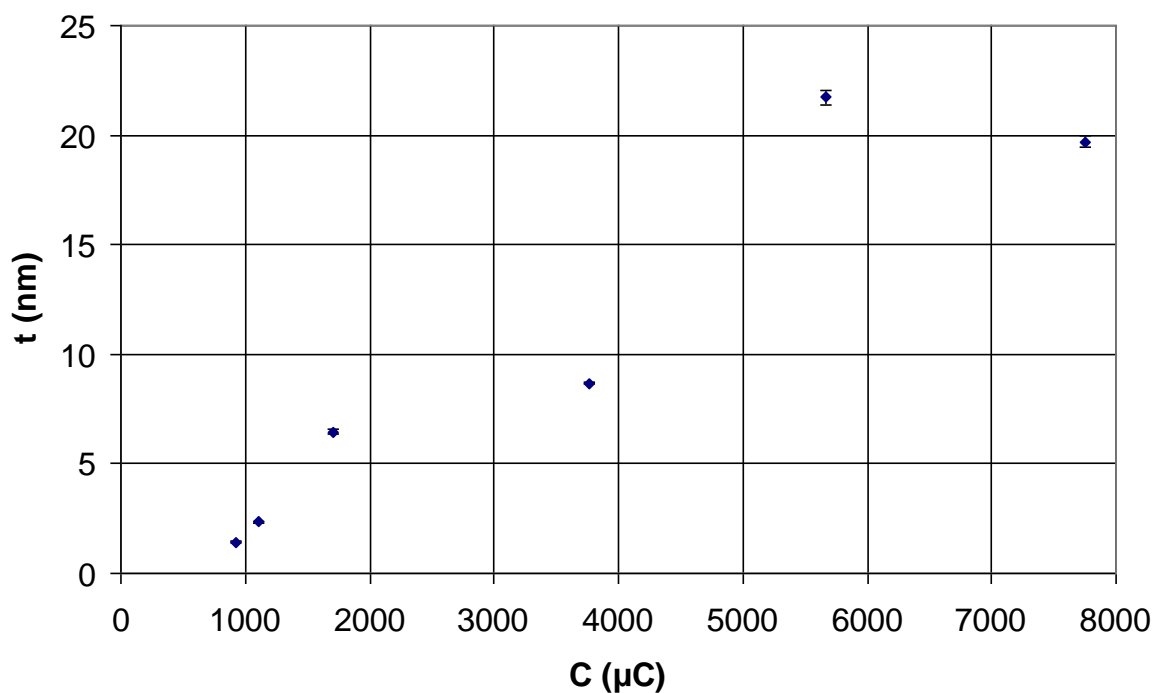


Figure 75. Correlation between PAN film thicknesses and the charge flown in the circuit. Films were electrografted by short pulses in between 0,02 s and 0,5 s at -2,5 V or -2,8 V.

On the basis of this experiment, the conditions for grafting ultra-thin PAN films were a potential of -2,8 V and a step time of 0,05 s. In these conditions films of about 2 nm were obtained.

## Carbon nanotubes adsorption

In a first time carbon nanotubes adsorption was effectuated as described in [152] on silicon wafers treated by APTS. This was done to exploit the low roughness of silicon substrates and be able to easily characterize them by microscopy techniques (AFM and SEM).

Figure 76 reports an AFM images of single walled carbon nanotubes on APTS treated silicon wafer. Carbon nanotubes are visible as straight lines. Electrical percolation in the plane is expected because a big amount of intersection in between carbon nanotubes is visible.

Some spherical particles are visible on the sample. They are likely to be residual carbon impurities in the sample. Although carbon nanotubes were purified by acidic treatment some carbon impurities are also resistant to the attack. More severe conditions could have been able to eliminate the particles but this would have resulted in an increased amount of faults formation on carbon nanotubes surface.

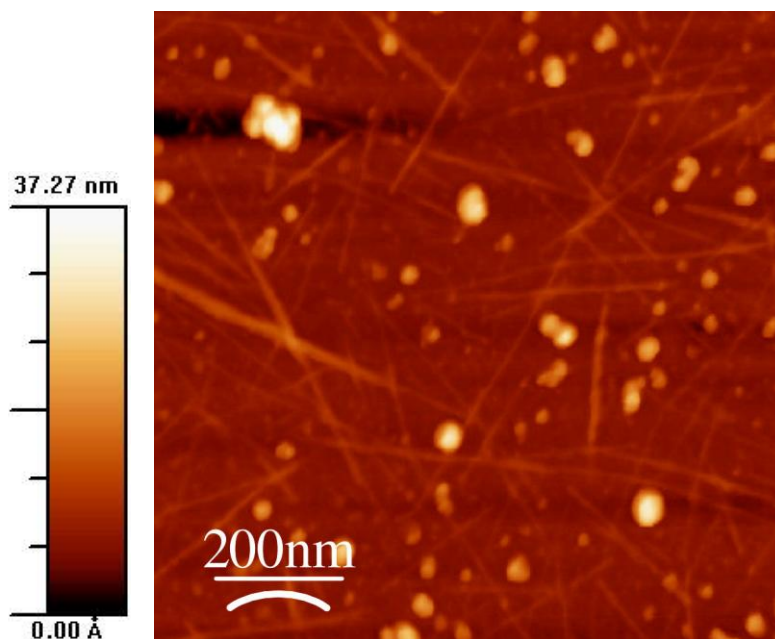


Figure 76. AFM image (tapping mode) of single walled carbon nanotubes 2D-network adsorbed on a silicon wafer treated by APTS.

Microscopy characterizations was more difficult for single walled carbon nanotubes on gold substrates either of the “evaporated gold” kind or “gold coupons” because the roughness of these substrates is comparable or greater than the diameter of the carbon nanotubes.

Therefore, on these substrates, more information has been obtained by resonant dispersive Raman spectroscopy. Figure 77 reports the recorded spectrum for a carbon nanotubes network adsorbed on gold surface modified by electrografting of PAN successively chemically reduced to PAA.

Figure 77a shows the region corresponding to the radial breathing mode. This mode is unique to single-walled carbon nanotubes. The observation of a peak at  $192\text{ cm}^{-1}$  proves the presence of single walled carbon nanotubes on the sample. The frequency of the radial breathing mode is proportional to the inverse of the nanotube diameter [153]. A frequency of  $192\text{ cm}^{-1}$  corresponds to carbon nanotubes with a diameter of about  $1,2\text{ nm}$  [153] which is in agreement with the specifications that were given by the fabricant.

Figure 77b shows the region corresponding to tangential modes (G band) and the D band. The first one is due to tangential vibrations of carbon atoms and it is characteristic of carbon nanotubes but also of other carbon-based materials.

The mode corresponding to the D band is also called “defects mode”. Observation of a peak at this frequency indicates the formation of some  $\text{sp}^3$  carbon atoms due to the formation of defects on carbon nanotubes structure. These are due to the opening of the tubes ends by the acidic treatment and a partial oxidation of the tube with formation of  $\text{sp}^3$  carbon bringing an acidic function.

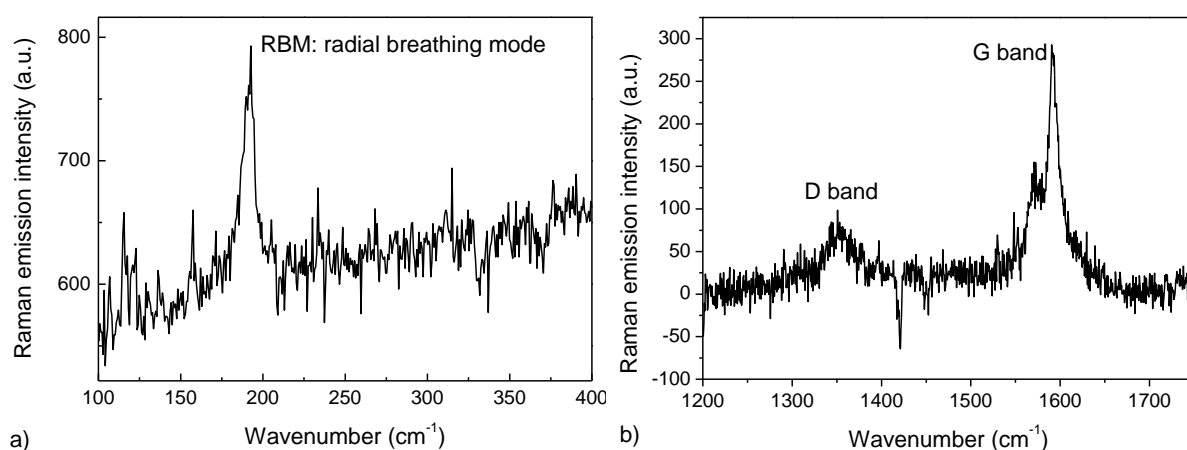


Figure 77. Resonant dispersive Raman spectroscopy spectrum of carbon nanotubes network adsorbed on PAA grafted on gold.

### Zonyl BA-L® grafting

Zonyl BA-L® is the commercial name of a technical product constituted of a fluorinated alcohol. Its structure is reported in Figure 78.

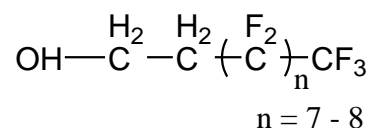
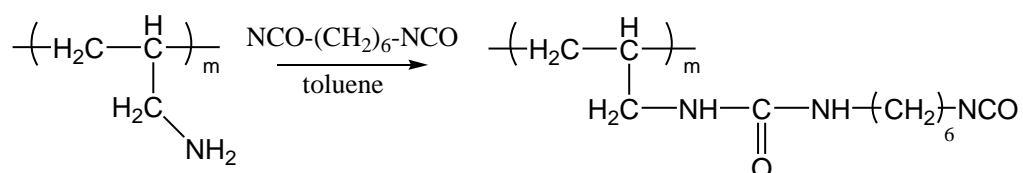


Figure 78. Chemical structure of Zonyl BA-L®.

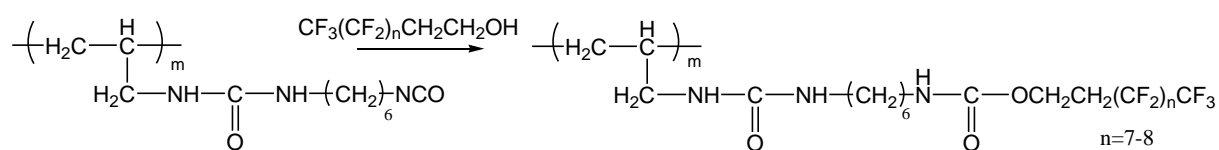
Covalent bonding of this molecule on the substrate was effectuated by the use of a diisocyanate in a two steps procedure.

In the first step the substrate with the carbon nanotubes adsorbed on the grafted PAA was made to react with 1,6-diisocyanatohexane. Reaction in between isocyanates and primary amines is a well known reaction which proceeds as represented in Scheme 6:



Scheme 6. Reaction in between the 1,6-diisocyanatohexane and the PAA grafted on the substrate.

The isocyanate group is also very reactive toward primary alcohols. In the second step the fluorinated alcohol Zonyl BA-L® was made to react with the surface isocyanate functionalized according to the following reaction:



Scheme 7. Grafting of Zonyl BA-L® on isocyanate functionalized surface.

The effectiveness of the reaction was followed by ATR-IR spectroscopy and XPS. Figure 79 reports the IR spectra recorded after each step in film fabrication.

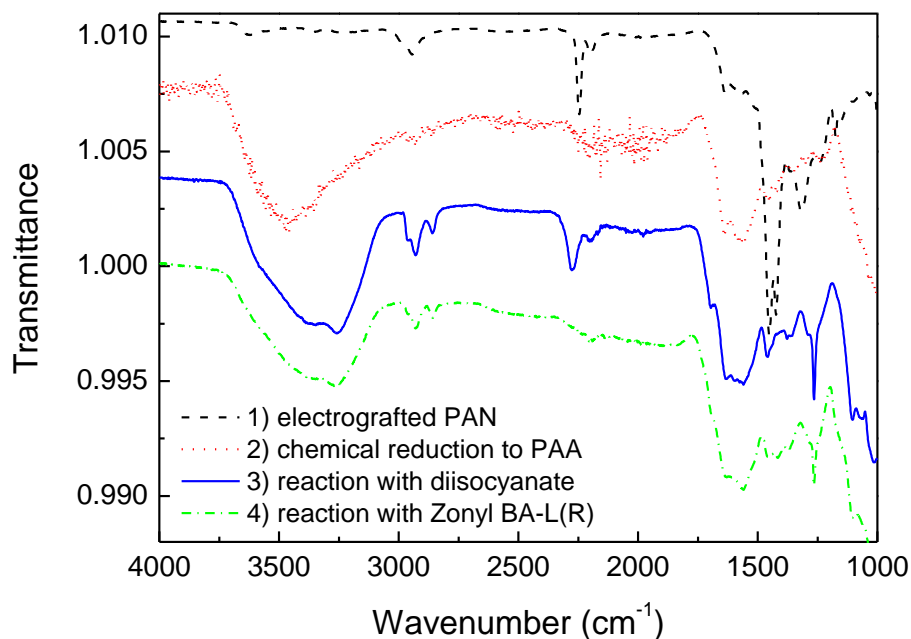


Figure 79. IR spectra collected after each step in the fabrication of Zonyl BA-L grafted films composite with carbon nanotubes.

The black dashed line reports the spectra after the electrografting of PAN, the same feature as in Figure 74 is found, but the peak corresponding to the inter-chain reticulation ( $2200\text{ cm}^{-1}$ ) is less intense. The height of this peak in all the different experiments it is not well reproducible and as the degree of reticulation might depends on parameters difficult to control as the residual oxygen in the dry box. Spectrum recorded after the reduction with  $\text{LiAlH}_4$  is reported as the red dotted line and the feature correspond to what expected as reported above. Also in this case we can see that the reticulation resists to chemical reduction.

Reaction with the 1,6-diisocyanatehexane leads to the appearance of a peak at  $2277\text{ cm}^{-1}$  (blue solid line). This is the signature of the presence of the isocyanate group at the surface at corresponds to the asymmetric stretching vibration of the  $-\text{N}=\text{C}=\text{O}$  group.

Reaction with the fluorinated alcohol leads to the disappearing of this band because of the formation of the urethane group which is less easily determined by IR spectroscopy. Anyway XPS spectra could prove the presence of fluorine atoms by the presence of F1s peaks and the modification of carbon peaks C1s by the appearance of the components at high energy due to  $-\text{CF}_2-$  and  $\text{CF}_3$  carbons.

Carbon nanotubes have been adsorbed on the substrate after the reduction of PAN to PAA, which means in between fabrication steps 2 and 3 of Figure 79.

A question that could arise is whether the use of such a reactive molecule as the diisocyanate can not modify the carbon nanotubes. Another possible objection is that if they can detach during the chemical reactions.

Therefore Raman spectra were recorded before and after the chemical reactions (reaction with the diisocyanate and Zonyl BA-L®). Results are reported in Figure 80. The solid line reports the spectrum recorded after carbon nanotubes adsorption on the PAA. The presence of the G band due to tangential modes and of the D bands due to defects was discussed above. The dotted line report the spectrum after that all chemical reaction have been carried out. It can be seen that the intensity of the G band is almost the same which insures that no major desorption of carbon nanotubes happened. Moreover if faults had been created on the nanotubes by the reaction of the diisocyanate this could be visible by an increase in the intensity of the D band and this is not the case. Therefore the chemical reactions conducted do not attack the carbon nanotubes or they cause carbon nanotubes desorption from the substrate.

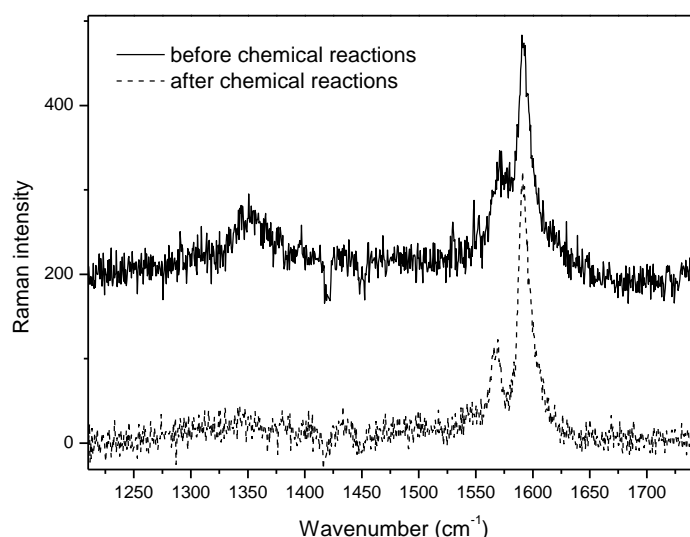


*Figure 80. Raman spectra (gold amine-rich surface) just after nanotubes deposition (solid line), and after chemical grafting of Zonyl BA-L (dashed line). Curves were shifted vertically for clarity.*

## PHFBM and PHFIPM electrografting

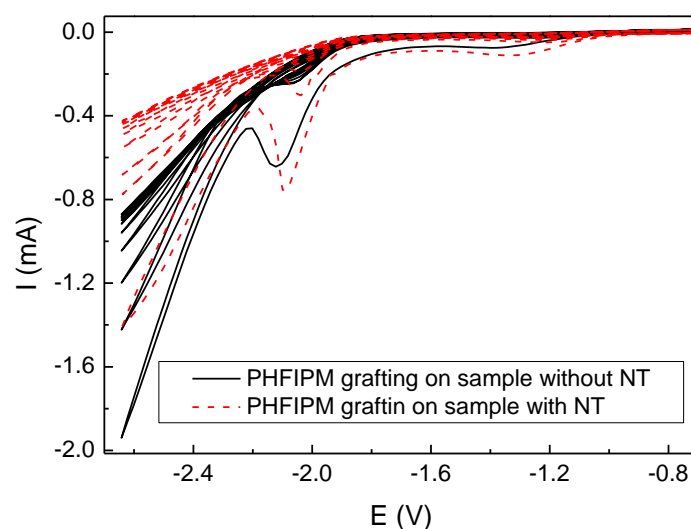
Chronologically when the studies of composites films of fluorinated poly(methacrylate)s and carbon nanotubes were done we had not yet found the way of obtaining very thin completely grafted films by electrografting in THF/DMF electrolyte. Therefore films were grafted in PC and the addition of carbon nanotubes was a strategy used for obtaining low contact electrical resistances.

Figure 81 reports the voltammograms recorded during the electrografting of PHFIPM on “gold coupons”. In one case the 2D-carbon nanotubes network was adsorbed on the substrate and in the other case it was not. In both cases the ultra thin PAN film chemically reduced to PAA was present on the substrate.

As expected the ultra thin PAA grafted films present on the surface is swollen by the electrolyte and does not hinder the electropolymerization.

The PHFIPM polymerization peak is observed at the usual potentials and films are present on the surface of the electrode when removed from the cell and analyzed.

The presence of carbon nanotubes on the substrate is visible in these electrochemical experiments. The current measured in the sample with the carbon nanotubes is lower than what recorded for the sample without. A different behavior could have been expected. Actually if the adsorbed 2D-carbon nanotubes network behaved as a good conductor an increase in the electrical current in electrochemistry experiments should be expected because of the increased effective area of the electrode.



*Figure 81. Electrografting of PHFIPM on gold coupons with (red dashed line) and without (black solid line) pre-adsorbed carbon nanotubes. Experiments conducted in PC and TEAP 0,05M, scan rate 20 mV s<sup>-1</sup>.*

The phenomenon could be explained by a bad electrons transfer from the metal to the carbon nanotubes because of the presence of the PAA film. This film is thin but could be sufficient to avoid direct contact between the carbon nanotubes and the metal electrode. Another possible explanation resides in the nature of the carbon nanotubes used. They mainly are single walled carbon nanotubes and they are therefore composed of a mixture of metallic carbon nanotubes and semiconducting carbon nanotubes. Thus a global semiconducting behavior could be expected for the network, resulting in a not well conducting material.

### **5.7 Study of the tribological properties of the composites of poly(methacrylates) and adsorbed nanotubes**

The friction coefficient that has been measure for the different films, with or without nanotubes, is reported in Figure 82. For each kind of polymer the films have been prepared in the same way except for the presence or not of the adsorbed nanotubes. That means that on each film is present the ultra thin PAA film.

The same differences in friction coefficient values have been found between PHFBM and PHFIPM as the effect of a linear or a branched later group as discussed in section 4.5.

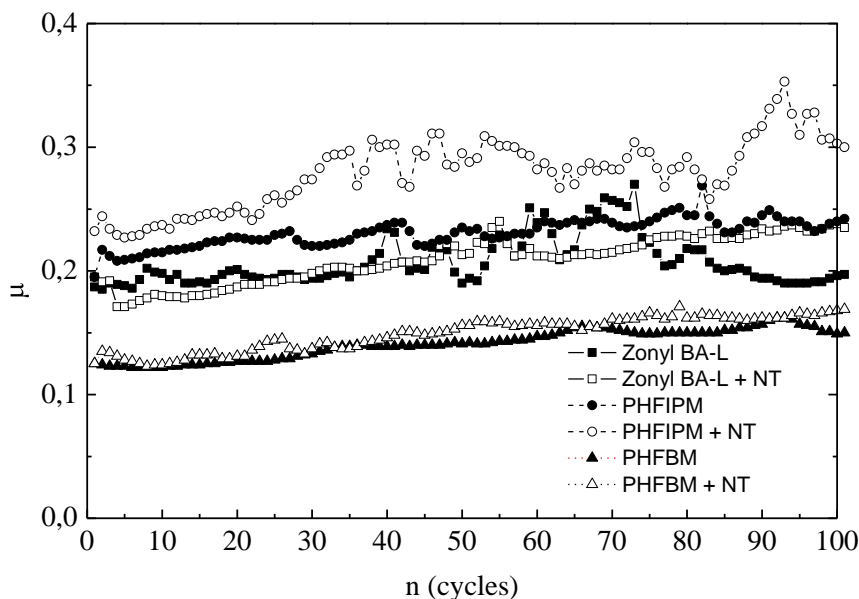


Figure 82. Mean friction coefficient comparison for the different matrixes with (empty symbols) or without (filled symbols) nanotubes. Chemically grafted 2-(Perfluoroalkyl)ethanol (squares), PHFIPM (circles), PHFBM (triangles). Applied normal force 1N.

The friction coefficient for the film obtained by grafting the fluorinate alcohol Zonyl BA-L® is in between the two electrografted poly(methacrylate)s. It is difficult to compare this systems with the other two electrografted poly(methacrylate)s because the molecular structures are quite different. Grafting on the ultra thin PAA film of an aliphatic diisocyanate followed by a fluorinated alcohol leads to the formation of a sort of polymer in which the “main chain” is constituted of the grafted PAA and in which the later groups are lengthen by successive post-functionalizations. But in fact the PAA being ultra thin, the main chain results having a length that is at least comparable with the length of the lateral groups. Moreover the post-funtionalizations lead to the formation of a chain that is just half fluorinated having a six-carbons spacer coming from the diisocyanate.

Therefore comparison with the directly electrografted poly(methacrylate)s is not straightforward.

Just from the point of view of the tribology experiments we can see that anyway the tribological behavior of this system (grafted Zonyl BA-L®) is not especially interesting. The fact that its fabrication requires quite long chemical steps renders it

less interesting for an industrial application. Thus the grafted Zonyl BA-L® films have not been longer studied.

It was reported that the introduction of carbon nanotubes in bulk polymer (PMMA[154], polyimide[155], UHMWPE[156], PTFE[157], polyacrylamide[158]) caused a decrease of the friction coefficient and of the wear rate of the material already for a contents minor of the 1%.

Although formed by two components our poly(methacrylate)s/carbon nanotubes films are somewhat outsider with respect to classical composites films. These latter ones are obtained by mechanical mixing of the components in the bulk either in a molten phase or in solution.

In our case, films composites of the fluorinated poly(methacrylate)s and the carbon nanotubes are obtained by successive surface reactions and they are thin films substrate supported.

If the friction coefficient evolution at 1N for the film containing the carbon nanotubes is compared to the film without nanotubes it can be seen that the effect of carbon nanotubes is inducing spikes in the curve. In the curve reported in Figure 83 the friction coefficient for a PHFBM film with our without carbon nanotubes is reported and compared to the values of the uncoated gold. It can be seen that both the polymer charged with the nanotubes and the polymer alone have a lubricating effect because the friction coefficient remain for all the experiment below the values of the uncoated gold. But while for the polymer alone the curve is quite smooth for the film with nanotubes “spikes” are observed. The friction coefficient shows sudden increases and at same points it reaches the values of the uncoated gold. More surprisingly few cycles later it comes back to low values measured for the film without nanotubes.

We interpret these friction coefficient fluctuations as collective displacements of the carbon nanotubes under the stress at the interface ball plane.

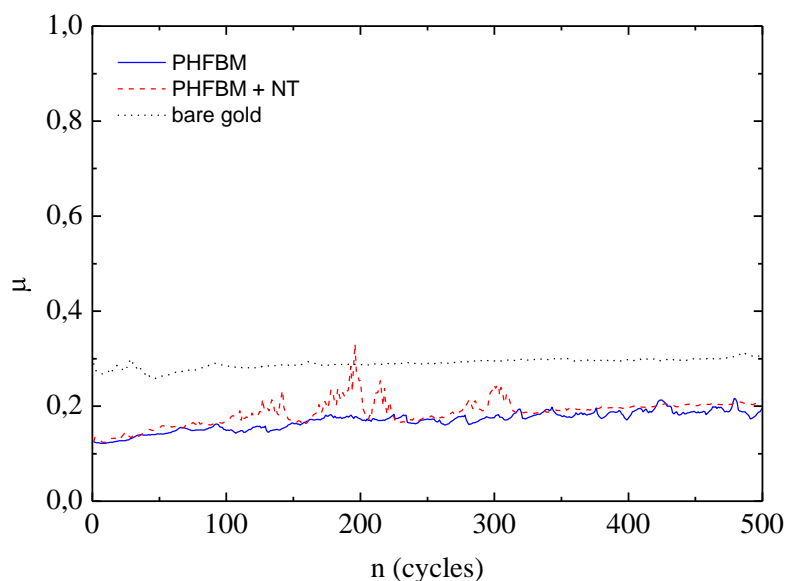


Figure 83. Mean friction coefficient measured during friction cycles in ball/plane configuration on PHFBM (solid line) and on the nanocomposite PHFBM + nanotubes network (dashed line). Dotted line shows the bare gold behavior. Applied normal force 1 N.

Some more information on these fluctuations can be collected by analyzing the local friction coefficient matrix (Figure 84). One can see the “high friction coefficient spikes” are initially localized at the track ends for the first fluctuations. Then a big fluctuation is observed at around 200 cycles. At that point of the wear test the spikes are also localized in the middle of the track. Anyway the “high friction points” are localized in the same position for all the cycles where a high friction coefficient is measured.

These high friction points are likely to correspond to nanotubes bundles, formed during the tribology experiment or already present in the sample before starting the experiment, causing high friction until they are wiped out of the track. The fluorinated polymer remains in the track and when the nanotube bundles are wiped out the friction coefficient can come back to lower values. Moreover it seems that when the mechanically weakest part due to bundles is wiped out (e.g. after cycle 320) the friction coefficient becomes again smooth as in the case of the polymer without the carbon nanotubes.

Correspondingly to the higher friction observed, more wear is also observed by optical microscopy. The wear track is larger and degraded for the films containing the carbon nanotubes than for the film of sole polymer.

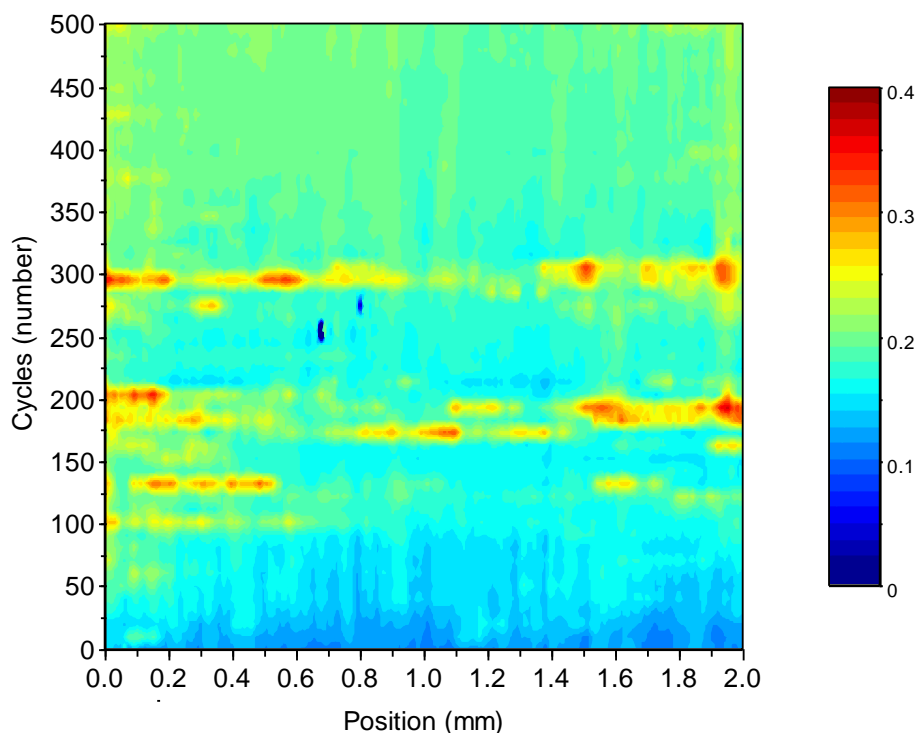


Figure 84. Local friction coefficient friction matrix for a composite film of PHFBM and carbon nanotubes. The data visualized correspond to data used for the curve in Figure 83.

The same trend in friction and wear when nanotubes are added is found for the three different organic matrixes. For all the cases, PHFBM, PHIPM and the grafted Zonyl BA-L®, worse tribological properties are observed for the films containing the carbon nanotubes and “friction coefficient spikes” are observed.

A radical difference is found between our results on thin film polymer/carbon nanotubes composites and the data reported in literature [154-158] on bulk composites. While in the cited works the carbon nanotubes ameliorated the tribological properties in our case it is evident that they are degraded. What plays a major role in separating the bulk and the thin films cases is the interface that receives mechanical solicitation.

In the case of a good polymer/nanotubes nanocomposite a good interface is necessary in between the nanoparticles and the polymer in order to obtain a material with good mechanical properties where the applied stress is transferred from the weaker polymer matrix into the stronger nanofibers.

In our case, of a substrate supported thin film, the interface playing a major role is the one in between the film and the substrate. While the polymer is strongly adhering to the substrate, because of the covalent bonding, nanotubes are just adsorbed on the amine functions of the substrate with a “weak” bond. The interface fluorinated polymer/carbon nanotubes is even weaker because no specific bond exists in between them.

The values of the contact electrical resistance evolution for PHFBM and PHFBM charged with carbon nanotubes are reported in Figure 85. The values of uncoated gold are also reported as reference.

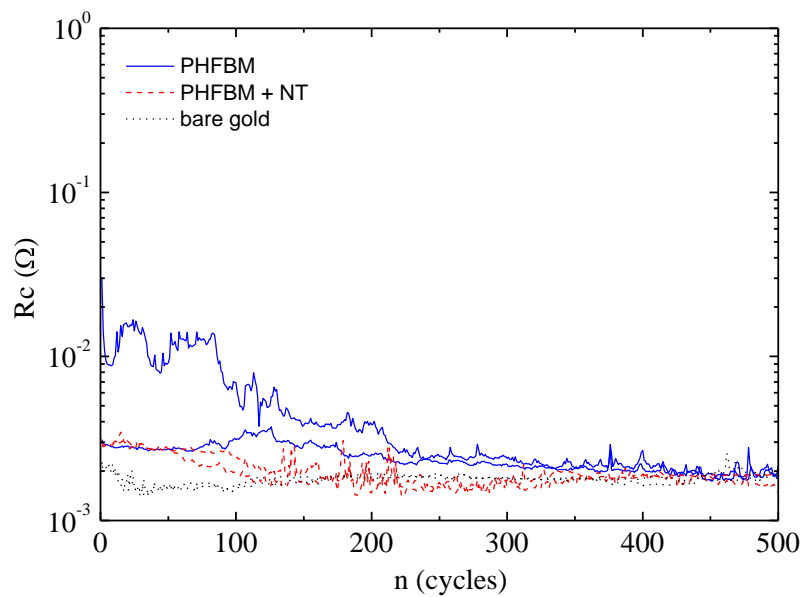


*Figure 85. Contact resistance measured at the two ends of the wear track during friction cycles in ball/plane configuration on PHFBM (solid line) and on the nanocomposite PHFBM + nanotubes network (dashed line). Dots line shows the behavior of bare gold. Applied normal force 1 N. Values have been measured during the same experiment of Figure 83.*

One can observe that the resistances measured at the two ends of the track are different on the sample without nanotubes. This indicated that there can be some accumulation of insulating material at one track end, pushed during the first cycle. This effect is not present in the sample with nanotubes and the contact resistance measured is the same at the two ends. This could be explained either by the fact that the addition of carbon nanotubes is efficacious in reducing the electrical resistance of the film and there is electrical percolation through the matter accumulated in the wear track end or that the nanotubes are effective in avoiding the accumulation of film debris at the track ends. Optical microscopy observation of the wear track shows

anyway that film debris are present at the track end after the experiment and that the first hypothesis as to be accepted.

In general one can see that there is a general trend in electrical resistance reduction with the number of cycles. At cycle 500 almost no difference is observed in between the coated gold and the samples with the film. This is probably due to “direct” contacts establishment between the asperities of the metal substrate and the asperities of the ball. Similar trends are found for the two others matrixes.

Figure 86 reports the values of the contact electrical resistance measured before starting the tribology experiment. In the case of Zonyl BA-L® grafted films no significant difference is found with respect to uncoated gold. This kind of film is very thin; the thickness is estimated below 10 nm (from the ellipsometry measurements on PAN and simple molecular mechanic simulations for estimating the diisocyanate + alcohol chain length).

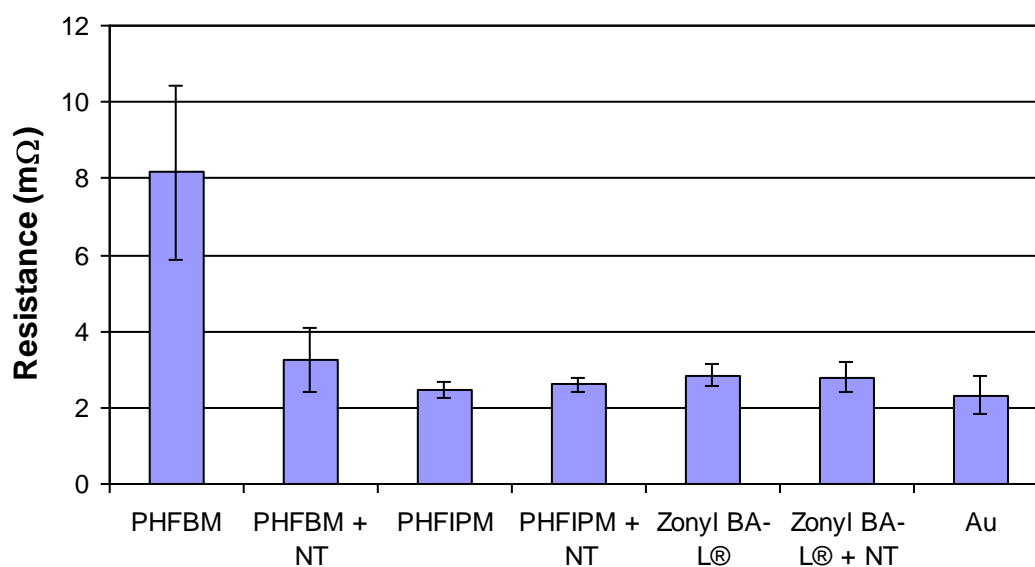


Figure 86. Static contact electrical resistance measured before starting the experiment. Measurements were made on substrates coated with the films charged with or without the carbon nanotubes and on the uncoated gold. Applied normal force 1 N.

This result, although exceptional, especially for the sample without carbon nanotubes, is comparable to what was measure on other lubricating thin films (as the very thin poly(methacrylate)s electrografted films or the diazonium salts films.

For the sample not charged with carbon nanotubes no conduction could be expected intrinsically by the polymer because its molecular structure is typical of insulating

organic matter. Therefore electrical conduction can be possible in between direct metal to metal contact were the film is pierced by the asperities, but this is hardly believable because of lubricating effect measured, or by tunneling through the film. Where the film is pinned between the asperities contacts, its thickness can be reduced by the mechanical pressure to truly nanometric or subnanometric dimension allowing electrons to be transferred by tunneling through the interface.

Films with PHFIPM also do not show significant difference with uncoated gold. But as discussed in 4.5 this matrix is weak and probably easily penetrated by gold asperities.

In the case of PHFBM film which are more mechanically robust with respect to PHFIPM ones and more thick than Zonyl BA-L® grafted films a significant difference is found for the sample with and without carbon nanotubes. In this case effectively carbon nanotubes network is able to reduce values of the contact resistance from about 8 mΩ to values comparable to uncoated gold. This means that electrical transport is effectuated through the conductive matrix which implies that there is a good electrical contact with carbon nanotubes and the two gold surfaces. The assumption is somewhat controversial with what was measured by electrochemistry and discussed above (section 5.8). During the electrografting of the poly(methacrylate)s on the surface on which carbon nanotubes were adsorbed no increase in the electrochemical current was observed with respect to the sample without carbon nanotubes. An increase in electrochemical current could be expected because of the increase in electrode real area by the presence of carbon nanotubes. On the contrary a small decrease in electrochemical current was observed. To explain the phenomenon we evoked either a bad contact in between the gold electrode and the carbon nanotube network (because of the ultra thin PAA film) or intrinsic bad electrical conduction properties of the network.

The second it is now to be rejected because of the “dry” electrical resistance measured. What looks like more reasonable is a different contact between the carbon nanotubes and the gold substrate in the two cases (electrochemical cell and dry ball/plane configuration).

In the case of the electrochemistry experiments the sample is immersed in the electrolytic solution and the thin PAA is swollen by the solvent. This is likely to increase the PAA film thickness over the about 2 nm measured by ellipsometry experiment in the dry state and separate the carbon nanotubes from the gold substrate.

The case of the ball/plane configuration is the opposite of the electrochemistry case. While in this latter case the electrolyte solution swells the PAA film separating the carbon nanotubes from the gold in the ball/plane configuration a normal force is applied exerting a mechanical pressure to the film. Therefore the contact in between the carbon nanotubes and the gold substrate is likely to be ameliorated by the applied external pressure.

### **5.8 Elaboration of composites of poly(methacrylate)s and grafted carbon nanotubes**

From the experimental results in the previous sections emerge as of primary importance improving the adhesion of carbon nanotubes to the substrate. The adsorption of carbon nanotubes on the primary amine functionalized substrate was not sufficient to avoid carbon nanotubes to be displaced by the stress applied during the friction experiment. As the polymer is covalently bonded to the surface we looked for a strategy for immobilizing the carbon nanotubes too.

In a first time the idea we had was to use the same amine functionalized substrate used for adsorbing carbon nanotubes but for covalently bonding them. Carbon nanotubes acid purified already contains carboxylic functions that could react with primary amines to form an amide bond.

The reaction in between carboxylic acid and primary amine, which is well known in organic chemistry [159], proceeds as represented in the following scheme:



*Scheme 8. Reaction between carboxylic acid and amine to form amide bond.*

Although the reaction has already been used for functionalizing carbon nanotube dispersed in solvents [160] the amount of acidic functions and their accessibility to

reactive groups seems too low to have an efficacious heterogeneous phase reaction with a surface.

Quite recently in our laboratory was developed a method for a facile polymer functionalization of carbon nanotubes [60]. The method is based on the chemical reduction of diazonium salts in presence of the nanotubes dispersion and of a vinyl monomer in water. The reduction of the diazonium salts leads to the formation of a radical, which attack a vinyl monomer thus initiating a radical polymerization. One of the possible termination reactions is the bonding of the polymer on carbon nanotube surface. Although operatively very simple the chemical mechanism is quite complex and not yet completely understood. The reader will find further details in [60].

At this step we worked with nanofibers as a model for carbon nanotubes.

We used this kind of process to functionalize carbon nanofibers with poly(acrylic acid). Poly(acrylic acid) is a polymer which has as lateral group a carboxylic group. Therefore by a "soft" functionalization, that means creating few defects on the nanofibers surface, a great number of carboxylic acid functionalities that can allow for bonding to the surface are created. A severe functionalization has to be avoided because each time a functionality is formed a  $sp^3$  carbon is created on the surface worsening electrical conduction properties.

Therefore poly(acrylic acid) functionalization presents an advantage to an extensive acid treatment of the nanofibers. By this latter treatment, in harsh conditions, a great number of acid functions can be created but it also creates a great number of defects and cuts nanotubes or nanofibers in smaller segments. Moreover, by our polymer functionalization, the presence of a "soft" polymer spacer in between the nanotubes and the carboxylic groups is likely to allow the steric accommodation of the nanofibers on the surface.

The effect of functionalization on nanofibers dispersability is evident. While pristine nanofibers have to be strongly sonicated and kept under continuous stirring to avoid precipitation in water, after the reaction dispersions are perfectly stable giving a grey transparent colloid.

So the carboxylic functionalized nanofibers can react with the primary amine functionalized substrate by forming strong and stable amide bonds.

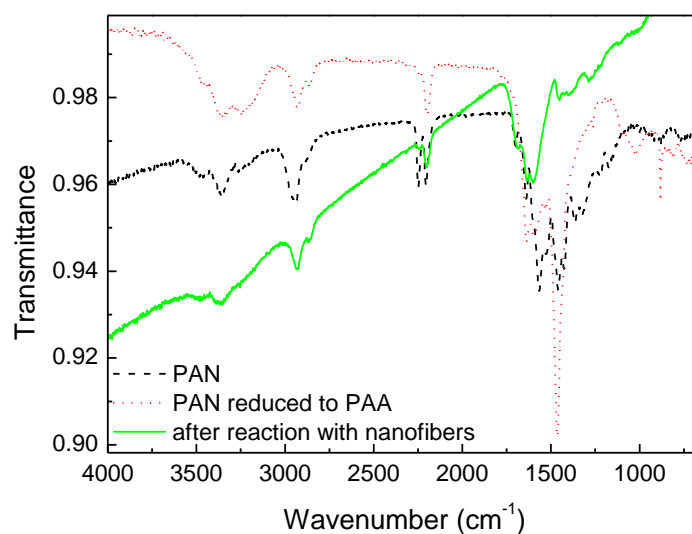


Figure 87. ATR-IR spectra recorded after each step necessary for chemical bonding poly(acrylic acid) functionalized carbon nanofibers to gold substrates.

Figure 87 reports the ATR-IR spectra recorded after each steps necessary to graft the poly(acrylic acid) functionalized carbon nanofibers to the gold substrate.

The black dashed curve corresponds to the thin PAN film obtained by cathodic electrografting. The red dotted curve corresponds to the spectrum recorded after the chemical reduction of PAN to PAA. Discussion of these spectra was reported above.

Finally the green solid curve corresponds to the spectrum recorded after the reaction with the carbon nanofibers.

The first thing that it is observable is the deriving of the spectrum baseline. This is a hint for the presence of widely adsorbing matter, i. e. the immobilized nanofibers. The presence of this widely absorbing nanofibers make difficult to identify peaks corresponding to other modes due to the polymer film. The strongest band corresponding to secondary amides are the I band (mainly due to  $-C=O$  stretching vibration) that is expected in the region  $1680-1630\text{ cm}^{-1}$  and the II band (mainly due N-H deformations and C-N stretching vibrations) in the region  $1570-1515\text{ cm}^{-1}$  [81].

The massive already present in the PAA film in the region  $1800-1200\text{ cm}^{-1}$  is modified in the spectrum after the reaction with functionalized carbon nanofibers. A peak appears at  $1675\text{ cm}^{-1}$  that is likely to correspond to the I band. The II band is normally less intense on secondary amides than the I band. No peak is observed appearing in

the II band region but a modification of the absorbance in  $1550\text{-}1300\text{ cm}^{-1}$  is observed after the reaction. The absorbance in this region decreases after the reaction when compared to the intensity of the other peaks.

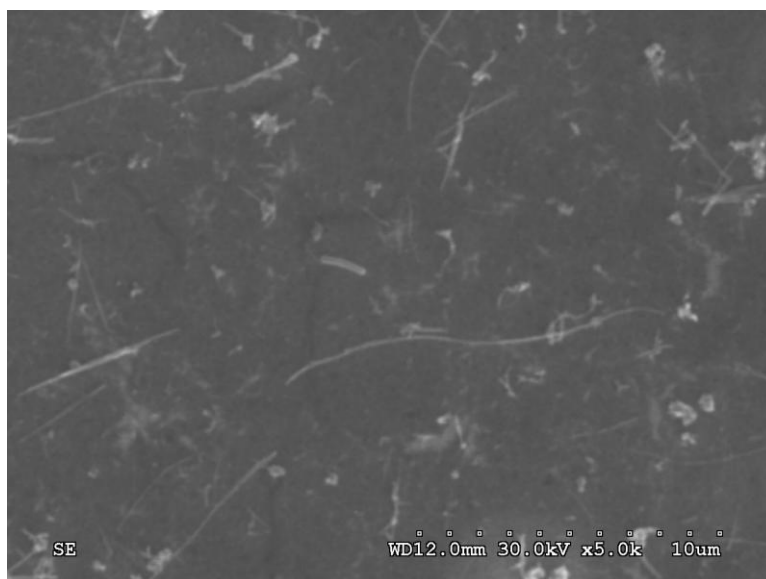
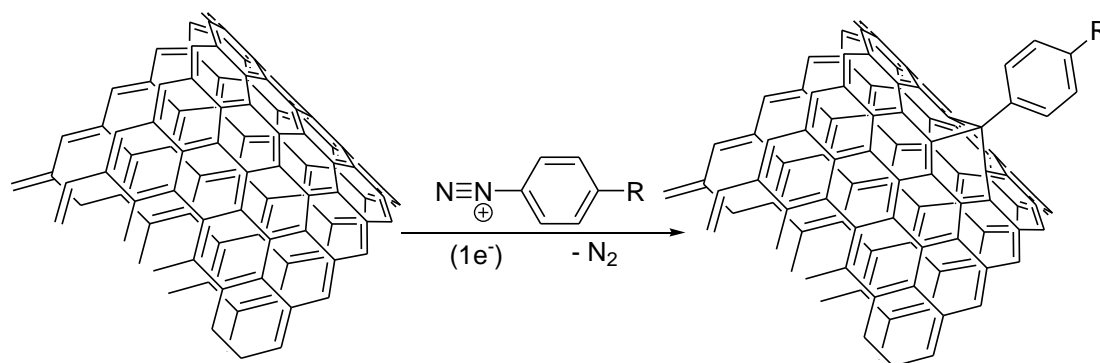


*Figure 88. SEM image of poly(acrylic acid) functionalized carbon nanofibers grafted on amine functionalized gold substrates.*

The presence of carbon nanofibers on the substrate was observed by SEM (see Figure 88). Anyway the grafting ratio seems quite low and the electric percolation through the structure not insured. Moreover the fabrication process is quite long because it requires an electrografting step, a carbon nano-objects functionalization and a grafting reaction in two steps (chemical reduction of PAN to PAA and coupling of the substrate with the nanofibers). Therefore we looked for a more efficient and simpler way of covalently bonding carbon nanotubes on the surface.

One of the most widespread ways to functionalize carbon nanotubes is the reaction with aromatic diazonium salts [161-165]. In some article the reaction in between the diazonium salt an the carbon nanotubes was reported to be spontaneous, while in some other works a chemical reducing agent was used or an electrochemical negative potential applied. Graphite particles have also been functionalized by diazonium salts grafting and it was reported that the amount of functionalization is the same for spontaneous reaction or when electrochemically activated [166].

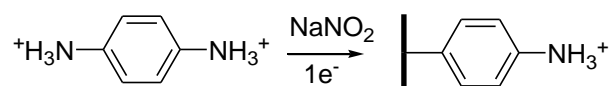
In the case of the spontaneous or temperature activated one as to assume that one electron is transferred from the carbon material to the diazonium salt in order to have the aryl radical formation [162].



*Scheme 9. Functionalization of carbon nanotube surface by attaching aryl ring by using of aromatic diazonium salts.*

In order to have a very reactive surface toward carbon nanotubes our idea was to functionalize a substrate in order to obtain aromatic diazonium group on it. This surface will be then “sticky” toward pristine carbon nanotubes.

This was obtained in two steps, in the first step a film containing aromatic amine was grafted on the gold surface, in the second step aromatic amine have been diazotized. Functionalization of surface with aromatic amine by the electrochemical reduction of in situ generated diazonium cations has already been reported by Lyskawa et al. [167]. They used a 1,4-benzenediamine that was transformed in situ to the corresponding aromatic diazonium salt by addition of 1 equivalent of sodium nitrite and electrografted as reported in Scheme 10. Experiments were conducted in aqueous solution at acidic pH.



*Scheme 10. Grafting of amine layer by reduction of the 4-aminobenzene diazonium in situ generated [167].*

As for other diazonium salts, film thicker than a monolayer can be obtained by a mechanism based on the addition on the aryl of the already grafted units (see Scheme 3).

In a first time we tried reproducing their experiments and grafting aminated layer by this way. But, even when trying to control extremely carefully the experimental conditions, the shape of the voltammograms was hardly reproducible from one experiment to another one, as thickness of the film obtained on the electrode as monitored by measuring the absorbance of ATR-IR bands. The 1,4-diamine is an unstable chemical product as for the generated diazonium radical. Moreover

experiments are conducted in aqueous solution, oxygen was removed by nitrogen bubbling but the conditions can not be as accurate as in a dry box. Oxygen can easily interfere with aryl radicals reducing the reproducibility in film growth.

Therefore we tried a second way to obtain this kind of film by using instead of the electrochemical reduction of the in situ generated diazonium cations a chemical reduction by metallic iron powder [168]. In this case also films were obtained. The thickness of the film can be controlled by changing the time during which the substrate is left in the reaction bath [169].

Anyway also with chemical reduction by iron powder the thickness of the film resulted scarcely reproducible and was impossible to obtain well controlled ultra-thin films as was done for electrografted PAN films (see page 116 and followings). It was anyway the procedure chosen because easier with respect to electrochemical one. The presence of a grafted film was always checked by IR spectroscopy before doing further experiments.

The second step consisted in the diazotization of the aromatic amine present on the substrate, done either in organic solution by using  $\text{NOBF}_4$  or aqueous acidic solutions of  $\text{NaNO}_2$  as represented in Scheme 11.



*Scheme 11. Diazotization of grafted aromatic amines [159].*

Figure 89 reports de IR spectra recorded after the two steps. Step 1 (red dashed curve): the grafting of aromatic amine. Step 2 (black solid line): diazotization of the amine on the surface to diazonium group.

The spectrum after step 1 does not bring specific signature as it is common for amine. The massive corresponding to N-H vibrations is anyways visible in the region 3600-3200  $\text{cm}^{-1}$ . It is also visible a peak corresponding to the frequency of aromatic ring carbon-carbon stretching vibrations at 1509  $\text{cm}^{-1}$ . Less intense peak are visible at 1580  $\text{cm}^{-1}$  and 1620  $\text{cm}^{-1}$  which are also due to the aromatic ring carbon-carbon vibrations.

After treating the film with the  $\text{NOBF}_4$  solution to transform amine group to diazonium group, the IR spectrum show a very characteristic peak at 2280  $\text{cm}^{-1}$  due to the  $\text{N}^+\equiv\text{N}$  stretching vibrations. Another modification observed is the shifting of

the peak at  $1585\text{ cm}^{-1}$  corresponding to aromatic ring  $\text{-C=C-}$  stretching vibration because of the presence of an electron attractive substituent group on the aryl ring. The very strong peak at  $1090\text{ cm}^{-1}$  corresponds to  $\text{BF}_4^-$  counterions vibrations.

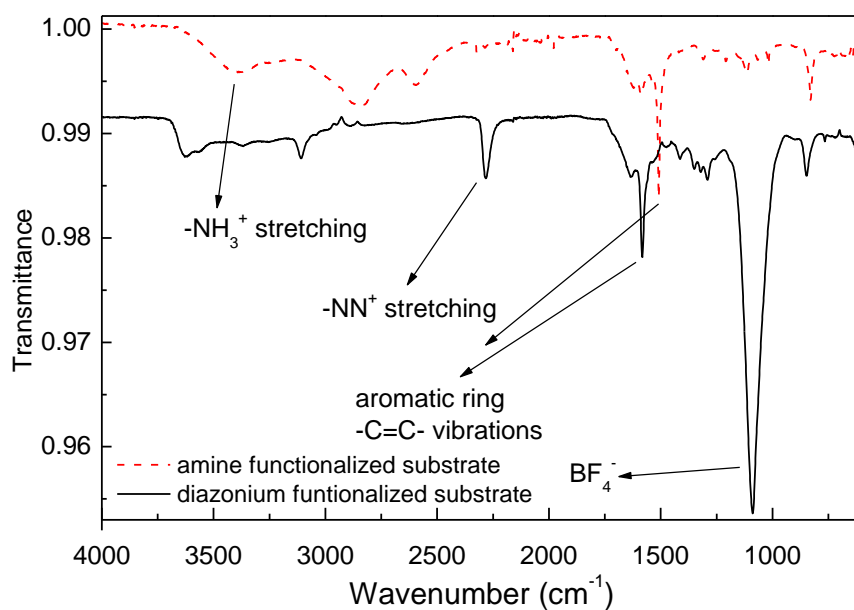


Figure 89. ATR-IR spectra recorded after each step necessary to diazonium functionalize the surface. The red dashed curve is recorded after aromatic amine grafting; the black dashed curve is recorded after diazotization of amines by  $\text{NOBF}_4$  solution.

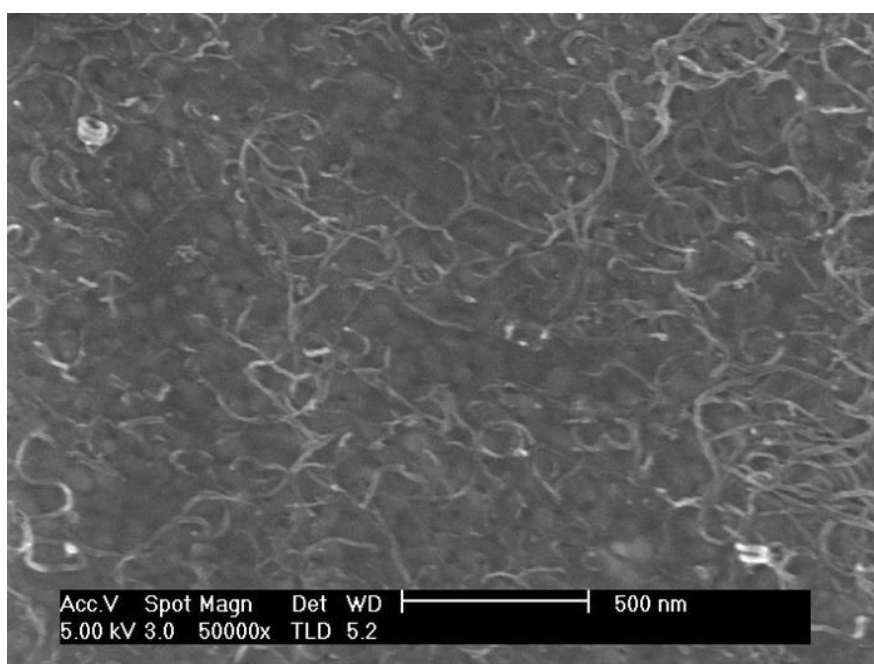


Figure 90. SEM image taken after grafting multiwalled carbon nanotubes on the diazonium functionalized substrate.

The diazonium substrate was made to react with multiwalled carbon nanotubes in suspension in NMP by heating at 100°C.

IR spectra recorded after grafting nanotubes do not present specific signatures but show the bleaching of the peak at 2280  $\text{cm}^{-1}$  due to diazonium stretching vibration. SEM images of the samples were taken which shows the presence of nanotubes on the sample. The morphology is radically different with respect to the adsorbed single walled nanotubes on primary amines which appeared as straight fibers. In this case the grafted multiwalled carbon nanotubes appear more like disordered entangling fibers.

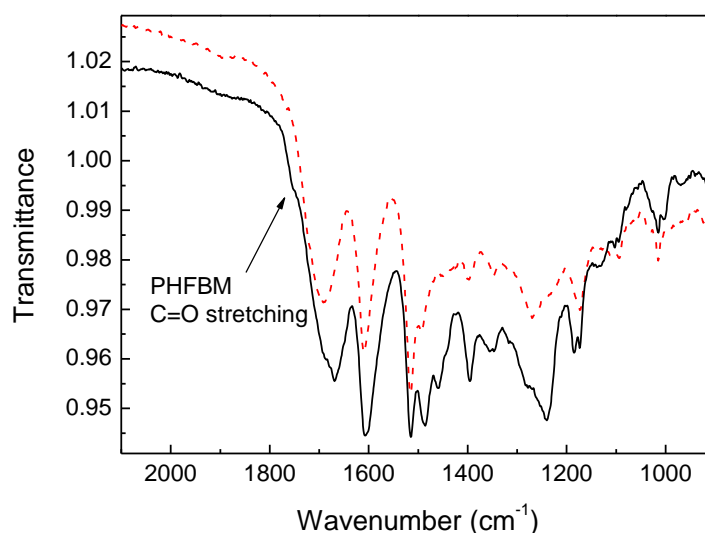


Figure 91. IR spectra recorded on the substrate after carbon nanotubes grafted (red dashed curve) and after the following step of PHFBM grafting through carbon nanotubes.

As already observed for adsorbed single walled nanotubes (but also for PEDOT) the grafting of carbon nanotubes on the surface induces a broad absorption of the IR light which complicates the IR analysis following this step.

Figure 91 reports the spectra collected after the carbon nanotubes grafting step (red dashed curve). PHFBM was grafted through the carbon nanotubes network as already presented for adsorbed tubes. The spectrum recorded after PHFBM grafting is reported as the solid black line.

The identification of the polymer peaks is quite difficult because of the preexistent adsorption of the organic layer used for grafting the tubes and the tubes itself. The

appearance of a shoulder at  $1780\text{ cm}^{-1}$  anyway insures the presence of the polymer. This frequency vibration corresponds to the C=O vibration of the fluorinated poly(methacrylate). To verify this assignment the reader can compare to the spectrum reported in Figure 40 of a pure PHFBM electrografted film.

### 5.9 Study of the tribological properties of the composites of poly(methacrylate)s and grafted carbon nanotubes

Ball/plane tribology tests were effectuated on the samples obtained by growing carbon nanotubes through the grafted carbon nanotubes. Figure 92a reports the evolution of the mean friction coefficient for a test at 2,5 N normal force. The friction coefficient shows a very smooth profile with a friction coefficient in between 0,1 and 0,2 for all the experiment.

It is interesting to remark that in this case no spikes due to nanotubes displacement have been observed as in the case of adsorbed carbon nanotubes. Therefore the chemical grafting of carbon nanotubes to the substrate (through the organic phenylene-like film) is efficacious in ameliorating their interface with the substrate and their friction properties.

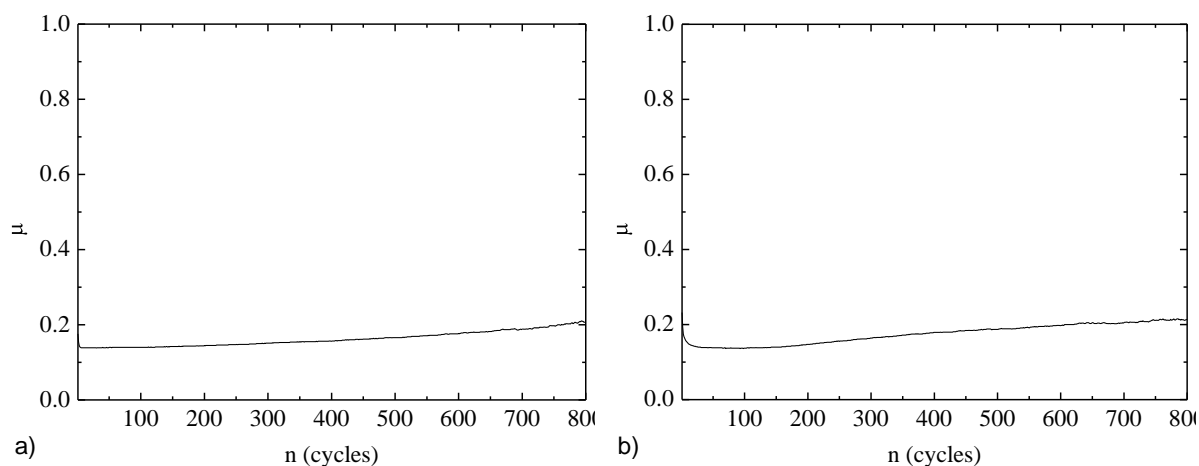


Figure 92. Mean friction coefficient evolution during tribology test. a) test effectuated on the composite film of PHFBM and grafted nanotubes, b) test effectuated simply on substrate with grafted nanotubes (no PHFBM).

The mean friction coefficient evolution represented in Figure 92a is similar to what was measured for BD-grafted films alone, that means a very smooth profile, friction coefficient in between 0,1 and 0,2 and a great withstand to wear (see e. g. Figure 31).

The structure of the film used for grafting the carbon nanotubes greatly resemble to the **BD**-grafted films: they both have a phenylene-like structure and they do not have substituent group on the phenyl ring (or a very short one).

For this reason tribology tests were effectuated on a “gold coupon” with just the carbon nanotubes grafted on the organic sub-layer. Friction coefficient results are reported in Figure 92b. As one can see the tribological behavior is almost the same. In fact grafting of PHFBM does not play a major role and the tribological properties depend essentially of the sub-layer.

With the process used for grafting the aromatic amine sub-layer it is difficult to control the thickness to a precise value because of the lack in reproducibility as discussed above. Films tested were quite “thick”, a rough estimation is around 50 nm. Thickness is anyway hard to measure on the substrates used for tribology (“gold coupons”) either by optical or mechanical profilometry because of the roughness. The fact that films are thick is visible also in the mean friction coefficient evolution curves because they show a decrease at the beginning as it was already measured for “thick” poly(methacrylate)s films (section 4.5).

Also the electrical contact resistance evolution is similar to that of thick poly(methacrylate)s films: it is high before starting the test but rapidly decreases after the first friction cycle. This can be explained by the removal of the mechanically weaker external part of the film during the first cycle. At the second cycle, when just a thin film is remaining in the wear track, contact resistances below 10 m $\Omega$  were measured.

The static contact resistances measured before starting the friction experiments are reported in Table 5. Results are not very good and show poor reproducibility and great variations.

	F (N)	R ( $\Omega$ )	$\Delta R/2$ ( $\Omega$ )
CNT	1	4.98E+06	7.04E+06
PHFBM + CNT	1	7.18E-03	6.22E-04
CNT	2.5	4.99E+06	7.05E+06
PHFBM + CNT	2.5	1.22E-01	7.67E-02

Table 5. Values of contact electrical resistance measures at 1 and 2,5 N for a substrate with grafted nanotubes (CNT), and a substrate with PHFBM and carbon nanotubes (CNT + PHFBM). F and R. represent normal force, electrical resistance and its standard deviation. Two measures were effectuated per table row;  $\Delta R/2$  represents the semi-difference in between the two R values.

This essentially reflects the lack in reproducibility of the grafting of the aromatic amine layer. The aromatic amine sub-layers of two samples on which the measures of Table 5 have been effectuated have been grafted in the same reaction bath in which they have been immersed and extracted together.

It also hints for inhomogeneity of the deposited film. Because of the experimental set-up just four measurements could be done for each sample which means two for each value of applied normal force. Anyway a great difference in the values is found.

If for the CNT + PHFBM film the electrical resistance at 1 N and 2,5 N is compared, it is found that the value is higher for the highest applied normal force. This is of course not possible for this kind of films.

The electrical contact resistance in a sphere/plane configuration in presence of a film at the interface is given by [31]:

$$R_{contact} = R_{constriction} + R_{film} = \frac{\rho_1 + \rho_2}{4a} + \frac{\rho_3 e}{\pi a^2}$$

$R_{constriction}$  is the contact resistance due to the constriction of current line in the contact surface of radius  $a$  and  $R_{film}$  is the resistance due to the presence of the film in the interface.  $\rho_1$ ,  $\rho_2$ , and  $\rho_3$  are the resistivity of the material composing the ball, the plane and of the polymer,  $e$  is the thickness of the film at the interface.

In the framework of Hertz theory of the mechanical contact the radius  $a$  of the circle of contact is:

$$a = \left( \frac{3 FR}{4 E} \right)^{1/3} \propto F^{1/3}$$

where  $R$  is the radius of the sphere and  $E$  the Young modulus.  $F$  is the applied normal force.

By combining the two equations it is found that:

$$R_{contact} \propto F^{-\alpha}$$

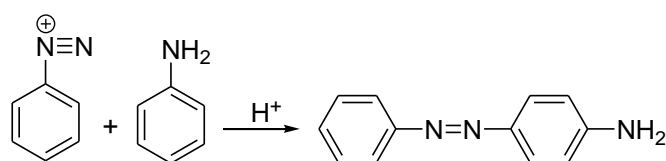
where the coefficient  $\alpha$  varies in between 0,33 and 0,66 depending on ratio in the amount of contribution to the contact resistance by the constriction or by the film. This model, which does not account for roughness or for piercing of the film by asperities, confirm the intuitive idea that the resistance of the contact has to reduce when increasing the normal force.

Therefore the increase in the contact resistance for the CNT + PHFBM film when passing from 1 to 2,5 N is an "artifact" due to the inhomogeneity of the film.

While the idea of using a diazonium functionalized surface to chemically bond carbon nanotubes seems working for improving the friction of the sample the method used for grafting the intermediate layer still has to be improved.

Amelioration in the reproducibility of the system could be obtained by optimizing the used process, e. g. by changing the chemical reducing agent. Iron powder leads to a heterogeneous phase reaction, the use of a water soluble reducing agent could improve the results.

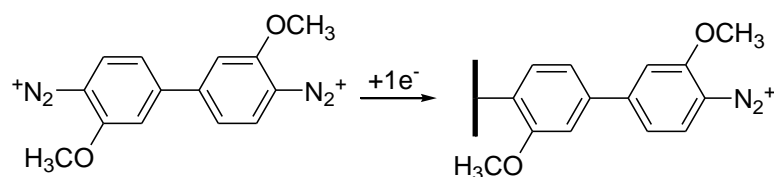
Anyway the use of the aromatic diamine and the following the generation of a mono diazonium salt seems the most delicate step and the one which is probably responsible of the lack in reproducibility by multiple sideways reactions. The reactivity of diazonium salts toward aromatic amines is well known. E. g. a classical reaction [159] is the one of benzene diazonium ion with excess aniline in acidic medium to give the aromatic substitution product *p*-aminoazobenzene (see Scheme 12).



Scheme 12. Reaction of benzenediazonium ion with aniline in acidic medium [159].

Moreover aromatic amines are often toxic and it seems therefore very meaningful, after all these consideration, to find an alternative and appropriate way for obtaining a diazonium functionalized surface.

It was reported [58] that the electrochemical reduction of a bidiazonium salt, the diazonium chloride of 3,3'-dimethoxy-4,4'-diamino biphenyl, a very common colorant sold under the commercial name of Fast Blue salt, lead to the formation of a diazonium functionalized surface. The reaction is reported in Scheme 13.



Scheme 13. Fast Blue salt grafting as reported in [58].

Although the one electron reduction seems quite delicate without further reducing the molecule by transferring an electron to the other diazonium group the method of the electrochemical grafting of bidiazonium salts promises to be a more elegant way to obtain a diazonium functionalized surface. It is a one step reaction and does not require further post functionalizations of the surface. Moreover the electrochemical reduction allow for easier control of the amount of reduced molecules and therefore make possible moving toward a monolayer or sub-monolayer film capable of attaching the carbon nanotubes without having a negative effect of the electrical resistance.

### **5.10 Summary and chapter conclusions**

#### **Fluorinated PEDOTs/PHFBM composites**

It was found that the addition of a substituent fluorinated chain on the dioxane ring of EDOT do not change dramatically the properties of the molecules in term of oxidation potential and possibility of polymerizing under anodic polarization.

Anyway for poly(**MB54**) and poly(**MB20**) it is hypothesized that the presence of the fluorinate group improves the supramolecular organization of the polymer. The hypothesis is supported by observation of steeper transition from insulating to doped states by EIS and by better defined peaks by cyclic voltammetry.

By combining EQCM measurements and from fitting and mathematical manipulation of EIS data, it is found that electrochemical doping of the PEDOTs is accompanied by solvent swelling the polymer. In the doped state the amount of solvent molecules for doping ion is estimated to about 1,4 for poly(**MB54**), the doping rate is estimated to about 4,3% by using EIS data.

When working on gold electrodes it was found that traces of water can increase the stability of the electrode.

When composite films made of PHFBM and fluorinated PEDOTs are tested in macroscopic ball/plane tribo-electrical experiments no reduction of the electrical contact resistance is found with respect to sole PHFBM.

### **Fluorinated poly(methacrylate) composites with adsorbed nanotubes**

To our knowledge, for the first time, nanocomposites polymer/carbon nanotubes thin films substrate supported and obtained by surface modification were fabricated and studied.

From the point of view of tribo-electrical tests it is found that the carbon nanotubes addition to electrografted PHFBM (in propylene carbonate) ameliorates the electrical conduction properties. Anyway friction is deteriorated by the observation of spikes in the friction coefficient evolution because of the wiping out of carbon nanotubes from the wear track. From this emerges the importance of ameliorating the adhesion at the interface substrate/carbon nanotubes.

### **Composites with grafted carbon nanotubes**

By using an intermediate sub layer, which renders sticky the surface, carbon nanotubes were covalently bonded on gold. No more spikes were observed in friction coefficient evolution.

The friction coefficient evolution is anyway dominated by the “thick” organic sub-layer added to the film to covalently bond the tubes. Moreover contact resistances are high because of the presence of this “thick” film and not well reproducible because the lack in homogeneity and reproducibility in film thicknesses. This aspect remains the critical point of the fabrication process and has to be ameliorated to obtain good films.

### **Chapter global conclusion**

This thesis chapter is the one which contains the most the spirit of the NANOCONECT project, the framework in which this thesis is inserted, as it was written three years ago before starting researches. One of the main ideas of the project was the realization of lubricating *and* conductive film to be good material to be inserted at the interface of electrical connectors in order to assure lubrication, wear protection and electrical conduction through the film. As good lubricant and mechanical properties are difficult to conciliate with good electrical conduction in one simple material the composite approach was prospected.

During the researches it became evident that the films showing the best mechanical, lubricating and wear withstanding properties are the thin films (with a thickness below 10 nm). Moreover these films, being extremely thin, do not increase the electrical resistance with respect to an uncoated gold/gold contact, when macroscopic measurements are conducted using industrial rough substrates.

It seems therefore logic to conclude that the composite approach, which requires a great effort and often complicate reaction steps for obtaining little gains in wanted properties, is not advantageous with respect to a simple and quick one step polymer thin films grafting.

It is anyway to be considered that the tribological and electrical characterization that were presented here refer just to a macroscopic test, which simulates low level electrical connectors. The contact configuration studied, where the ball and the plane have a roughness much greater than the thicknesses of the films, is characterized by a great number of asperities to asperities contacts which makes possible to have the same contact resistance when measuring a thin film coated substrate and an uncoated substrate.

One of the principal reason for studying immobilized covalently bonded organic films as dry lubricants is the limitation that liquid lubricants present in "extreme condition" as in MEMS (because of the miniaturization), high vacuum and space operating as this was presented in introductory chapter.

In MEMS, for example, the electrical contacts will have the size of just one of the multiple asperities that composes the macroscopic contact and radical differences could be expected in contact electrical resistance and the effect of it of a nanometric polymer coating. We consider therefore worth continuing the tribo-electrical studies of composites films in conditions more pertinent to the intended applications.

## **6 Discussion and comparison of tribological behaviors**

### **6.1 Introduction to the chapter**

In the previous chapters we presented the experimental results on the fabrication, characterization and tribo-electrical properties of different kinds of films: poly(methacrylate)s, phenylene-like films obtained from the reduction of aryl diazonium salts and different composite films.

One of the first questions that might arise is: “What is then the best film for the protection and lubrication of electrical contacts?”

We also wrote in the introduction chapter that one of the goals of this thesis was to understand the role of the grafted polymers structure on friction properties. I.e. the role of the kind of chemical bond in between the carbons of the polymer main chain, the role of fluorination, the presence of lateral groups, etc.

While the answer of some of these questions will be left for the conclusions, the present chapter has the aim to investigate the differences that can be found in physical chemistry properties and in tribo-electrical behavior in between the family of electrografted poly(methacrylate)s and the phenylene-like films obtained from the diazonium salts. We will therefore compare the electrochemical growth mechanism of the two families and we will point out the obscure points that still exist in the literature on the subject. We will present then a few EIS measurements that could give some hints to the corrosion protection of the two kinds of films. Finally we will compare and discuss the tribological and electrical properties of the two films, trying to elucidate the mechanisms of wear and the main differences between the two families.

### **6.2 Films growth mechanisms**

The principal lines of the growth mechanisms of the two polymers families: the electrografted poly(methacrylate)s and the phenylene-like films obtained by the reduction of aryl diazonium salts, were known much before this thesis and presented in the introduction chapter. In this section, we would like to point out the peculiar

aspects of the growth mechanisms that come out when comparing the two families and that we consider worth of interest.

At a first impression the growth of the two families looks quite similar: a negative potential is applied to the substrate, a metal grafted film is obtained and in both cases, the film is thin and it is not possible to make it grow more than a few tens of nanometers. But when looking more accurately the two families seem completely different: the growth of one involves an anionic polymerization while the other is based on radical attacks, one leads to films that have a grafting ratio of maximum 40% while the other leads to films that are very compact. The substrate functionalization with one family leads to electrode that are still electroactive while the other to films that are completely electro-blocking. But more intriguingly both lead to a film growth of thin nanometric films that are somewhat self-limiting.

Why the truly grafted films in the two cases can not grow more than a few tens of nanometers?

While much research effort has been devoted in trying to get thicker films by cathodic electrografting of vinyl monomers, less research was conducted to investigate why thin films are obtained. A first simple reason is that growth of cathodic electrografted films involves an anionic polymerization. Although experimental conditions in such cases are carefully controlled, the lifetime of a carbanion is short, and  $H^+$  coming from some residual water or taken to the solvent quickly terminates the polymerization propagation, resulting in low polymerization degrees for the electrografted macromolecular chains.

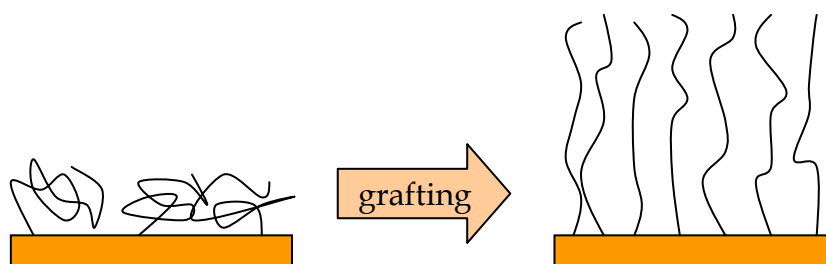


Figure 93. Electrografted polymer passing from “bushes” configuration to “brush” configuration by increasing grafting ratio.

Anyway it was found that the thickness of the films increases with the grafting ratio. When the grafting ratio is low the polymer is in “bushes” configuration. By increasing the number of grafted chain (by effectuating further cathodic potential

pulses or voltammetry cycles) the polymer pass to a “brush” configuration [170] which results in thicker films (as shown in Figure 93).

This configuration change is possible because the cathodic electro grafting mechanism is a “grafting from” mechanism, which means that the macromolecular chains grow from the electrode surface toward the bulk of the solution.

Grafting of poly(phenylene)-like films from the aromatic diazonium salts proceeds with a “grafting to” mechanism. The reactive radicals are generated by electron transfer from the electrode to the aromatic diazonium salt in the solution then these radicals “graft to” the electrode surface causing the film growth.

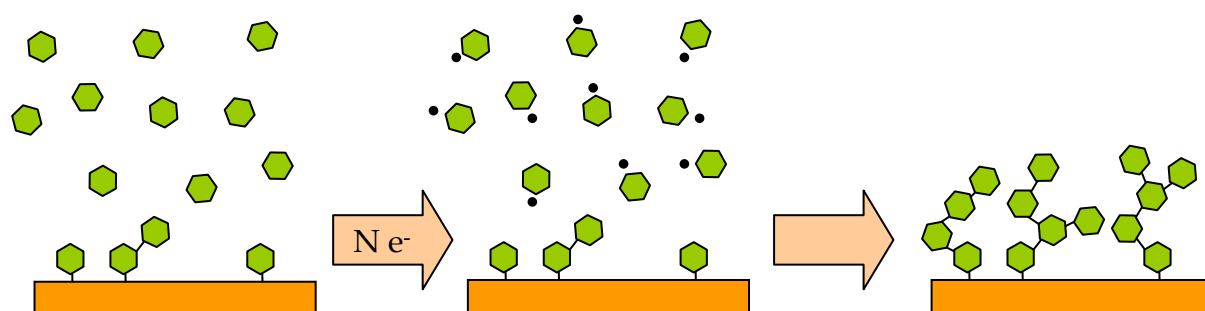


Figure 94. Schematic representation poly(phenylene)-like films growth from the reduction of aromatic diazonium salts.

Pinson and coworker have shown that radicals can be created on the film too and that they can attack diazonium cations in the solution [85]. The mechanism should be there more accurately defined as a hybrid “grafting to”/“grafting from”. The “grafting from” reaction path is anyway secondary and the mechanism remains mainly “grafting to”.

What limits then the grafted film thicknesses to a few tens of nanometers in the two cases?

In the case of cathodic electrografting we have told that the two limiting factors are the polymerization degree of the chains and the grafting ratio. The fact that the polymerization degree is limited by reactions with  $H^+$  or other cations is more easily understandable. But why can not grafting ratios be higher than 40% if moreover the surface is still electroactive and monomer reduction can be observed in cyclic voltammetry?

The fact that monomer reduction is still observable and that no more film is grafted means that from a certain grafting ratio, the solution polymerization is the only polymerization reaction possible and all the reduced monomers initiate solution polymerization.

Therefore it seems likely that the maximum grafting ratio is somewhat like an intrinsic property of the electrografted films.

What limits the thickness of the poly(phenylene)-like grafted films obtained from diazonium salts is more clear and already mentioned in this text. When the first layer of diazonium salt is grafted, the electrode surface is strongly passivated (as reported by many authors [42, 69, 167, 171, 172]) and the electrode shows almost no electrochemical activity. Therefore what limits the thickness of the films is their electrochemical insulating behavior. The electron transfer from the metal to the solution is hindered and therefore the growth is "self limiting".

It was reported anyway that thick films could grow from electrochemical reduction of diazonium salts when they present a group having an electrochemical activity. It is the case of 4-nitrobenzenediazonium tetrafluoroborate [173] and of a special diazonium salts bringing ruthenium complex as substituent group [174]. An electron can be transferred to the electroactive group when its potential is reached. The charge carrier can then move through the film by a hopping mechanism between the groups [173, 174]. Therefore films at that potential are not insulating but can transport electron through this hopping mechanism. Electron can then be transferred to the diazonium salts in the solution, with the formation of the reactive aryl radicals, and film growth can continue.

### **6.3 EIS measurements and corrosion protection**

The measurement of the current blocking behavior of the films deposited on the electrode can be a first indication of their potential protection toward environmental corrosion of the substrates [42].

A good way to measure it is to evaluate the charge transfer resistance to a redox couple by EIS when the electrode is coated with the different films. We measured EIS spectra at open circuit potential for the different films, in aqueous solution with

$\text{Fe}(\text{CN})_6^{3-/4-}$  0,005 M. Figure 95 reports the EIS spectra recorded for the different films left in the electrolytic solution for 15 h.

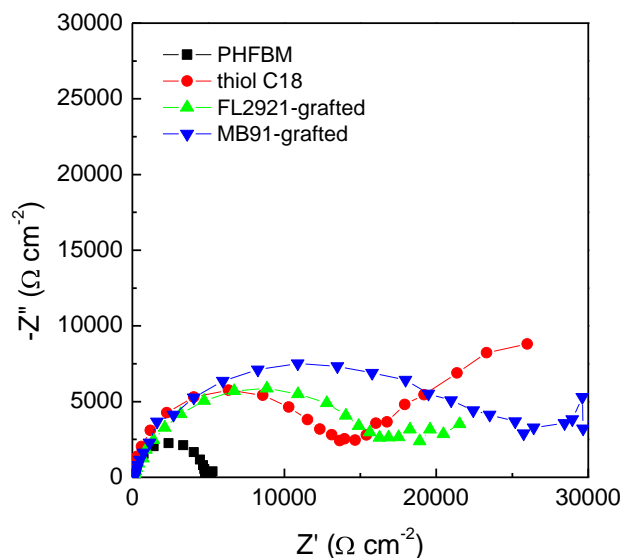


Figure 95. a) Nyquist Electrochemical Impedance Spectroscopy diagrams on “evaporated gold” electrodes grafted with films obtained from different molecules in water with  $\text{KCl}$  0,1 M and  $\text{Fe}(\text{CN})_6^{3-/4-}$  0,005 M.

Charge transfer resistances on the  $\text{Fe}(\text{CN})_6^{3-/4-}$  system can be estimated from the width of the semicircle at high frequencies on the Nyquist plot. The EIS measurements were also conducted on octadecanethiol grafted on the gold as a very well known “reference” to ease up comparisons.

It can be seen that the poly(phenylene)-like film obtained by grafting the aliphatic **FL2921** diazonium salt gives a charge transfer resistance which is comparable to that of the octadecanethiol. Thiols grafting is well known to bring to the formation of very dense and organized film [175]. The observation that the measured charge transfer values are near in the two cases confirms the very dense structure of the films obtained by the grafting of aromatic diazonium salts.

The charge transfer resistance measured for the fluorinated film obtained from **MB91** is even higher. The hydrophobic character of the chain reduces the water penetration in the film: this results in even more blocking films toward electron transfer on the  $\text{Fe}(\text{CN})_6^{3-/4-}$  system in aqueous solutions.

For the PHFBM grafted film the measured charge transfer resistance is “only” 50000  $\Omega \text{ cm}^{-2}$ . This remains anyway a high value to be compared to the charge transfer of 9  $\Omega \text{ cm}^{-2}$  measured on uncoated gold.

EIS data confirm the assumption already made on the electrografted poly(methacrylate)s film being less compact. For this kind of films the penetration of the  $\text{Fe}(\text{CN})_6^{3-/4-}$  complexes until the electrode surface is easier probably because of the more free volume present in the film.

We think that the free volume of the films can be a key for the interpretation of the different compactness of the films and of the limited grafting ratio for poly(methacrylate)s. PHFBM is a polymer which has the main chain composed by  $\text{sp}^3$  carbon atoms which give to the macromolecular chain a conformational space with a higher degree of freedom. We expect therefore the macromolecular chains to be more disordered and thus more spaced. Moreover poly(methacrylate)s (as e.g. PMMA) are polymers which are well known [176] to have a poor degree of crystallinity and to be mainly in a glassy state at room temperature (glass transition temperature of PHFBM is 65 °C, Aldrich).

Less studies exist on the conformation of poly(phenylene)-like films obtained from diazonium salts reduction. In a first order approximation we can imagine that their properties will have to correspond roughly to that of poly(p-phenylene) that has been more widely studied as a polyconjugated fluorescent and semiconducting polymer. This kind of polymers presents a very high degree of crystallinity and the chains have a good supramolecular organization because of the  $\pi$ -stacking of the aromatic rings.

Moreover Allongue et al. [38] have studied the attachment of diazonium salts on Si-H surfaces and the conditions for obtaining monolayer. They have shown that very compact layer (with a surface occupation near to the unity) can be obtained.

We deduce then, that the differences in the film compactness of two families and of the maximum grafting ratio obtainable depend on the intrinsic molecular structure which determines the conformation of the main macromolecular chain and the kind of allowed supramolecular organization.

Better corrosion protection is expected for poly(phenylene)-like film with respect to the PHFBM. Anyway EIS measurements are previsual and corrosion tests (in a corrosive atmosphere) on the films are planned in September 2008.

The corrosion test, standard tests for electrical connectors, are done by exposing the samples for 20 days at 30 °C to an atmosphere containing NO<sub>2</sub> (200 ppb), SO<sub>2</sub> (200 ppb), H<sub>2</sub>S (100 ppb) and Cl<sub>2</sub> (20 ppb) at 70% relative humidity.

#### 6.4 Wear comparison

Figure 96 reports the optical microscopy pictures of the stamped ball and of the wear track after a tribology test on a substrate protected by PHFBM and a substrate protected by a **MB91**-grafted film. In both cases the friction remained low for all the experiment and no rupture of the film was observed.

Uncoated gold

PHFBM

**MB91**

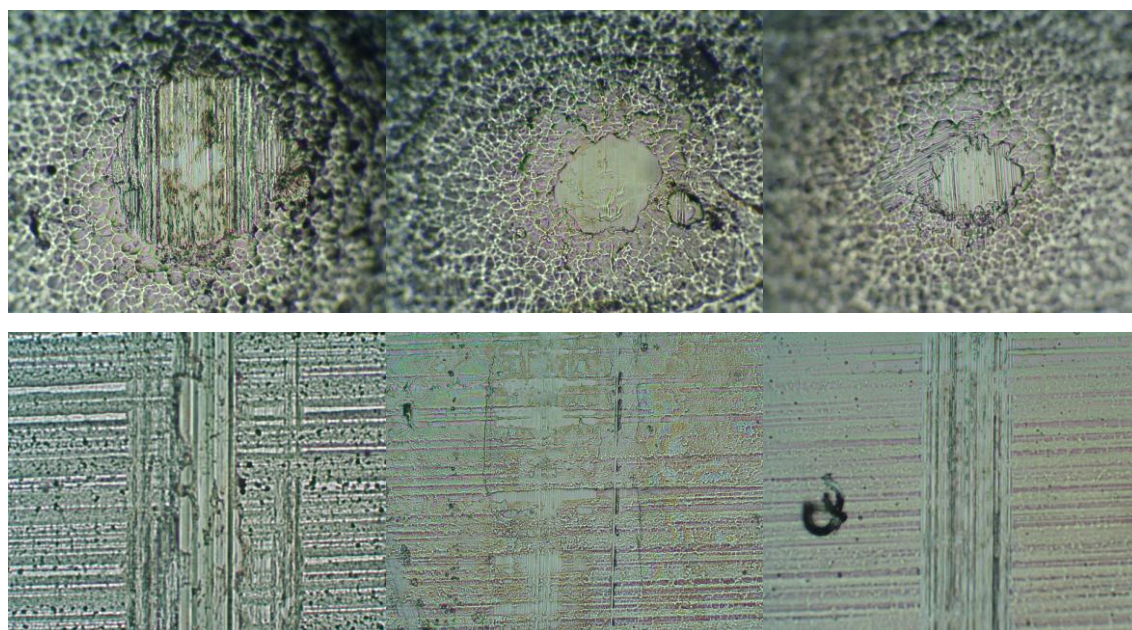


Figure 96. Ball (top) and wear track (bottom) optical micrography after tribology test (800 cycles 1 N). From left to right: uncoated gold, PHFBM, **MB91**-grafted film.

The films are effective in reducing wear because the area of the worn surface on the ball is smaller when the friction test were conducted on film coated substrates than on uncoated ones. That means that the wear rate is lower.

The flattened surface area on the ball is about the same for the two organic film coated substrates which indicates similar wear rates.

The main difference observed between the PHFBM coated and **MB91** coated substrates is the morphological aspect of the ball and of the wear track after the test. The ball, in the case of the PHFBM coated substrate, looks much smoother than the one that has slid on the **MB91**-grafted substrate. In the first case the surface looks almost flat while in the second vertical scratches are visible on the flattened surface.

A similar feature is observable for the wear track. It is almost invisible for the PHFBM coated substrate; it is revealed by the flattening of the top of the substrate lamination stripes. In the case of the **MB91** grafted film the wear track is more easily detectable and vertical scratches are also visible in track as it was on the sphere. Although the track is visible by optical microscopy, when observed in optical profilometry it is very difficult to see the depth of the wear track which confirms that the wear is low in both cases.

We interpret the differences observed for the two kinds of films as due to a difference in “mechanical hardness” of the organic films. The poly(phenylene)-like films wear in a different manner than poly(methacrylate) films. The former have a more rigid structure (as discussed in the section above) and are hard (as measured by AFM approach curves reported in section 3.6). The electrochemical grafting leads to the formation of homogenous films which follow the topography of the sample. Therefore the film covers the sample following the roughness profile (we remember that  $R_a$  for the substrates is  $0,25\ \mu\text{m}$ , the thickness of the film is estimated to about 10 nm). The vertical scratches are likely to be due to the asperities contacts in between the sample and ball which is confirmed by these vertical scratches being also visible for the uncoated gold.

PHFBM polymer chains have a more conformational freedom and therefore are likely to accommodate at the interface. In this way the roughness of the substrate is somehow reduced, by accumulation of the polymer in the cavities resulting in a smoother friction surface.

The wear described above was observed after the tribology tests when low values of the friction coefficient were measured for all the experiment long. We reported in section 5.5, for PHFBM films, that the application of a load of 2,5 N caused at a certain point during the tribology test a sudden increase of the friction coefficient to

values of about 0,6. After this transition, tracks about 2  $\mu\text{m}$  deep were observed by optical profilometry. One of these tracks is shown again in Figure 97. In chapter 5 we made the assumption that the observation of such a deep track corresponded to a fail in the nickel/gold interface. The assumption is supported by the thickness of the gold layer deposited by galvanoplasty on the substrate being 2 $\mu\text{m}$  and that horizontal lamination stripes are visible in the bottom of the track.

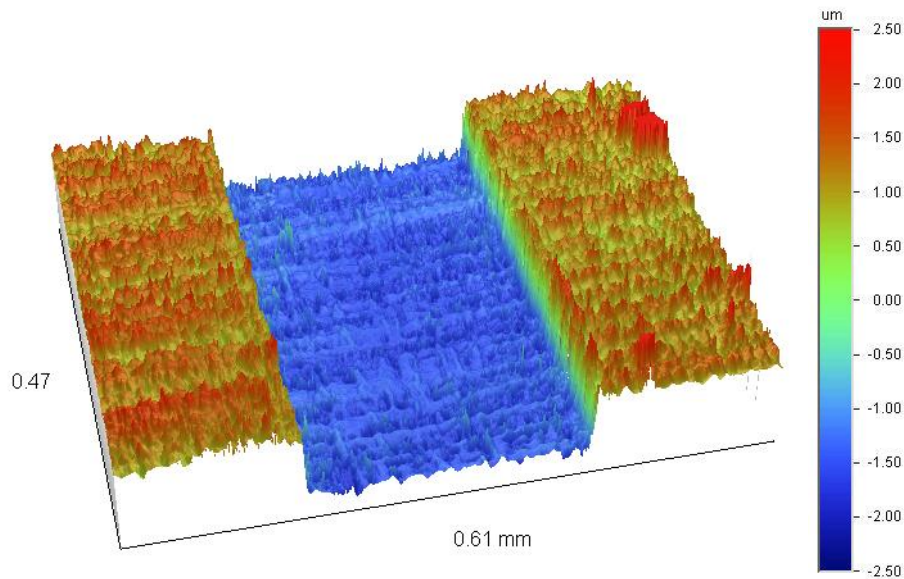


*Figure 97. Optical profilometry image of a wear track after a tribology test (800 cycles, 2,5 N) on a PHFBM + poly(MB20) film.*

We performed XPS spectra in the wear track of Figure 97. The track has a width of about 270  $\mu\text{m}$  while the XPS spot has a diameter of 50  $\mu\text{m}$ . The spot was centered in the track by acquiring a XPS cartography before taking the focalized XPS spectra. Therefore we made sure that the collected signal was really coming from the bottom of the wear track and that no contribution was coming from the film outside the track.

The characteristic core spectra of gold, nickel, carbon and fluorine are reported in Figure 98. The appearance of the Ni 2p peak in the spectrum taken inside the track supports the idea that the gold is removed and the nickel is exposed at the surface. An alternative solution is that the nickel is deposited in the wear track by the ball (that is made in the same material of the substrate, i.e. bronze/nickel/gold).

Gold 4f peaks intensities are reduced in the wear track with respect to outside the track and slightly shifter toward higher energies. This suggests that the overlaying coating is modified by the tribology experiment.

Anyway the ratio between the nickel and the gold remains low. The ratio between Ni 2p<sub>3/2</sub> and Au 4f<sub>7/2</sub> peak areas normalized by Scofield factor give a value of 2,2%. Thus the predominant metal remaining at the interface is gold.

What is more impressing is the area and the shape of the carbon C 1s and fluorine F 1s peaks.

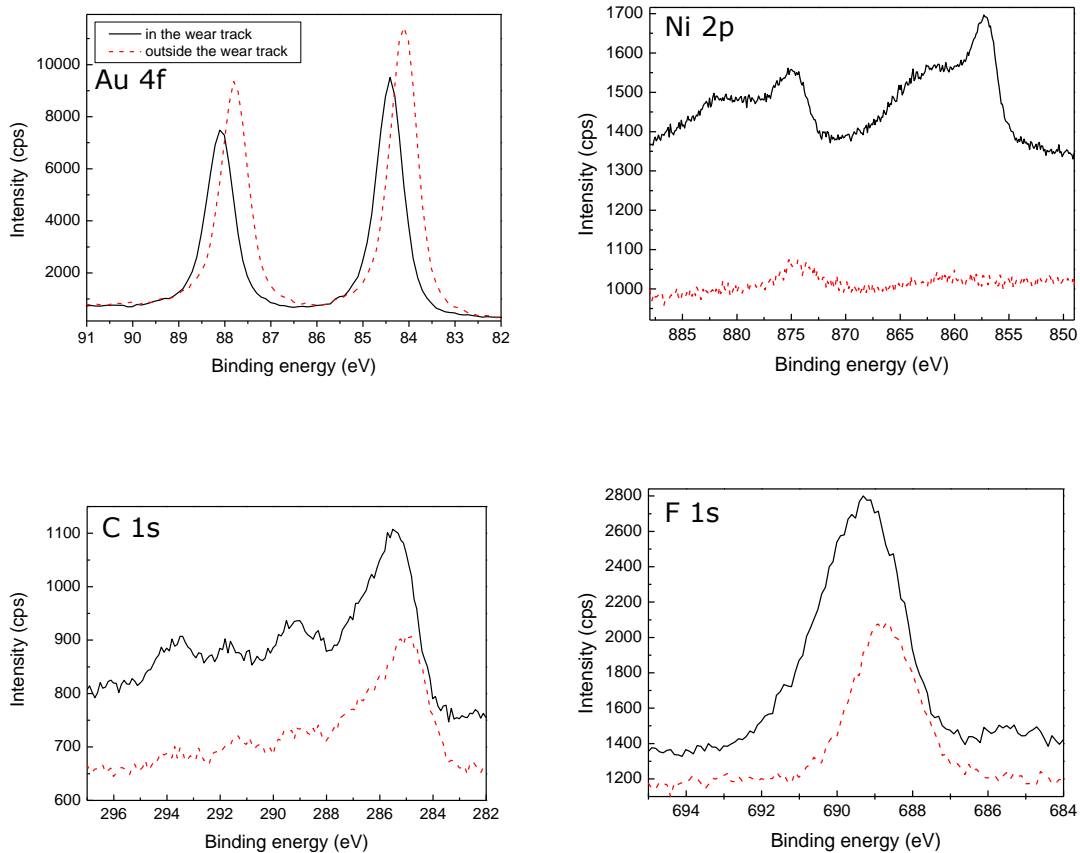


Figure 98. XPS core spectra of a PHFBM films + poly(MB20) recorded inside (black solid line) and outside the wear track (red dashed line) after a tribology test (800 cycles, 2,5N).

The area and the shape of C1s peak and F1s peak is almost the same in the wear track and outside the wear track. Moreover their shapes are not modified which insures that the molecular structure of the organic films as not been modified by phenomena like oxidation or tribochemistry reactions.

It is quite hard to explain how a 2 μm wear track can be produced in the substrate while the intensity and the shape of carbon and fluorine peaks are not modified.

A possible explanation, but quite complicate, is that the biggest part of gold is squeezed off from the nickel/gold interface and the gold polymer interface, while the polymer with a small part of the gold remain in the track (like when the mayonnaise squeeze of a sandwich). Nickel signal could be then detected by XPS either because the remaining film is thin enough to allow for the photoelectron coming from the nickel to come out and being detected or because some nickel is deposited from the ball.

Measurements presented in this section are quite intriguingly although preliminary. To fully explain the phenomenon further experiments would be necessary. This first experiment shows anyway the solidity of the organic coatings and their ability to withstand in an interface under mechanical sollicitation.

## 7 General conclusion and outlook

### 7.1 Conclusions

The objective of this work was to study the covalent grafting of thin lubricant films on metal surfaces to act as dry lubricants for the protection of the electrical contacts.

Two main families of electrografted organic films have been studied: the poly(methacrylate)s and the poly(phenylene)-like films obtained by grafting of aromatic diazonium salts. For this work studies were concentrate on grafting on bronze gold coated substrates which are a model for the industrial gold coated connectors.

It was shown that the fluorinate poly(methacrylate)s can effectively lubricate the studied substrates by reducing friction and wear as measured in macroscopic ball/plane tribology tests.

With respect to the macromolecular structure it was found that presence of fluorinated lateral group is essential to have a good lubricant because purely hydrogenated electrografted poly(methacrylate) PBUMA proved a poor dry lubricant. For these kinds of polymer films the adhesion at the ball/organic film interface plays a major role on the tribological properties.

It has also been shown that the presence of a linear, rather than a ramified fluorinated later group, can improve the resistance to wear and reduce the friction because of the better organization of the macromolecular chains.

For the point of view of electrical conduction it was shown that using thin purely grafted film does not induce increases to the electrical resistance with respect to the uncoated gold contact. Thin purely grafted films could be obtained by choosing appropriate conditions for the electrochemical grafting.

In order to ameliorate electrical conduction properties nanocomposite films were fabricated by interpenetrating the electrografted fluorinated poly(methacrylate) by intrinsic conducting polymers or by carbon nanotubes.

The fabrication of these materials is original and presents interesting physico-chemical properties.

Anyway amelioration of electrical conduction for thin films was not efficacious. Considering moreover the complicate fabrication steps, it does not seem an interesting solution at least for macroscopic low-level electrical connectors.

Poly(phenylene)-like films obtained from the electroreduction of aromatic diazonium films seems very interesting materials for the lubrication and the protection of electrical contacts.

Both (phenylene)-like films bringing a hydrogenated or a fluorinated later group act as good lubricants for gold substrates. Because of the reduction of adhesion better results are found for fluorinated films. Anyway, mechanical properties being better (poly(phenylene) skeleton is hard and compact) adhesion play a less important than for poly(methacrylate).

With a purely poly(phenylene)-like films without any lateral group the better lubricant and wear reduction properties are found (benzenediazonium films).

Films obtained this way are thin and show good electrical conduction properties. The same contact resistance is found in a macroscopic ball/plane configuration with or without the organic protective film.

Moreover because of the compactness of the film and their high gold surface passivation they are expected to effectively reduce environmental corrosion.

## **7.2 Outlooks**

Except the studies on the PAN acting as solid lubricant [177], to our knowledge, no other is has been conducted on electrochemically grafted organic film as dry lubricants. Moreover the field of lubricants for electrical contacts is especially challenging because of supplementary matters about electrical conduction.

Thus, although this thesis tried in exploring this subject, many questions and research ways remain open after this work.

### **Short term outlooks**

On the presented results two arguments still need to be clarified.

The first is the way in which the electrical conduction is possible through the interface presenting an organic film in it. Is the conduction due to asperities piercing the film and establishing direct metal/metal contacts? And in that case why the friction is low and no adhesion is observed after the tests on the ball and on the plane?

Or, is the conduction possible by tunneling where the film is pinned and extremely thinned?

In the poly(phenylene)-like film is conduction possible through the poly(conjugated) structure? And in that case what is the intrinsic resistance of the film?

Many of these questions could be resolved by experiments on the static electrical contact resistance as a function of pressure and temperature in a smooth ball/plane configuration. Inquiring these phenomena at the microscopic scale of the AFM could also bring responses on the role of the single asperities.

The second question which remains open is what happens to the organic film during the tribology tests and what modifications are caused to its molecular structure. What looks particularly intriguing is the first XPS results which show that the polymer is remaining in the wear track also when severe wear is observed and the track is "deep". These results will need to be confirmed and integrated by other local surface analysis techniques (IR microscopy, SIMS, etc.)

### **Long term outlooks**

Poly(phenylene)-like films seem very promising as organic films playing the role of dry lubricants. Some molecular structures have been studied. Sophisticated structures, bringing substituent groups inspired from traditional liquid lubricants, have been studied at the beginning of this thesis. It has shown anyway that the use of the simple benzenediazonium tetrafluoroborate leads to very good lubricant properties. The use of other simple commercial salts such as the 4-nitrobenzenediazonium could lead to interesting results. It will be also interesting to study aromatic salts bringing as lateral group a very short fluorinated substituent group such as the trifluoromethyl group or having a fluorinated benzene ring.

A research way that has not been explored but looks very interesting is studying electrografted dry lubricants on more industrial other than gold.

Gold is added on bronze based electrical contacts because it does not present a stable insulating oxide, is soft (allowing for low contact resistances) and therefore presents low adhesion. Anyway coating the bronze with a noble metal severely increases its corrosion (the bronze act as a “sacrificial metal”) and for that reason the inter-layer of nickel has to be added. The organic film could efficiently replace the roles played by the gold (lubrication and avoiding formation of an oxidized interface) without promoting the corrosion of the bronze. Moreover removal of a noble metal from the fabrication process will have industrial and economic interest.

Therefore it will be interesting to study the lubrication of other metal substrates such as bronze, copper, nickel or tin.

## Appendix A – List of acronyms and abbreviations

AFM	Atomic Force Microscopy
<b>BD</b>	Benzenediazonium tetrafluoroborate
APTS	3-(aminopropyl)triethoxysilane
ATR	Attenuated total reflection
BUMA	Butyl methacrylate (see Figure 8)
DMF	N,N-Dimethylformamide
EDOT	2,3-Dihydrothieno[3,4-b]-1,4-dioxin
EIS	Electrochemical impedance spectroscopy
EQCM	Electrochemical Quartz Crystal Microbalance
<b>FL2921</b>	4-Hexylthiophenyldiazonium tetrafluoroborate (see Figure 12)
HFBM	2,2,3,3,4,4,4-Heptafluorobutyl methacrylate (see Figure 8)
HFIPM	1,1,1,3,3,3-Hexafluoroisopropyl methacrylate (see Figure 8)
IR	Infrared
ITO	Indium Thin Oxide
<b>MB83</b>	4-Perfluorohexyl-ethyl-thiophenyl diazonium tetrafluoroborate) (see Figure 12)
<b>MB91</b>	4-Perfluorohexylthiophenyldiazonium tetrafluoroborate (see Figure 12)
MEMS	Micro Electrical Mechanical Systems
MOD	4-Methoxybenzenediazonium tetrafluoroborate
<b>NBD</b>	4-Nitrobenzenediazonium tetrafluoroborate
NEMS	Nano Electrical Mechanical Systems
NT	nanotubes
PAA	poly(allylamine)
PAN	poly(acrylonitrile)
PBUMA	poly(butylmethacrylate)
PEDOT	poly(ethylenedioxythiophene)
PFPE	Perfluoropolyether
PHFBM	poly(2,2,3,3,4,4,4-Heptafluorobutyl methacrylate)

PHFIPM	poly(1,1,1,3,3,3-Hexafluoroisopropyl methacrylate)
PTFE	polytetrafluoroethylene
PZC	potential of zero charge
SAM	Self Assembled Monolayer
SEM	Scanning Electron Microscopy
SFA	Surface-force apparatus
SIMS	Secondary ion mass spectrometry
TEAP	Tetraethylammonium perchlorate
THF	Tetrahydrofuran
UHV	Ultra high vacuum
XPS	X-ray photoelectron spectroscopy

## Appendix B – Introduction to electrical contacts

### B.a Introduction – Contact surfaces

Typically a contact is established by pushing together two conducting solids. The surface of these solids result from the combinations of three elements: physical-chemical structure, roughness and macroscopic shape, as represented in Figure 99. Actually the contact is established in an area which has a roughness [178, 179] and a physical-chemical structure quite complicated. There are multiple superficial layers [180] which have variable thicknesses and compositions. They are due to the fabrication processes and the following reactions of the surface and the environment.

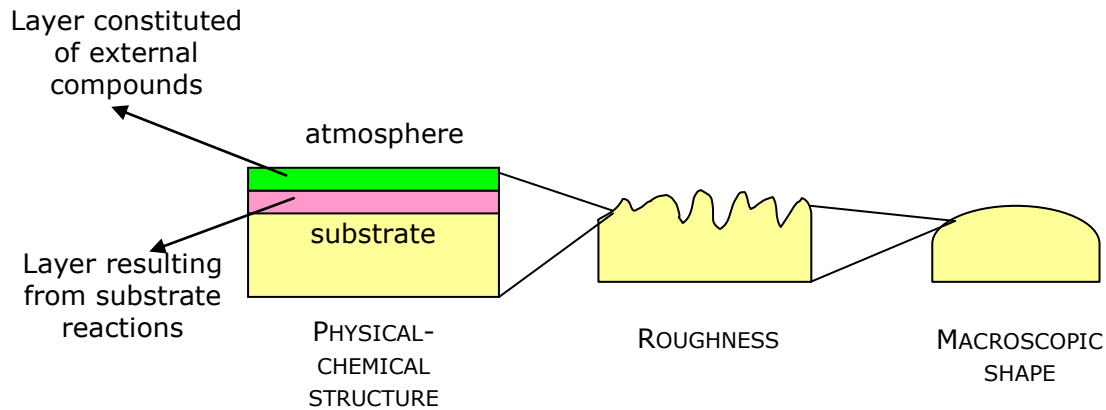


Figure 99. The three elements of the initial surface of an electrical contact [181].

All those parameters are difficult to control, therefore experimental work is often conducted on simplified contact models which are easier to control.

The shape of the contact surface depends on the shape of the solids which compose the contact. In the research field of electrical contact the configuration is often ball/plane, cylinder/cylinder or cylinder/plane.

### B.b Mechanics of electrical contacts

#### Elastic regime

The contact area is determined by the macroscopical shape of the two solids and their intrinsic mechanical properties as defined by Young modulus  $E$  and Poisson ratio  $\nu$ .

The case of an elastic contact in between a ball and a plane having smooth surfaces can be described by Hertz theory [182]. The contact surface is a circle with radius  $a$

$$a = \sqrt[3]{\frac{3FR}{4E^*}}$$

where  $R$  is the radius of the ball,  $F$  the applied normal force and  $E^*$  the equivalent elastic modulus defined as

$$\frac{1}{E^*} = \frac{1-\nu_1^2}{E_1} + \frac{1-\nu_2^2}{E_2}$$

where the subscripts 1 and 2 refer to the two solids establishing the contact.

The average pressure as the expression

$$P_m = \frac{F}{\pi a^2} = \frac{2}{3} \sqrt[3]{\frac{6FE^{*2}}{\pi^3 R^2}}$$

and the local pressure  $p(r)$  at a distance  $r$  from the center, represented in xx, is

$$p(r) = \frac{3}{2} \frac{F}{\pi a^2} \sqrt{1 - \frac{r^2}{a^2}}$$

Hertz theory is constructed by considering ideally smooth surfaces. But real surfaces are always rough. The presence of roughness greatly complicates the theoretical treatment. Greenwood and Tripp have studied a smooth ball/rough plane contact [183]. Their model assumes the height of asperities is much smaller than the radius  $R$  of the ball and that they follow a quadratic statistical distribution  $R_q$ . The radius  $a^*$  of the apparent contact area, represented in Figure 100, is given by

$$a^* = a \left( 1 + \alpha \right)$$

$$\alpha = \frac{RR_q}{a^2}$$

The effect of roughness is enhanced when the applied normal force is low.

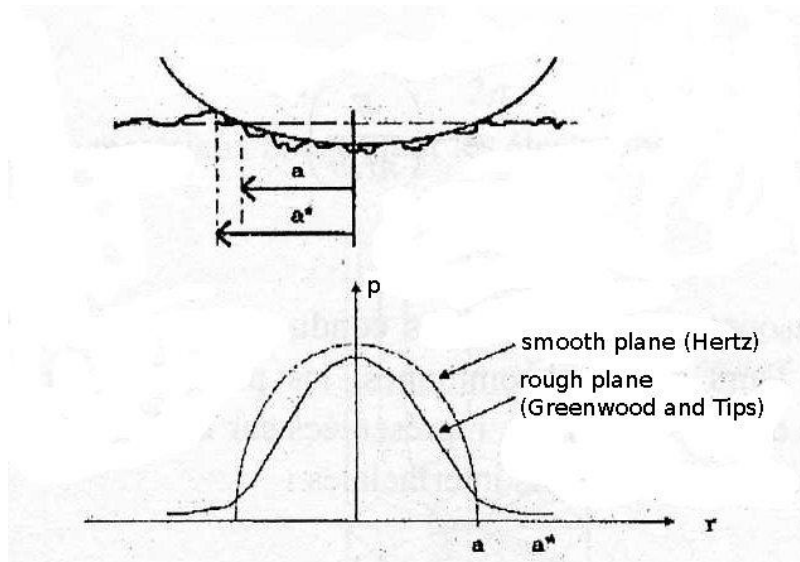


Figure 100. Contact in between a smooth ball and a rough plane: apparent contact radius and local pressure.

The true contact area is smaller than the apparent contact area and composed of an ensemble of spots and the area of the mechanical contact is smaller than the apparent area as represented in Figure 101.

### Plastic regime

The contact is in the plastic regime when the deformation becomes irreversible. In that case the radius of the deformed region can be determined from Brinell hardness as

$$a = \sqrt{\frac{F}{\pi H_B}}$$

where  $H_B$  is Brinell hardness.

### B.c Contact electrical resistance

#### Contact with conductors quasi-continuity

The simplest case is that of two smooth perfectly conductive electrodes in the ball/plane configuration. They communicate through a singular circular surface which has a radius as calculated by Hertz.

If the radius of the surface is much bigger than electrons free path than the electrical resistance due to the confinement of current lines is given by

$$R_c = \frac{\rho}{2a}$$

where  $\rho$  is the resistivity of the electrodes material.

When the contact radius is smaller than electrons free path the contact electrical resistance is given by Sharvin formula:

$$R_c = \frac{4\rho l}{3\pi a^2}$$

- electrical contact area
- +● mechanical contact area (no zero stress)
- +●+○ apparent contact area

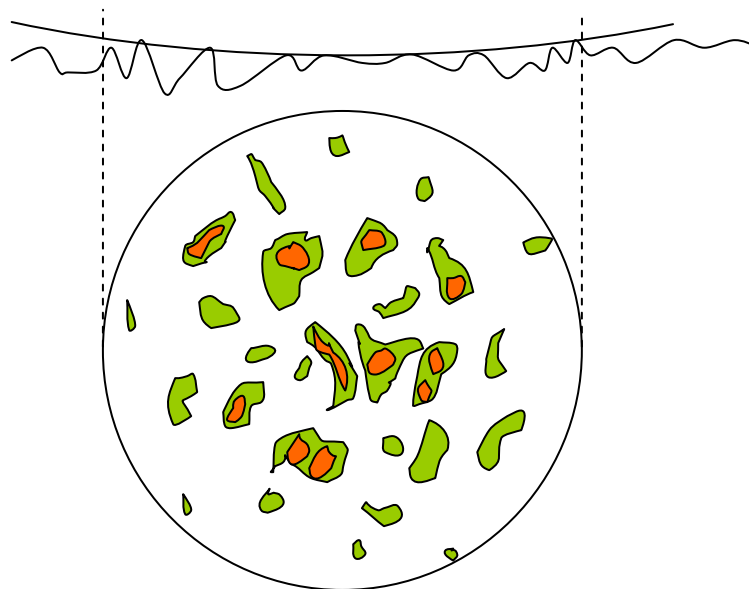


Figure 101. Contact areas for a ball/plane configuration.

When surfaces are rough the contact is established by an ensemble of spots within the apparent contact surface. The resulting contact resistance is obtained by a parallel off all the contact resistances of each spot.

The simplest case is that of  $n$  circular spots having the same radius  $b$  and regularly distributed within the apparent contact surface of radius  $a$ . In that case the resistance is given by

$$R_c = \frac{\rho}{2} \left( \frac{1}{a} + \frac{1}{nb} \right)$$

### Contact with discontinuous conductors

This is the case when the conductors are coated by a less conducting film (such as metal oxide or a lubricant).

In the case of a singular contact (smooth surfaces) in a ball plane configuration the total contact resistance is given by

$$R_t = R_c + R_f = \frac{\rho}{2a} + \frac{\rho_f e}{\pi a^2}$$

where  $\rho_f$  is the resistivity of the film and  $e$  its thickness.

In the case of multiple circular passages, when  $n$  spots or  $b$  radius are uniformly distributed in the apparent contact area, the resistance is

$$R_t = \frac{\rho}{2a} + \frac{1}{n} \left( \frac{\rho}{2b} + \frac{\rho_f e}{\pi b^2} \right)$$

For certain spots the film resistance can be much greater than constriction resistance while for other spots the contrary is possible. The current conduction will be then occurs mainly through these latter spots.

The size, the shape and the distribution of the spots as the resistivity of the film are often unknown and it is thus difficult to give analytic expression of the total contact resistance.

The content of this appendix is mainly inspired from [24, 31]. The reader can refer to these theses for further information or to the references cited in the appendix.

## Appendix C – Introduction to EIS

### C.a Introduction

EIS approach is based on perturbing an electrochemical cell with an alternating signal of small magnitude and observing the way in which the system follows the perturbation at steady state.

### C.b Definition of impedance and representation

To the electrochemical cell a perturbation sinusoidal electrical potential  $e$  is applied:

$$e = E \exp j\omega t$$

where  $\omega$  is the angular frequency, which is  $2\pi$  the conventional frequency in Hz. If the perturbation is small and thus the system behave as linear at the steady state a current  $i$  will be measured

$$i = I \exp j(\omega t + \phi)$$

where  $\phi$  is the phase shift of current with respect to voltage perturbation. It is then possible to define the impedance as:

$$Z = \frac{e}{i} = Z_0 \exp j\phi = Z_0 (\cos\phi + j \sin\phi) = Z' + jZ''$$

Different kind of EIS can be performed by varying one parameter of the voltage perturbation and measuring the current response. The most common impedance technique is based on a frequency spectroscopy. The frequency of the perturbation signal is varied from low to high frequencies (or the contrary) and the complex current is measured which allow for calculating the impedance value at each frequency.

The values of the impedance are then commonly plotted in a Nyquist or a Bode plot. An example of Nyquist plot is represented in Figure 102. In this kind of plot for each measured point the opposite of the imaginary part of the impedance is reported as a function of the real part.

This kind of plot often allows electrochemists to individuate relevant phenomena.

Anyway Nyquist plot does not reports explicitly the values of the angular frequency.

When this is necessary data can be plotted in a Bode plot which reports the values of

the modulus and the phase of the impedance as a function of the angular frequency ( $\omega = 2\pi\nu$ ) or of the frequency ( $\nu$ ). An example is reported in Figure 103.

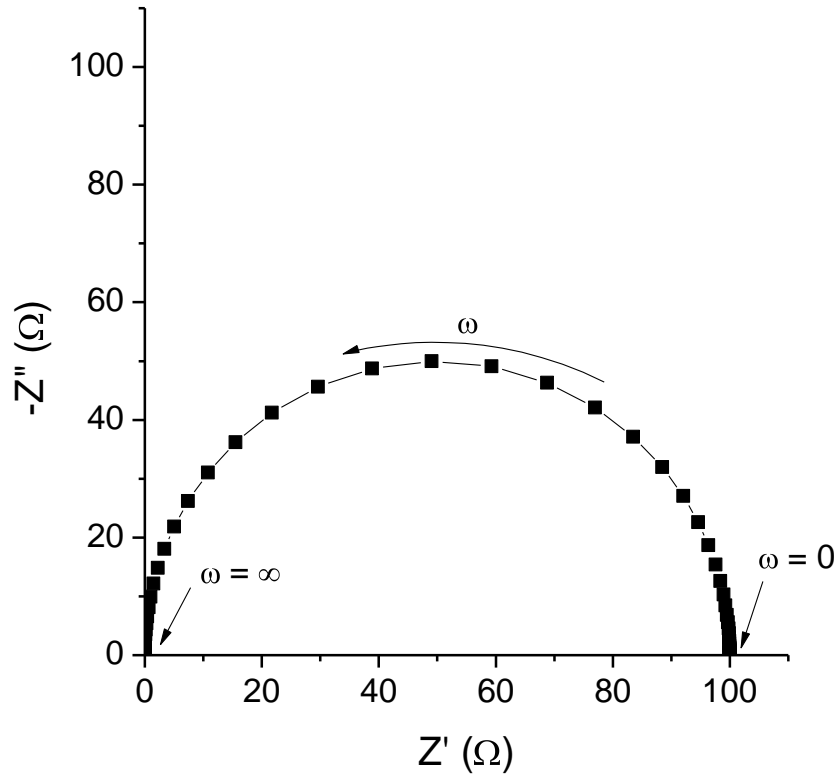


Figure 102. Nyquist plot of impedance measured as a function of perturbation frequency.

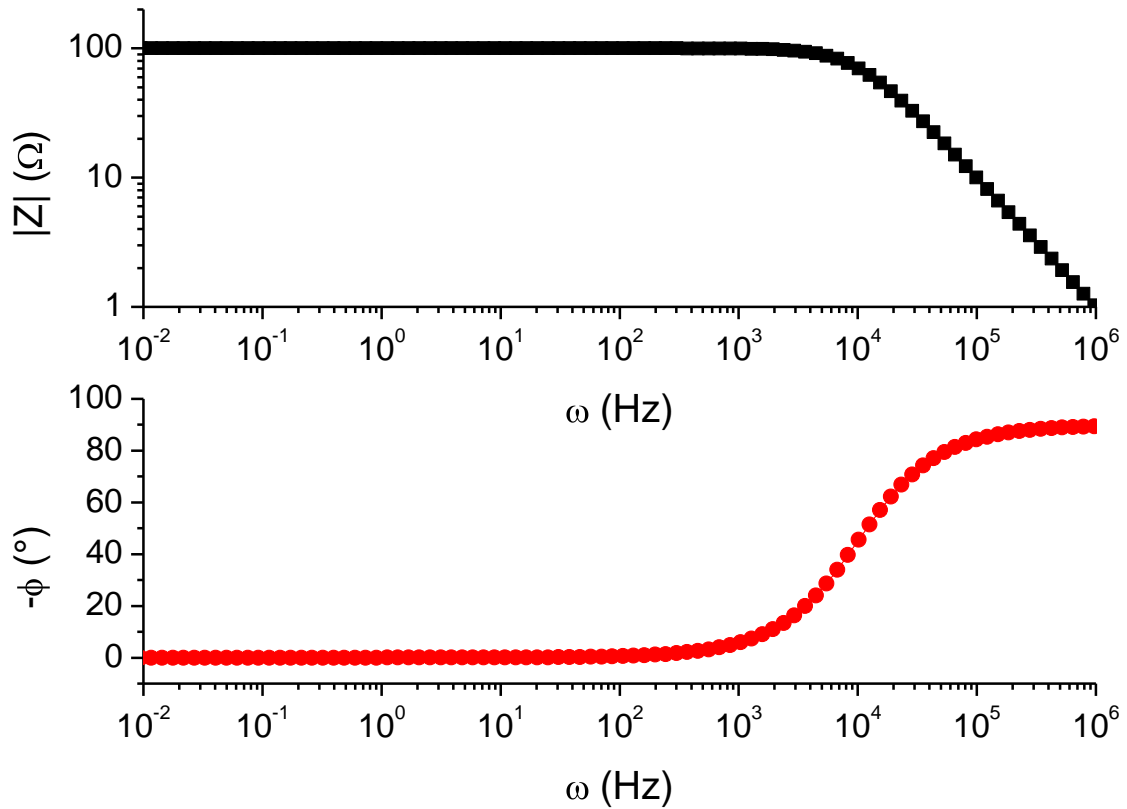
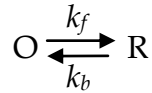


Figure 103. Bode plot of the same data reported in Figure 102.

### C.c Charge-transfer resistance

Let consider the following electrode process, wherein species O and R engage in a one-electron transfer at the interface without being involved in any other chemical step:



The rate of the forward and backward processes will then be:

$$\begin{aligned} v_f &= k_f C_O(\theta, t) \\ v_b &= k_b C_R(\theta, t) \end{aligned}$$

where  $C_O(\theta, t)$  and  $C_R(\theta, t)$  are the concentration of O and R at the electrode surface at the time  $t$ .

In the framework of the *transition state theory* it is found that the rate constants  $k_f$  and  $k_b$  are expressed by:

$$\begin{aligned} k_f &= A_f \exp\left(-\frac{\Delta G_{oc}^\ddagger}{RT}\right) \exp\left\{\alpha f (E - E^{0'})\right\} \\ k_b &= A_b \exp\left(-\frac{\Delta G_{oa}^\ddagger}{RT}\right) \exp\left\{-\alpha f (E - E^{0'})\right\} \end{aligned}$$

where  $A_f$  and  $A_b$  are Arrhenius prefactors,  $\Delta G_0^\ddagger$  the activation energy of the cathodic and anodic reactions in standard conditions,  $R$  the perfect gases constant,  $T$  the temperature,  $\alpha$  the transmission coefficient,  $E$  the applied potential and  $E^{0'}$  the formal potential of the redox couple,  $f$  is defined as  $F/RT$  where  $F$  is the Faraday constant (96485 C). The term containing the transmission coefficient  $\alpha$  expresses the variation of the rate constants when passing from standard to generic conditions. The activation free energy in general conditions  $\Delta G_a^\ddagger$  is less than the  $\Delta G_{0a}^\ddagger$  by a fraction  $(1 - \alpha)$  of the total energy change when a  $\Delta E$  is applied with respect to the formal potential.

The forward and backward rate constants can be expressed in term of  $k^0$  the *standard rate constant*:

$$\begin{aligned} k_f &= k^0 \exp\left\{\alpha f (E - E^{0'})\right\} \\ k_b &= k^0 \exp\left\{-\alpha f (E - E^{0'})\right\} \end{aligned}$$

$k^0$  is a measure of the kinetic facility of a redox couple. A system with a large  $k^0$  will achieve the equilibrium on a short time scale, but a system with small  $k^0$  will be sluggish.

Kinetic equation containing  $k^0$  involve the formal potential which is a quantity of more difficult experimental access with respect to the overpotential  $\eta$  which is the potential applied with respect to the equilibrium potential of the system, a facile measurable quantity ( $\eta = E - E_{eq}$ ).

Therefore a quantity called *exchange current* is introduced

$$i_0 = FAk^0 C_O^{*\alpha} C_R^{*\alpha}$$

where  $A$  is the area of electrode surface, and  $C^*$  the bulk concentration of the specie  $O$  and  $R$ .

At the equilibrium, when the applied potential  $E$  is equal to  $E_{eq}$  the net current is zero. Anyway a faradaic activity is present, reduction and oxidation exists simultaneously. But the cathodic current  $i_c$  is equal to anodic current  $i_a$  and this balance current is the exchange current which value is  $i_0$ . Thus  $i_0$  measures the faradaic activity at the equilibrium.

When the solution is well stirred or current are kept so low that the surface concentrations do not differ appreciably from bulk values the current flowing in the electrochemical cell  $i$  as a function of the overpotential  $\eta$  is expressed by *Butler-Volmer equation*

$$i = i_0 \left[ e^{-\alpha f \eta} - e^{\alpha f \eta} \right]$$

When little a little potential perturbation with respect to the equilibrium is applied, which means that  $\eta$  is small, the Butler-Volmer equation can be linearized as

$$R_{ct} = -\frac{\eta}{i} = \frac{RT}{Fi_0}$$

The *charge transfer resistance*  $R_{ct}$  serves as a convenient index of kinetic facility. For very large  $k^0$  values it approaches 0.

### **C.d Determination of $R_{ct}$ from EIS measurements**

$R_{ct}$  can be easily determined by EIS in the *high-frequency* limits when the mass transfer is unimportant on the expression of the impedance. This means assuming the same

approximation necessary for obtaining the Butler-Volmer equation reported above, that the electrode surface concentrations are equal to the solution bulk concentrations. This condition can be obtained by stirring the solution using a rotating disk electrode [184].

In that case the expression of impedance is

$$Z = R_{\Omega} - j \frac{R_{ct}}{R_{ct}C_d\omega - j}$$

Hence the Nyquist plot is a semicircle centered at  $Z' = R_{\omega} + R_{ct}/2$  and  $Z'' = 0$  and having a radius  $R_{ct}/2$ . Where  $R_{\omega}$  is the resistance of the solution and  $C_d$  the capacity of the electrochemical double layer. The shape of the Nyquist plot is represented in Figure 104.

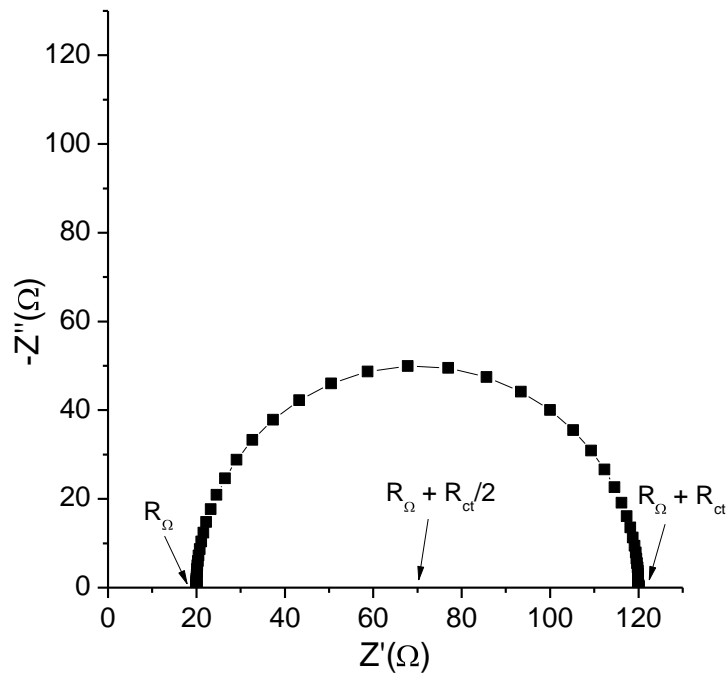


Figure 104. Nyquist plot obtained for a system kinetically controlled (no mass transfer limitations).

The equation described above is obtained for a system which is controlled by kinetic aspects and in which mass transfer is not limiting. Even in absence of stirring this is generally a good approximation at high frequencies.

The opposite case is that of a system that is totally limited by diffusion (no stirring is provided and kinetic is extremely rapid).

In that case the impedance of the Electrochemical cell is the *Warburg impedance*

$$Z_w = \sigma \sqrt{\omega} (-j)$$

$$\sigma = \frac{RT}{n^2 F^2 A \sqrt{2}} \left( \frac{1}{C_o^* \sqrt{D_o}} + \frac{1}{C_R^* \sqrt{D_R}} \right)$$

where  $D_O$  and  $D_R$  are the diffusion coefficient of O and R. In the Nyquist plot it is represented by a straight line inclined at  $45^\circ$  (see Figure 105).

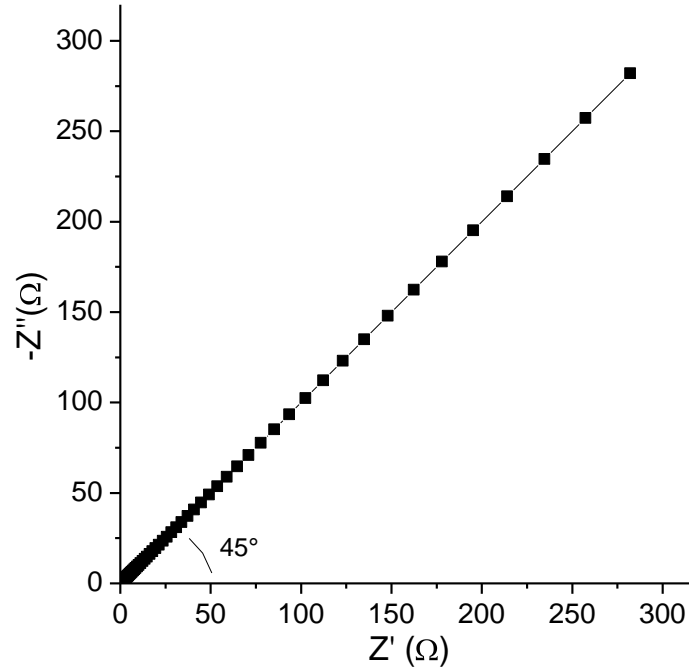


Figure 105. Nyquist plot obtained of the Warburg impedance.

Actually a system purely mass controlled for all the frequencies measured in typical EIS experiments it is hardly observable. At high frequencies almost all the systems exhibits a kinetic-controlled behavior. Warburg impedance is observed as a *low frequencies* limit where impedance of the electrochemical cell is dominated by diffusive phenomena.

Real systems are typically characterized by a kinetic controlled region at high frequencies, showing a semicircle shape in the Nyquist plot, while at low frequencies impedance is dominated by diffusive phenomena and the straight line at  $45^\circ$  degrees typical of Warburg impedance shows up. An example of such system is reported in Figure 106.

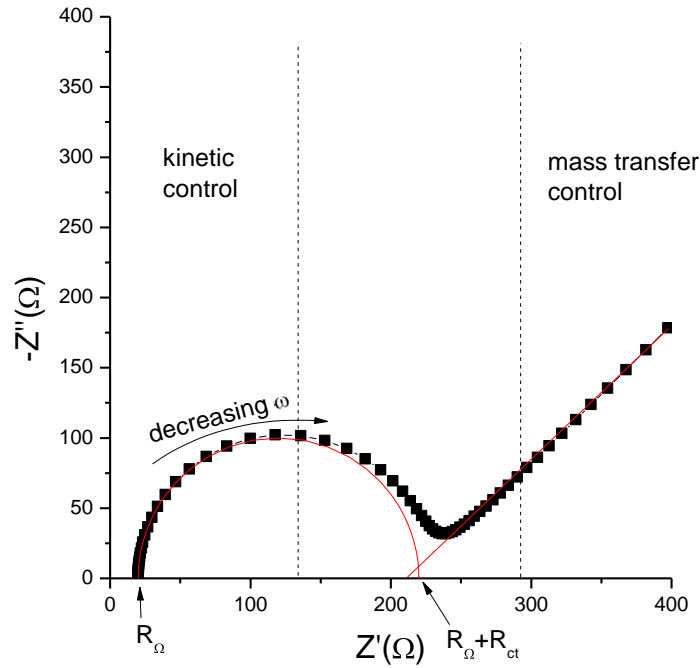


Figure 106. Impedance plot for an electrochemical system. Regions of mass-transfer and kinetic control are found respectively at low and high frequencies.

### C.e Fitting with equivalent circuits

Although some relevant quantities can already be quickly grasped from Nyquist and Bode plots the determination of physical quantities from EIS measurements passes by fitting experimental data with a theoretical model.

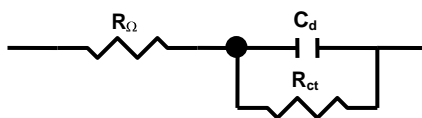
The simplest electrochemical cell that can be imagined is that of a solution containing just the supporting electrolyte. In that case the impedance will be given by

$$Z = R_{\Omega} + \frac{1}{j\omega C_d}$$

where  $R_{\Omega}$  is again the resistance of the solution and  $C_d$  the double-layer capacitance (the electrochemical double layer acting somewhat as a plane capacitor). Another way to imagine the system is to represent it into an equivalent electrical circuit that in this case will be simply

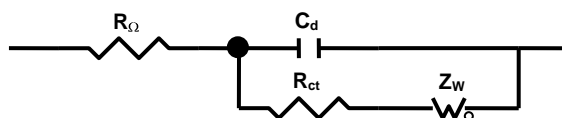


A system that is purely kinetic controlled (see analytic expression of impedance above) will be represented by a *Randles circuit*



If the expression of impedance of this circuit is calculated the same equation reported above is found.

To account for the diffusion a “new” circuital element as to be considered, this will have the Warburg impedance. The data reported in Figure 106 is obtained with the following equivalent circuit



In all these simple cases the equivalent circuits have determined from the analytical expression of electrochemical cell impedance.

A great number of theoretical model and of semi-empirical equivalent circuits exists in the literature for fitting different problems that can be studied by EIS.

This appendix is written by summing up (and sometime oversimplifying) contents from [185-188]. The reader will refer to these texts for more rigorous and complete information.

## 8 Index

Ringraziamenti.....	5
Summary.....	7
1 Introduction.....	8
1.1 Objective of the work.....	8
1.2 Previous works on the tribology of grafted organic films .....	10
1.3 Specific studies on the lubrication on electrical contacts.....	12
1.4 Electrografting. A versatile method for covalent surface functionalization. 14	
Grafting of aromatic diazonium salts.....	15
Electrografting of poly(methacrylate)s .....	16
2 Methodologies .....	18
2.1 ANR Project NANOCONNECT .....	18
2.2 Molecules choice and design .....	19
2.3 The role of this thesis in the NANOCONNECT project.....	22
2.4 Substrates.....	23
2.5 General experimental details.....	26
Electrochemical equipment.....	26
Surface spectroscopies .....	26
Contact angle measurements.....	26
Tribology experiments.....	26
Atomic force microscopy.....	27
3 Grafting of aromatic diazonium salts.....	28
3.1 Introduction.....	28
3.2 Experimental section.....	29
Reagents and electrochemistry .....	29
3.3 Electrochemical grafting of diazonium salts on polycrystalline gold substrates .....	29
Electrochemical grafting of benzenediazonium tetrafluoroborate (BD).....	39
3.4 Physical chemistry characterization of the films .....	41
Infrared spectroscopy .....	41

---

X-ray photoelectron spectroscopy .....	45
3.5 Surface energy measurements .....	48
3.6 AMF approach/withdraw curves .....	49
FL2921 diazonium salt modified gold sample .....	50
MB83 diazonium salt modified gold sample .....	52
3.7 Tribological tests .....	53
Effect of the fluorination .....	53
Effect of the lateral group .....	59
3.8 Chapter conclusions .....	62
4 Grafted poly(methacrylate)s .....	63
4.1 Introduction .....	63
4.2 Experimental section .....	64
Reagents .....	64
4.3 Electrochemical grafting .....	65
Monomers electrochemical behavior .....	65
Electrografting in different solvents .....	66
4.4 Physical chemistry characterization of the films .....	70
IR characterization .....	70
XPS characterization .....	71
Contact angle measurements .....	73
4.5 Tribological tests .....	73
Effect of the solvent used for electrografting .....	74
Effect of fluorination .....	77
Effect of the lateral chain on tribological properties .....	79
4.6 Chapter conclusions .....	81
5 Composites of grafted poly(methacrylate)s and conductive charges .....	83
5.1 Chapter introduction .....	83
Composites with PEDOT and fluorinated PEDOT .....	83
Composites with carbon nanotubes .....	84
Present chapter structure .....	86
5.2 Experimental details .....	86

---

Electrochemistry and electrochemistry reagents .....	86
Carbon nanotubes 2D-networks adsorption and characterization .....	86
Carbon nanofibers functionalization and grafting .....	86
Carbon nanotubes 2D-networks grafting .....	87
Zonyl BA-L® grafting .....	87
5.3 Electrochemical study and characterization of fluorinated PEDOTs .....	87
Films deposition .....	87
Electrochemical impedance spectroscopy characterization .....	88
Electrochemical Quartz Crystal Microbalance analysis .....	95
XPS analysis .....	100
5.4 Grafting of poly(methacrylates)s/PEDOTs composites and physical chemistry characterizations .....	102
Electropolymerization of EDOT and derivatives on gold electrodes .....	102
XPS characterization .....	107
Infra Red characterization .....	109
5.5 Study of the tribological properties of the poly(methacrylates)s/PEDOTs composites .....	110
5.6 Elaboration of composites of poly(methacrylate)s and adsorbed nanotubes 116	
Grafting of PAN and chemical reduction to PAA .....	116
Carbon nanotubes adsorption .....	119
Zonyl BA-L® grafting .....	121
PHFBM and PHFIPM electrografting .....	124
5.7 Study of the tribological properties of the composites of poly(methacrylates) and adsorbed nanotubes .....	125
5.8 Elaboration of composites of poly(methacrylate)s and grafted carbon nanotubes .....	133
5.9 Study of the tribological properties of the composites of poly(methacrylate)s and grafted carbon nanotubes .....	141
5.10 Summary and chapter conclusions .....	145
Fluorinated PEDOTs/PHFBM composites .....	145

Fluorinated poly(methacrylate) composites with adsorbed nanotubes.....	146
Composites with grafted carbon nanotubes.....	146
Chapter global conclusion.....	146
6 Discussion and comparison of tribological behaviors .....	148
6.1 Introduction to the chapter .....	148
6.2 Films growth mechanisms .....	148
6.3 EIS measurements and corrosion protection.....	151
6.4 Wear comparison.....	154
7 General conclusion and outlook.....	159
7.1 Conclusions .....	159
7.2 Outlooks.....	160
Short term outlooks.....	160
Long term outlooks .....	161
Appendix A - List of acronyms and abbreviations.....	163
Appendix B - Introduction to electrical contacts.....	165
Elastic regime .....	165
Plastic regime .....	167
Contact with conductors quasi-continuity .....	167
Contact with discontinuous conductors .....	169
Appendix C - Introduction to EIS.....	170
8 Index.....	178
9 Bibliography.....	182

## 9 Bibliography

1. Lee, H., B.P. Lee, and P.B. Messersmith, *A reversible wet/dry adhesive inspired by mussels and geckos*. *Nature*, 2007. **448**(7151): p. 338.
2. Autumn, K., et al., *Evidence for van der Waals adhesion in gecko setae*. *Proceedings of the National Academy of Sciences of the United States of America*, 2002. **99**(19): p. 12252.
3. Sun, T.L., et al., *Bioinspired surfaces with special wettability*. *Accounts of Chemical Research*, 2005. **38**(8): p. 644.
4. Hu, D.L., B. Chan, and J.W.M. Bush, *The hydrodynamics of water strider locomotion*. *Nature*, 2003. **424**(6949): p. 663.
5. Urbakh, M., et al., *The nonlinear nature of friction*. *Nature*, 2004. **430**(6999): p. 525.
6. Yoshizawa, H., Y.L. Chen, and J. Israelachvili, *Fundamental mechanisms of interfacial friction. 1. Relation between adhesion and friction*. *J. Phys. Chem.*, 1993. **97**(16): p. 4128.
7. Maboudian, R. and C. Carraro, *Surface Chemistry and Tribology of MEMS*. *Annual Review of Physical Chemistry*, 2004. **55**(1): p. 35.
8. Georges, J.-M., *Frottement, usure et lubrification*. 2000, Paris: CNRS Editions. 424.
9. Bhushan, B., J.N. Israelachvili, and U. Landman, *Nanotribology: friction, wear and lubrication at the atomic scale*. *Nature*, 1995. **374**(6523): p. 607.
10. Israelachvili, J.N. and D. Tabor, *The shear properties of molecular films*. *Wear*, 1973. **24**(3): p. 386.
11. Yamada, S. and J. Israelachvili, *Friction and Adhesion Hysteresis of Fluorocarbon Surfactant Monolayer-Coated Surfaces Measured with the Surface Forces Apparatus*. *J. Phys. Chem. B*, 1998. **102**(1): p. 234.
12. Yoshizawa, H., C. You-Lung, and J. Israelachvili, *Recent advances in molecular level understanding of adhesion, friction and lubrication*. *Wear*, 1993. **168**(1-2): p. 161.
13. Yoshizawa, H. and J. Israelachvili, *Relation between Adhesion and Friction Forces across Thin-Films*. *Thin Solid Films*, 1994. **246**(1-2): p. 71.
14. Liu, H. and B. Bhushan, *Nanotribological characterization of molecularly thick lubricant films for applications to MEMS/NEMS by AFM*. *Ultramicroscopy*, 2003. **97**(1-4): p. 321.
15. Tas, N., et al., *Stiction in surface micromachining*. *Journal of Micromechanics and Microengineering*, 1996. **6**(4): p. 385.
16. Miller, S.L., et al., *Failure modes in surface micromachined microelectromechanical actuation systems*. *Microelectronics Reliability*, 1999. **39**(8): p. 1229.
17. Liu, H.W., et al., *Investigation of the adhesion, friction, and wear properties of biphenyl thiol self-assembled monolayers by atomic force microscopy*. *Journal of Vacuum Science & Technology a-Vacuum Surfaces and Films*, 2001. **19**(4): p. 1234.
18. Noël, S., et al., *Adhesion properties and surface analyses of monolayers of  $n$ -dodecanethiol self-assembled on galvanic gold*. *Surface and Interface Analysis*, 1998. **26**(12): p. 889.
19. Tambe, N.S. and B. Bhushan, *Nanotribological characterization of self-assembled monolayers deposited on silicon and aluminium substrates*. *Nanotechnology*, 2005. **16**(9): p. 1549.

20. Devaprakasam, D., et al., *Boundary lubrication additives for aluminium: A journey from nano to macrotribology*. Tribology International, 2005. **38**(11-12): p. 1022.
21. Mekhalif, Z., et al., *Self-assembled monolayers of n-dodecanethiol on electrochemically modified polycrystalline nickel surfaces*. Langmuir, 1997. **13**(8): p. 2285.
22. Mekhalif, Z., et al., *Surface modifications of nickel substrates with self-assembled monolayers of alkanethiols for electrical contact applications*. Surface and Coatings Technology, 1998. **100-101**: p. 463.
23. Noel, S., et al., *Self-assembled monolayers of alkanethiols on nickel surfaces for low level electrical contact applications*. Ieee Transactions on Components and Packaging Technologies, 1999. **22**(1): p. 79.
24. Alamarguy, D., *Etude de couches moléculaires organiques pour la protection des contacts électriques bas niveau*, 2004, Thesis of Université de Paris XI
25. Alamarguy, D., et al., *Corrosion behaviour of gold surfaces protected with bonded perfluoro polyethers*. Surface and Interface Analysis, 2004. **36**(8): p. 780.
26. Noel, S., et al., *Tribological Behavior of Heat-Treated Thin-Films of Electropolymerized Polyacrylonitrile*. Surface and Interface Analysis, 1994. **22**(1-12): p. 393.
27. Houze, F., et al., *ELABORATION OF HEAT-TREATED THIN-FILMS OF POLYACRYLONITRILE FOR CONNECTOR APPLICATION*. Ieee Transactions on Components Packaging and Manufacturing Technology Part A, 1995. **18**(2): p. 364.
28. Newton, P., et al., *Elaboration and chemical topography, tribological and electrical characterization of heat-treated thin-films of polyacrylonitrile for connector applications*. Journal De Physique Iii, 1995. **5**(6): p. 661.
29. Newton, P., et al., *Atomic force microscopy study of the topographic evolution of polyacrylonitrile thin films submitted to a rapid thermal treatment*. Thin Solid Films, 1997. **303**(1-2): p. 200.
30. Guessab, S., et al., *Influence of temperature and pressure on the static contact resistance of vacuum heat-treated polyacrylonitrile films*. Synthetic Metals, 2001. **118**(1-3): p. 121.
31. Guessab, S., *Etude de films de polyacrylonitrile post-traités en vue d'une utilisation comme revêtements de contacts électriques bas-niveau*, 1998, Thesis of Université de Paris XI
32. Delamar, M., et al., *Covalent modification of carbon surfaces by grafting of functionalized aryl radicals produced from electrochemical reduction of diazonium salts*. J. Am. Chem. Soc., 1992. **114**(14): p. 5883.
33. Andrieux, C.P. and J. Pinson, *The Standard Redox Potential of the Phenyl Radical/Anion Couple*. J. Am. Chem. Soc., 2003. **125**(48): p. 14801.
34. Pinson, J. and F. Podvorica, *Attachment of organic layers to conductive or semiconductive surfaces by reduction of diazonium salts*. Chemical Society Reviews, 2005. **34**(5): p. 429.
35. Laforgue, A., T. Addou, and D. Belanger, *Characterization of the Deposition of Organic Molecules at the Surface of Gold by the Electrochemical Reduction of Aryldiazonium Cations*. Langmuir, 2005. **21**(15): p. 6855.
36. Adenier, A., et al., *Covalent Modification of Iron Surfaces by Electrochemical Reduction of Aryldiazonium Salts*. J. Am. Chem. Soc., 2001. **123**(19): p. 4541.

37. Bernard, M.C., et al., *Organic layers bonded to industrial, coinage, and noble metals through electrochemical reduction of aryldiazonium salts*. *Chemistry of Materials*, 2003. **15**(18): p. 3450.
38. Allongue, P., et al., *Phenyl layers on H-Si(111) by electrochemical reduction of diazonium salts: monolayer versus multilayer formation*. *Journal of Electroanalytical Chemistry*, 2003. **550-551**: p. 161.
39. Uetsuka, H., et al., *Electrochemical grafting of boron-doped single-crystalline chemical vapor deposition diamond with nitrophenyl molecules*. *Langmuir*, 2007. **23**(6): p. 3466.
40. Kuo, T.C., R.L. McCreery, and G.M. Swain, *Electrochemical modification of boron-doped chemical vapor deposited diamond surfaces with covalently bonded monolayers*. *Electrochemical and Solid State Letters*, 1999. **2**(6): p. 288.
41. Jiang, D.E., B.G. Sumpter, and S. Dai, *Structure and bonding between an aryl group and metal surfaces*. *Journal of the American Chemical Society*, 2006. **128**(18): p. 6030.
42. Chausse, A., et al., *The electrochemical reduction of diazonium salts on iron electrodes. The formation of covalently bonded organic layers and their effect on corrosion*. *Chemistry of Materials*, 2002. **14**(1): p. 392.
43. Boukerma, K., et al., *X-ray photoelectron spectroscopy evidence for the covalent bond between an iron surface and aryl groups attached by the electrochemical reduction of diazonium salts*. *Langmuir*, 2003. **19**(15): p. 6333.
44. Liu, Y.-C. and R.L. McCreery, *Reactions of Organic Monolayers on Carbon Surfaces Observed with Unenhanced Raman Spectroscopy*. *J. Am. Chem. Soc.*, 1995. **117**(45): p. 11254.
45. Liu, Y.C. and R.L. McCreery, *Raman Spectroscopic Determination of the Structure and Orientation of Organic Monolayers Chemisorbed on Carbon Electrode Surfaces*. *Anal. Chem.*, 1997. **69**(11): p. 2091.
46. Actis, P., et al., *Functionalization of Glassy Carbon with Diazonium Salts in Ionic Liquids*. *Langmuir*, 2008. **24**(12): p. 6327.
47. Combellas, C., et al., *Time-of-flight secondary ion mass spectroscopy characterization of the covalent bonding between a carbon surface and aryl groups*. *Langmuir*, 2005. **21**(1): p. 280.
48. Lecayon, G., et al., *Grafting and growing mechanisms of polymerised organic films onto metallic surfaces*. *Chemical Physics Letters*, 1982. **91**(6): p. 506.
49. Palacin, S., et al., *Molecule-to-Metal Bonds: Electrografting Polymers on Conducting Surfaces*. *ChemPhysChem*, 2004. **5**(10): p. 1468.
50. Baute, N., et al., *Electrografting of acrylic and methacrylic monomers onto metals: Influence of the relative polarity and donor-acceptor properties of the monomer and the solvent*. *European Journal of Inorganic Chemistry*, 1998(11): p. 1711.
51. Deniau, G., et al., *Comparative study of acrylonitrile, 2-butenenitrile, 3-butenenitrile, and 2-methyl-2-propenenitrile electropolymerization on a nickel cathode*. *Langmuir*, 1992. **8**(1): p. 267.
52. Viel, P., S. Decayeux, and G. Lecayon, *Spectroscopic studies of the interface built-up during the formation of an electropolymerized polyacrylonitrile thin-film on a copper surface cathode*. *Surface and Interface Analysis*, 1993. **20**(5): p. 468.

53. Charlier, J., et al., *Mask-free localized grafting of organic polymers at the micrometer or submicrometer scale on composite conductors or semiconductor substrates*. *Advanced Functional Materials*, 2004. **14**(2): p. 125.
54. Jerome, C., et al., *Preparation of reactive surfaces by electrografting*. *Chemical Communications*, 2003(19): p. 2500.
55. Viel, P., et al., *New concept to remove heavy metals from liquid waste based on electrochemical pH-switchable immobilized ligands (vol 253, pg 3263, 2007)*. *Applied Surface Science*, 2007. **254**(5): p. 1543.
56. Cuenot, S., et al., *First insights into electrografted polymers by AFM-based force spectroscopy*. *Macromolecules*, 2006. **39**(24): p. 8428.
57. Deniau, G., et al., *Carbon-to-metal bonds: Electrochemical reduction of 2-butenenitrile*. *Surface Science*, 2006. **600**(3): p. 675.
58. Delamar, M., et al., *Modification of carbon fiber surfaces by electrochemical reduction of aryl diazonium salts: Application to carbon epoxy composites*. *Carbon*, 1997. **35**(6): p. 801.
59. Bouizem, Y., et al., *Ellipsometric study of acrylonitrile electropolymerization on nickel*. *Journal of Electroanalytical Chemistry*, 1984. **172**(1-2): p. 101.
60. Mevellec, V., et al., *Grafting polymers on surfaces: A new powerful and versatile diazonium salt-based one-step process in aqueous media*. *Chemistry of Materials*, 2007. **19**(25): p. 6323.
61. Deniau, G., et al., *Surface electroinitiated emulsion polymerization: Grafted organic coatings from aqueous solutions*. *Chemistry of Materials*, 2006. **18**(23): p. 5421.
62. Ricci, A., C. Bonazzola, and E.J. Calvo, *An FT-IRRAS study of nitrophenyl mono- and multilayers electro-deposited on gold by reduction of the diazonium salt*. *Physical Chemistry Chemical Physics*, 2006. **8**(37): p. 4297.
63. Adenier, A., et al., *Formation of polyphenylene films on metal electrodes by electrochemical reduction of benzenediazonium salts*. *Chemistry of Materials*, 2006. **18**(8): p. 2021.
64. Delamar, M., et al., *Covalent modification of carbon surfaces by grafting of functionalized aryl radicals produced from electrochemical reduction of diazonium salts*. *Journal of the American Chemical Society*, 1992. **114**(14): p. 5883.
65. Allongue, P., et al., *Covalent modification of carbon surfaces by aryl radicals generated from the electrochemical reduction of diazonium salts*. *Journal of the American Chemical Society*, 1997. **119**(1): p. 201.
66. Griveau, S., et al., *Electrochemical grafting by reduction of 4-aminoethylbenzenediazonium salt: Application to the immobilization of (bio)molecules*. *Electrochemistry Communications*, 2007. **9**(12): p. 2768.
67. Ranganathan, S. and R.L. McCreery, *Electroanalytical performance of carbon films with near-atomic flatness*. *Analytical Chemistry*, 2001. **73**(5): p. 893.
68. Baranton, S. and D. Belanger, *Electrochemical derivatization of carbon surface by reduction of in situ generated diazonium cations*. *Journal of Physical Chemistry B*, 2005. **109**(51): p. 24401.
69. Brooksby, P.A. and A.J. Downard, *Electrochemical and Atomic Force Microscopy Study of Carbon Surface Modification via Diazonium Reduction in Aqueous and Acetonitrile Solutions*. *Langmuir*, 2004. **20**(12): p. 5038.
70. Lamy, C., J.M. Leger, and J. Clavilier, *Structural Effects in the Electrooxidation of Methanol in Alkaline-Medium - Comparison of Platinum Single-Crystal and*

- Polycrystalline Electrodes*. Journal of Electroanalytical Chemistry, 1982. **135**(2): p. 321.
71. Rodes, A., et al., *The Influence of Polyoriented Gold Electrodes Modified by Reversibly and Irreversibly Adsorbed Ad-Atoms on the Redox Behavior of the Cr(II)/Cr(I) Couple and the Effect of Chloride-Ions*. Journal of Electroanalytical Chemistry, 1989. **271**(1-2): p. 127.
  72. Clavilier, J., et al., *Electrochemistry at Platinum Single-Crystal Surfaces in Acidic Media - Hydrogen and Oxygen-Adsorption*. Journal De Chimie Physique Et De Physico-Chimie Biologique, 1991. **88**(7-8): p. 1291.
  73. Lipkowski, J., et al., *Molecular adsorption at metal electrodes*. Electrochimica Acta, 1994. **39**(8-9): p. 1045.
  74. Lang, P. and J. Clavilier, *Influence of the crystalline surface-structure of platinum on the electropolymerization of 3-methylthiophene*. Synthetic Metals, 1991. **45**(3): p. 297.
  75. Trasatti, S., *Systematic Trends in the Crystal-Face Specificity of Interfacial Parameters - the Cases of Ag and Au*. Journal of Electroanalytical Chemistry, 1992. **329**(1-2): p. 237.
  76. Hamelin, A., et al., *The Electrochemical Double-Layer on Sp Metal Single-Crystals - the Current Status of Data*. Journal of Electroanalytical Chemistry, 1983. **145**(2): p. 225.
  77. Alessandrini, A. and U. Valdre, *Work function dependence on the thickness and substrate of carbon contamination layers by Kelvin probe force microscopy*. Philosophical Magazine Letters, 2003. **83**(7): p. 441.
  78. Hamelin, A., *Double-layer properties at sp and sd metal single-crystal electrodes*, in *Modern Aspects of Electrochemistry*, B.E. Conway, J.O.M. Bockris, and R.E. White, Editors. 1985, Plenum Press: New York and London. p. 1.
  79. Leon y Leon, C.A. and L.R. Radovic, *Interfacial Chemistry and Electrochemistry of Carbon Surfaces*, in *Chemistry and physics of carbon*, P. Thrower, Editor. 1994, New York: Dekker: New York. p. 213.
  80. Zhang, L., et al., *Conductivity and surface potential studies in carbon films by conductive scanning probe microscopy*. Japanese Journal of Applied Physics Part 1- Regular Papers Short Notes & Review Papers, 2000. **39**(6B): p. 3728.
  81. Socrates, G., *Infrared Characteristic Group Frequencies*. 1980, Chichester - New York - Brisbane - Toronto: John Wiley & Sons. 153.
  82. Hurley, B.L. and R.L. McCreery, *Covalent bonding of organic molecules to Cu and Al alloy 2024 T3 surfaces via diazonium ion reduction*. Journal of the Electrochemical Society, 2004. **151**(5): p. B252.
  83. Adenier, A., et al., *Grafting of nitrophenyl groups on carbon and metallic surfaces without electrochemical induction*. Chemistry of Materials, 2005. **17**(3): p. 491.
  84. Combellas, C., et al., *Spontaneous grafting of iron surfaces by reduction of aryl diazonium salts in acidic or neutral aqueous solution. Application to the protection of iron against corrosion*. Chemistry of Materials, 2005. **17**(15): p. 3968.
  85. Doppelt, P., et al., *Surface modification of conducting substrates. Existence of azo bonds in the structure of organic layers obtained from diazonium salts*. Chemistry of Materials, 2007. **19**(18): p. 4570.
  86. Demarconnay, L. and D. Belanger, *Modification of glassy carbon and gold electrodes with halogenated phenyl groups by electrochemical reduction of in situ generated*

- diazonium cations, in *The 58th Annual Meeting of the International Society of Electrochemistry*. 2007: Banff, Canada.
87. Owens, D.K. and R.C. Wendt, *Estimation of the surface free energy of polymers*. *Journal of Applied Polymer Science*, 1969. **13**(8): p. 1741.
  88. Strom, G., M. Fredriksson, and P. Stenius, *Contact angles, work of adhesion, and interfacial tensions at a dissolving Hydrocarbon surface*. *Journal of Colloid and Interface Science*, 1987. **119**(2): p. 352.
  89. Jasper, J.J., *The Surface Tension of Pure Liquid Compounds*. *Journal of Physical and Chemical Reference data*, 1972. **1**(4): p. 859.
  90. Alamarguy, D., et al., *Tribological and electrical study of fluorinated diazonium films as dry lubricants for electrical contacts*. *Surface and Interface Analysis*, 2008. **40**(3-4): p. 802.
  91. Guo, D.Z., et al., *Conductance fluctuation and degeneracy in nanocontact between a conductive AFM tip and a granular surface under small-load conditions*. *Applied Surface Science*, 2006. **252**(14): p. 5149.
  92. Miura, Y.F., et al., *Wettabilities of self-assembled monolayers generated from CF<sub>3</sub>-terminated alkanethiols on gold*. *Langmuir*, 1998. **14**(20): p. 5821.
  93. Gabriel, S., et al., *Electrografting of poly(ethylene glycol) acrylate: A one-step strategy for the synthesis of protein-repellent surfaces*. *Angewandte Chemie-International Edition*, 2005. **44**(34): p. 5505.
  94. Deniau, G., et al., *Study of the simultaneous electro-initiated anionic polymerization of vinylic molecules*. *Journal of Electroanalytical Chemistry*, 2006. **586**(1): p. 62.
  95. Deniau, G., et al., *Polymer-film formation on the surface of a cathodically polarized nickel electrode in the presence of 4-chlorostyrene*. *Journal of the Chemical Society-Perkin Transactions 2*, 1990(8): p. 1433.
  96. Charlier, J., C. Bureau, and G. Lecayon, *Electropolymerization of methacrylonitrile and N-vinyl-2-pyrrolidone as probed by an EQCM*. *Journal of Electroanalytical Chemistry*, 1999. **465**(2): p. 200.
  97. Voccia, S., et al., *Electrografting of thin polymer films: Three strategies for the tailoring of functional adherent coatings*. *Progress in Organic Coatings*, 2006. **55**(2): p. 175.
  98. Houze, F., et al., *Electrical-Properties of Very Thin Heat-Treated Polyacrylonitrile Layers Electropolymerized on Nickel for Contact Application*. *Synthetic Metals*, 1994. **62**(3): p. 207.
  99. Deniau, G., et al., *Study of the polymers obtained by electroreduction of methacrylonitrile*. *Journal of Electroanalytical Chemistry*, 2001. **505**(1-2): p. 33.
  100. Mertens, M., et al., *The electroreduction of acrylonitrile: A new insight into the mechanism*. *Macromolecules*, 1996. **29**(14): p. 4910.
  101. Bureau, C., et al., *The electroreduction of acrylonitrile: A new insight into the mechanism - Comments*. *Macromolecules*, 1997. **30**(2): p. 333.
  102. Bureau, C., J.M. Soudan, and G. Lecayon, *On the influence of RRC and RSC dimerizations on the shape of semi-integrated voltammograms: a mixed asymptotic and numerical analysis*. *Electrochimica Acta*, 1999. **44**(19): p. 3303.
  103. Bureau, C., *Polymerization reaction coupled to charge transfer: propagation versus termination as a source of permanent travelling waves and multi-peak voltammograms*. *Journal of Electroanalytical Chemistry*, 1999. **479**(1): p. 43.

104. Tanguy, J., et al., *Study of the grafting and the electrochemical polymerization of acrylic-monomers on a metallic surface by impedance spectroscopy*. *Electrochimica Acta*, 1993. **38**(11): p. 1501.
105. Deniau, G., *Etude de l'influence de la structure moléculaire de composés vinyliques sur leur aptitude à former des films de polymère par electropolymerization sous polarisation cathodique*, 1990, Thesis of Université de Paris VI
106. Erhardt, M.K. and R.G. Nuzzo, *Driven Pattern Formation in Organic Thin Film Materials: Complex Mesoscopic Organization in Microcontact Printing on Si/SiO<sub>2</sub> via the Spontaneous Dewetting of a Functionalized Perfluoropolyether Ink*. *J. Phys. Chem. B*, 2001. **105**(37): p. 8776.
107. Rolland, J.P., et al., *Solvent-Resistant Photocurable "Liquid Teflon" for Microfluidic Device Fabrication*. *J. Am. Chem. Soc.*, 2004. **126**(8): p. 2322.
108. Lin, D.S., et al., *The friction and wear behaviour of nickel-base alloys in air at room temperature*. *Wear*, 1973. **24**(3): p. 261.
109. Mishina, H., *Atmospheric characteristics in friction and wear of metals*. *Wear*, 1992. **152**(1): p. 99.
110. Mathieson, D., et al., *Effect of progressive wear on the friction characteristics of nickel LIGA processed rotors*. *Wear*, 1996. **192**(1-2): p. 199.
111. Drummond, C. and J. Israelachvili, *Dynamic phase transitions in confined lubricant fluids under shear*. *Physical Review E*, 2001. **6304**(4).
112. Bhuyan, S., et al., *Boundary lubrication properties of lipid-based compounds evaluated using microtribological methods*. *Tribology Letters*, 2006. **22**(2): p. 167.
113. Tartaglino, U., et al., *Impact of molecular structure on the lubricant squeeze-out between curved surfaces with long range elasticity*. *Journal of Chemical Physics*, 2006. **125**(1).
114. Homola, A.M., H.V. Nguyen, and G. Hadziioannou, *INFLUENCE OF MONOMER ARCHITECTURE ON THE SHEAR PROPERTIES OF MOLECULARLY THIN POLYMER MELTS*. *Journal of Chemical Physics*, 1991. **94**(3): p. 2346.
115. Pooley, C.M. and D. Tabor, *Friction and molecular structure - behavior of some thermoplastics*. *Proceedings of the Royal Society of London Series a-Mathematical and Physical Sciences*, 1972. **329**(1578): p. 251.
116. Jerome, C., et al., *Full-electrochemical preparation of conducting/insulating binary polymer films*. *Chemistry of Materials*, 2001. **13**(5): p. 1656.
117. Labaye, D.E., et al., *Full electrochemical synthesis of conducting polymer films chemically grafted to conducting surfaces*. *Langmuir*, 2002. **18**(13): p. 5222.
118. Gabriel, S., et al., *Synthesis of adherent hydrophilic polypyrrole coatings onto (semi)conducting surfaces*. *Chemistry of Materials*, 2007. **19**(9): p. 2364.
119. Sato, M. and M. Sano, *van der Waals layer-by-layer construction of a carbon nanotube 2D network*. *Langmuir*, 2005. **21**(24): p. 11490.
120. Auvray, S., et al., *Chemical optimization of self-assembled carbon nanotube transistors*. *Nano Letters*, 2005. **5**(3): p. 451.
121. Kong, J. and H.J. Dai, *Full and modulated chemical gating of individual carbon nanotubes by organic amine compounds*. *Journal of Physical Chemistry B*, 2001. **105**(15): p. 2890.

122. Nan, X., Z. Gu, and Z. Liu, *Immobilizing Shortened Single-Walled Carbon Nanotubes (SWNTs) on Gold Using a Surface Condensation Method*. Journal of Colloid and Interface Science, 2002. **245**(2): p. 311.
123. Rosario-Castro, B.I., et al., *Attachment of single-wall carbon nanotubes on platinum surfaces by self-assembling techniques*. Reviews on Advanced Materials Science, 2005. **10**(4): p. 381.
124. Jung, M.S., et al., *Electrical and field-emission properties of chemically anchored single-walled carbon nanotube patterns*. Applied Physics Letters, 2005. **87**(1).
125. Wei, Z., et al., *Rectifying diodes from asymmetrically functionalized single-wall carbon nanotubes*. Journal of the American Chemical Society, 2006. **128**(10): p. 3134.
126. Flatt, A.K., B. Chen, and J.M. Tour, *Fabrication of carbon nanotube-molecule-silicon junctions*. Journal of the American Chemical Society, 2005. **127**(25): p. 8918.
127. Vorotyntsev, M.A., J.-P. Badiali, and G. Inzelt, *Electrochemical impedance spectroscopy of thin films with two mobile charge carriers: effects of the interfacial charging*. Journal of Electroanalytical Chemistry, 1999. **472**(1): p. 7.
128. Mulder, W.H., et al., *Tafel current at fractal electrodes - connection with admittance spectra*. Journal of Electroanalytical Chemistry, 1990. **285**(1-2): p. 103.
129. Hass, R., J. Garcia-Canadas, and G. Garcia-Belmonte, *Electrochemical impedance analysis of the redox switching hysteresis of poly(3,4-ethylenedioxythiophene) films*. Journal of Electroanalytical Chemistry, 2005. **577**(1): p. 99.
130. Yamamoto, T., et al., *Extensive studies on pi-stacking of poly(3-alkylthiophene-2,5-diyl)s and poly(4-alkylthiazole-2,5-diyl)s by optical spectroscopy, NMR analysis, light scattering analysis, and X-ray crystallography*. Journal of the American Chemical Society, 1998. **120**(9): p. 2047.
131. Percec, V., et al., *Self-organization of supramolecular helical dendrimers into complex electronic materials*. Nature, 2002. **419**(6905): p. 384.
132. Sauerbrey, G., *Verwendung von Schwingquarzen zur Wagung dünner Schichten und zur Mikrowagung*. Zeitschrift Fur Physik, 1959. **155**(2): p. 206.
133. Kanazawa, K.K. and J.G. Gordon, *Frequency of a quartz microbalance in contact with liquid*. Anal. Chem., 1985. **57**(8): p. 1770.
134. Viel, P., et al., *Erratum to "New concept to remove heavy metals from liquid waste based on electrochemical pH-switchable immobilized ligands" [Appl. Surf. Sci. 253 (2007) 3263-3269]*. Applied Surface Science, 2007. **254**(5): p. 1543.
135. Groenendaal, L., et al., *Electrochemistry of poly(3,4-alkylenedioxythiophene) derivatives*. Advanced Materials, 2003. **15**(11): p. 855.
136. Greczynski, G., T. Kugler, and W.R. Salaneck, *Characterization of the PEDOT-PSS system by means of X-ray and ultraviolet photoelectron spectroscopy*. Thin Solid Films, 1999. **354**(1-2): p. 129.
137. Kissner, R., *HALIDE CATALYSIS OF THE ELECTROCHEMICAL OXIDATION OF GOLD IN ACETONITRILE*. Journal of Electroanalytical Chemistry, 1995. **385**(1): p. 71.
138. Otero, T.F., et al., *ELECTROGENERATION OF THICK POLYTHIOPHENE FILMS ON STAINLESS-STEEL*. Synthetic Metals, 1993. **55**(2-3): p. 1574.
139. Sakmeche, N., et al., *Usefulness of aqueous anionic micellar media for electrodeposition of poly-(3,4-ethylenedioxythiophene) films on iron, mild steel and aluminium*. Electrochimica Acta, 2000. **45**(12): p. 1921.

140. Mekhalif, Z., F. Plumier, and J. Delhalle, *Electropolymerisation of poly(3,4-ethylenedioxythiophene) on nickel substrates*. Applied Surface Science, 2003. **212**: p. 472.
141. Biallozor, S. and A. Kupniewska, *Conducting polymers electrodeposited on active metals*. Synthetic Metals, 2005. **155**(3): p. 443.
142. Xiao, Y.H., X.Y. Cui, and D.C. Martin, *Electrochemical polymerization and properties of PEDOT/S-EDOT on neural microelectrode arrays*. Journal of Electroanalytical Chemistry, 2004. **573**(1): p. 43.
143. Angersteinkozłowska, H., et al., *ELEMENTARY STEPS OF ELECTROCHEMICAL OXIDATION OF SINGLE-CRYSTAL PLANES OF AU .2. A CHEMICAL AND STRUCTURAL BASIS OF OXIDATION OF THE (111) PLANE*. Journal of Electroanalytical Chemistry, 1987. **228**(1-2): p. 429.
144. Angersteinkozłowska, H., et al., *ELEMENTARY STEPS OF ELECTROCHEMICAL OXIDATION OF SINGLE-CRYSTAL PLANES OF AU .1. CHEMICAL BASIS OF PROCESSES INVOLVING GEOMETRY OF ANIONS AND THE ELECTRODE SURFACES*. Electrochimica Acta, 1986. **31**(8): p. 1051.
145. Hamelin, A. and L. Stoicoviciu, *STUDY OF GOLD LOW INDEX FACES IN KPF6 SOLUTIONS .1. EXPERIMENTAL BEHAVIOR AND DETERMINATION OF THE POINTS OF ZERO CHARGE*. Journal of Electroanalytical Chemistry, 1987. **234**(1-2): p. 93.
146. Hamelin, A., *Cyclic voltammetry at gold single-crystal surfaces .1. Behaviour at low-index faces*. Journal of Electroanalytical Chemistry, 1996. **407**(1-2): p. 1.
147. Hamelin, A. and A.M. Martins, *Cyclic voltammetry at gold single-crystal surfaces .2. Behaviour of high-index faces*. Journal of Electroanalytical Chemistry, 1996. **407**(1-2): p. 13.
148. Groenendaal, L., G. Zotti, and F. Jonas, *Optical, conductive and magnetic properties of electrochemically prepared alkylated poly(3,4-ethylenedioxythiophene)s*. Synthetic Metals, 2001. **118**(1-3): p. 105.
149. Barbalace, K. *Periodic Table of Elements - Sorted by Electrical Conductivity*. 1995 - 2008 [cited Accessed on-line: 7/17/2008]; Available from: <http://EnvironmentalChemistry.com/yogi/periodic/electrical.html>.
150. Mathieu, D., et al., *Theoretical and experimental study of the molecular structure absorbing at 2190 cm<sup>-1</sup> in electroinitiated polyacrylonitrile*, in *Polymer-Solid Interfaces: First International Conference*, J.J. Pireaux, Editor. 1992, Taylor & Francis Group Namur, Belgium. p. 379.
151. Viel, P., *Etude de la modification d'une surface métallique par greffage et croissance d'un film de polyacrylonitrile électropolymerisé sous polarisation cathodique*, 1990, Thesis of Université de Paris VI
152. Valentin, E., et al., *High-density selective placement methods for carbon nanotubes*. Microelectronic Engineering, 2002. **61-62**: p. 491.
153. Popov, V.N., L. Henrard, and P. Lambin, *Resonant raman intensity of the radial breathing mode of single-walled carbon nanotubes within a nonorthogonal tight-binding model*. Nano Letters, 2004. **4**(9): p. 1795.
154. Yang, Z., et al., *A study on carbon nanotubes reinforced poly(methyl methacrylate) nanocomposites*. Materials Letters, 2005. **59**(17): p. 2128.
155. Cai, H., F. Yan, and Q. Xue, *Investigation of tribological properties of polyimide/carbon nanotube nanocomposites*. Materials Science and Engineering A, 2004. **364**(1-2): p. 94.

156. Zoo, Y.S., et al., *Effect of carbon nanotube addition on tribological behavior of UHMWPE*. Tribology Letters, 2004. **16**(4): p. 305.
157. Chen, W.X., et al., *Tribological behavior of carbon-nanotube-filled PTFE composites*. Tribology Letters, 2003. **15**(3): p. 275.
158. Li, X., et al., *Fabrication and atomic force microscopy/friction force microscopy (AFM/FFM) studies of polyacrylamide-carbon nanotubes (PAM-CNTs) copolymer thin films*. Materials Chemistry and Physics, 2004. **88**(1): p. 53.
159. Streitwieser, A. and C.H. Heathcock, *Introduction to Organic Chemistry*. third ed. 1989, New York: Maxwell Macmillan International Editions.
160. Ramanathan, T., et al., *Amino-functionalized carbon nanotubes for binding to polymers and biological systems*. Chemistry of Materials, 2005. **17**(6): p. 1290.
161. Bahr, J.L. and J.M. Tour, *Covalent chemistry of single-wall carbon nanotubes*. Journal of Materials Chemistry, 2002. **12**(7): p. 1952.
162. Dyke, C.A., et al., *Diazonium-based functionalization of carbon nanotubes: XPS and GC-MS analysis and mechanistic implications*. Synlett, 2004(1): p. 155.
163. Buffa, F., H. Hu, and D.E. Resasco, *Side-wall functionalization of single-walled carbon nanotubes with 4-hydroxymethylaniline followed by polymerization of epsilon-caprolactone*. Macromolecules, 2005. **38**(20): p. 8258.
164. Ellison, M.D. and P.J. Gasda, *Functionalization of Single-Walled Carbon Nanotubes with 1,4-Benzenediamine Using a Diazonium Reaction*. J. Phys. Chem. C, 2008. **112**(3): p. 738.
165. Pagona, G., N. Karousis, and N. Tagmatarchis, *Aryl diazonium functionalization of carbon nanohorns*. Carbon, 2008. **46**(4): p. 604.
166. Toupin, M. and D. Belanger, *Thermal stability study of aryl modified carbon black by in situ generated diazonium salt*. Journal of Physical Chemistry C, 2007. **111**(14): p. 5394.
167. Lyskawa, J. and D. Belanger, *Direct Modification of a Gold Electrode with Aminophenyl Groups by Electrochemical Reduction of in Situ Generated Aminophenyl Monodiazonium Cations*. Chem. Mater., 2006. **18**(20): p. 4755.
168. Viel, P., X.T. Le, and A. Benedetto, *Rediazotization*. 2008.
169. Le, X.T., et al., *Electro-switchable surfaces for heavy metal waste treatment: Study of polyacrylic acid films grafted on gold surfaces*. Electrochemistry Communications, 2008. **10**(5): p. 699.
170. Tanguy, J., et al., *Cathodic electropolymerization of methacrylonitrile studied in situ by quartz crystal microbalance, cyclic voltammetry, and impedance spectroscopy*. Journal of Electroanalytical Chemistry, 1996. **417**(1-2): p. 175.
171. Saby, C., et al., *Electrochemical modification of glassy carbon electrode using aromatic diazonium salts .1. Blocking effect of 4-nitrophenyl and 4-carboxyphenyl groups*. Langmuir, 1997. **13**(25): p. 6805.
172. Benedetto, A., et al., *Electro-reduction of diazonium salts on gold: Why do we observe multi-peaks?* Electrochimica Acta, 2008. **53**(24): p. 7117.
173. Bureau, C., E. Levy, and P. Viel, *Method for grafting and growing a conductive organic film on a surface*, 2008, Patent WO03018212
174. Jouselme, B., et al., *One-step electrochemical modification of carbon nanotubes by ruthenium complexes via new diazonium salts*. Journal of Electroanalytical Chemistry. **In Press, Corrected Proof**.

175. Laibinis, P.E. and G.M. Whitesides, *Self-assembled monolayers of n-alkanethiolates on copper are barrier films that protect the metal against oxidation by air*. Journal of the American Chemical Society, 1992. **114**(23): p. 9022.
176. Guaita, M., et al., *Fondamenti di Scienza dei Polimeri*. 1998, Pisa: Pacini Editore. 923.
177. Newton, P., *Etude physico-chimique, électrique et tribologique de films minces de polyacrylonitrile pyrolysés en vue de leur application comme revêtements terminal de connecteurs électriques bas-niveau*, 1995, Thesis of Université de Paris VI
178. Thomas, T.R., *Rough Surfaces*. 1982, London: Longman.
179. Majumdar, A. and B. Bhushan, *Fractal model of elastic-plastic contact between rough surfaces*. Journal of Tribology-Transactions of the Asme, 1991. **113**(1): p. 1.
180. Féchant, L., *Le contact électrique. Tome I: Phénomènes physiques et matériaux*. 1996, Paris: Hermes.
181. Le Gall, C., *Etude des phénomènes de dégradation dans les contacts de bas niveau soumis à des micro vibrations*, 1995, Thesis of Université de Paris XI
182. Johnson, K.L., *Contact Mechanics*. 1989, Cambridge: Cambridge University Press.
183. Greenwood, J.A. and J.H. Tripp, *Elastic contact of rough spheres*. Journal of Applied Mechanics, 1967. **34**(1): p. 153.
184. Gabrielli, C., et al., *A model for copper deposition in the damascene process*. Electrochimica Acta, 2006. **51**(8-9): p. 1462.
185. Gabrielli, C., *Identification of electrochemical processes by frequency response analysis. Technical report*. 1998, Solartron.
186. Bard, A.J. and L.R. Faulkner, *Electrochemical methods: Fundamentals and Applications*. 2nd ed. 2001, New York: John Wiley & Sons Inc.
187. Barsoukov, E. and J.R. Macdonald, eds. *Impedance Spectroscopy: Theory, Experiment, and Applications*. 2nd ed. 2005, John Wiley & Sons Inc.: New York.
188. Macdonald, D.D., *Reflections on the history of electrochemical impedance spectroscopy*. Electrochimica Acta, 2006. **51**(8-9): p. 1376.